Universidade do Minho
Escola de Engenharia

Sidonie Fernandes Costa

Free Form Extrusion - Extrusion of 3D
components using complex Polymeric systems

Sidonie Fernandes Costa Free Form Extrusion - Extrusion of 3D
components using complex Polymeric systems

UMinho | 2012

Agosto de 2012

Universidade do Minho
Escola de Engenharia

Sidonie Fernandes Costa

Free Form Extrusion - Extrusion of 3D
components using complex Polymeric systems

Agosto de 2012

DECLARAÇÃO

Nome: Sidonie Fernandes Costa

Endereço eletrónico: sidonie@dep.uminho.pt   **Telefone:** 964850501

Número do Cartão de Cidadão: 13407518

Título tese:

Free Form Extrusion - Extrusion of 3D components using complex Polymeric systems

Orientador:

Professor Doutor Fernando Moura Duarte

Co-orientador:

Professor Doutor José António Colaço Gomes Covas

Ano de conclusão: 2012

Designação do Doutoramento:

Programa Doutoral em Ciência e Engenharia de Polímeros e Compósitos

É AUTORIZADA A REPRODUÇÃO INTEGRAL DESTA TESE APENAS PARA EFEITOS DE INVESTIGAÇÃO, MEDIANTE DECLARAÇÃO ESCRITA DO INTERESSADO, QUE A TAL SE COMPROMETE.

Universidade do Minho,   de Agosto de 2012

Assinatura: _____

ACKNOWLEDGEMENTS

My first acknowledgments are made to my supervisor Professor Doctor Fernando Duarte, for all the support, guidance and encouragement during these past years. He showed always to be available and spent a lot of time helping me, overall in making the connection between mathematics and engineering. His unquestionable patience and great ability in transmitting his knowledge were fundamental for the accomplishment of this work. I've learned a lot during this time and I am greatly thankful for this.

To Professor Doctor José António Covas, my co-supervisor, for his knowledgeable, professionalism and careful supervision. He always showed to have a great scientific view and gave me important advices and ideas that contributed to the improvement of my work. When I was less sure of myself, he always showed me the positive sides and gave me the correct way for which I should go. Meetings with him always give me a great "refresh" and courage to continue.

To the technicians of the University of Minho, namely João Paulo Peixoto, Francisco Mateus, Serafim Sampaio and Mauricio Malheiro.

I am also sincerely grateful to Paulo Antunes for the help on manipulating ABAQUS® software. Without his support, the familiarization with this software would have been a difficult and slow task.

To my colleagues of Escola Superior de Tecnologia e Gestão de Felgueiras, especially to Doctor Aldina Correia, for the understanding and encouragement. Her support was fundamental in the accomplishment of this work.

I also would like to express my sincere thanks to my colleagues at the old Biblioteca do Departamento de Polímeros, for their help and friendship.

To my friends of Violodorata, Acanthus and Tuna Feminina de Engenharia da Universidade do Minho, for the good moments that they provide me during this period, especially to Flora Ferreira, an eternal and especial friend since I came to Portugal.

I cannot also forget my friend Oscar, for his tireless companionship along all my work, for all the days and hours that he spent always by my side.

To my grandfather Guy Sivignon, who will always be in my heart.

By last, my final words go out to the most special person to me, my husband and best friend Rui. Without him, everything would be much more difficult, in particular in the final phase of this work. His great ability to listen to what I had to say, always with love, care and patience, gives me the strength to keep going on. Thank you for being by my side in all the moments and for letting me be part of your life. To him I dedicated this thesis.

Free Form Extrusion:

Extrusion of 3D components using complex Polymeric systems

ABSTRACT

Free Form Extrusion (FFE) is a 3D fabrication process that involves depositing an extruded filament onto successive horizontal planes, in order to build a physic part with a specific geometry. The method is an adaptation of Fused Deposition Modeling (FDM), whereby a commercial pre-extruded ABS filament is replaced by a mini-extruder capable of processing a wide range of materials, including homopolymers, polymer blends and nanocomposites.

The mechanical performance of FFE parts is controlled by the bonding quality between adjacent filaments both in the horizontal and vertical plans. Adjacent filaments must be sufficiently hot to ensure adhesion, but should then cool down fast enough to avoid excessive deformation due to gravity and weight of the filaments on top. Therefore, it is important to know the evolution in time of the filaments temperature and how it is affected by the major process variables.

Although several heat transfer models have been proposed in literature, most assume simplifications without verifying their effective importance. In this work, a detailed analysis of the contributions to the global heat transfer was made using the ABAQUS® software. Heat exchanges with ambient by convection and between adjacent filaments by conduction were found to be the most important. Consequently, these were taken in the energy balance, in order to obtain a rigorous FFE heat transfer analytical model.

This analytical solution was then embedded into a routine capable of considering three different deposition patterns, for parts with specific geometries. Moreover, an adhesion criterion was implemented, in order to predict whether the operating conditions and deposition patterns selected for the manufacture of a given part are adequate. The deformation of the filaments was investigated by performing computational experiments with the ABAQUS® software, assuming a temperature dependent viscoelastic response. Since the maximum differences were shown to be quite small ($< 0.2\%$), this phenomenon was considered negligible.

The consequence of this work is then a computer code that rigorously considers and inter-relates the three phenomena, with the potential of assisting the FFE user in selecting the ideal process parameters in order to obtain a part with good performance. This also allows testing the influence of many process variables and concluding about the most important.

Free Form Extrusion:

Extrusão de componentes 3D utilizando sistemas poliméricos complexos

RESUMO

Free Form Extrusion (FFE) é um processo 3D de fabricação que envolve a deposição de um filamento extrudido em planos horizontais sucessivos, por forma a obter uma peça com uma geometria específica. O método é uma adaptação do Fused Deposition Modelling (FDM), através do qual um filamento de ABS comercial pré-extrudido é substituído por uma mini-extrusora com a capacidade de processar uma grande variedade de materiais, incluindo homopolímeros, misturas de polímeros e nanocompósitos.

O desempenho mecânico das peças obtidas através da técnica FFE é influenciado pela qualidade de adesão entre filamentos adjacentes, nos planos horizontais bem como verticais. Os filamentos adjacentes devem ser suficientemente quentes para assegurar a adesão, mas ter um arrefecimento suficientemente rápido para evitar a deformação excessiva devido à gravidade e ao peso dos filamentos posicionados nas camadas superiores. Consequentemente, é importante o conhecimento da evolução da temperatura dos filamentos em função do tempo, e como este é afetado pelas principais variáveis do processo.

Apesar de vários modelos de transferência de calor terem sido propostos na literatura, na maior parte, simplificações são assumidas sem verificar a sua efetiva importância. Neste trabalho, uma análise detalhada dos intervenientes na transferência de calor foi elaborada usando o software ABAQUS®. Trocas de calor com o ambiente por convecção e entre filamentos adjacentes por condução mostraram ser os mais importantes. Consequentemente, estes foram incluídos no balanço de energia, a fim de obter um modelo analítico rigoroso de transferência de calor para o processo FFE.

Esta solução analítica foi então incorporada numa rotina com a capacidade de considerar três tipos diferentes de deposição, para peças com geometrias específicas. Além disso, um critério de adesão foi implementado, a fim de prever se as condições operatórias e os tipos de deposição selecionados para a construção de uma dada peça são adequados.

A deformação dos filamentos foi investigada através da realização de experiências com o software computacional ABAQUS®, assumindo uma resposta viscoelástica dependente da temperatura. Uma vez que as diferenças máximas mostraram ser muito baixas ($< 0.2\%$), este fenômeno foi considerado negligenciável.

A consequência deste trabalho é portanto um código computacional que considera rigorosamente e inter-relaciona os três fenómenos, com a potencialidade de auxiliar o utilizador do processo FFE na seleção ideal dos parâmetros de processo, a fim de obter uma peça com bom desempenho. Também permite testar a influência de diversas variáveis de processo e concluir quais são as mais importantes.

CONTENTS

LIST OF FIGURES

xiv

LIST OF TABLES

LIST OF ABBREVIATIONS AND NOMENCLATURE

CAD   –   Computer Aided Design

RP   –   Rapid Prototyping

LOM   –   Laminated Object Manufacturing

SLS   –   Selected Laser Sintering

3DP   –   Ink-jet Printing

FDM   –   Fused Deposition Modeling

ABS   –   Acrylonitrile Butadiene Styrene

FFE   –   Free Form Extrusion

PED   –   Precision Extruding Deposition

PCL   –   Poly-ε-CaproLactone

MED   –   Mini Extruder Deposition

FEM   –   Finite Element Methods

FDC   –   Fused Deposition of Ceramics

t –   Time (sec)

L –   Filament Length (m)

Φ –   Bonding Potential (K.s)

T_c –   Critical temperature above which

                   bonding process is activated (ºC)

$T_{\text{interface}}$ –   Temperature at the interface between two adjacent filaments (ºC)

T_g –   Glass Transition Temperature (ºC)

L_c –   Length of polymer chain (m)

$t_{reptation}$ –   Reptation time (s)

χ –   Interpenetration Depth (m)

χ_∞ –   Ultimate Interpenetration Distance (m)

$\sigma(t)$ –   Bond Strength (MPa)

$D_h(t)$ –   Degree of Healing (%)

$t_{reptation}^{*}$ –   Reptation time (s) obtained at the average temperature

M_c –   Critical Entanglement Molecular Weight (kg/kmol)

                   Probability of finding a particular chain segment at a position s and

$P(s,t)$ –   time t

D	–	Reptation Diffusion Coefficient (m^2/s)
δ	–	Dirac Delta function (m^{-1})
$t_w(T)$	–	Welding time with temperature dependence (s)
R	–	Universal Gas Constant (J/K.mol)
AD	–	Average Absolute Deviation (inches)
SCF	–	Optimal Shrinkage Compensation (%)
δ	–	Flattening height (mm)
h_{conv}	–	Heat transfer coefficient (W/$m^2 \cdot$ ºC)
T_L	–	Extrusion temperature (ºC)
T_E	–	Environment temperature (ºC)
ε	–	Emissivity coefficient
$F_{A\to B}$	–	Ratio of the radiation energy leaving surface A and that is intercepted by surface B
r_c	–	Thermal contact Resistance ($m^2 \cdot$ ºC/W)
h_c	–	Thermal contact Conductance (W/$m^2 \cdot$ ºC)
A_a	–	Area of the contacting surfaces (m^2)
N	–	Total number of filaments of a given sequence
$T_r(x,t)$	–	Temperature on the point x at the instant t of the rth filament ($r \in \{1,\ldots,N\}$)
k	–	Thermal Conductivity (W/m· ºC)
A	–	Filament cross-section Area (m^2)
n	–	Physical number of contacts with adjacent filaments or with support
h_i	–	Thermal contact Conductance for contact $i \in \{1,\ldots,n\}$ (W/m$^2 \cdot$ ºC)
T_{r_i}	–	Temperature (ºC) of the adjacent filament or support at contact i ($r_i \in \{1,\ldots, N+1\}$, $r_i \neq r$.
ρ	–	Density (kg/m^3)
C	–	Heat Capacity (J/kg · ºC)
$(A_r)_{conv}$	–	Area of filament exposed to environment (m^2)
$(A_r)_i$	–	Area of filament for contact i with the rth filament (m^2)

P	–	Filament Perimeter (m)
λ_i	–	Fraction of P that is in contact with another or with the support
a_{r_i}	–	Indicator of activated contact i for the rth filament
m	–	Filament Mass (kg)
$t_r(x)$	–	Instant at which the cross section x of the rth filament starts cooling down or enters in contact with another cross section (s)
T_{r0}	–	Filament temperature at t_r (ºC)
B_i	–	Biot Number
Δt	–	Incremental time (s)
w	–	Filament Diameter (m)
TCV	–	Thermal Condition Variable
Φ	–	"Raster angle" (Bellini and Güçeri 2003)
M	–	Matrix that defines the deposition sequence
m	–	Number of layers of a given sequence
μ	–	Convergence Temperature Error (ºC)
v	–	Deposition Velocity (m/sec)
$T_{up\text{-}dating}$	–	Instants at which the thermal conditions are up-dated (s)
$temp$	–	Matrix with all the temperatures for all the filaments
$save\_lim$	–	Vector composed by the values of TCV_1
T_begin	–	Vector composed by the values of TCV_2
$abcissa$	–	Vector composed by the computation incremental times
$Biot$	–	Vector composed by the Biot number values for each filament
t_{last}	–	Last instant before the deposition of the actual filament (s)
$canto\_0$	–	Vector composed by the start local of deposition for each layer (only for perpendicular sequences)
h	–	Filament cross-section Height (m)
$G(t)$	–	Time-dependent Shear Modulus (Pa)
G_0	–	Initial Shear Modulus (Pa)
g_i	–	i^{th} Prony constant
τ_i	–	i^{th} Prony retardation time constant (s)
n_p	–	Number of Prony terms
E	–	Young modulus (MPa)

R	–	Universal Gas Constant (R = 287 J/kg·K)
Ra_d	–	Rayleigh Number
Pr	–	Prandtl Number
v_k	–	Kinematic Viscosity (m^2/s)
α	–	Thermal Diffusivity (m^2/s)
Gr_d	–	Grashof Number
g	–	Gravity Acceleration (g = 9.8 m/s^2)
β	–	Volumetric Thermal Expansion Coefficient
T_s	–	Cylinder Temperature (ºC)
B_p	–	Break Point (cm)

1 INTRODUCTION

1.1 FREE FORM EXTRUSION

In 1986, Charles Hull developed a technology for creating physical objects from computer data: stereolithography (Jacobs 1992, Kochan 1993). This process makes solid parts, layer by layer, through the solidification of a liquid photopolymer, using a laser beam that is projected in the shape of the part cross-section (Cooper 2001, Bártolo 2011). Based on this technology, Hull founded the 3D Systems of Valencia, which marks the beginning of the rapid prototyping industry. Since then, the concept has been explored by many institutions, especially in the area of three dimensional computer aided design (CAD) (Chua, Leong and Lim 2005). Currently, Rapid Prototyping (RP) denotes a group of techniques in which a three-dimensional model is directly built layer by layer, without any mould, from a CAD data (Menges, Michaeli and Mohren 2001, Grimm 2004). In contrast with traditional manufacturing techniques, these processes offer the possibility of creating very complex parts at reduced cost, manufacturing time and human intervention (Gibson, Rosen and Stucker 2009, Silva and Simões 2010). Moreover, a rapid feedback of prototype quality is done before the fabrication: this maximizes quality, competitiveness and reduces the costs and the production cycle time (Tseng and Tanaka 2001). The range of processable materials has increased significantly (polymers, ceramics, metals), improving the flexibility of the technique (Pérez 2002). Other similar Technologies include Laminated Object Manufacturing (LOM), Selected Laser Sintering (SLS), Ink-jet Printing (3DP) and Fused Deposition Modeling (FDM) (Hopkinson 2006, Jacobs 1996).

FDM was developed in 1988 by Scott Crump (Ogot and Okudan-Kremer 2004), who co-founded Stratasys Inc., in U.S.A, where the first FDM machine, the 3D Modeler®, was commercialized in 1992 (Gebhardt 2003). A plastic or wax filament is fed through a nozzle and deposited onto the support as a series of 2D slices of a 3D part (Venuvinod and Ma 2004). The nozzle moves in the X–Y plane to create one layer. These movements are computer controlled in accordance with the deposition strategy generated by the QuickSlice® or Insight® software (Ahn, et al. 2002). When each layer is completed, the support moves vertically in the Z direction so that the nozzle deposits a new layer on top of the previous one (Figure 1.1). Since the filament is extruded as a melt, the newly deposited material welds with the previously deposited material.

Adequate adhesion requires the control of the thermal environment. Therefore, the complete system is enclosed in a chamber kept at a temperature just below the melting point of the deposited material (Bellini and Güçeri 2004).
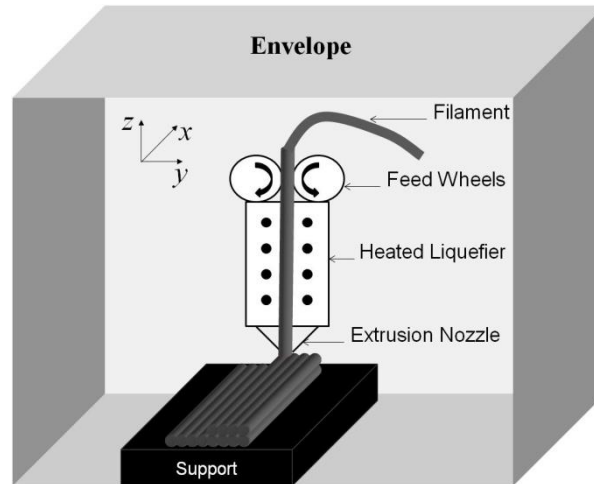
Figure 1.1 – FDM process

The extrusion of two distinct materials may be of interest, so that one of them is used as support and then removed after complete building of the part by washing it in a water-based solution (Chua, Leong and Lim 2005). This can eliminate surface defects and increases the geometric complexity of the parts that can be made by FDM.

In order to obtain a dimensionally accurate part, the extruded material must exhibit low shrinkage upon cooling. Consequently, amorphous polymers are more popular than crystalline ones (Gibson, Rosen and Stucker 2010). Also, their shape is largely maintained after extrusion, as their solidification is quick and easy. ABS (Acrylonitrile Butadiene Styrene) is the most commonly employed material in FDM (Rauwendaal 2001, Timings and Wilkinson 2003), since it provides good impact resistance, toughness, heat stability, chemical resistance and rigidity. Applications include automotive and consumer electronics (Kamrani and Nasr 2006). However, others materials are possible like wax, polyester and elastomers. Green ceramic, bioceramic or metallic parts can be also made (Fellow and Tzou 2004).

Free Form Extrusion (FFE) is a variant of FDM, where the material is melted and deposited by an extruder & die. FFE enables the use of a wider range of materials (e.g., filled compounds, polymer blends, composites, nanocomposites, foams), thus yielding parts with superior performance. Moreover, the adoption of co-extrusion or sequential extrusion techniques confers the possibility to combine different materials for specific

2

properties, such as soft/hard zones or transparent/opaque effects. Finally, pellets or powders can be directly used in FFE, in contrast with FDM where the material must be supplied as a filament, which requires extra cost in manufacturing. FFE has been used by several authors, although with different designations: Wang and co-workers (2004) used the Precision Extruding Deposition (PED) to fabricate poly-ε-caprolactone (PCL) tissue scaffolds and Bellini and co-workers (2005) developed the "Mini Extruder Deposition" (MED) to create ceramic parts.

a) The Process

b) MED screw
(Bellini, Shor and Güçeri 2005)
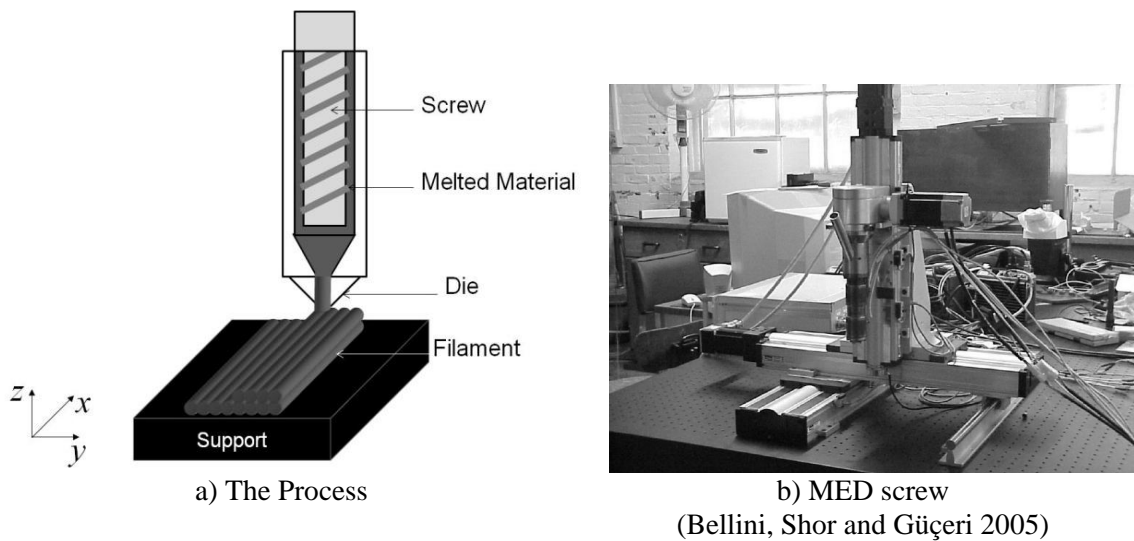
Figure 1.2 – The MED set-up.

1.2 MOTIVATION

Despite the multiples vantages, FDM/FFE needs to be improved in order to satisfy the demanding manufacturing requirements (Venkata 2010). These improvements can be made by minimization of part cost and build time (process objectives), and by maximization of dimensional accuracy, surface quality and mechanical performance (quality part objectives).

Most of the research has been directed towards determining how mechanical properties and dimensional accuracy can be maximized: experimental work, optimization routines, and process modelling have been developed. However, the available know-how is still sufficient to generalize the correlations between process conditions and performance.

Consequently, the present thesis study focuses the two most important/complex phenomena that control the final quality of the prototype:

i) the filament deformation, which causes insufficient dimensional accuracy and, ii) the bonding quality between adjacent filaments that influences the mechanical resistance. Deformation and bonding are mainly controlled by the heat transfer, i.e., adequate bonding requires that the filaments remain sufficiently hot during enough time to ensure adhesion and, simultaneously, to cool down fast enough to avoid excessive deformation due to gravity and weight of the filaments above them (Figure 1.3). So, three inter-dependent phenomena will be considered during the FFE process: heat transfer, adhesion/bonding and creep deformation (Figure 1.4). The process variables can be divided into three categories: operational, material and geometrical/machine (Table 1.1). The objective is to develop a general model for filaments deposition, where the three phenomena are considered, in order to evaluate the effect of the process parameters or define the ideal conditions to optimize the final product quality.
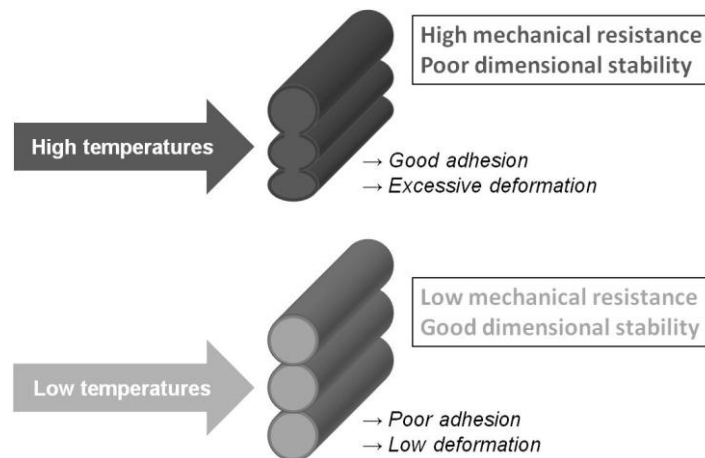
Figure 1.3 – Problems occurring in FFE and their relation with temperature.
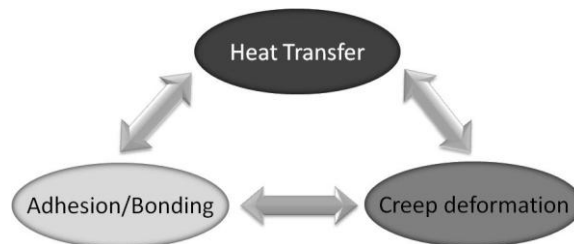
Figure 1.4 – Main process phenomena in FFE.

Table 1.1 – Main process variables in FFE

Operation parameters	Material parameters	Geometrical/machine parameters
- Deposition velocity; - Extrusion temperature; - Environment temperature; - Deposition strategy.	- Thermal conductivity; - Specific heat; - Density; - Melt viscosity; - Stiffness.	- Filament geometry; - Part geometry; - Support structure.

4

1.3 OBJECTIVES AND THESIS OUTLINE

The central objective of this work is to model the heat transfer during the FFE process. Then, the two others components (deformation and bonding) must be introduced and inter-related with computed temperatures. The second aim is to increase the potential of the model, by considering different deposition sequences and parts made by two different materials, which allows evaluating a wider range of part geometries and deposition strategies. This will give us the possibility of reaching the last goal, that is, to make a parametric study of the process.

This thesis comprises eight chapters including this introduction. A literature review about the theme is presented in Chapter 2. The analysis and modelling of heat transfer in FFE are described in Chapter 3. This study gave rise to a computational code in MatLab® which computes the temperature evolution of all the filaments for three possible deposition sequences, with the possibility of including two distinct materials for one of these. Chapter 4 explains how the scope of the model was expanded, by addition of a bond/adhesion criterion and by including the possibility of evaluating bi-material part. A mechanical deformation study with ABAQUS® was also made to evaluate the degree of dimensional stability. In Chapter 5, the results of the experimental validation of the code are shown, and finally, Chapter 6 presents a parametric study of the process, obtained from the MatLab® code, in order to conclude about the most important variables of process. Fundamental inter-relations between process conditions and specific objectives were then deduced. The last chapter includes the most important conclusions and recommendations for future work.

2 MODELLING OF FFE

The improvement of the quality of FDM/FFE parts has attracted significant research. Analytical models, experimental results and optimization routines have been proposed with the aim of reducing costs, improving the mechanical properties, the dimensional accuracy and the surface finish quality of the final part. In this study, three phenomena are analyzed: heat transfer, adhesion and mechanical deformation.

2.1 HEAT TRANSFER

2.1.1 Analysis of the problem

In FFE, when the first filament is extruded and deposited onto the support, its temperature is considerably higher than the ambient temperature. Then, heat exchanges with ambient by convection and radiation, and with support by conduction occur. In addition, heat by conduction along the filament and gradient temperatures throughout its cross section must be also considered and, since the filament is progressively deposited, each cross section has a different temperature history (Figure 2.1).
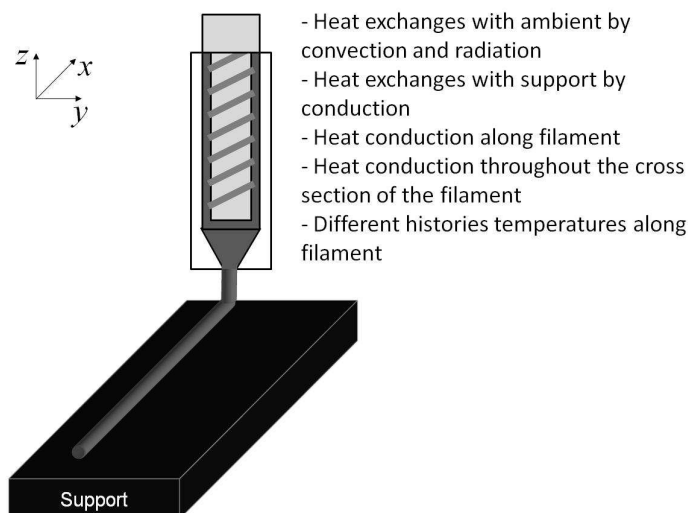
Figure 2.1 – Heat Transfer Analysis during the deposition of the first filament.

When the others filaments of the first layer are deposited, physical contacts are present between the adjacent filaments. Then, in addition to the heat transfer conditions described before, heat exchanges between adjacent filaments by conduction and by radiation must be considered (Figure 2.2).

- Heat exchanges with ambient by convection and radiation
- Heat exchanges with support by conduction
- Heat conduction along filament
- Heat conduction throughout the cross section of the filament
- Different histories temperatures along filament
- Heat exchanges between adjacent filaments by conduction and by radiation
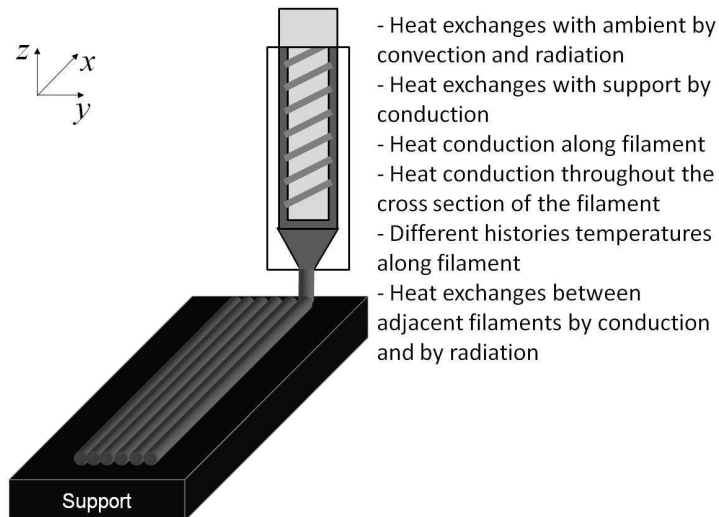
Figure 2.2 – Heat Transfer Analysis during the deposition of the filaments of the 1st layer.

When others layers are deposited on top of the first one, another heat transfer condition enters into account; the small voids presented between filaments are heated by these (Figure 2.3), so, their temperatures are higher than the ambient temperature. Beyond the large number of thermal conditions, these appear and vary along the FFE process, due to the progressive deposition of filaments. Consequently, the modelling of heat transfer in FFE is a complex procedure, where many non-constant phenomena enter into account at determined instants of the process (Figure 2.4).

Voids between filaments
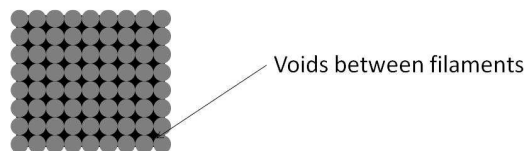
Figure 2.3 – Presence of small voids in FFE process.

- Heat exchanges with ambient by convection and radiation
- Heat exchanges with support by conduction
- Heat conduction along filament
- Heat conduction throughout the cross section of the filament
- Different histories temperatures along filament
- Heat exchanges between adjacent filaments by conduction and by radiation
- Higher temperatures of the voids

During the FFE process, all these thermal conditions start and vary at different times.

Figure 2.4 – Heat Transfer Analysis during the deposition of the filaments of others layers.

8

In addition to the complexity of the heat transfer phenomena, many forms of creating a layer in FDM/FFE exist, which will influence the thermal boundary conditions. As illustrated in Figure 2.5, each layer can be filled in three different ways (Agarwala, et al. 1996):

- "*Raster fill*": the filament material is deposited back and forth inside the defined perimeter to fill the entire area;

- "*Contour fill*": the head makes closed loop contour movements inside the defined perimeter until the area is completely filled;

- "*Raster and contour fill*": the two deposition forms are combined, where the perimeter region is made by a contour fill, and the internal area is completed by a raster fill.

Contour fill   Raster fill   Contour and raster fill
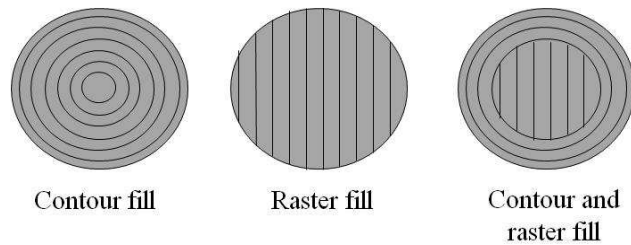
Figure 2.5 – Top view of a layer with many fulfills forms.

The most common used approach is the raster fill, due to its speed and the aptitude to vary the direction of the movements in adjacent layers. In fact, for this deposition strategy, the filaments can have different orientations, which are defined by the "raster angle" Φ (Bellini and Güçeri 2003): this angle is relative to the loading direction of the part and it can vary from layer to layer (Figure 2.6).

$\Phi = [0^\circ]$

$\Phi = [90^\circ]$

$\Phi = [0^\circ / 90^\circ]$
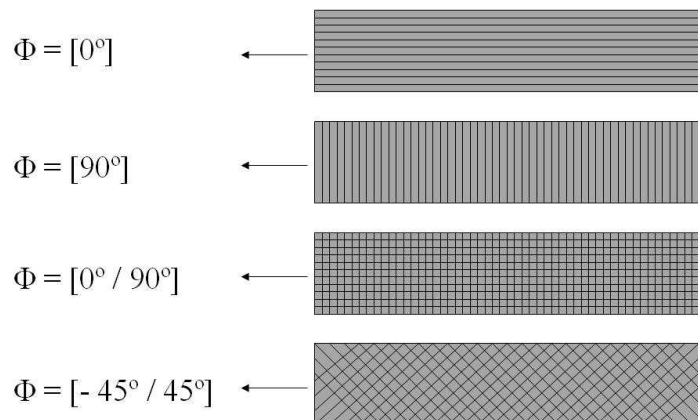
$\Phi = [-45^\circ / 45^\circ]$

Figure 2.6 – Top view of a layer with different raster angles.

Filaments can be perpendicular (orientations $\Phi = [0° / 90°]$ and $\Phi = [- 45° / 45°]$), or unidirectional (raster angles $\Phi = 0°$ and $\Phi = 90°$). For the unidirectional case, there exist two possible configurations, as depicted in Figure 2.7: aligned or skewed filaments (Rodriguez, Thomas and Renaud 2000).

Aligned configuration   Skewed configuration
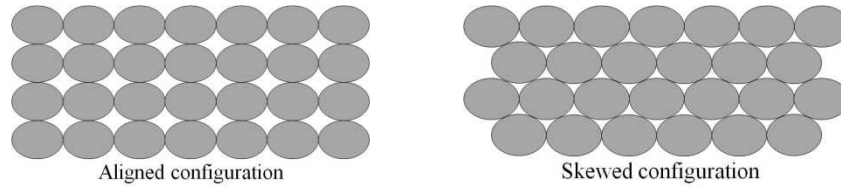
Figure 2.7 – Two different configurations for unidirectional filaments (cross section view).

Since the deposition sequence type strongly affects the quality of the final product, with respect to the mechanical properties (Bellini and Güçeri 2003), the surface finish quality and the total build time (Thrimurthulu, Pandey and Reddy 2004), this must be considered in the conditions of the heat transfer during the manufacturing of a part by FFE.

2.1.2 Existing heat transfer models:

In 1999, Rodriguez studied the cooling of five elliptical filaments deposited on top of each other, using finite element methods (FEM) and later found a 2D analytical solution by using the separation of variables method for rectangular cross-sections (Rodríguez 2000). Figure 2.8 illustrates the specific situation that was considered to develop this last model, with the defined boundary conditions.
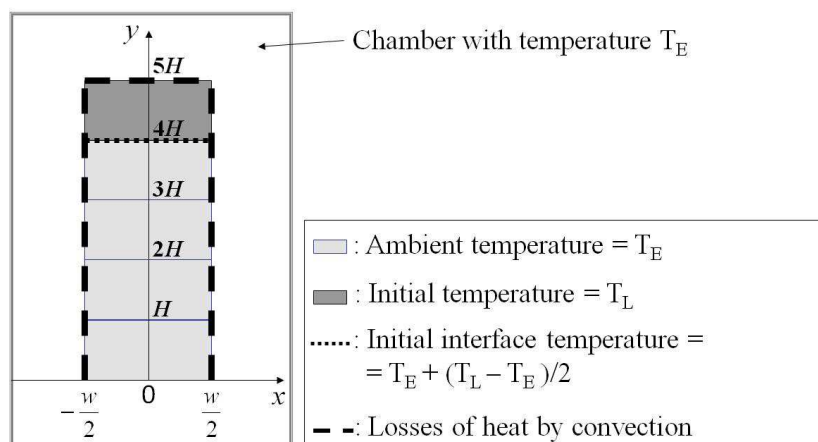
Figure 2.8 – Schematic of the conditions used in Rodriguez's analytical model.

On the other hand, Yardimci (Yardimci and Güçeri 1996) developed a heuristic numerical model for Fused Deposition of Ceramics (FDC) to simulate the cooling/bonding process for any part, but without experimental validation. Li and co-workers (Li 2002) developed an analytical 1D transient heat transfer analysis in good agreement with experimental results, but only valid for a single filament (Figure 2.9). In this analysis, the deposition process was divided into two phases (Figure 2.10): during the deposition of the filament and after this. In the 1st phase ($t = 0$), a semi infinite model was used to obtain all the temperatures along the filament, at the instant of the end of deposition. In the 2nd phase ($t > 0$), a Lumped Capacity analysis is used to obtain all the temperatures along the filament, at any instant from the end of deposition. This gave rise to a simple exponential function that devolves simply and quickly the temperature for any point x of the filament.
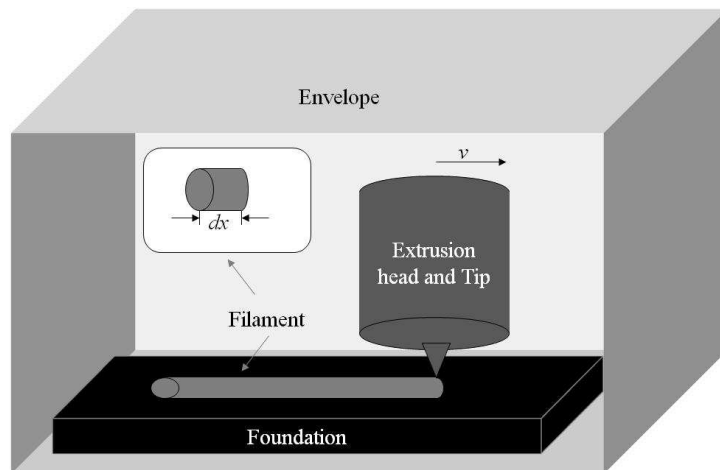
Figure 2.9 - Schematic of the conditions used in Li's analytical model.
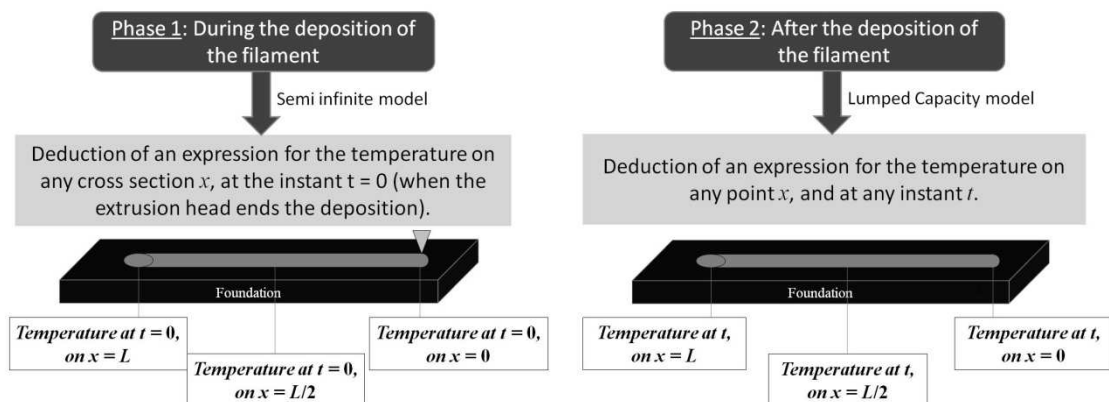
Figure 2.10 – Schematic of the phases in Li's analytical model ($t = 0$ and $t > 0$), where L is the filament length (m).

All the proposed models can be compared by observation of Table 2.1, where a detailed description for each is presented. Most of them are only valid for a specific situation, so inapplicable to all the possible deposition sequences and part geometries, and some heat transfer phenomena such as radiation heat were neglected, without verification of their importance degree. Finally, in all the models, the contacts between filaments were assumed to be perfect, but in reality, a thermal resistance exists and must be considered (Yardimci 1999).

Table 2.1 – Characteristics of existing heat transfer models for FDM/FDC.

	YARDIMCI'S MODEL (Yardinci and Güçeri 1996)	**1ST RODRIGUEZ'S MODEL** (J. F. Rodriguez 1999)	**2ND RODRIGUEZ'S MODEL** (Rodriguez, Thomas and Renaud 2000)	**LI'S MODEL** (Li 2002)
Model type	2D numerical model	2D numerical model	2D analytical model	1D analytical model
Applicable for …	Any part (Generic model)	Five vertically filaments		One elliptical filament
Heat Transfer Conditions		Heat losses only by convection		
Cross Section Geometry	Elliptical cross section	Elliptical cross section	Rectangular cross section	Elliptical cross section
Contact between adjacent filaments	Perfect (zero thermal resistance)			Not applicable (one filament).
Predictions	Cooling and Bonding		Cooling	
Experimental validation		Not done.		Done.
Neglected aspects	- Different temperatures of previous filaments; - Thermal contacts by conduction; - Contact with eventual support structures; - Radiation heat.	- Different temperatures of previous filaments; - Thermal contacts by conduction; - Contact with eventual support structures; - Radiation heat; - Temperatures along the filaments.		- Heat conduction along filament; - Gradient temperatures throughout the cross section; - Contact with eventual support structures; - Radiation heat.
Main Conclusion(s)	Heat transfer coefficient has a great effect on bonding.	Environment temperature has a greater influence on cooling comparing with extrusion temperature.	Temperature gradients throughout the cross section filament are small (< 3 %).	- Environment temperature and heat transfer coefficient have a greater influence on cooling; - Filament temperature reaches rapidly the environment temperature (< 5 sec).

Due to the lack of flexibility and/or rigor, few conclusions were made about the influence of process variables and none of these models was explored to optimize the technique. In particular, the importance degree of build strategy, part geometry, deposition velocity, heat exchanges between adjacent filaments by conduction could not be evaluated. Consequently, FDM-FFE needs a new heat transfer model, with the following characteristics:

- The model must be simple, fast and generic, applicable to different part geometries and deposition sequence types;
- Others heat transfer quantities must be analyzed: these can have an important weight on temperature evolution;
- A thermal resistance between adjacent filaments must be considered;
- Cooling and bonding must be predicted, with an inter-relation-ship between them;
- The model must be validated by experimental results.

2.2 ADHESION

2.2.1 Different approaches in studying the mechanical properties of FFE parts

The final mechanical properties of the parts made by FFE have been studied through three different approaches:

i) by experimental results on a specific part, as made by Hoekstra and co-workers (2001), who studied the effect of six distinct build strategies (A-0º, A-45º, B-0º, B-45º, C-0º and C-45º) on six mechanical properties (tensile strength, flexural strength, flexural modulus, impact strength, hardness and shear strength) for a specific ABS part (Figure 2.11). The authors concluded that the build strategies B-0º and B-45º exhibit the best overall properties (Hoekstra, Kraft and Newcomer 2001). However, these experimental results cannot give general inter-relationship between process variables and specific objectives;

ii) by theoretical prediction of stiffness and strength of the part, as proposed by Wu et al. (Wu, et al. 1997), who predicted the stress-strain response on unaxial compression tests of SLA samples by using an elastic-viscoplastic material model, or Gray et al. (Gray, Baird and Bohn 1998), who used the classic composite mechanics to predict the final mechanical properties of short thermotropic liquid crystalline polymer fiber

14

reinforced polypropylene FD parts. Rodriguez et al. (Rodriguez, Thomas and Renaud 2003) also modelled the strength and stiffness of unidirectional FD-ABS components, but with dependence on three mesostructures (Figure 2.12). This model showed to be in good agreement with experimental results, but two assumptions were made by the researchers: the ABS filaments are linear-elastic and isotropic and, the bonding between adjacent filaments is assumed to be perfect. In fact, with this approach, only the void density and the bond length are considered, but in reality, the quality of bond plays a fundamental role in the mechanical properties of the part, then, this must be considered and analyzed, with its relation with temperature evolution.

iii) by prediction of the adhesion degree between adjacent filaments, rarely used in the existing studies; Yardimci (1996) and Sun (2004) were the few researchers who studied the mechanical properties through the computation of the bonding degree.
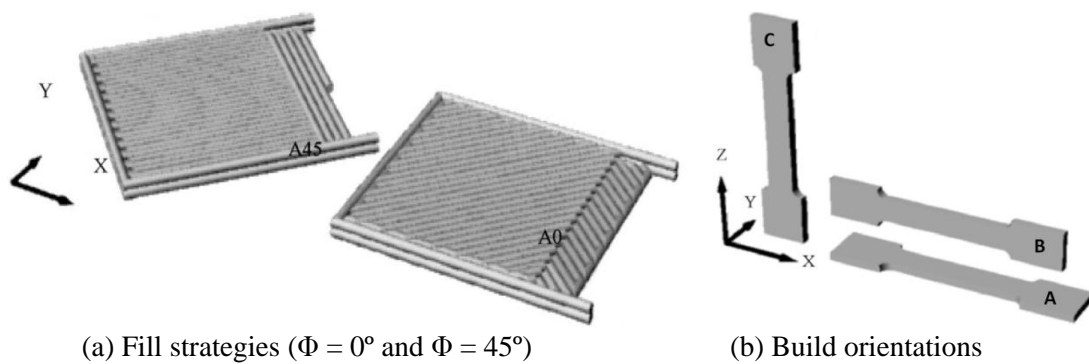
| (a) Fill strategies ($\Phi = 0°$ and $\Phi = 45°$) | (b) Build orientations |

Figure 2.11 – Tested build strategies for a specific ABS part (Hoekstra, Kraft and Newcomer 2001)
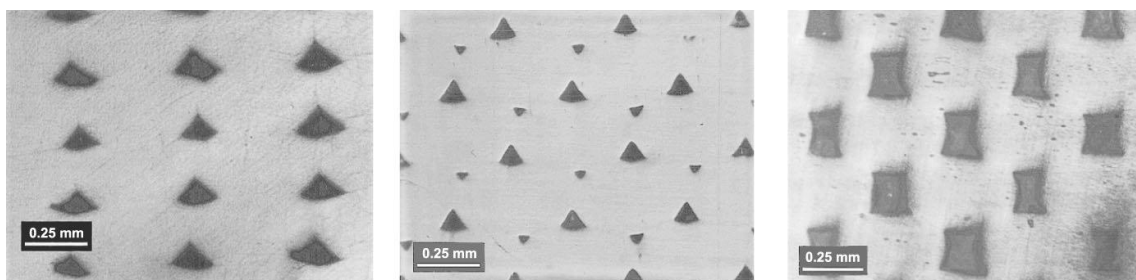
Figure 2.12 – Considered mesostructures in Rodriguez's model to predict the strength and the stiffness of FD-ABS components (Rodriguez, Thomas and Renaud 2003).

2.2.2 Yardimci's model

Yardimci (1996) proposed a cooling/bonding model for fused deposition process, whose cooling component has been described in section 2.1. In this model, a bonding potential Φ (K·s) was proposed to quantify the adhesion degree (Yardimci and Güçeri 1996):

$$\phi = \int_0^t \left(T_{\text{interface}} - T_c \right) d\tau \quad (2.1)$$

Where T_c (°C) is the critical temperature above which bonding process is activated and below which bonding does not occur, and $T_{\text{interface}}$ (°C) is the temperature at the interface.

However, the variable T_c is difficultly quantified, and $T_{\text{interface}}$ depends on the temperatures computed by a cooling model, where many simplifications were made (e.g. thermal interactions between filaments were ignored). Moreover, since the filaments remain above their glass transition temperature for a relative long period of time (Sun 2004), the used route for solution is more related with the molecular diffusion occurring at the interface. So, an adequate diffusion model could predict the development of the bond and how the bond strength can be maximized.

2.2.3 Polymer Interdiffusion: the Reptation Theory

When two identical amorphous polymers enter in contact above their Glass Transition Temperature (T_g), the interface progressively disappears due to the interdiffusion of polymer chain segments, back and forth across the interface (Lee 1991). During this interdiffusion, the mechanical strength of this boundary increases with time until achievement of a unique material (Sperling 2006). To model the motion of the individual chains, the Reptation Theory proposed by DeGennes and Edwards has been used (DeGennes 1971). Several researchers applied this theory to the problem of polymer-polymer interface under isothermal conditions namely, Prager & Tirrell (1981), Wool et al (1981), Mantel & Springer (1992), and Butler & McCullough (1998). The Reptation model considers a polymer chain of length L_c (m) to be confined in a tube, which represents constraints to lateral movements of monomers imposed by the neighbouring chains (Ewen and Richter 1997, Elias 2008). This tube restricts the motion of the chain that can only move along its curvilinear length. At the beginning of the process ($t = 0$), the chain is totally enclosed in the initial tube, as illustrated in Figure 2.13. Due to the Brownian motion, and after a certain time $t = t_1$, some chain ends with a length $l_c(t)$ (m) that increases with time escape from the initial tube (Wool 1995). Finally, at $t = t_{reptation}$, where $t_{reptation}$ is the Reptation time (s), the chain escapes from the original tube and $l_c(t_r) \rightarrow L_c$.
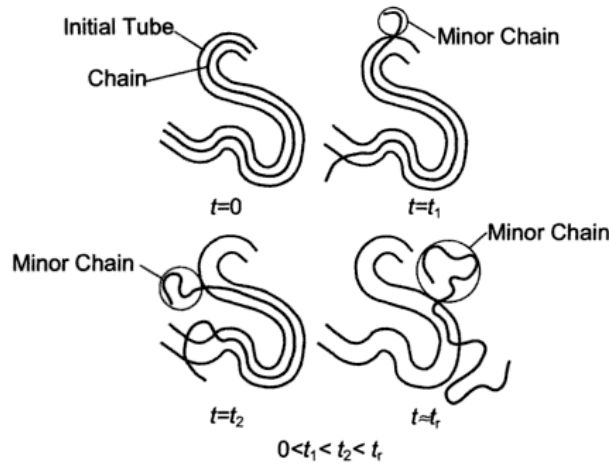
Figure 2.13 – Reptation theory: polymer chain migration from its initial tube, emergence and growth of the minor chains (Wool, McGarel and O.J.Yuan 1989)

This model can be used to describe the polymer molecular motion that occurs during the healing process at the interface between two polymers (Figure 2.14). At the instant $t = 0$, all the minor chains have zero length ($l_c(t) = 0$), as represented by the points in Figure 2.14. Then, the minor chains emerge and grow out, and some of these move across the interface with an interpenetration depth $\chi(t)$ (m), which influences the bond strength evolution and can be related with the minor chain length $l_c(t)$ as (Wool and O'Connor 1981):

$$\frac{\chi}{\chi_\infty} = \left(\frac{l_c}{L_c}\right)^{1/2} \qquad (2.2)$$

Where χ_∞ is the ultimate interpenetration distance (m).

(a) $t = 0$ (b) $t = t_1$ (c) $t = t_r$
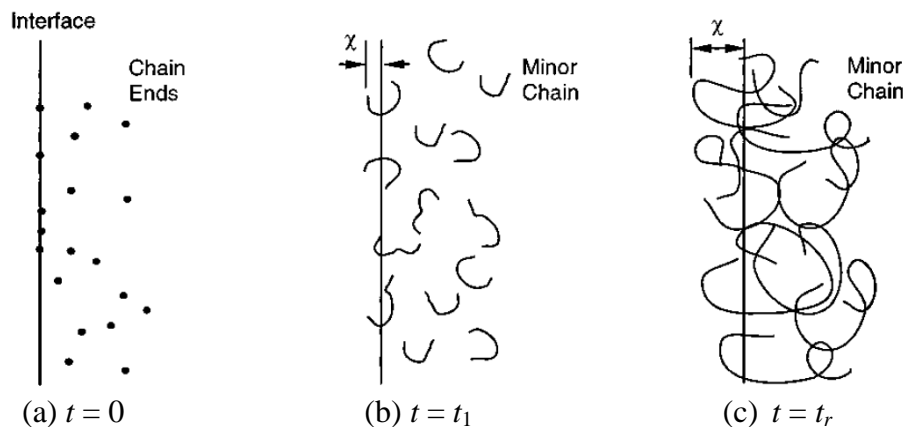
Figure 2.14 – Interdiffusion of minor chains at a polymer-polymer interface (Yang and Pitchumani 2002)

From the Reptation time $t = t_{reptation}$, all the polymer chains are interpenetrated and the interface starts having the same molecular configuration as the original material. The bond strength $\sigma(t)$ (MPa) is proportional to the interpenetration $\chi(t)$, and it reaches the ultimate bond strength σ_∞ (MPa) when $\chi(t) = \chi_\infty$ and $l_c(t) = L_c$. Then, assuming that the factor of proportionality of the strength with the square root of minor chain length is the same for $\sigma(t)$ and σ_∞, the degree of healing $D_h(t)$ can be defined as (Prager and Tirrell 1981, DeGennes 1971):

$$D_h(t) = \frac{\sigma}{\sigma_\infty} = \frac{\chi}{\chi_\infty} = \left(\frac{l_c}{L_c} \right)^{1/2} \quad (2.3)$$

Equation (2.3) can be used for both isothermal and non isothermal conditions.

2.2.4 Yang and Pitchumani's model

Bastien and Gillespie (1991) used the Reptation Theory to propose a non isothermal healing model, where the temporal domain is subdivided into q time intervals, and the process is assumed to be isothermal in each of these intervals. The healing degree along time was then expressed as a sum of the incremental bond strength values (Bastien and Gillespsie 1991):

$$D_h(t) = \frac{\sigma}{\sigma_\infty} = \sum_{i=0}^{t/\Delta t} \left[\frac{t_{i+1}^{1/4} - t_i^{1/4}}{t_{reptation}^{*}{}^{1/4}} \right] \quad (2.4)$$

Where $t_{reptation}{}^{*}$ is the Reptation time (s) obtained at the average temperature.

Sonmez and Hahn (1997) proposed later another similar non isothermal healing model. Through simple integrations, an expression for the healing degree under non isothermal conditions was obtained (Sonmez and Hahn 1997):

$$D_h(t) = \frac{\sigma}{\sigma_\infty} = \sqrt{\frac{l_c}{L_c}} = \left[\int_0^t \frac{d\tau}{2\sqrt{\tau\, t_{reptation}(\tau)}} \right]^{1/2} \quad (2.5)$$

Yang and Pitchumani (2002) presented two important limitations for the two models:

- The two models are only valid if the process is isothermal in each increment with an average temperature: this does not correspond to the real temperature history, so they are not appropriate for non isothermal conditions;

- These models are based on the Reptation Theory, which is only valid for low molecular weights (kg/kmol) (between M_c and $8M_c$, where M_c is the critical entanglement molecular weight (kg/kmol)). But, for many thermoplastics, the molecular weight range is higher than $8M_c$ so, for these materials, the equation (2.3) cannot be used.

Then, Yang and Pitchumani (2002) developed a model for the healing process under non isothermal conditions that can be used for any thermoplastic. As in the previous studies, the Reptation motion of a polymer chain enclosed in a surrounding tube was first considered. A probability density function $P(s,t)$ is defined as the probability of finding a particular chain segment at a position s and time t, where s is the curvilinear coordinate along the tube. This function is governed by a diffusion equation (Prager and Tirrell 1981):

$$\frac{\partial P}{\partial t} = D \frac{\partial^2 P}{\partial s^2} \qquad (2.6)$$

Where D is the Reptation diffusion coefficient related to the movements of the polymer chain in the encompassing tube (m^2/s) and only influenced by the temperature and time by hypothesis.

The initial condition corresponding to the equation (2.6) was written as:

$$P(s,0) = \delta(0) \qquad (2.7)$$

Where δ is the Dirac delta function (m^{-1}).

The diffusion domain was assumed to be infinitely large ($|s| \rightarrow \infty$), and since the chains cannot move across an infinite distance, the following natural boundary conditions were defined:

$$P(s,t) = 0; \frac{\partial P(s,t)}{\partial t} = 0 \quad \text{as} \quad |s| \rightarrow \infty \quad (2.8)$$

Using the separation of variables techniques and a Fourrier transformation, the non isothermal healing degree was obtained (Yang and Pitchumani 2002):

$$D_h(t) = \frac{\sigma}{\sigma_\infty} = \left[\int_0^t \frac{1}{t_w(T)} dt \right]^{1/4} \quad (2.9)$$

Where $t_w(T)$ is the welding time with temperature dependence (s).

Experimental validation of this model was presented by the authors, using measured interfacial strength data on different thermoplastic materials and processing conditions. The model predictions showed to be in good agreement with the experimental results.

2.2.5 Application of the Yang and Pitchumani's model by Sun (2004)

Sun (2004) used the Yang and Pitchumani's model (equation (2.9)) to predict the healing degree between filaments in FDM process. For this, two components are needed:

- *The welding time*: Sun (2004) used the welding time proposed by Rodriguez (1999), who made fracture tests on FDM ABS P400 parts and used an Arrhenius equation to predict the welding time with temperature dependence (J. F. Rodriguez 1999):

$$t_w = 1.080 \times 10^{-47} \exp\left(\frac{Q_d}{RT} \right) \quad (2.10)$$

Where $Q_d = 388.7$ kJ/mol and R is the universal gas constant.

- *The temperature evolution with time*: Temperature profiles were experimentally measured for two sets of parts, with the following dimensions: 31 mm × 19.1 mm × 3.1 mm and 100 mm × 19.1 mm × 3.1 mm.

Then, equation (2.9) was numerically implemented using a MatLab® code, combined with the welding time defined by equation (2.10) and the measured temperature profiles. Two assumptions were made in this procedure: i) the numerical integration was carried out until the bonding degree reached the value 1, or until the total fabrication time was achieved, and ii) the healing phenomenon was considered active only if the material temperature is above its glass transition point (for amorphous material).

20

In this study, the bonding degree is computed by using an expression where the material properties and the Reptation theory play an important role, but depends too on experimentally measured temperatures for two particular parts. Consequently, the authors only made one conclusion: the healing degree is lower for the longer part, which is not sufficient to understand how the quality of FFE parts can be generally improved.

2.3 MECHANICAL DEFORMATION

In FFE process, filaments are deposited in a semi-molten state: top and bottom of the filaments would slightly deform, phenomenon that is improved by the weight of top filaments deposited later (Figure 2.15). This deformation compromises the dimensional accuracy of the final part, then, some research has been made on this topic, with the aim of identifying the process variables that have a significant effect on deformation of filaments.
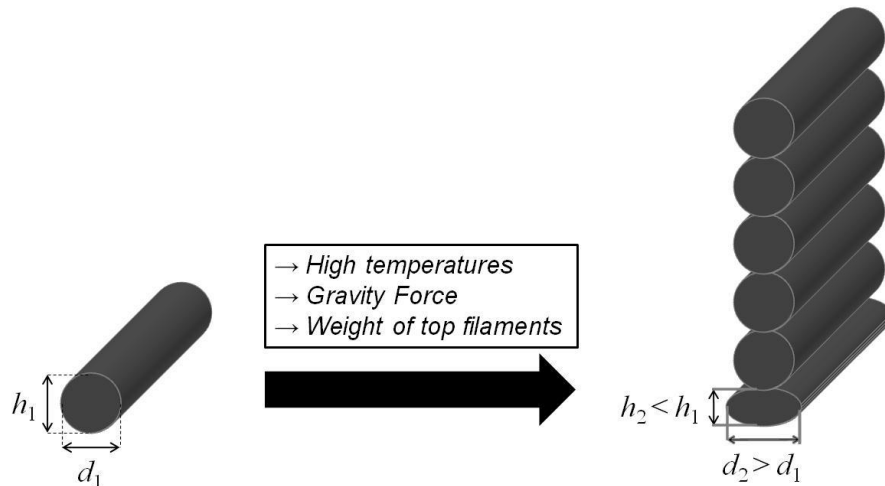
Figure 2.15 – Deformation of a filament due to high temperatures, gravity force and weight of top filaments.

Ziemian and Crawn (2001) developed a multi-objective decision support system to aid the FDM user in setting the process variables that maximize the final part quality. For this, the authors realized some experiences to quantify the weight of each build goal, and deduced the effects of some FDM process variables on these objectives. Four FDM process variables were considered – build orientation, layer thickness, filament width and interior fill strategy, and the following purposes were assumed: build time, dimensional accuracy and surface quality.

The dimensional accuracy was quantified as the average absolute deviation (AD), in inches, between measured points from the actual part surface, and the associated nominal part surfaces as representing within the CAD model (Ziemian and Crawn 2001). The experimental results demonstrated that build orientation, layer thickness and filament width don't affect the dimensional accuracy, in opposition to the layer fill strategy that has a relative weight. The authors deduced that the accuracy may be more related to variables that were not included in this study, and pointed to the placement of the part within the support table, the cooling behavior and the air flow within the work envelope. However, no verification of these relations was made. Similarly, Gregorian et al. (2001) chosen a specific ABS part to be made by a Stratasys 1650 FDM machine and found the most optimal shrinkage compensation factor (SCF), a parameter that determines the amount a part should be enlarged/stretched so that it can be closed to the required dimensions. The authors concluded that SFC = 0.7% and suggested that future investigation must consider the great influence of temperature and build speed on the dimensional stability of FDM parts (Gregorian, et al. 2001). On the contrary, Pennington et al. (2005) experimentally tested the weight of the factors recommended by the previous research. For this, an ABS part with six features commonly used in products was manufactured using a Stratasys 2000 FDM. Twelve dimensions of the six part features including height, length and thickness, were measured with a coordinate measurement machine and digital callipers. This analysis allows concluding that part size, location of part in the work envelope, and envelope temperature, have a significant effect on the dimensional accuracy (Pennington, Hoekstra and Newcomer 2005).

On the other hand, Li (2002) presented a theoretical analysis of void geometry, where the deformation of the filament due to the high temperatures is considered. An analytical expression for the void fraction is proposed, which depends on the "flattening height" δ (mm). This parameter δ was experimentally measured: unidirectional cubic specimens of dimension $10 \times 8 \times 20$ mm were made, cut in the middle plane, cleaned and polished. Photos of cross-section were then taken under a microscope and analyzed by using an image processing software. Values for δ were then measured and used to calculate the void fraction between filaments. Once more, this deformation was measured experimentally for a specific part.

As a conclusion, all the research on this topic has been always based on experimental results, where a specific part is constructed, dimensional stability is measured, and some conclusions are made from this.

3 ANALYSIS AND MODELLING OF HEAT TRANSFER IN FFE

3.1 CONTRIBUTION OF THE INDIVIDUAL THERMAL PHENOMENA

As described in chapter 2, heat transfer in FFE comprises many non-constant phenomena difficult to describe by simple mathematical equations. Therefore, the use of numerical methods to solve more realistic and complex mathematical equations, namely the finite element methods, is a feasible approach to compute the temperature histories of the filaments during the FFE process.

ABAQUS® is a software application for Finite Element Analysis, developed in 1978 by Hibbitt, Karlsson & Sorensen, Inc (Hibbitt 1997). This software is used to predict how solid bodies will behave under load, stress, temperature, contact, and other conditions, and enables to make many types of analysis (linear, nonlinear, static or dynamic) for mechanical, civil, biomedical and related engineering applications (Helwany 2007, Liu and Quek 2003). The available materials include metals, soils, plastics, foam, composites and rubber. Some of the specific capabilities of ABAQUS® are stress analysis (both static and dynamic responses), dynamic studies (linear and nonlinear problems), element removal and replacement, heat transfer problems and coupled heat transfer and stress analysis (Tan, et al. 2011). Figure 3.1 resume the general operation of the software.
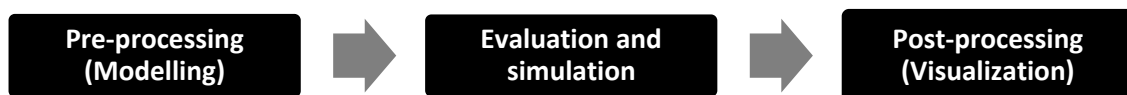
Figure 3.1 – The three stages of a complete Finite Element analysis with ABAQUS® software.

In order to define the problem to obtain the required computational results, the user must introduce model data and history data. In the model data, the object geometry, the material, the loads and others conditions are characterized, by selecting and defining the distinct options available in the software. The sequence of events is defined in the history data, which is subdivided into "steps", where conditions are activated/inactivated at determined instants of the simulation time.

Consider the above mentioned, ABAQUS® software is a valid option for the modeling of heat transfer in FFE: the total deposition time can be subdivided into many steps, where the thermal conditions are activated/inactivated depending on the location of the

extrusion head and, complex thermal conditions such as radiation can be easily defined by a simple selection/definition of a software option. However, after a thorough study of the potential of ABAQUS® for the modeling of FFE heat transfer, three important limitations were found:

- The total computational time is very large;
- A generic/automatic model (results computation for any part) cannot be created: for each geometry, a new software document must be made from the beginning;
- Since all the filaments are progressively deposited, they need to be subdivided into small elements with a maximum length of 1-2.5 mm (for a typical extrusion velocity of 0.025 m/sec) in order to ensure the rigor of results. However, this involves a considerable computational time and a hard task for the generation of the ABAQUS® document. As an example, 1000 filaments with a length of 5 cm, subdivided into 20 small cylinders (with a length of 2.5 mm), correspond to a parallelepiped of dimension 3 cm $\times$ 3 cm $\times$ 5 cm. In this case, 20 000 steps, 60 000 convection conditions, 60 0000 radiation conditions, etc. need to be manually generated, one by one.

Despite these limitations, ABAQUS® was used with the main objective of evaluate the relative the importance of each thermal phenomenon involved in FFE, allowing conclude if some of these can be neglected in order to simplify the FFE heat transfer problem.

The considered thermal conditions were deduced by analysis of two situations, as illustrated in Figure 3.2. If one filament is deposited, heat exchanges with ambient by convection and radiation, and with support by conduction are present. In the other hand, if many filaments are deposited, others thermal phenomena also occur, that is, heat exchanges between adjacent filaments by conduction and radiation, and with the small voids by convection.

-Heat Exchanges with ambient by convection and by radiation at the free boundaries;
- Heat exchanges with support by conduction for the filaments of the 1st layer;

Heat Exchanges with ambient by convection and by radiation

Heat Exchanges between adjacent filaments by conduction and by radiation

Support

Heat Exchanges with the support by conduction

Support

Heat Exchanges with the ambient delimited by the filaments by convection

Figure 3.2 – Thermal phenomena occurring during the FFE process.

3.1.1 Heat Exchanges with ambient by convection

Since the extruded filaments are deposited into an environment with a lower temperature, they exchange heat with ambient by convection. This thermal condition was included in all the existing heat transfer models and considered as the unique phenomenon that governs the temperature history. This heat amount is controlled by the heat transfer coefficient h_{conv}. Rodriguez (1999) used the Churchill correlation for natural convection of a long cylinder to conclude that $h_{conv} = 67$ W/$m^2 \cdot$ ºC, by considering an elliptical filament with semiaxis lengths of 0.508 mm and 0.254 mm respectively, an extrusion temperature of 270ºC and an environment temperature of 70ºC (Rodriguez, Thomas and Renaud 2000).

In order to evaluate the importance of this heat amount, a 3D thermal simulation was made with ABAQUS® software. The temperature evolution of a unique filament was computed during 15 s, with a unique thermal condition: heat exchanges by convection with the environment at the free boundaries (Figure 3.3). The cross-section of the filament is assumed to be circular with an area equal to that of the filaments used in FDM techniques, which corresponds to a circle with diameter of 0.359 mm. The values for extrusion and environment temperature were defined respectively as $T_L = 270$ºC and $T_E = 70$ºC, which are typical values for a Stratasys 1600 FDM machine (Rodriguez, Thomas and Renaud 2000). The material properties values (density, thermal conductivity and specific heat) are relative to a P400 ABS plastic, usually used in FDM technology (Rodriguez, Thomas and Renaud 1999).

Since the exact value of the heat transfer coefficient is unknown, three values were tested: $h_{conv} = 5$ W/$m^2 \cdot$ °C, $h_{conv} = 60$ W/$m^2 \cdot$ °C and $h_{conv} = 150$ W/$m^2 \cdot$ °C. The FFE variables and material properties are listed in Table 3.1.
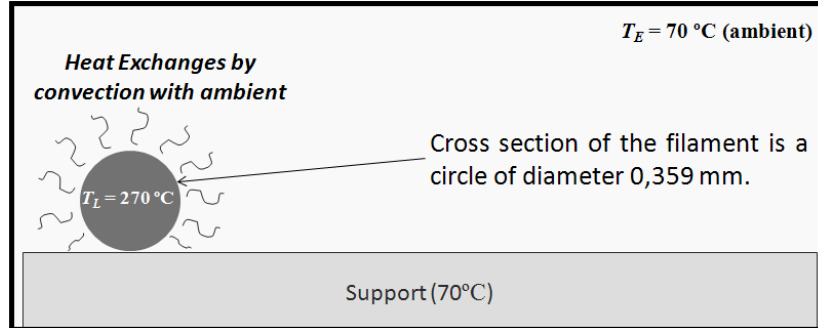
Figure 3.3 – Heat exchanges with ambient by convection for one filament (2D visualization).

Table 3.1 – FFE variables and material properties for the convection study.

Property	Value
Extrusion temperature (°C)	270
Environment temperature (°C)	70
Filament length (m)	0.02
Cross section diameter (m)	0.0003
Heat transfer coefficient (W/$m^2 \cdot$ °C)	5-60-150
Thermal conductivity (W/m $\cdot$ °C)	0.18
Specific heat (J/kg $\cdot$ °C)	2020
Density	1.05

The values of ABAQUS® parameters, which will be also used for all the future simulations, are shown in Table 3.2.

Table 3.2 – ABAQUS® parameters for all the simulations.

Property	Value
Elements Number	524
Mesh Type	Hex-dominated
Element Type	DC3D8: 8-node linear heat transfer brick
Step Type	Heat Transfer
Increment Size	Initial = 10^{-6} s
	Minimum = 10^{-12} s / Maximum = 0.1 s
Solution Technique	Full Newton
Default Load Variation with Time	Instantaneous
Output Request	NT, Nodal Temperature

The temperatures along time can be devolved on any node of the filament. So, three cuts along filament were chosen, and, for each cut, three nodes were selected (Figure 3.4).
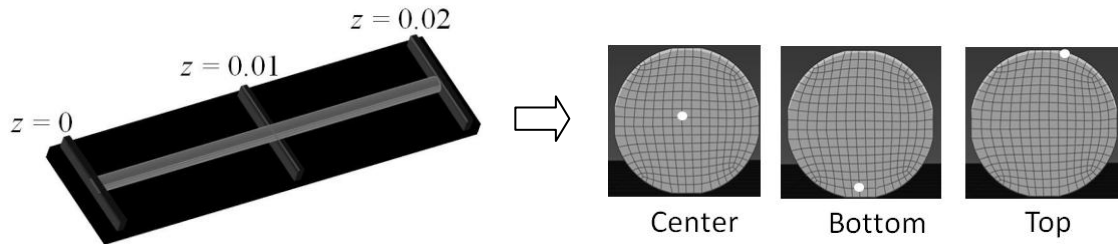
Figure 3.4 – Selected cuts (m) and nodes for extracting temperatures.

The 9 temperature curves for each heat transfer coefficient value are shown in Figure 3.5, Figure 3.6 and Figure 3.7, respectively. From these results, two important conclusions could be made:

- The heat exchanges with ambient by convection, which is mainly controlled by the heat transfer coefficient, is a very important thermal condition;

- The temperatures along filament length (*z*-axis) and throughout the cross section are uniform, as shown by Li (2002). Consequently, for the next studies, only temperatures on the central node of the filament middle will be shown, except in cases where this uniformity ceases to be valid.
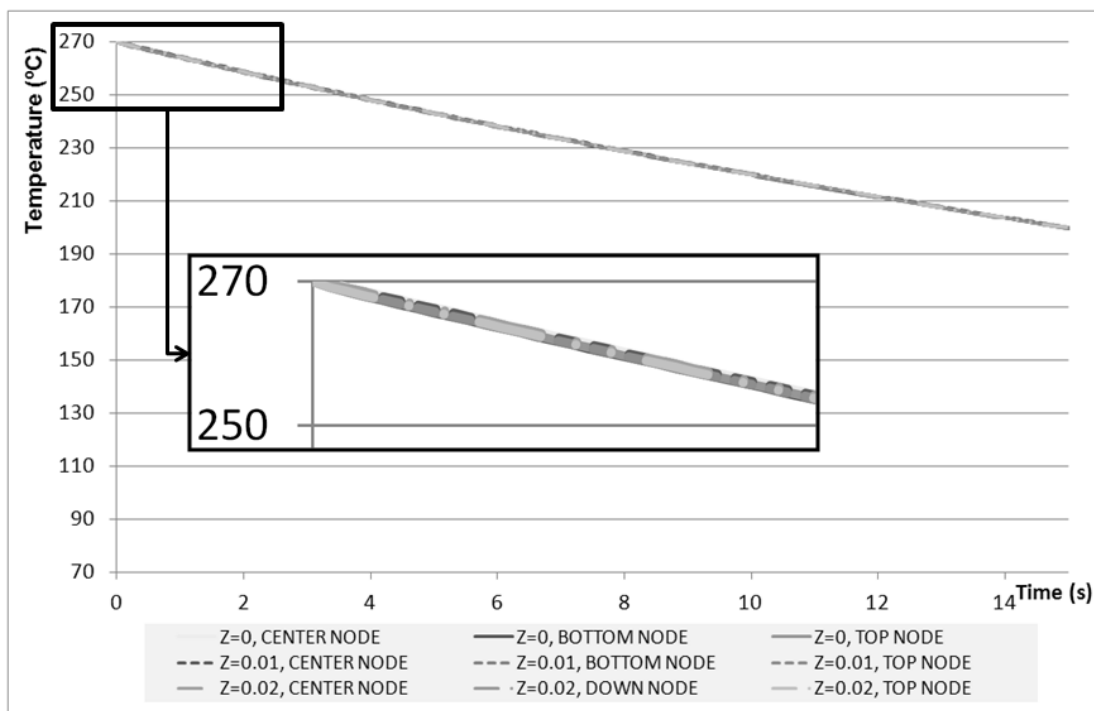
Figure 3.5 – Temperature evolution of a unique filament for h_{conv} = 5 W/m^2 · ºC.

27
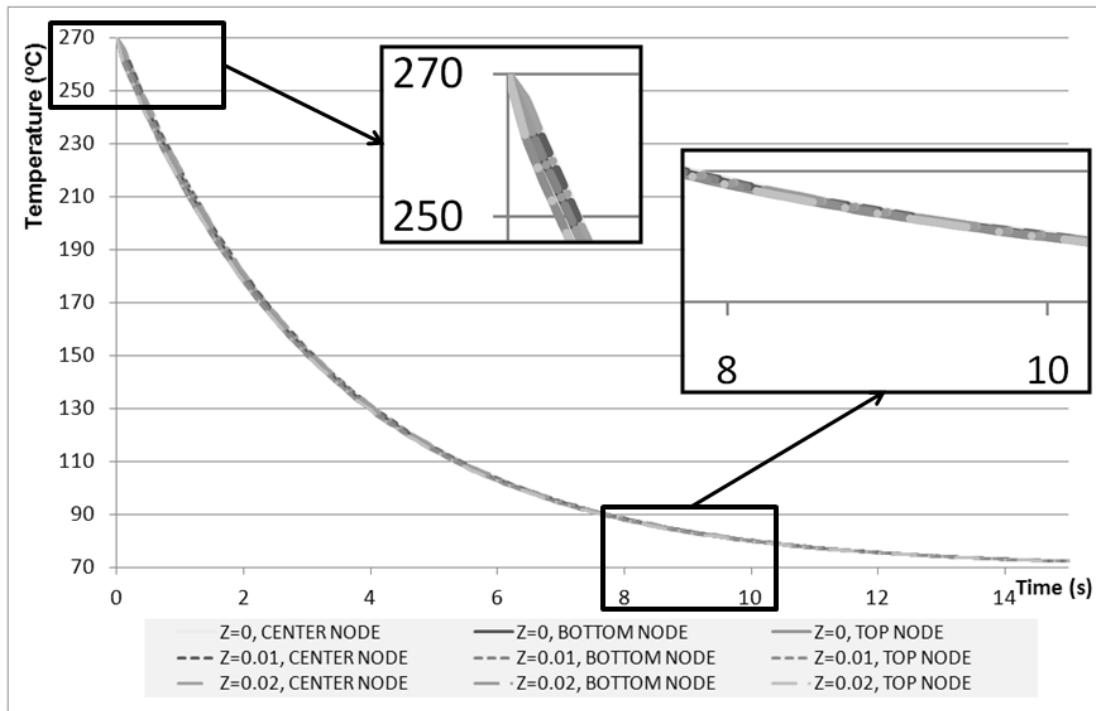
Figure 3.6 – Temperature evolution of a unique filament for $h_{conv} = 60$ W/m^2 · °C.
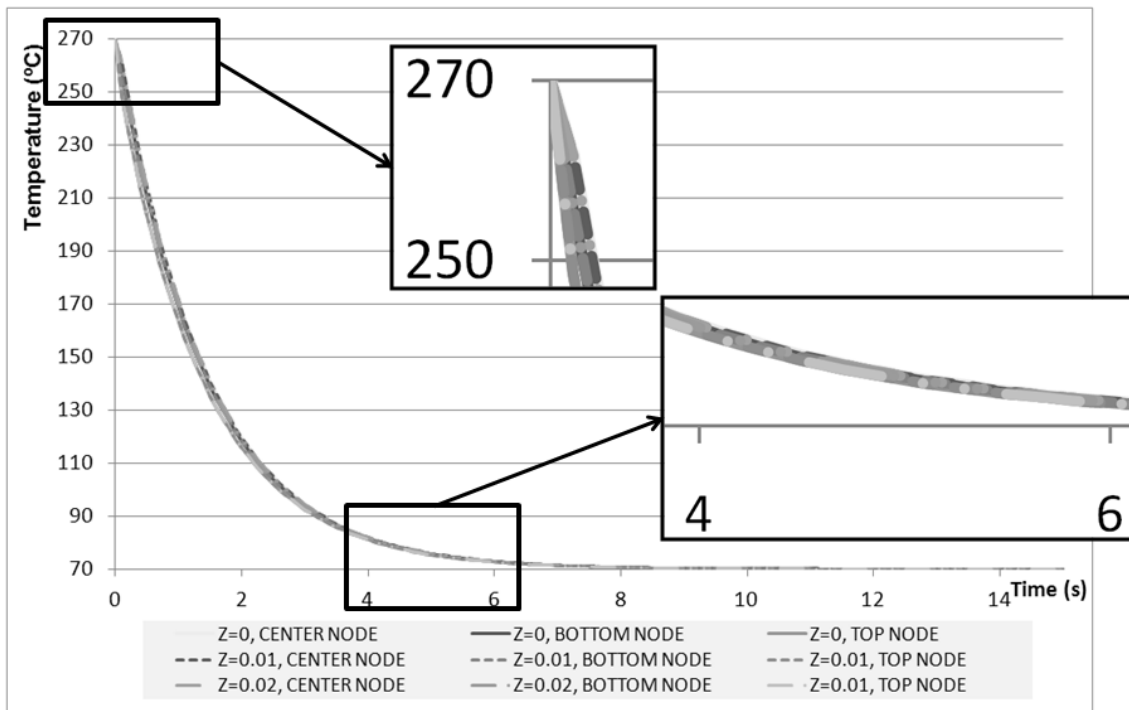
Figure 3.7 – Temperature evolution of a unique filament for $h_{conv} = 150$ W/m^2 · °C.

3.1.2 Heat Exchanges with ambient by radiation

As referred before, heat exchanges with ambient by radiation also occur at the free boundaries of the filament. This phenomenon is referred by Yardimci (1999), nevertheless neglected, without verification of its importance in the temperature history of the filament. To evaluate the importance degree of this amount of heat, was used the last simulation (variables and values) adding the radiation condition with $\varepsilon = 0.96$, which corresponds to the emissivity coefficient of an ABS (Liu, Wu and Wang 2010). Temperatures results are shown in Figure 3.8, Figure 3.9 and Figure 3.10 for the three respective values of heat transfer coefficient $h_{conv} = 5$ W/$m^2 \cdot$ °C, $h_{conv} = 60$ W/$m^2 \cdot$ °C and $h_{conv} = 150$ W/$m^2 \cdot$ °C. In each Figure, three situations are represented: i) convection, ii) radiation, iii) convection and radiation.
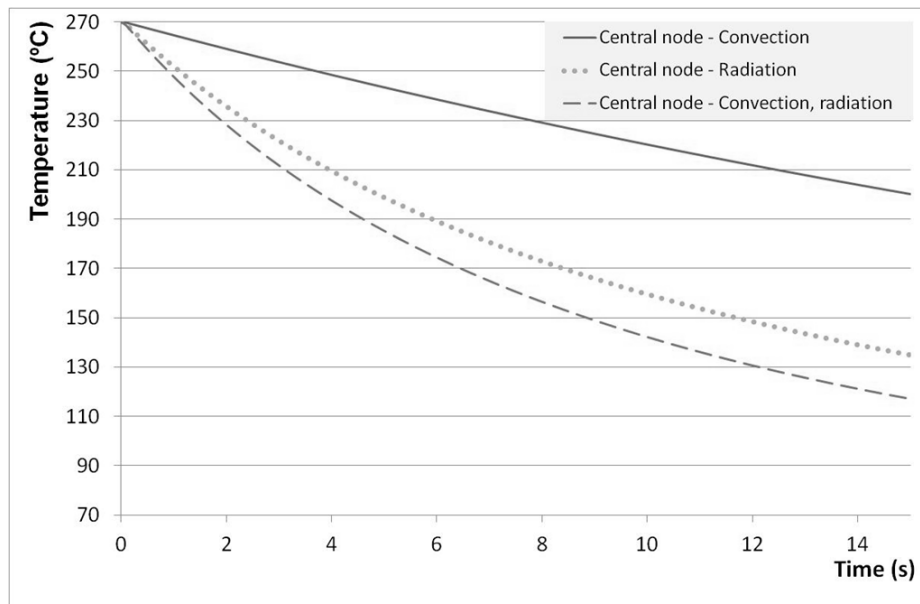
Figure 3.8 – Temperature evolution of a unique filament for the three situations ($z = 0.01$, central node, $h_{conv} = 5$ W/$m^2 \cdot$ °C and $\varepsilon = 0.96$).
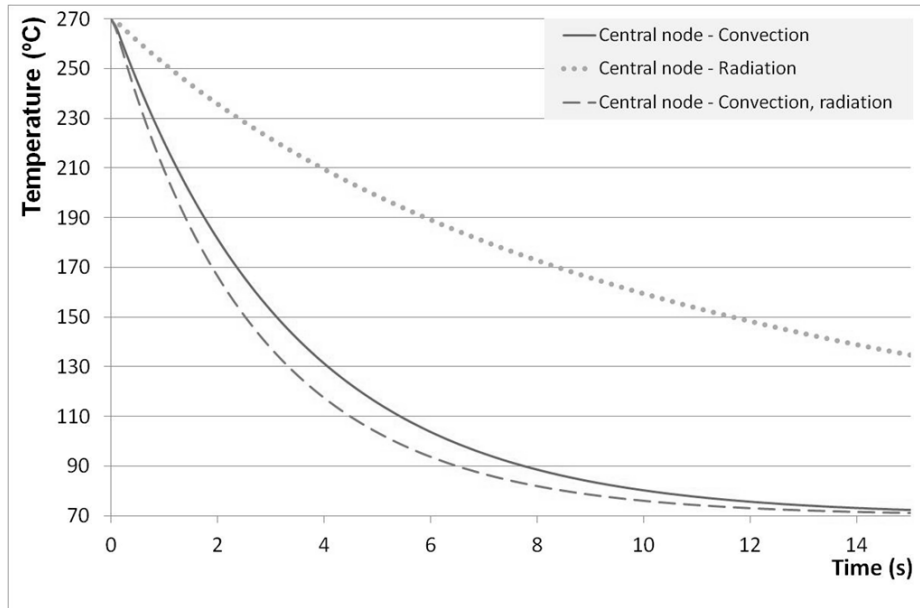
Figure 3.9 – Temperature evolution of a unique filament for the three situations ($z = 0.01$, central node, $h_{conv} = 60$ W/m$^2 \cdot$ °C and $\varepsilon = 0.96$).
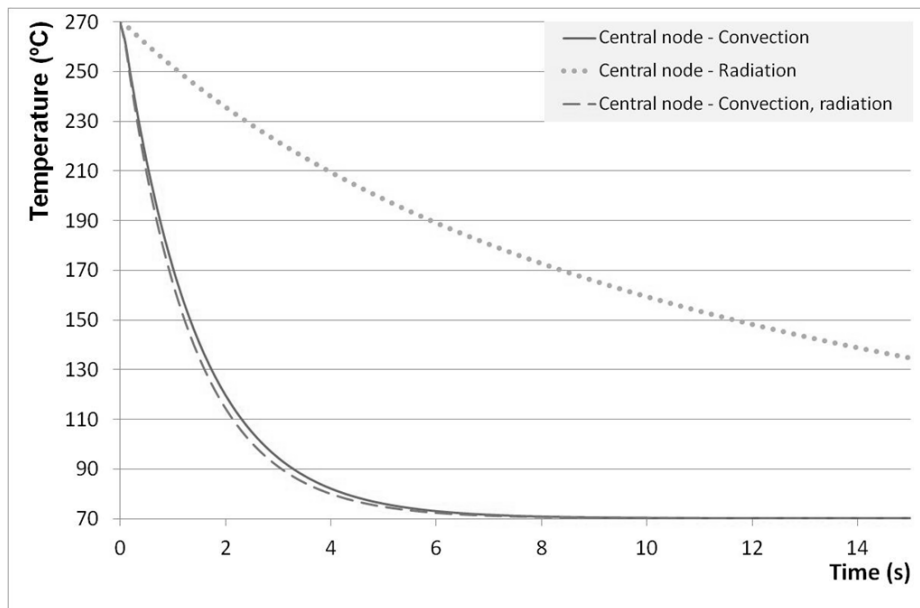
Figure 3.10 – Temperature evolution of a unique filament for the three situations ($z = 0.01$, central node, $h_{conv} = 150$ W/m$^2 \cdot$ °C and $\varepsilon = 0.96$).

The influence of the heat exchanges with ambient by radiation depends on the heat transfer coefficient value: for $h_{conv} = 5$ W/m$^2 \cdot$ °C, the differences between the three different cases are considerable. This is due to the low weight of convection, so the temperature evolution is mainly controlled by radiation heat. Otherwise, for $h_{conv} = 150$ W/m$^2 \cdot$ °C, the differences between "with convection" and "with convection and radiation" are insignificant. Then, the increase of h_{conv} reduces the importance degree of this phenomenon. Since the most of authors who studied heat transfer in FDM

30

concluded that the heat transfer coefficient is around 60 W/m^2 · ºC, we can conclude that the heat exchanges by radiation with ambient have a relative impact on temperature evolution (maximum differences of 10ºC) and the convection condition has a very much higher weight on heat transfer.

3.1.3   Heat exchanges with support by conduction

When two materials at different temperatures are placed in contact, heat transfer by conduction occurs between them. However, this transfer is not perfect, due to a thermal contact resistance r_c (Figure 3.11): a temperature difference $\Delta T_{interface}$ occurs at the interface (Kothandaraman and Subramanyan 2006).
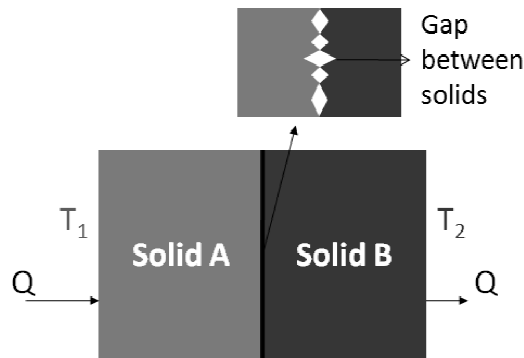
Figure 3.11 – Thermal contact resistance between two solids.

The contact resistance r_c (m^2 · ºC/W) depends on the surface roughness, the hardness of the materials, the applied pressure, the gap material and the temperature (Kaviany 2002). It is defined by:

$$r_c = \frac{\Delta T_{\text{interface}}}{Heat\,Transferred\,through\,the\,interface} \qquad (3.1)$$

Thermal contact conductance h_c (W/m^2 · ºC) and contact resistance r_c are related by (Madhusudana 1996):

$$h_c = \frac{1}{A_a r_c} \qquad (3.2)$$

Where A_a is the area of the contacting surfaces (m^2).

Due to the difficult determination of h_c, two situations will be considered in this study in order to evaluate the importance of this thermal condition: low conduction between the filament and the support, and great conduction between them. For this, the "gap conductance" is required by the software in order to specify the thermal conduction degree between the two contacting bodies: a large "gap conductance" corresponds to a high thermal conduction and vice versa (Gaal and Gaal 2010). The used values for this variable are shown in Table 3.3 and temperature evolution for the two cases is shown in Figure 3.12, assuming that $h_{conv} = 60$ W/$m^2 \cdot$ °C.

Table 3.3 – Used values for gap conductance.

Property	Value
Gap conductance with support for low conduction (W/m$^2 \cdot$ °C)	10
Gap conductance with support for great conduction (W/m$^2 \cdot$ °C)	500
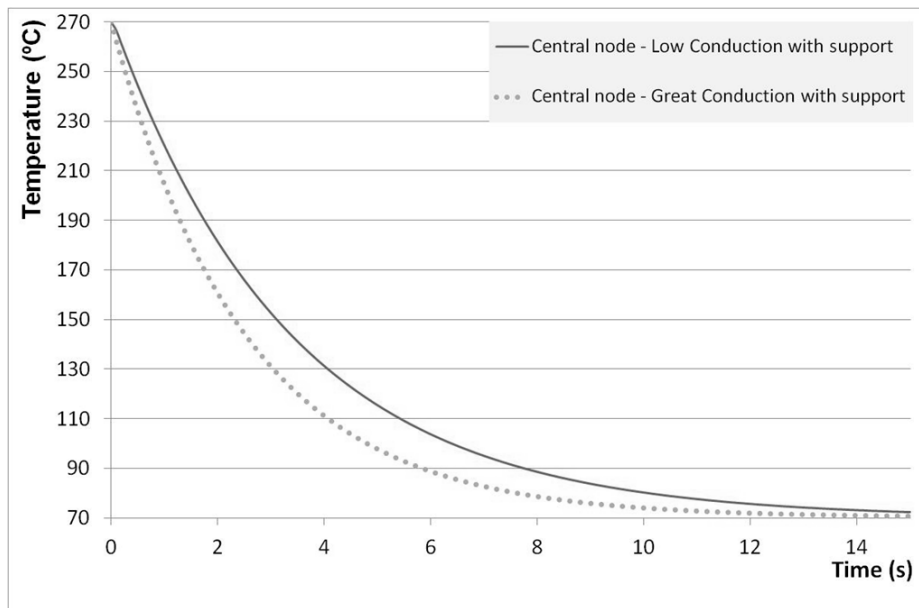
Figure 3.12 – Temperature evolution of a unique filament for the two situations, with a circular filament cross-section ($z = 0.01$, central node, 5% of contact).

The results allowed concluding that the conduction with support has a relative importance in the temperature evolution (until 20ºC). However, these results were obtained assuming a circular cross-section, where the contact with support is minimal (about 5%). Figure 3.13 shows the temperature results for a squared cross-section with 0.359 mm of side, where the contact is higher (25%).
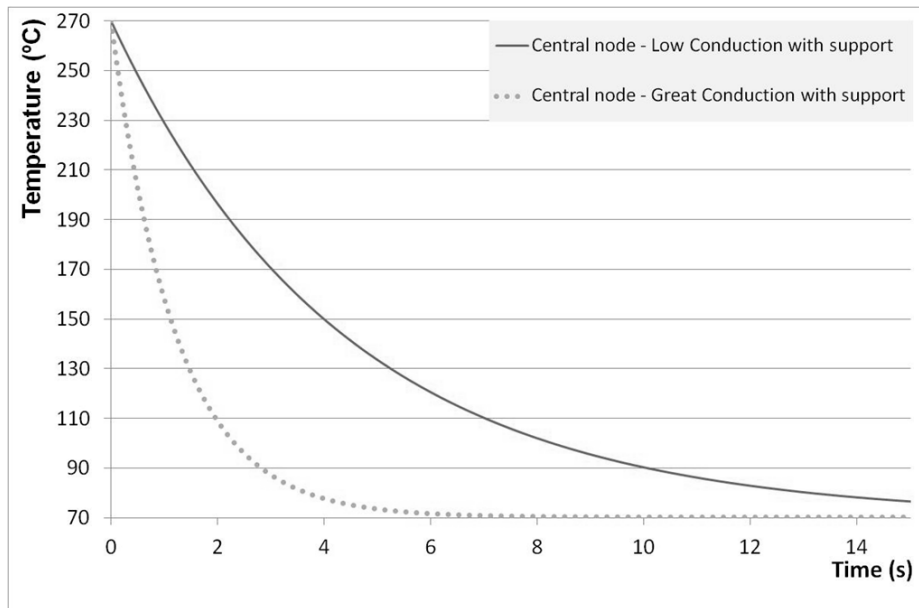
Figure 3.13 – Temperature evolution of a unique filament for the two situations, with a squared filament cross-section ($z = 0.01$, central node, 25% of contact).

With a higher contact, the temperature differences are very much more important (until 80°C). As a conclusion, heat exchanges with support by conduction can have a great importance in the FFE heat transfer, but depend strongly on the thermal contact conductance (support material properties, roughness…) and the contact length.

3.1.4 Heat exchanges between adjacent filaments by radiation

During the manufacture of a part by FFE, the filaments are deposited sequentially starting cooling down at different times having different temperature evolutions. So, unlike assumptions of the others existing models, exchanges of heat energy via thermal radiation need to be considered. In order to study the importance of these heat exchanges, four filaments of 2 *cm* of length were considered, where each is deposited every second (Figure 3.14).

Since the deposition velocity is approximately $0.2 - 0.25$ m/s:

At $t = 0$ s: the 1st filament is deposited, it cools down during [0 s, 15 s];

At $t = 1$ s: the 2nd filament is deposited, it cools down during [1 s, 15 s];

At $t = 2$ s: the 3rd filament is deposited, it cools down during [2 s, 15 s];

At $t = 3$ s: the 4th filament is deposited, it cools down during [3 s, 15 s].
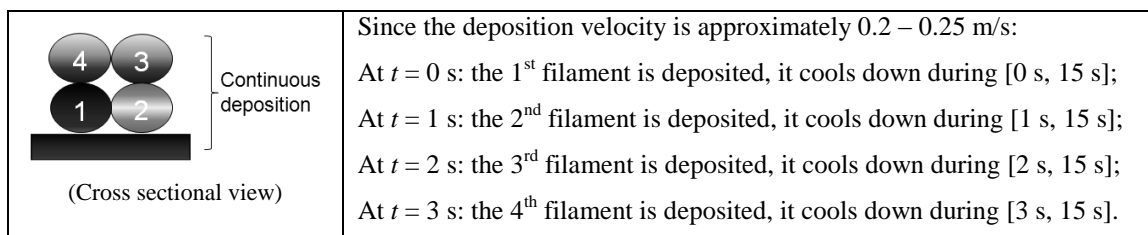
Figure 3.14 – Conditions of the case study (Heat exchanges by radiation).

The heat exchanges by radiation are controlled by a parameter called "radiation view factor", also known as form factor, shape factor or geometric factor. The radiation view factor of surface A with respect to surface B is denoted by $F_{A \to B}$ and it is defined as the ratio of the radiation energy leaving surface A and that is intercepted by surface B (Rathore and Kapuno 2010):

$$\text{View factor} \, F_{A \to B} = \frac{\left(\begin{array}{c} Radiation \; energy \; leaving \; surface \; A \\ and \; that \; reaches \; surface \; B \; directly \end{array} \right)}{Total \; energy \; leaving \; surface \; A} \quad (3.3)$$

The view factor $F_{A \to B}$ represents the fraction of radiation energy leaving surface A that strikes surface B, and view factor $F_{B \to A}$ represents the fraction of radiation energy leaving surface B that strikes surface A. The "reciprocity rule" relates them as:

$$Area(A) \times F_{A \to B} = Area(B) \times F_{B \to A} \quad (3.4)$$

To simplify the calculus of the view factors between the filaments, the surfaces that are in contact with the ambient voids are assumed to be rectangles: as illustrated in Figure 3.15, heat exchanges by radiation occur between the filaments 1 and 2, 1 and 4, 2 and 3, 3 and 4 (perpendicular surfaces), and, between 1 and 3, 2 and 4 (parallel surfaces).
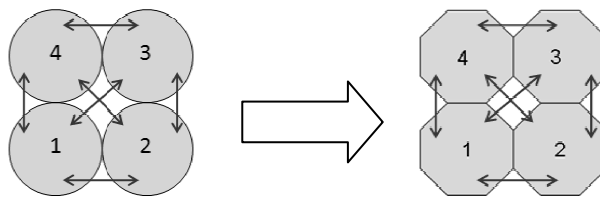
Figure 3.15 – Simplification of the filaments geometry for the heat exchanges by radiation (Cross sectional view).

Since these surfaces are rectangles with same area, and by using relation (3.7), the factor form controlling the exchanges by radiation between two filaments i and j is done by:

$$F_{i-j} = F_{i \to j} = F_{j \to i} \quad (3.5)$$

For parallel and identical planes, the factor form can be calculated using this expression (Siegel and Howell 1992):

$$
F_{1-2} = \frac{2}{\pi XY} \left\{ \begin{array}{l} \ln\left[\dfrac{\left(1+X^2\right)\left(1+Y^2\right)}{1+X^2+Y^2}\right]^{1/2} + X\sqrt{1+Y^2}\,\tan^{-1}\left(\dfrac{X}{\sqrt{1+Y^2}}\right) + \\[3mm] + Y\sqrt{1+X^2}\,\tan^{-1}\left(\dfrac{Y}{\sqrt{1+X^2}}\right) - X\tan^{-1}X - Y\tan^{-1}Y \end{array} \right\} \qquad (3.6)
$$

The variables X and Y are expressed as:

$$
X = \frac{a}{c} \qquad Y = \frac{b}{c} \qquad (3.7)
$$

Where a, b and c are defined in Figure 3.16.
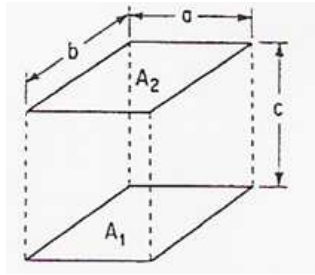
Figure 3.16 – Variables a, b and c, to compute the factor form for identical, parallel, and directly opposed rectangles (Siegel and Howell 1992).

For perpendicular and identical planes, the factor form can be calculated using this expression (Siegel and Howell 1992):

$$
F_{1-2} = \frac{1}{\pi W}\left\{ W\tan^{-1}\frac{1}{W} + H\tan^{-1}\frac{1}{H} - \sqrt{H^2+W^2}\,\tan^{-1}\left(\frac{1}{\sqrt{H^2+W^2}}\right) + \right.
$$
$$
\left. + \frac{1}{4}\ln\left[\frac{\left(1+W^2\right)\left(1+H^2\right)}{1+W^2+H^2}\left(\frac{W^2\left(1+W^2+H^2\right)}{\left(1+W^2\right)\left(W^2+H^2\right)}\right)^{W^2}\left(\frac{H^2\left(1+H^2+W^2\right)}{\left(1+H^2\right)\left(H^2+W^2\right)}\right)^{H^2}\right] \right\} \qquad (3.8)
$$

The variables H and W are expressed as:

$$H = \frac{h}{l} \qquad W = \frac{w}{l} \qquad (3.9)$$

Where h, l and w are defined in Figure 3.17.
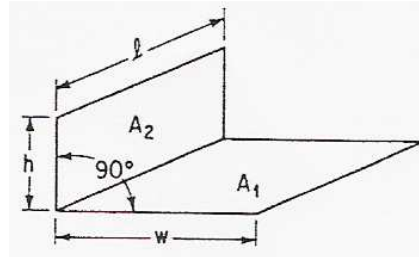
Figure 3.17 – Variables h, l and w, to compute the factor form for two finite rectangles of same length, having one common edge and having an angle of 90º to each other (Siegel and Howell 1992).

The cross-section of the voids between filaments is assumed as a square of width:

$$a = c = h = w = \frac{perimeter\ cross-section\ filament}{4} \qquad (3.10)$$

Then, the following factor forms were obtained:

Parallel planes: $\qquad\qquad F_{1-3} = F_{2-4} \approx 0.4139$

Perpendicular planes: $\quad F_{1-2} = F_{1-4} = F_{2-3} = F_{3-4} \approx 0.2928$ $\qquad (3.11)$

In order to evaluate the importance degree of considering these thermal exchanges, two simulations were made: i) with the inclusion of these heat exchanges and ii) without these. The conditions of the simulations and parameters values are shown in Table 3.4 and temperatures differences between simulation 1 (with exchanges by radiation) and simulation 2 (without exchanges by radiation) were computed (Figure 3.18). Note that temperatures were extracted on the three nodes, but only on a cut ($z = 0$), due to the verified uniformity of temperatures along filament length.

Table 3.4 – FFE variables, material properties and thermal conditions for the heat exchanges by radiation study.

Property	Value	Thermal conditions
Extrusion temperature (ºC)	270	- Heat exchanges with ambient by convection and radiation at the free boundaries of the filaments;
Environment temperature (ºC)	70	
Filament length (m)	0.02	
Cross-section diameter (m)	0.0003	- Heat exchanges with support by conduction for the filaments of the 1st layer;
Heat transfer coefficient (W/m$^2 \cdot$ ºC)	60	
Emissivity Coefficient	0.96	
Gap conductance with support (W/m$^2 \cdot$ ºC)	10	- Simulation1: with heat exchanges by radiation / Simulation2: without heat exchanges by radiation
Thermal conductivity (W/m$\cdot$ ºC)	0.18	
Specific heat (J/kg$\cdot$ ºC)	2020	
Density	1.05	

Figure 3.18 – Temperatures differences versus time between with and without exchanges by radiation, for each filament, at $z = 0$, on 3 nodes (central, bottom and top).

The graphics show the temperature differences between the two simulations. These low differences (approximately 0.22ºC) allowed concluding that the thermal exchanges by radiation between filaments have an insignificant impact on heat transfer.

3.1.5 Heat exchanges between adjacent filaments by conduction

In the FFE process, when a filament is deposited, it enters in contact with the previous that was deposited before (colder) and will enter in contact with the next filaments (hotter).

Then, heat exchanges by conduction between adjacent filaments must be considered and can influence the heat transfer process. These were referred and neglected by Yardimci (1999): however, the author recommended their consideration in future works.

In order to test the importance of this thermal condition, four filaments were newly considered with four physical contacts: between filaments 1 and 2, 2 and 3, 3 and 4, and 1 and 4 (Figure 3.19).
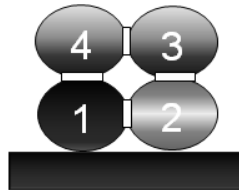
Figure 3.19 – Existing physical contacts for two layers of two filaments (Cross sectional view).

In order to define this heat amount, the value of thermal contact conductance must be calculated. However, since it depends on variables which are hardly quantified (as referred previously for the heat exchanges with support), the determination of an exact value is a difficult task. Furthermore, in FFE process, the value of thermal contact conductance is not constant along time, due to the adhesion that occurs between the adjacent filaments (Figure 3.20).
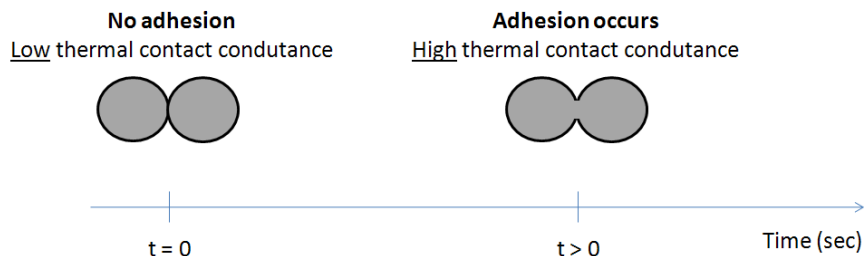
Figure 3.20 – Evolution of the thermal contact conductance with the adhesion, for two adjacent filaments.

Despite the difficult determination of h_c, a low value is expected in a first phase due to the low thermal conductivity of the material (polymer). In contrast, from the instant where the adhesion occurs, a high value is expected. Consequently, three situations will be considered in this study: no conduction, low conduction and perfect conduction.

In order to simulate these situations with ABAQUS® software, the gap conductance must be introduced, as referred previously for the thermal contact between filaments and support: a low value is introduced for low conduction (high thermal resistance) and a high value is introduced for perfect conduction (low thermal resistance).

38

The conditions of the simulations are shown in Table 3.5 and temperature results were extracted at $z = 0$, on the three nodes (Figure 3.22).

Table 3.5 – FFE variables, material properties and thermal conditions for the heat exchanges by conduction study.

Property	Value	Thermal conditions
Extrusion temperature (ºC)	270	- Heat exchanges with ambient by convection and radiation at the free boundaries of the filaments;
Environment temperature (ºC)	70	
Filament length (m)	0.02	
Cross section diameter (m)	0.0003	
Heat transfer coefficient (W/m² · ºC)	60	- Heat exchanges with support by conduction for the filaments of the 1st layer;
Emissivity Coefficient	0.96	
Gap conductance with support (W/m² · ºC)	10	
Thermal conductivity (W/m· ºC)	0.18	- Simulation1: without heat exchanges by conduction / Simulation2: with heat exchanges by conduction (low conduction) / Simulation3: with heat exchanges by conduction (perfect conduction).
Specific heat (J/kg· ºC)	2020	
Density	1.05	

Figure 3.21 – Temperature evolution versus time of the three simulations (no, low and perfect conduction), for each filament, at $z = 0$, on 3 nodes (central, bottom and top), with radiation.

Each graphic contains nine temperatures curves: these curves were obtained selecting three nodes (center, bottom and top) at $z = 0$, with the three different conditions (no conduction, low and high conduction). Some conclusions were made from these results:

- The thermal exchanges by conduction have a large influence on heat transfer, depending on the conduction degree, which is controlled by the adhesion and the material properties.

- The heat exchanges by conduction also influence the temperature gradients throughout the cross section. With perfect conduction, the temperatures throughout the cross section cease to be uniform: temperature differences until 20ºC were obtained (filament 1, difference between the top node and the bottom node). On the other hand, with low or no conduction, the uniformity of the temperatures remains.

Now, the same simulations were made, but without the heat exchanges with ambient by radiation (Table 3.6).

Table 3.6 – FFE variables, material properties and thermal conditions for the heat exchanges by conduction study, without heat exchanges with ambient by radiation.

Property	Value	Thermal conditions
Extrusion temperature (ºC)	270	- Heat exchanges with ambient only by convection at the free boundaries of the filaments;
Environment temperature (ºC)	70	
Filament length (m)	0.02	
Cross section diameter (m)	0.0003	
Heat transfer coefficient (W/m$^2 \cdot$ ºC)	60	- Heat exchanges with support by conduction for the filaments of the 1st layer;
Emissivity Coefficient	0.96	
Gap conductance with support (W/m$^2 \cdot$ ºC)	10	
Thermal conductivity (W/m· ºC)	0.18	- Simulation1: without heat exchanges by conduction / Simulation2: with heat exchanges by conduction (low conduction) / Simulation3: with heat exchanges by conduction (perfect conduction).
Specific heat (J/kg· ºC)	2020	
Density	1.05	

The results are shown in Figure 3.22, in order to evaluate the importance degree of heat exchanges by radiation with ambient, comparing with the others thermal conditions (convection with ambient and conduction between adjacent filaments).
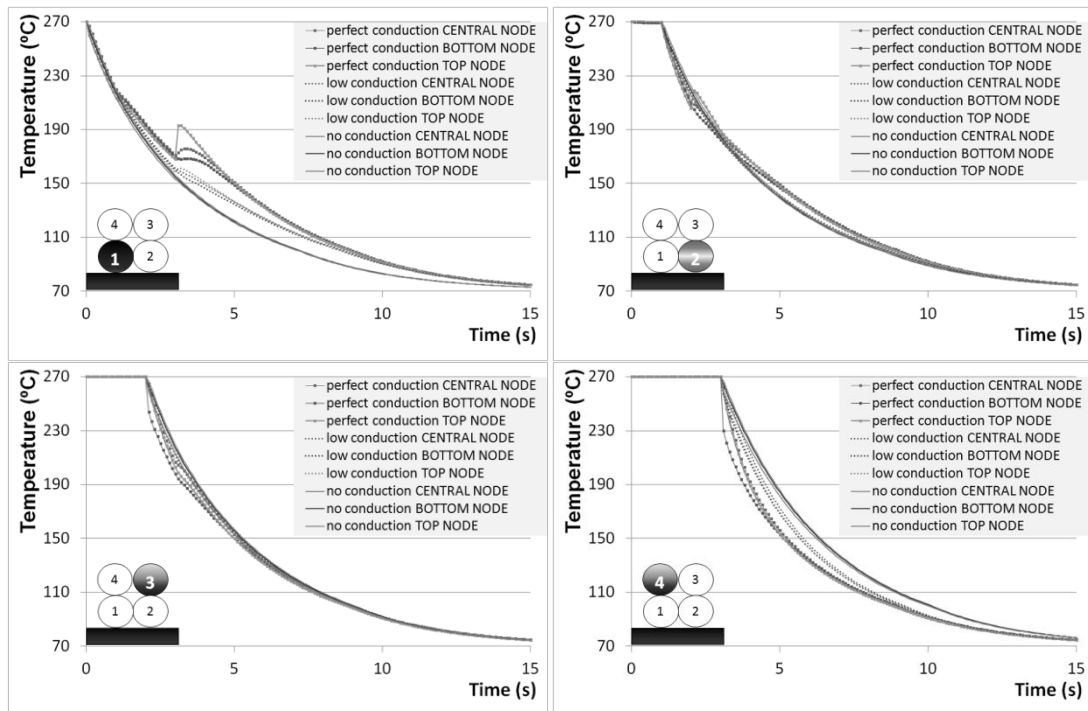
Figure 3.22 – Temperature evolution versus time of the three simulations (no, low and perfect conduction), for each filament, at $z = 0$, on 3 nodes (central, bottom and top), without radiation.

Comparing the results of Figure 3.21 and Figure 3.22, low temperature differences can be observed (until 10ºC), and the behavior still the same in the two cases. Consequently, heat exchanges by convection with ambient and by conduction between adjacent filaments and support have the most significant impact, comparing with the heat exchanges with ambient by radiation.

3.1.6   Heat exchanges with voids by convection

Due to the characteristics of the FFE process (sequential deposition of filaments), very small voids can be present between filaments. Then, a high temperature for these voids is expected, comparing with the ambient temperature:
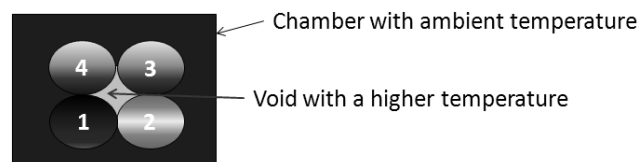
Figure 3.23 – Existing voids between filaments (Cross sectional view).

Although this condition was not mentioned in previous research, its occurrence is unquestionable so its importance must be studied. For this study, four filaments were newly considered, and a simulation in ABAQUS® was first made in order to determine the temperature evolution of the void delimited by these. The void geometry was simplified, by considering quadratic filaments, and the material properties of the void are defined as the air properties at 70ºC (Figure 3.24).
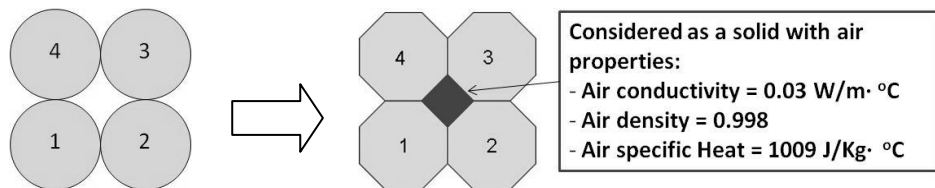
Figure 3.24 – Assumptions and simplification of the filaments geometry (Cross sectional view).

Since the void is only totally formed from the instant where the last filament is deposited, the void temperature along time were computed from $t = 4$ sec (Figure 3.25).
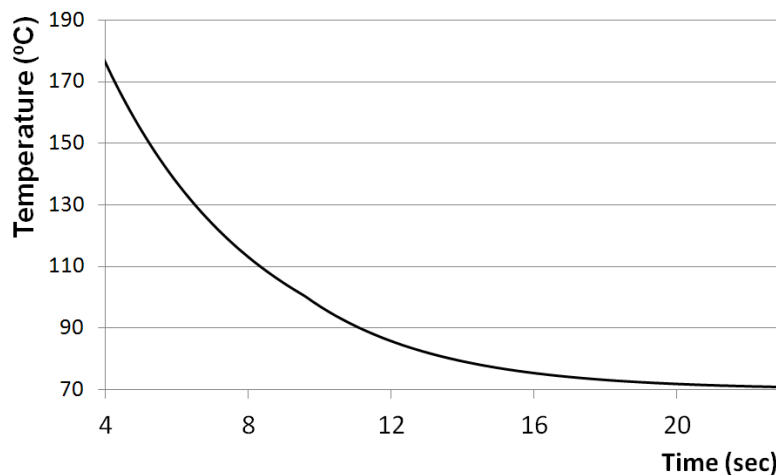
Figure 3.25 – Temperature evolution of the central node of the void.

Then, the thermal conditions of the surfaces that are in contact with the void were defined by using these temperature results. Two situations were considered: i) with higher temperatures of the void and ii) with a void temperature equal to the ambient temperature. Differences temperatures were computed in order to evaluate the importance of this boundary condition (Figure 3.26).
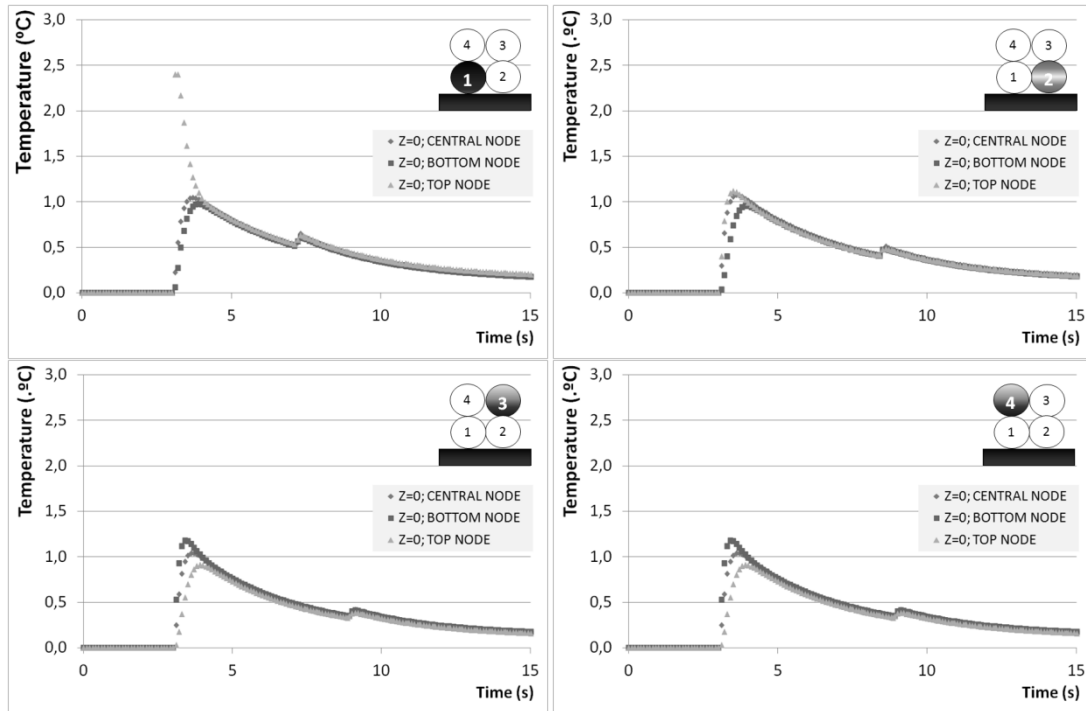
Figure 3.26 – Temperatures differences versus time between with and without higher temperatures of the void, for each filament, at $z = 0$, on 3 nodes (central, down and top).

The maximum observed difference temperature is 2.5ºC (1st filament), but during a short time period. In general, the differences temperatures are equal to 1ºC. These low values show that the higher voids temperatures have not a significant impact on heat transfer.

3.1.7 Conclusions

From this study with ABAQUS® software, some conclusions were made:

- Heat exchanges by convection with ambient and by conduction between adjacent filaments and support have the highest impact on FFE heat transfer. In the existing models of literature, the convection was considered as the unique responsible of the temperature evolution, but these previous results show that others heat amounts also have a great importance;

- The importance degree of the heat exchanges by radiation with ambient depends on the heat transfer coefficient: for high values of h_{conv} ($h_{conv} > 60$ W/m$^2 \cdot$ ºC), this thermal condition can be neglected;

- Heat exchanges by radiation between adjacent filaments and by convection with ambient voids showed to be insignificant in the heat transfer process, so they can be ignored;

- Temperatures throughout the filaments cross section are uniform, excepting when thermal contacts are assumed to be perfect: the increase of the conduction degree reduces the uniformity of temperatures;

- As concluded by Li (2002), temperatures along filament length are always uniform, that is, conduction heat along filaments can be neglected;

The most important aspects that must be taken into account in heat transfer process during FFE are described in Figure 3.27.

Most important aspects in Heat Transfer during FFE process				
Heat exchanges by convection with ambient at the free boundaries	Heat exchanges by conduction between adjacent filaments	Heat exchanges by conduction between filaments and support	Uniformity of temperatures along filament length	Uniformity of temperatures throughout the filament cross section
(controlled by the heat transfer coefficient)	(related with the adhesion)	(controlled by the thermal contact conductance)		(except for perfect conduction between filaments)

Figure 3.27 – The most important conclusions made from the ABAQUS®'s study.

3.2 ANALYTICAL SOLUTION FOR THE HEAT TRANSFER

Regardless the deposition sequence, during the manufacture of a part by FFE each individual filament is subjected to the same heat transfer mechanism with boundary conditions changing along the time deposition. As shown in Figure 3.28, one may have to consider heat flux with the support, with the surrounding environment, with colder filaments (deposited before) and with younger hotter filaments (deposited afterwards).
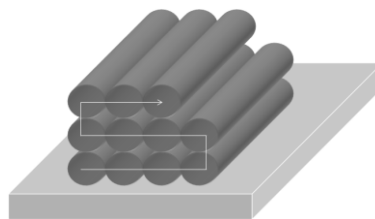
Figure 3.28 – Possible sequence of filaments deposition.

As demonstrated before, heat exchanges with ambient by convection and between adjacent filaments and support by conduction are the most important thermal conditions. The heat transfer by radiation will not be considered in this study due to its lower influence in the total heat exchange (section 3.1.2) and due to the complex analytical solutions that this boundary conditions provides.

Consider this, the energy balance for an element dx of the rth filament was written as (Figure 3.29):

$$\begin{cases} \textit{Energy in at one face} - \textit{Heat exchanges by convection with ambient} \\ -\textit{Heat exchanges by conduction between adjacent filaments or} \\ \textit{between filaments and support} \end{cases} =$$

$$= \textit{Change in internal energy} + \textit{Energy out at opposite face}$$
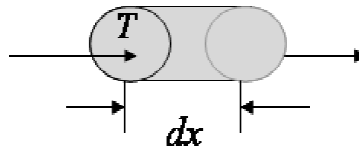
Figure 3.29 – Energy balance for an element dx of the rth filament.

Mathematically:

$$-kA\frac{\partial T_r}{\partial x} - h_{conv}(A_r)_{conv}(T_r - T_E) - \sum_{i=1}^{n} h_i(A_r)_i(T_r - T_{r_i}) =$$

$$= \rho \, CA\frac{\partial T_r}{\partial t}dx - A\left[k\frac{\partial T_r}{\partial x} + \frac{\partial\left(k\dfrac{\partial T_r}{\partial x}\right)}{\partial x}dx \right] \quad (3.12)$$

Where T_r is the temperature on the point x at the instant t of the rth filament ($r \in \{1,\dots,N\}$ where N is the total number of deposited filaments), T_L and T_E are respectively extrusion and environment temperatures (ºC), k is thermal conductivity (W/m· ºC), A is the filament cross-section area (m^2), n is the physical number of contacts with adjacent filaments or with support, h_i is thermal contact conductance for contact $i \in \{1,\dots,n\}$ (W/m^2 · ºC), T_{r_i} is the temperature (ºC) of the adjacent filament or support at contact i ($r_i \in \{1,\dots, N+1\}$, $r_i \neq r$, $T_1,\dots, T_N$ are temperatures of filaments and T_{N+1} is support

temperature), ρ is density (kg/m^3) and C is heat capacity (J/kg· ℃). $(A_r)_{conv}$ is area exposed to environment (m^2) and $(A_r)_i$ is area of contact i for the rth filament (m^2), given by (Figure 3.30):

$$\left(A_r\right)_i = a_{r_i}\lambda_i P\,dx, i \in \{1,\cdots,n\} \qquad \left(A_r\right)_{conv} = \left(1 - \sum_{i=1}^{n} a_{r_i}\lambda_i\right)P\,dx \qquad (3.13)$$

In this expression, P is the filament perimeter (m), λ_i is the fraction of P that is in contact with another, or with the support and a_{r_i} is defined by:

$$a_{r_i} = \begin{cases} 1 \text{ if the } r^{th} \text{ filament has the } i^{th} \text{ contact} \\ \\ 0 \text{ otherwise} \end{cases}, \forall i \in \{1,...,n\}, \forall r \in \{1,...,N\} \qquad (3.14)$$
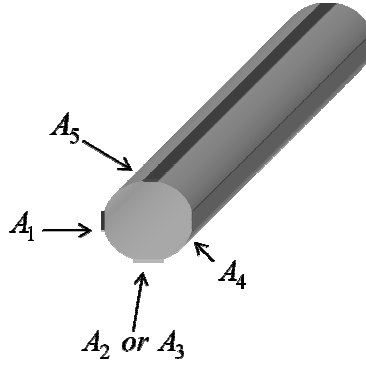
Figure 3.30 – Contact areas of a filament, for particular case of $n = 5$.

After some simplifications, and using the expressions of $(A_r)_{conv}$ and $(A_r)_i$, equation (3.12) can be written as (details in Appendix 1):

$$\frac{\partial T_r}{\partial t} = \frac{k}{\rho\,C}\frac{\partial^2 T_r}{\partial x^2} - \frac{P}{\rho\,CA}\left(h_{conv}\left(1 - \sum_{i=1}^{n} a_{r_i}\lambda_i\right)(T_r - T_E) + \sum_{i=1}^{n} h_i a_{r_i}\lambda_i\left(T_r - T_{r_i}\right)\right) \qquad (3.15)$$

Equation (3.15) shows that the temperature evolution in the filament is governed by:

- The conduction along filament length, controlled by the parameter $\dfrac{k}{\rho\,C}$;

- The heat exchanges by convection with the surroundings, governed by $\dfrac{Ph_{conv}}{\rho\,CA}$;

46

- The heat exchanges by conduction between adjacent filaments, controlled by $\dfrac{P h_i}{\rho\, CA}$.

The magnitude of each of these parameters was computed (Table 3.7).

Table 3.7 – Magnitude of the parameters that control the temperature variation.

	$\rho\,,C$	A	P	k	h_{conv}	h_i	$\dfrac{k}{\rho\, C}$	$\dfrac{h_{conv}P}{\rho\, CA}$	$\dfrac{h_i P}{\rho\, CA}$
Order	10^3	10^{-7}	10^{-3}	10^{-1}	10^1	10^2	10^{-7}	10^{-1}	10^0

From the results, it's possible to conclude that due to the low thermal conductivity of polymers and the small filament radius, the axial heat conduction can be neglected when compared with the convection and the conduction between adjacent filaments. This is in accordance with the previous results obtained by ABAQUS® simulations. Considering this, the energy equation can be simplified and rewritten as:

$$\frac{\partial T_r}{\partial t} = -\frac{P}{\rho\, CA}\left(h_{conv}\left(1 - \sum_{i=1}^{n} a_{r_i}\lambda_i\right)(T_r - T_E) + \sum_{i=1}^{n} h_i a_{r_i}\lambda_i\left(T_r - T_{r_i}\right)\right) \tag{3.16}$$

Equation (3.16) was solved analytically using the characteristic polynomial method (Meirovitch 1970, Palais and Palais 2009) to yield the evolution in time of the filament temperature (details in Appendix 2):

$$T_r(t) = C_1 e^{\frac{-P\, b\left(a_{r_1},...,a_{r_n}\right)}{\rho AC}(t - t_r(x))} + Q\left(a_{r_1},...,a_{r_n}\right) \tag{3.17}$$

$t_r(x)$ is the instant where the cross section x of the rth filament starts cooling down or enters in contact with another cross section, and C_1 is defined as:

$$C_1 = T_{r0} - Q\left(a_{r_1},...,a_{r_n}\right) \tag{3.18}$$

Where T_{r0} is the filament temperature at t_r ($T_{r0} = T_r(t_r)$).

Functions $b\left(a_{r_1},...,a_{r_n}\right)$ and $Q\left(a_{r_1},...,a_{r_n}\right)$ depend on contacts:

$$b\left(a_{r_1}, \ldots, a_{r_n}\right) = h_{conv}\left(1 - \sum_{i=1}^{n} a_{r_i} \lambda_i\right) + \sum_{i=1}^{n} a_{r_i} h_i \lambda_i$$

$$Q\left(a_{r_1}, \ldots, a_{r_n}\right) = \frac{h_{conv}\left(1 - \sum_{i=1}^{n} a_{r_i} \lambda_i\right) T_E + \sum_{i=1}^{n} a_{r_i} h_i \lambda_i T_{r_i}}{b\left(a_{r_1}, \ldots, a_{r_n}\right)}$$

(3.19)

In this case, the Biot number is defined by (Bejan 1993):

$$B_i = \frac{A}{P} \frac{b\left(a_{r_1}, \ldots, a_{r_n}\right)}{k}$$

(3.20)

If the Biot number is smaller than 0.1, temperature gradients can be negligible throughout the filament cross-section and the equation (3.17) can be used to obtain the temperature evolution of the filaments. Resuming:

$$B_i \leq 0.1 \Rightarrow T_r(t) = C_1 e^{\frac{-P\, b\left(a_{r_1}, \ldots, a_{r_n}\right)}{\rho AC}(t - t_r(x))} + Q\left(a_{r_1}, \ldots, a_{r_n}\right)$$

(3.21)

The Biot number is mainly controlled by the values of the heat transfer coefficient, the thermal contact conductance and the contact area of the filament with others bodies. Figure 3.31 shows the intervals of possible values for h_{conv} and h_i to guarantee that $B_i < 0.1$, considering a cylindrical filament of diameter $w = 0.0003$ m, a thermal conductivity of $k = 0.1768$ W/m· ºC and three values for the contact fraction with another body (25%, 50% and 75%).
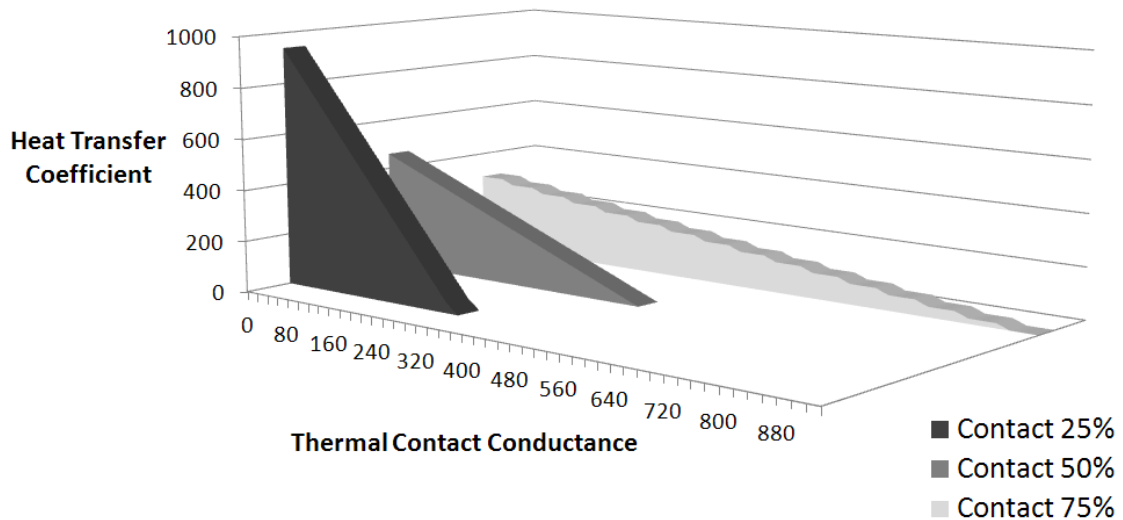
Figure 3.31 – Possible values for h_{conv} (W/m² · °C) and h_i (W/m² · °C) to guarantee that $B_i < 0.1$, for a cylindrical filament of diameter $w = 0.0003$ m, with 25%, 50% and 75% of contact with adjacent filaments or with support.

3.3 DEVELOPMENT OF A COMPUTATION CODE FOR HEAT TRANSFER IN FFE

Equation (3.17) quantifies the temperature evolution of a single filament along the deposition time for any point x. However, during the manufacture of part, consecutive filaments are deposited according a predefined deposition strategy. Therefore, in order to predict the temperature history in all filaments comprising the part, it is mandatory to generalize the previous computations to obtain the temperature evolution of each filament fragment at any point x of the part, for different deposition techniques and 3D configuration structures. This requires the development of some procedures, computational strategies/techniques as well as some simplifications, which are described below.

3.3.1 Generalizing the computation of temperatures

a) *Discretization of filaments:*

Since the temperature is uniform across the section (considering $B_i < 0.1$) and the axial conduction can be neglected (Table 3.7), a discretization of the filaments can be used in order to simulate the continuous filament deposition.

With this procedure, which considers that at each time increment Δt, an element of the filament is deposited (Figure 3.32), is possible to simulate the sequential filament deposition required to generate a part.
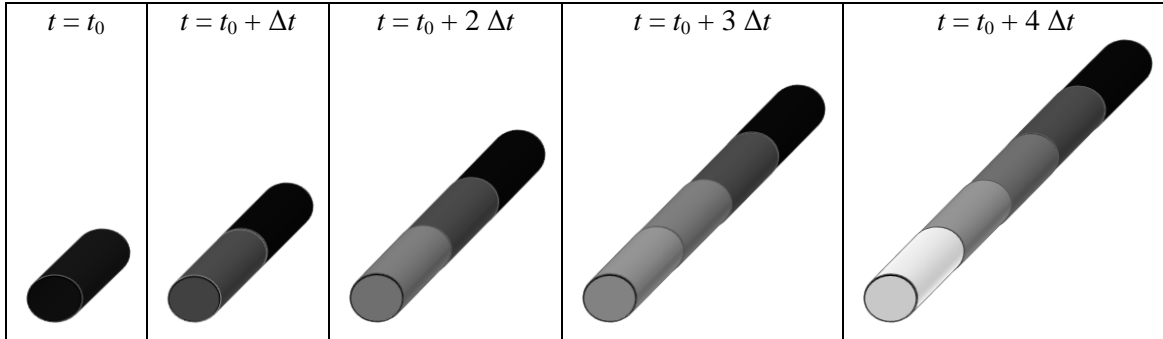
Figure 3.32 – Discretization of a filament.

The length of these elements must be set ensuring a good compromise between computation time and accuracy: high length leads to lower computations and less accuracy and vice versa.

b) *Filaments deposition:*

FFE is a continuous process, i. e., the extrusion doesn't stop the deposition between two consecutives filaments or between two consecutives layers. This requires a change of the deposition direction every time a new filament is deposited, and, consequently, a change in the thermal/boundary conditions along the deposition time. Figure 3.33 presents an example of a sequence of 7 filaments, where the successive deposition is illustrated.
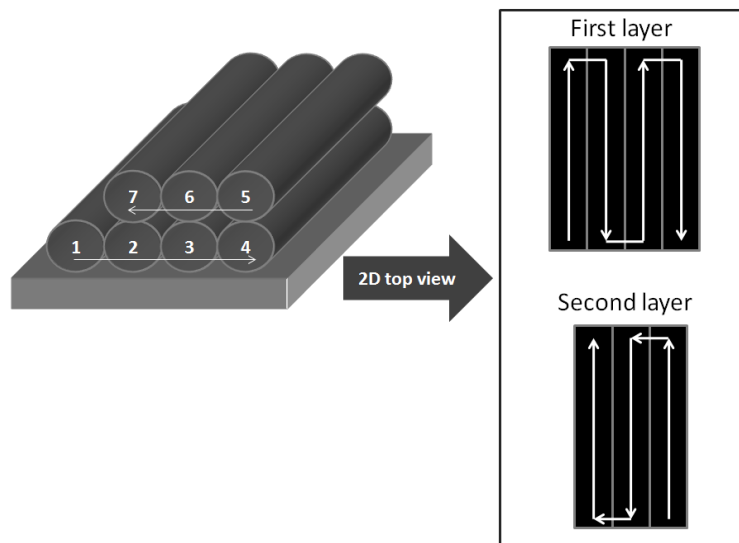
Figure 3.33 – Illustration of the successive deposition, for two layers of filaments.

c) *Up-dating of the thermal conditions:*

Since the filaments are progressively deposited, the thermal boundary conditions are not constant along the FFE process. The different physical contacts arise during the deposition process and consequently, the initial conditions (time and temperature) must be up-dated every time a new contact occurs. Contacts and initial conditions are governed by the following *Thermal Condition Variables* (TCV) that depends on the specific filament position, time and deposition sequence:

- time $t_r(x)$ ($TCV_1(r)$): instant at which the cross-section x of the rth filament starts cooling down or contacts with another;

- temperature T_{r0} ($TCV_2(r)$): temperature at $t_r(x)$;

- vector a_{r_i} ($TCV_3(r)$): in equation (3.14), it sets the contacts for the rth filament ($i \in \{1,...,n\}$, where n is the number of contacts).

For the filaments of the first layer, only horizontal contacts are available. Then, every time a new filament is deposited, the thermal conditions are defined for it, and up-dated only for the previously deposited filaments. A simple example of a layer of three consecutive adjacent filaments with the description of the thermal conditions evolution is illustrated in Figure 3.34.
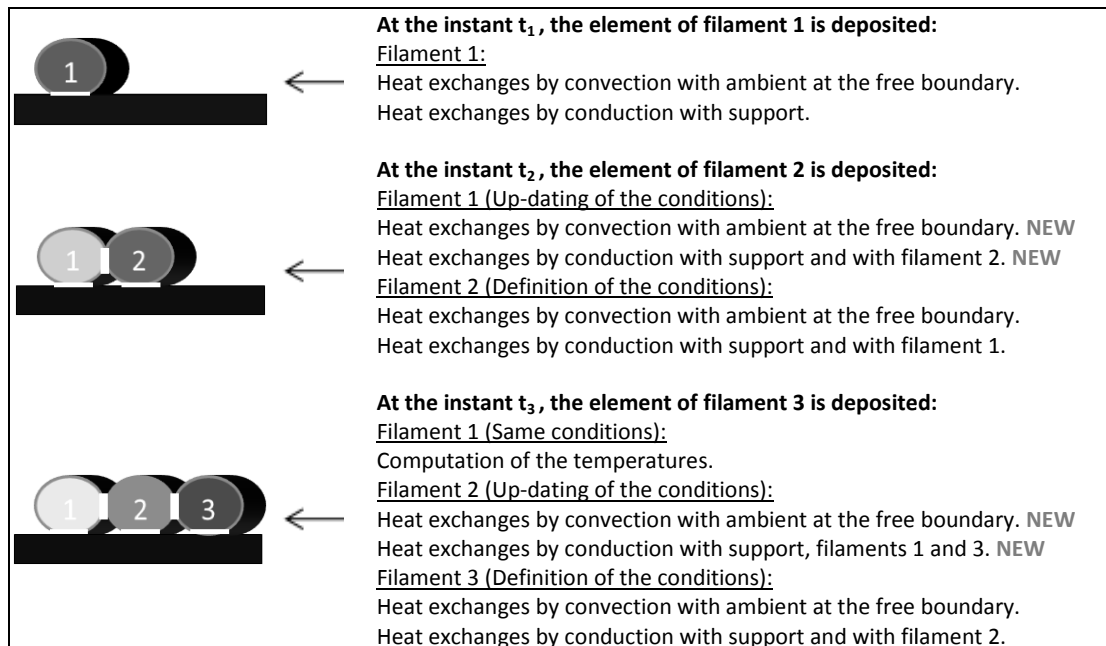
Figure 3.34 – Description of the thermal conditions evolution for a layer of three filaments.

Then, for the first layer, when the element of the rth filament starts cooling down ($r > 1$):

    i)   Thermal conditions $TCV_1(r)$, $TCV_2(r)$ and $TCV_3(r)$ are defined;

    ii)   Thermal conditions $TCV_1(r-1)$, $TCV_2(r-1)$ and $TCV_3(r-1)$, are up-dated (previous filament).

If new layers are deposited on top of the first, another type of contacts – the vertical contacts – must be considered. Therefore, for the 2nd and next layers, when the element of the rth filament starts cooling down:

    i)   Thermal conditions $TCV_1(r)$, $TCV_2(r)$ and $TCV_3(r)$ are defined;

    ii)   Thermal conditions $TCV_1(r-1)$, $TCV_2(r-1)$ and $TCV_3(r-1)$ are up-dated;

    iii)   Thermal conditions $TCV_1(r-p)$, $TCV_2(r-p)$ and $TCV_3(r-p)$ are up-dated, where $r-p$ is the position of the filament that allows to the previous layer and enters in contact with the rth.

An example of two layers of 3 filaments is illustrated in Figure 3.35, with the description of the thermal conditions at the instant t_6, when the element of the 6th filament starts cooling down.
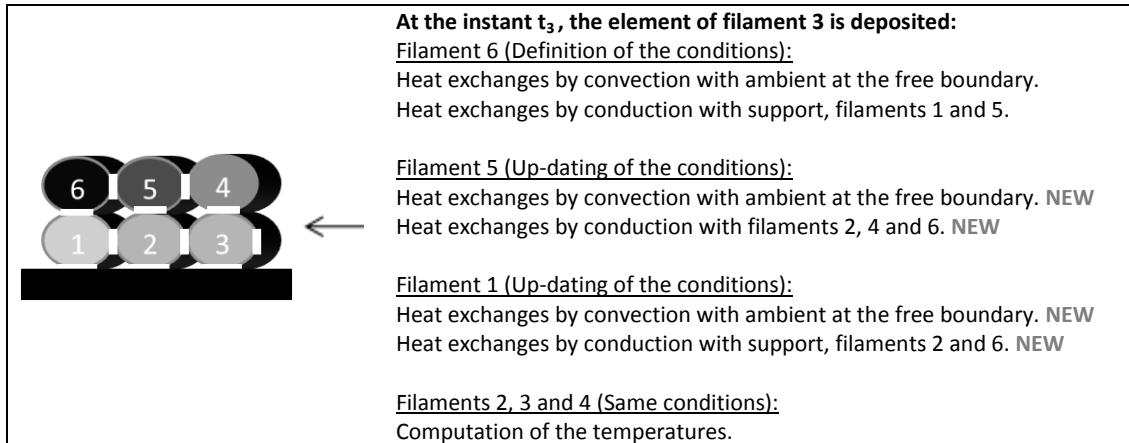
Figure 3.35 – Description of the thermal conditions when the last filament is deposited, for two layers of three filaments.

d) *Deposition sequences:*

Three different deposition sequences are considered in this study: unidirectional and aligned, unidirectional and skewed, and perpendicular filaments (Figure 3.36).
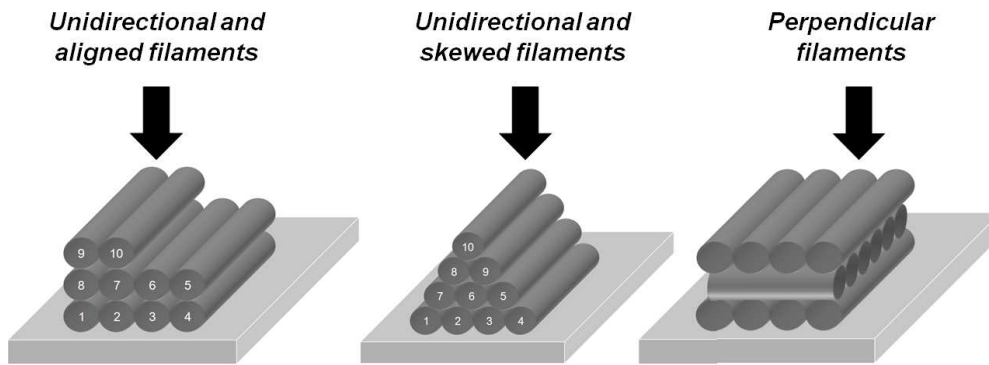
Figure 3.36 – Considered deposition sequence types.

The deposition sequence type fixes the nature and the number of contacts as well as the up-dating times. In addition, it also influences the computation procedure. For example, if the objective is to obtain the temperature evolution across a section x of a part, is only required to compute the temperature on the selected cut, if the unidirectional filaments are being used, or, the temperature evolution for the entire part must be computed, if perpendicular sequence strategy has being adopted (due to the change of filaments orientation from layer to layer).

    e) *Simultaneous computation of the filaments temperatures:*

During the FFE process, some filaments are reheated when new contacts with hotter filaments occur; simultaneously, the last filaments cool down faster due to these same contacts. Since this requires a simultaneous computation of the filaments temperature, an iterative process is needed, with a convergence error that must be chosen as a good compromise between accuracy of results and computation time.

3.3.2 Input parameters

In the MatLab® command window, the following variables need to be introduced:

- The deposition sequence;
- The cross section x (location of the part where the temperatures are studied);
- The filaments in contact with lateral supports, if these contacts exist.

Deposition sequence:

The deposition sequence is defined by a matrix M of m rows and 2 columns, where m is the layers number:

$$M = \begin{bmatrix} i_1 & j_1 \\ i_2 & j_2 \\ \vdots & \vdots \\ i_m & j_m \end{bmatrix}$$

(3.22)

In the matrix M, i_α is the filaments number of the αth layer, and j_α is the deposition sequence type of the αth layer ($\alpha \in \{1,...,m\}$).

As mentioned before, three deposition sequence types can be evaluated, corresponding one code for each one: 0 to unidirectional and aligned filaments, -1 or 1 for unidirectional and skewed filaments, and values higher than 1 for perpendicular cases. Table 3.8 resume the codes used while Table 3.8 shows an example of each deposition sequence type with the corresponding input matrix.

Table 3.8 – Codes for specification of the deposition type in the MatLab® code.
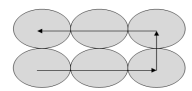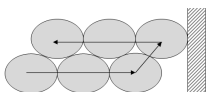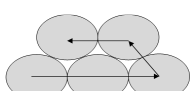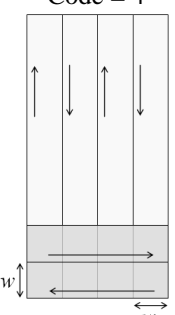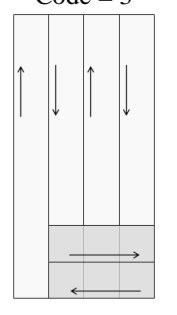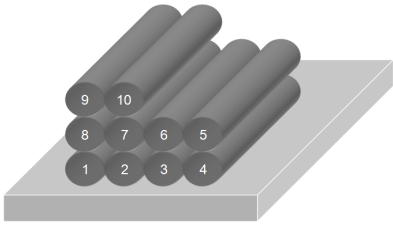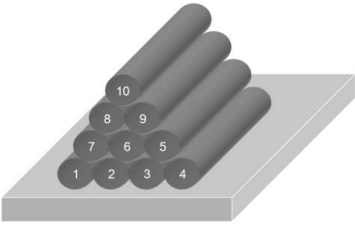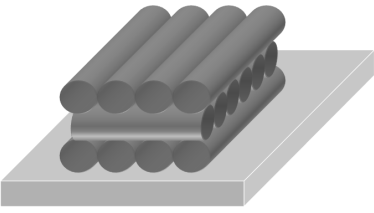
Orientation	Configuration	Example - Cross section view	Code value
Unidirectional filaments	Aligned		Code = 0
	Skewed to right		Code = 1
	Skewed to left		Code = -1
Perpendicular filaments	---	**Example - Top view** 	Code > 1 (number of filaments of the last layer covered by the actual layer)

Table 3.9 – Deposition sequence examples and its corresponding matrix.

DEPOSITION SEQUENCE	DESCRIPTION	CORRESPONDING MATRIX
	➢ 4 filaments in the layer 1, aligned (0) ➢ 4 filaments in the layer 2, aligned (0) ➢ 2 filaments in the layer 3, aligned (0)	$M = \begin{bmatrix} 4 & 0 \\ 4 & 0 \\ 2 & 0 \end{bmatrix}$
	➢ 4 filaments in the layer 1, aligned (0) ➢ 3 filaments in the layer 2, skewed to left (-1) ➢ 2 filaments in the layer 3, skewed to right (1) ➢ 1 filament in the layer 4, skewed to left (-1)	$M = \begin{bmatrix} 4 & 0 \\ 3 & -1 \\ 2 & 1 \\ 1 & -1 \end{bmatrix}$
	➢ 4 filaments in the layer 1, aligned (0) ➢ 6 filaments in the layer 2, perpendicular to the 4 previous filaments (4) ➢ 4 filaments in the layer 3, perpendicular to the 6 previous filaments (6)	$M = \begin{bmatrix} 4 & 0 \\ 6 & 4 \\ 4 & 6 \end{bmatrix}$

Cross section x:

The cross section x is the part location where the user wants to obtain the temperatures. It is introduced in the format number, in meters, taking into account the defined referential illustrated in Figure 3.37 for a layer of 4 filaments. As an example, if the objective is to know the temperature evolution on the middle of a part with a length of 0.01 m, the value that must be introduced is 0.005.
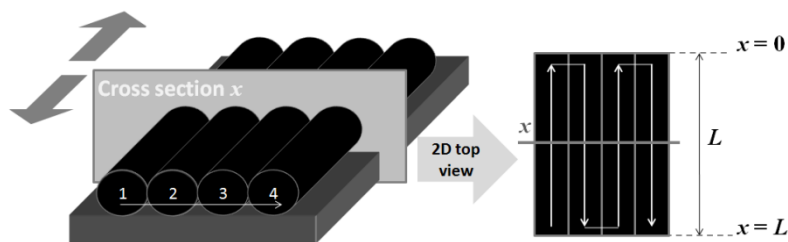
Figure 3.37 – Definition of the *x*-axis for a layer of 4 filaments.

Filaments in contact with lateral supports:

Especially for skewed configurations, a lateral support can be needed to avoid the fall of the filaments positioned in the extremities.

The existence of these contacts with lateral supports modifies the boundary conditions, and consequently influences the temperature evolution. Then, in order to transmit this information to the code, two vectors need to be introduced: *left* and *right*. In the vector *left*, the positions of the filaments (only for the 2nd and next layers) that are in contact with a left lateral support are introduced and, the vector *right* contains the filaments in contact with a right lateral support. In Figure 3.38, an example of a skewed configuration is illustrated: in this case, *left* = [0] because no filament of 2nd or next layers has contact with left lateral support and *right* = [8,9] because the 8th and the 9th filaments need a right lateral support.
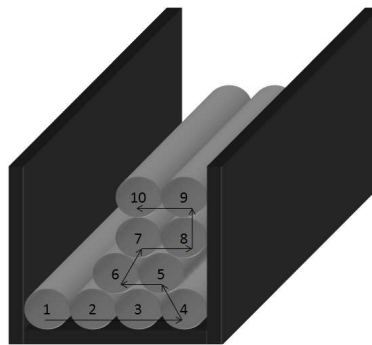
Figure 3.38 – Example of skewed sequence where lateral support is needed.

3.3.3 Output parameters

As output, a *.txt* document is generated, with the computation times and the respective temperatures, for all the filaments of the sequence. The first column corresponds to the consecutive instants at which the temperatures were computed (in seconds), the 2nd column corresponds to the temperatures of the 1st filament (ºC), the 3rd column contains the temperatures of the 2nd filament and consecutively. The last column shows the value of environment temperature (ºC). Figure 3.39 shows an example of *.txt* output document, for a sequence of two filaments with T_L = 200 ºC and T_E = 47 ºC, between t = 7.59 *s* and t = 7.8 *s*. Note that this document can be opened with Microsoft Office Excel® software, where graphics are quickly made and easily analyzed.
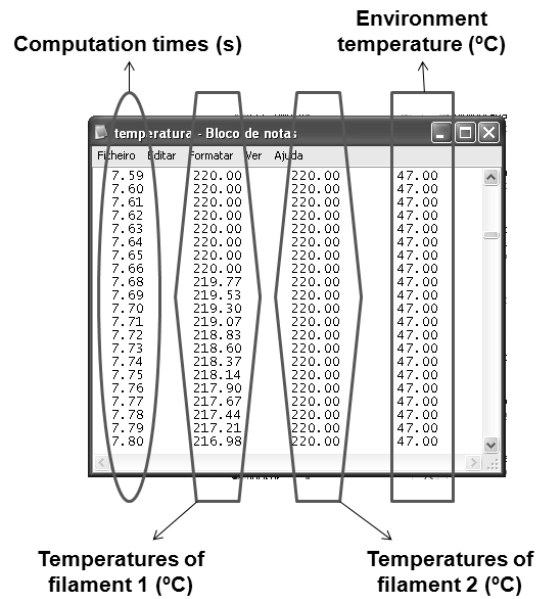
Figure 3.39 – Example of .txt output document for a sequence of two filaments.

3.3.4 Computing sequences

A MatLab® code was developed to devolve the temperature evolution time for all the filaments of any sequence, using the expression (3.17) and including the procedures described before. The computational flowchart is shown in Figure 3.40. In order to illustrate how the computer code was implemented, the segment dealing with the temperature along the deposition time for the first layer of filaments, using one or two distinct materials, is presented in Appendix 3.

MATLAB CODE

Definition of the variables

- Deposition sequence parameters - **STEP 1**
- Computation variables - **STEP 2**
- Dimensions of vectors and matrices - **STEP 3**
- FFE variables - **STEP 4**
- Up-dating times - **STEP 5**
- Contact matrix and contacts with support (TCV_3) - **STEP 6**
- Matrix of temperature values - **STEP 7**

MatLab code

INPUT COMMAND WINDOW

- Deposition sequence;
- Deposition mode (unidirectional and aligned, skewed, or perpendicular);

- Cross section x.

Computation of the temperature of the 1st filament (1st layer)

- Computation of b and Q - **STEP 8**
- Definition of the values of TCV_1 and TCV_2 for the 1st filament - **STEP 9**
- Computation of the temperatures - **STEP 10**
- Verification of the Biot Number value (Bi) - **STEP 11**

Computation of the temperature of the rth filament, r > 1 (1st layer)

- Up-date of the contact matrix (horizontal contacts) - **STEP 12**
- Up-date of b - **STEP 13**
- Definition of an additional time period for the last filament deposited - **STEP 14**
- Definition of the values of TCV_1 and TCV_2 for the rth filament - **STEP 15**
- Up-date of the values of TCV_1 and TCV_2 for the $(r-1)$th filament - **STEP 16**
- Iterative process to compute the temperatures of the filaments - **STEP 17**
- Verification of the value of Bi - **STEP 18**

Computation of the temperature of the rth filament, r > 1 (jth layer, j > 1)

- Up-date of the contact matrix (horizontal and vertical contacts) - **STEP 19**
- Up-date of b;
- Definition of an additional time period for the last filament deposited;
- Definition of the values of TCV-1 and TCV-2 for the rth filament;
- Up-date of the values of TCV-1 and TCV-2 for the filaments with new contacts;
- Iterative process to compute the temperatures of the filaments;
- Verification of the value of Bi.

MatLab code

OUTPUT

Text Document with evolution of temperature during deposition for all the filaments.

Figure 3.40 – General procedure to compute the temperatures of all the filaments.

58

Deposition sequence parameters – STEP 1

From the matrix *M* introduced by the user, some values are computed: the total number of filaments *N*, the total number of layers *m*, and the position of 1st and last filament of each layer.

Computation variables – STEP 2

Three computation variables need to be introduced: i) the time increment Δt, ii) the additional computation time and, iii) the convergence error.

i)   As referred in section 3.3.1, a time increment is needed to discretize the filaments: a low time increment value increases the results precision, but implies a considerable computation time. In order to guarantee the rigor of temperature results, a maximum value of $\Delta t_{max} = 0.1$ s is usually selected, for unidirectional filaments, but it must be adapted depending on the filaments number. Details about this value are more described later in section 4.3. For perpendicular filaments, a lower value must be chosen, due to the computation of temperatures on the totally of part: $\Delta t_{max} = (w/v)/5 \approx 0.0025$ s is usually used.

ii) When the last filament of a sequence is deposited, all the part continues to cool down. So, the computation of the temperatures evolution must continue during a certain time period ensuring the environment temperature is reached. This additional time is introduced in this section.

iii) As stated in section 3.3.1, the simultaneous computation of the filaments temperature includes the use of an iterative process, whose convergence error is usually set at $\mu = 0.001$ ºC, as a good compromise between accuracy and computation time.

Dimensions of vectors and matrices – STEP 3

During the computation of temperatures, a lot of information must be saved for each filament: temperatures along time, activated contacts, Biot number, adjacent filaments number, temperatures of adjacent filaments, initial temperature... These values must be saved into matrices, whose dimensions depend on the filaments number, the total deposition time and the deposition sequence type. For perpendicular configurations, since the temperatures are computed along the part, 4D matrices are required to save all the values while for the unidirectional filaments 2D matrices are sufficient. Then, at this step, dimensions of these matrices are deduced from the input matrix *M*.

In this section, the values of FFE variables are defined. These are divided into four categories:

- Process variables: deposition velocity (m/s), extrusion temperature (ºC) and environment temperature (ºC).

- Filament dimensions: filament cross-section area (m^2), filament cross section perimeter (m) and filament length (m).

- Material properties: thermal conductivity (W/m· ºC), material density (kg/m^3) and specific heat (J/kg· ºC).

- Heat transfer parameters: Heat transfer coefficient (W/m^2 · ºC), thermal contact conductances (W/m^2 · ºC) and fraction of contact with adjacent filaments (%), for each contact.

Up-dating times – STEP 5

As mentioned before, thermal conditions must be up-dated at specifics moments of the deposition process, i. e., every time a new contact occurs. These instants, designated by "up-dating times", strongly depend on the deposition sequence type, specifically on the orientation of the filaments.

> ➢ Unidirectional filaments

For this deposition sequence, temperatures T_1, T_2, T_3, …, T_N, where N is the number of filaments, are computed on the cross-section x introduced by the user in the MatLab® window. Then, thermal conditions TCV_1, TCV_2 and TCV_3 are defined/up-dated every time the cut x of the actual deposited filament starts cooling down, only for the actual deposited filament and the others filaments that enter in contact with it. Taken as an example 2 layers of 4 filaments (Figure 3.41), the extrusion head reaches the cross section x at the following successive instants:

$$t_{up-dating} = \left[\frac{L-x}{v} \quad \frac{L+x}{v} \quad \frac{3L-x}{v} \quad \frac{3L+x}{v} \quad \frac{5L-x}{v} \quad \frac{5L+x}{v} \quad \frac{7L-x}{v} \quad \frac{7L+x}{v} \right]^T \quad (3.23)$$
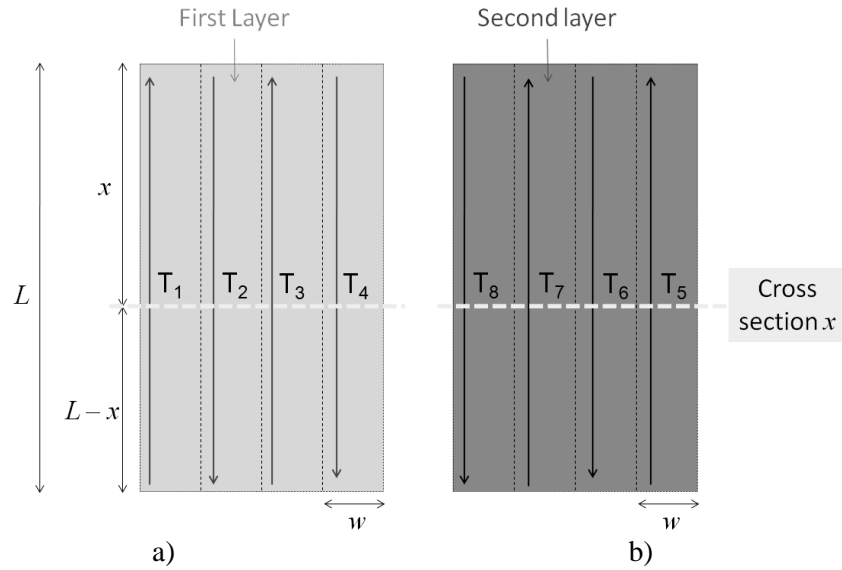
Figure 3.41 – Top simplified view of two deposited layers of unidirectional filaments. a) Deposition of the first layer. b) Deposition of the second layer.

A general mathematical expression in function of the actual deposited filament r and the cross section x was found for unidirectional filaments (aligned and skewed):

$$\left(t_{up-dating}\right)_r = \left[\left(r - \cos\left(\frac{\pi}{4}\left(1-(-1)^r\right)\right)\right)L + (-1)^r x\right] / v, r \in \{1,2,...,N\}$$ (3.24)

> ➤ Perpendicular filaments

For perpendicular deposition, and since the orientation changes along the adjacent layers (with $\Phi = [0^o / 90^o]$), the filaments are subdivided into square elements, and the temperature of these squares, $T_{(lay)ij}$, must be computed along deposition time, where *lay* is the layer number, i is the vertical position and j is the horizontal position (Figure 3.42). This involves a considerable large computation time when compared with the unidirectional case where only the temperatures on the point x are computed.
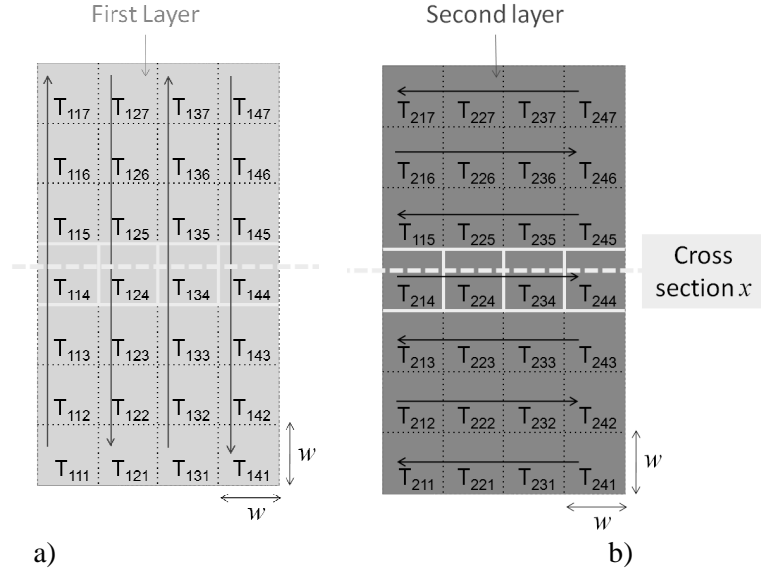
Figure 3.42 – Top simplified view of two deposited layers of perpendicular filaments.
a) Deposition of the first layer. b) Deposition of the second layer.

In this case, the three variables TCV_1, TCV_2 and TCV_3 must be up-dated every w/v second, which correspond to 0.01 s for a typical deposition velocity of $v = 0.025$ m/s and a diameter of $w = 0.0003$ m. then, the up-dating time are defined by:

$$t_{up-dating} = \left[\frac{w}{v} \quad \frac{2w}{v} \quad \frac{3w}{v} \quad \frac{4w}{v} \quad \frac{5w}{v} \quad ... \quad \frac{55w}{v} \quad \frac{56w}{v} \right]^T \qquad (3.25)$$

In a general way, for perpendicular filaments, vector $t_{up\text{-}dating}$ can be defined as:

$$\left(t_{up-dating} \right)_e = (ew)/v, e \in \{1,...,NT\} \qquad (3.26)$$
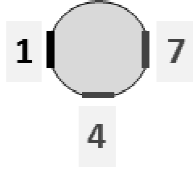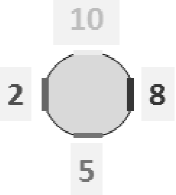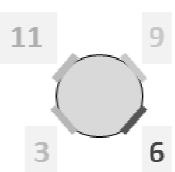
Where NT is the total number of square elements and e is the last deposited element. Based on the deposition sequence defined by the input matrix M, the values of the up-dating times $t_{up\text{-}dating}$ are computed using expressions (3.24) or (3.26), and saved in the matrix *limite*.

Contact matrix and contacts with support (TCV_3) – STEP 6

The activation of the contacts are made by the function a_{r_i}, defined by equation (3.14), where $i \in \{1,...,n\}$ and n is the number of physical contacts. In this study, for the three

considered deposition sequences and the possibility of existing lateral supports, $n = 11$ contacts were identified as described in Table 3.10.

Table 3.10 – Identification of the contacts used in the Matlab® code (cross sectional view).

Contacts with support	Contacts with an adjacent filament	
	Aligned filaments	Skewed filaments

In a first phase, variable a_{r_i} is assumed to be a 2D zero matrix ($N\times11$) for unidirectional filaments, and a 4D zero matrix ($m\times11\times ver\times hor$, where m is the layers number, ver is the vertical filaments number and hor is the horizontal filaments number) for perpendicular filaments. After the definition of the dimension of the contact matrix a, the contacts with support are activated: contacts with lateral supports are set depending on the vectors *left* and *right* introduced by the user, and contacts with bottom support are activated for the filaments of the first layer.

Note that this matrix a is one of the thermal condition variables that must be up-dated along the FFE process (TCV$_3$), as the different contacts appear. An example of a sequence deposition with its corresponding contact matrix a is illustrated in Figure 3.43.
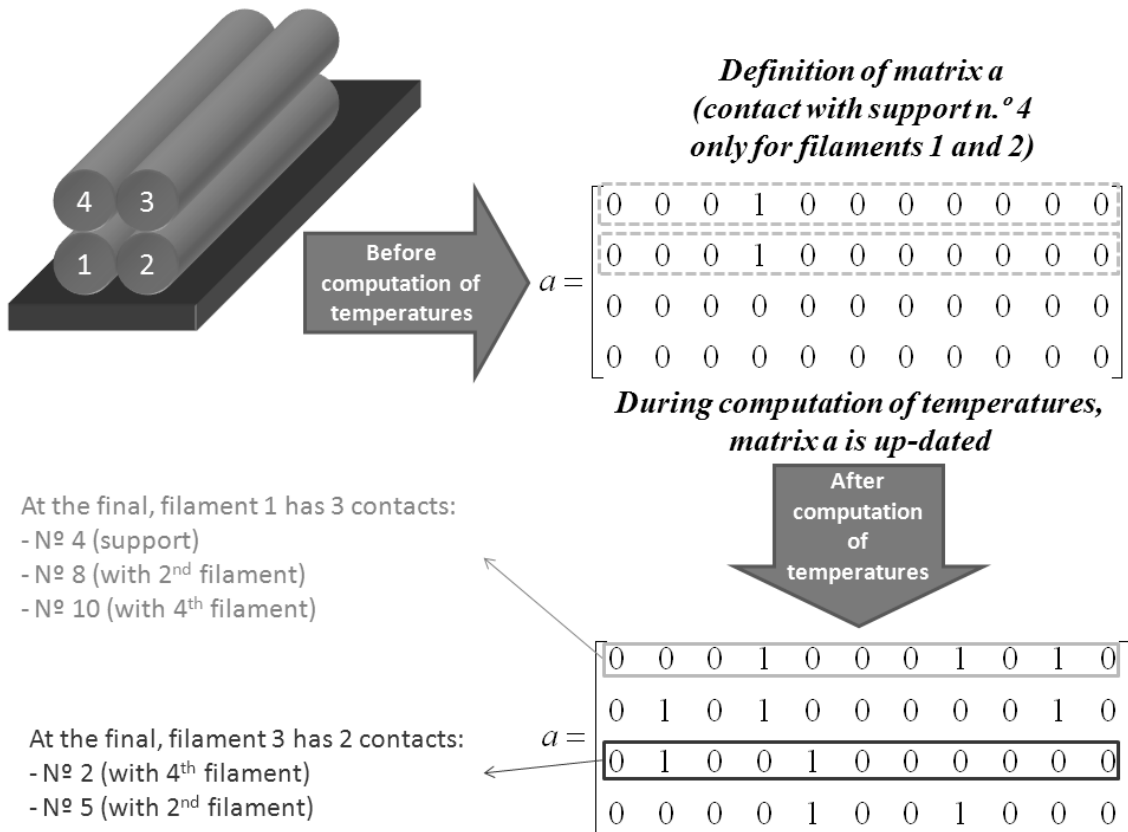
Figure 3.43 – Example of a sequence with its corresponding contact matrix *a*.

Matrix of temperature values – STEP 7

The objective of the code is to obtain a matrix of temperature values along time, for all the filaments. This matrix *temp* has N_t lines and N columns, where $N_t = (total\ time)/(\Delta t)$ is the number of time increments and N is the filaments number. Before the computation of the temperatures, *temp* is defined by (Figure 3.44):

$$temp_{i,j} = T_L, \qquad i = 1,..., N_t; j = 1,...N \tag{3.27}$$
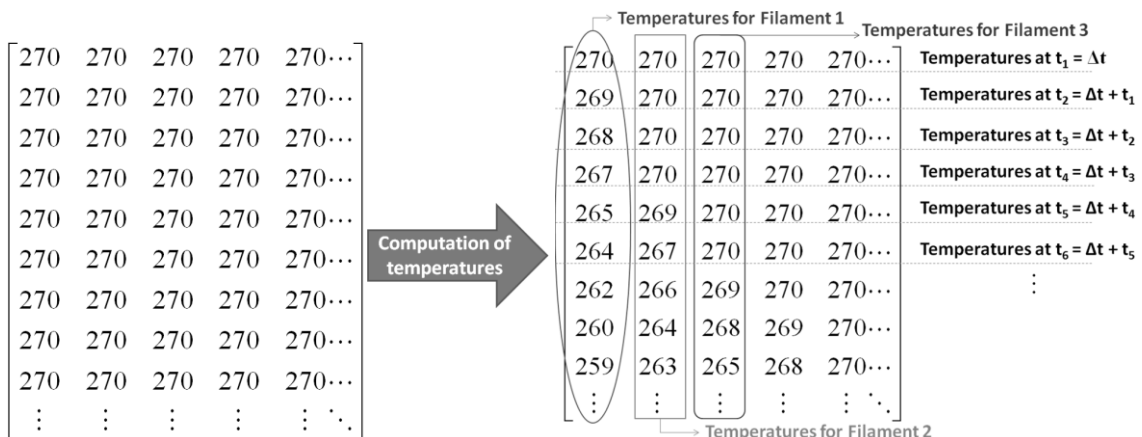
Figure 3.44 – Definition of matrix *temp* for $T_L = 270°C$.

Computation of b and Q – STEP 8

Variables b and Q defined by equation (3.19) depend on contacts and are used for the computation of temperatures, as expressed by equation (3.21). Since the filaments don't have the same contacts and the same temperature history, each of them has different values for b and Q. Then, in the code, for unidirectional filaments, b and Q are vectors of dimension N:

$$b = \begin{bmatrix} \text{value of } b(a_{r_1},...,a_{r_n}) \text{ for filament } 1 \\ \text{value of } b(a_{r_1},...,a_{r_n}) \text{ for filament } 2 \\ \text{value of } b(a_{r_1},...,a_{r_n}) \text{ for filament } 3 \\ \vdots \\ \text{value of } b(a_{r_1},...,a_{r_n}) \text{ for filament } N \end{bmatrix} ; Q = \begin{bmatrix} \text{value of } Q(a_{r_1},...,a_{r_n}) \text{ for filament } 1 \\ \text{value of } Q(a_{r_1},...,a_{r_n}) \text{ for filament } 2 \\ \text{value of } Q(a_{r_1},...,a_{r_n}) \text{ for filament } 3 \\ \vdots \\ \text{value of } Q(a_{r_1},...,a_{r_n}) \text{ for filament } N \end{bmatrix} \quad (3.28)$$

These vectors are computed at this stage and will be up-dated every time the contact matrix a is up-dated.

For perpendicular filaments, the values of b and Q are computed for all the square elements of width w, defined by the layer number and the vertical/horizontal positions (Figure 3.42). In this case, two 3D matrices are used to save and up-date these values.

Definition of the values TCV$_1$ and TCV$_2$ for the 1st filament – STEP 9

The Thermal Conditions Variables 1 and 2 are defined for the 1st filament. Taken as example the unidirectional deposition:

$$TCV_1(1) = \frac{L-x}{v}$$
$$TCV_2(1) = T_L \quad (3.29)$$

The expression of TCV$_1$(1) was deduced from the expression (3.24) of $(t_{up\text{-}dating})_1$.

For unidirectional filaments, the vectors *save_lim* and *T_begin* of dimension N comprise the values of TCV$_1$ and TCV$_2$, respectively, for all the filaments:

$$
save\_lim =
\begin{bmatrix}
\text{value of } T\text{CV}_1(1) \ (\text{filament} \ \ 1) \\
\text{value of } T\text{CV}_1(2) \ (\text{filament} \ \ 2) \\
\text{value of } T\text{CV}_1(3) \ (\text{filament} \ \ 3) \\
\vdots \\
\text{value of } T\text{CV}_1(N) \ (\text{filament} \ \ N)
\end{bmatrix}
; T\_begin =
\begin{bmatrix}
\text{value of } T\text{CV}_2(1) \ (\text{filament} \ \ 1) \\
\text{value of } T\text{CV}_2(2) \ (\text{filament} \ \ 2) \\
\text{value of } T\text{CV}_2(3) \ (\text{filament} \ \ 3) \\
\vdots \\
\text{value of } T\text{CV}_2(N) \ (\text{filament} \ \ N)
\end{bmatrix}
\qquad (3.30)
$$

At this step, the dimension of these vectors and the values of $TCV_1(1)$ and $TCV_2(1)$ are defined; the others values $TCV_1(2)$, ..., $TCV_1(N)$ and $TCV_2(2)$, ..., $TCV_2(N)$ will be computed/up-dated as the deposition progresses, every time a new contact occurs. For perpendicular filaments, these values are also saved and up-dated along the computation process, but for all the square elements (Figure 3.42). Then, two 3D matrices are used for this deposition sequence type.

Computation of the temperatures – STEP 10
Temperatures of the first filament can be now computed using expression (3.21), i. e., the first column of the matrix *temp* is up-dated (first filament). Additionally, the time increments are saved in the vector *abcissa* with dimension $1 \times N_t$, where $N_t = (total\ time)/(\Delta t)$ is the number of time increments.

Verification of the Biot Number value – STEP 11
As stated before, each filament has a specific value for the variable *b*, depending on their boundary conditions. Since the Biot number B_i is influenced by *b*, the value for B_i must be computed every time *b* is up-dated. In the code, and for the unidirectional deposition, *Biot* is a vector of dimension *N*, comprising the Biot number values for each filament:

$$
\text{Biot} =
\begin{bmatrix}
\text{value of } B_i \text{ for filament } \ 1 \\
\text{value of } B_i \text{ for filament } \ 2 \\
\text{value of } B_i \text{ for filament } \ 3 \\
\vdots \\
\text{value of } B_i \text{ for filament } \ N
\end{bmatrix}
\qquad (3.31)
$$

66

With the aim to ensure that the temperatures across section remain uniform, the MatLab® code window will send a warning message if one of these values is higher than 0.1. For perpendicular sequences, *Biot* is a 3D matrix including all the values of B_i for each square element.

Up-date of the contact matrix (horizontal contacts) – STEP 12

The existing contacts between adjacent filaments of the first layer are horizontal, that is, only contacts nº 2 and nº 8 (see Table 3.10) are activated during the computation of temperatures for the first layer: contact nº 2 is defined for the actual deposited filament and contact nº 8 is activated for the previous filament.

For unidirectional sequences, if *r* is the specific position of the actual deposited filament ($r > 1$):

$$\begin{cases} a_{r2} = 1 \\ a_{(r-1)8} = 1 \end{cases} \tag{3.32}$$

For perpendicular sequences, if *i/j* is the vertical/horizontal position of the actual deposited square element:

$$\begin{cases} a_{12(i)(j)} = 1 & (1^{st} \text{ layer, contact n.º 2}) \\ a_{18(i-1)(j)} = 1 & (1^{st} \text{ layer, contact n.º 8}) \end{cases} \tag{3.33}$$

Up-date of b – STEP 13

Since the contact matrix of the rth and the $(r-1)^{th}$ filaments are up-dated before, the value of *b* need to be actualized.

Definition of an additional time period for the last filament deposited – STEP 14

At this point, a procedure is made to identify if the actual deposited filament is the last. In this case, a new higher limit is defined for the computational time, according with the data introduced in STEP 2.

Definition of the values of TCV₁ and TCV₂ for the rth filament – STEP 15

Before the computation of temperatures at the next instant, the values of $TCV_1(r)$ and $TCV_2(r)$ need to be computed and consequently vectors *save_lim* and *T_begin* are updated. For unidirectional sequences:

$$\text{Initial time} \rightarrow TCV_1(r) = \frac{\left[\left(r - \cos\left(\frac{\pi}{4}\left(1-(-1)^r\right)\right)\right)L + (-1)^r x\right]}{v} \qquad (3.34)$$

$$\text{Initial temperature} \rightarrow TCV_2(r) = T_L$$

Up-date of the values of TCV₁ and TCV₂ for the $(r – 1)^{th}$ filament – STEP 16

Since the $(r – 1)^{th}$ filament contacts with the rth filament, the values of $TCV_1(r – 1)$ and $TCV_2(r – 1)$ need to be once more computed. As expressed in equation (3.35), the new initial time (TCV_1) is equal to the instant at which the contact arises, i. e., when the rth filament starts cooling down and the new initial temperature (TCV_2) is equal to the last computed temperature (just before the beginning of this new contact).

For unidirectional sequences, if t_{last} is the last time before the deposition of the rth filament:

$$\text{New initial time} \rightarrow TCV_1(r-1) = \frac{\left[\left(r - \cos\left(\frac{\pi}{4}\left(1-(-1)^r\right)\right)\right)L + (-1)^r x\right]}{v} \qquad (3.35)$$

$$\text{New initial temperature} \rightarrow TCV_2(r-1) = T_{r-1}(t_{last})$$

Then, these values replace the previous values of $TCV_1(r–1)$ and $TCV_2(r –1)$ in the vectors *save_lim* and *T_begin*.

Iterative process to compute the temperatures of the filaments – STEP 17

Considering that the temperatures of two adjacent filaments are known at the instant t. The objective is to compute simultaneously the temperatures of these two adjacent filaments at the next instant, that is, at $t + \Delta t$ (Figure 3.45).

68
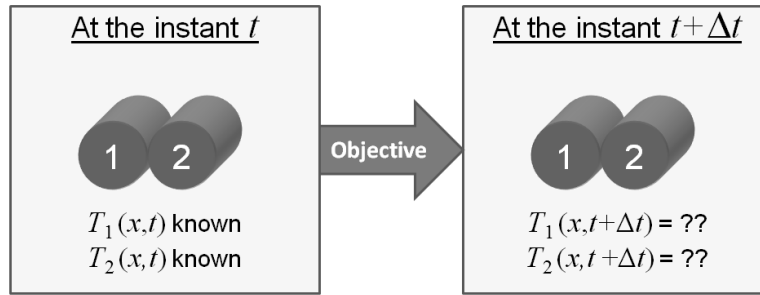
Figure 3.45 – Example of two adjacent filaments at two consecutive instants.

Since the two filaments 1 and 2 are in contact, the computation of $T_1(x,t + \Delta t)$ requires the value of $T_2(x,t + \Delta t)$, which is unknown, and vice versa. Consequently, an iterative process with a convergence error μ (ºC), must be applied to compute the temperatures for all the pairs of adjacent filaments (Figure 3.46).
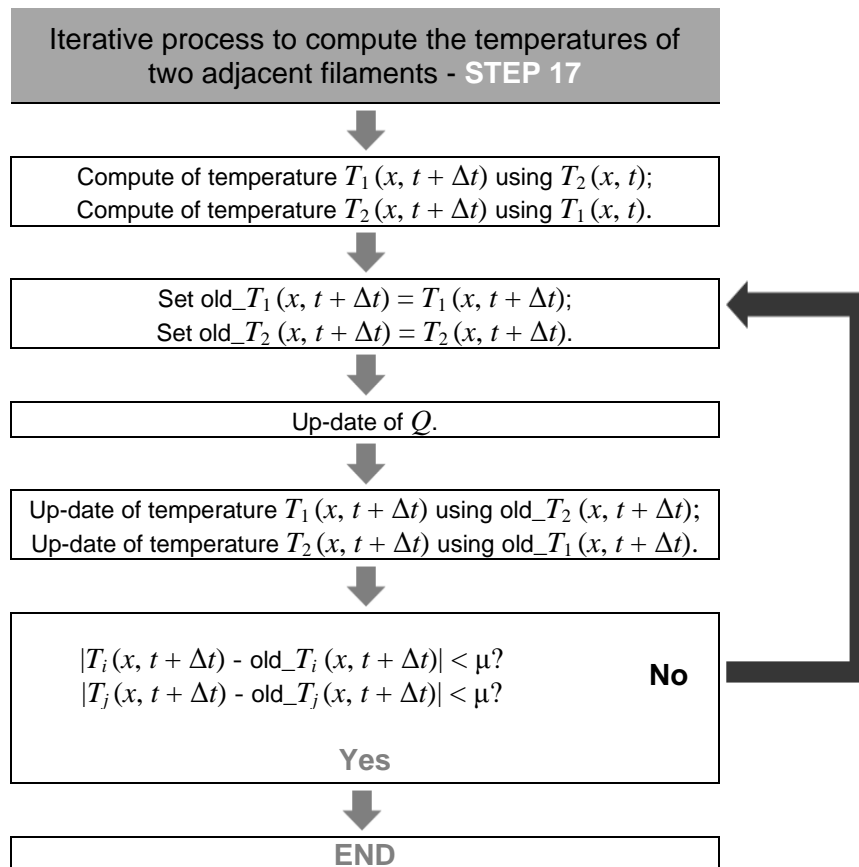
Figure 3.46 – Iterative process to compute the temperatures.

Verification of the value of B_i – STEP 18

Since new conditions were defined for the two last filaments, the values of Biot number B_i are actualized in order to verify if these remain lower than 0.1. The same procedure as STEP 11 is followed.

Following the same procedure for the first layer, the contacts must be previously activated, considering two differences:

- The horizontal contacts also occur between actual and the previous filaments, but due to the continuous deposition, a direction change occurs every time a new layer is deposited. For unidirectional filaments, this modifies the number of the activated contact, that switches between n.º 2 and n.º 8 (Table 3.8), as shown in the example of Figure 3.47, while for perpendicular sequences, a more complex change due to the different orientations of filaments. Details about perpendicular sequences are more described later.

- The vertical contacts need to be now considered between filaments of two distinct adjacent layers.

When the element of filament 6 is deposited:
Horizontal contacts for the last filament (6):
Contact nº 8 is activated for filament 6.
Horizontal contacts for the previous filament (5):
Contact nº 2 is activated for filament 5.

When the element of filament 9 is deposited:
Horizontal contacts for the last filament (9):
Contact nº 2 is activated for filament 9.
Horizontal contacts for the previous filament (8):
Contact nº 8 is activated for filament 8.

Figure 3.47 – Change of the horizontal contacts number between two successive layers (unidirectional filaments).

Consequently, a procedure must be developed in order to adapt the contacts number as a function of the deposition direction and to identify the filament position of the previous layer that contacts with the actual one. Since this procedure depends on the deposition sequence type, three distinct strategies were created and implemented in the code.

➢ *Unidirectional and aligned filaments*

For unidirectional and aligned filaments, the horizontal contacts must be defined as a function of the deposition direction. If r is the actual deposited filament and $r > n_{prev\_lay} + 1$, where n_{prev_lay} is the position of the last filament that allows to the previous layer:

$$\text{If the position layer is even :} \begin{cases} a_{r8} = 1 \\ a_{(r-1)2} = 1 \end{cases}$$

$$\text{else :} \begin{cases} a_{r2} = 1 \\ a_{(r-1)8} = 1 \end{cases} \tag{3.36}$$

With respect to the vertical contacts, the bottom contact for the last deposited filament r with the adjacent filament of the previous layer is activated (contact n.° 5):

$$a_{r5} = 1 \tag{3.37}$$

And, this contact must be also activated for the filament of the previous layer (top contact). The position of this filament is calculated by:

$$-r + 2 \times n_{prev\_lay} + 1 \tag{3.38}$$

Thus, the contact for this is activated (contact n.° 10):

$$a_{(-r+2 \times n_{prev\_lay}+1)(10)} = 1 \tag{3.39}$$

➢ *Unidirectional and skewed filaments*

For skewed filaments, two possibilities are included: skewed to right and skewed to left (Figure 3.38). In each case, the contacts are different, and also depend on the layer number (odd or even position of layer). With respect to the horizontal contacts, the procedure is the same as for aligned filament (equation (3.36)). For vertical contacts, the process is different.

For skewed to right and even layers, if the rth filament is not the first of the layer, the following contacts are activated:

$$\begin{cases} a_{r6} = 1 \\ a_{(-r+2 \times n_{prev\_lay}+2)(11)} = 1 \end{cases} \tag{3.40}$$

and, if the rth filament does not have contact with left lateral support:

71

$$\begin{cases} a_{r3} = 1 \\ a_{(-r+2\times n_{prev\_lay}+1)(9)} = 1 \end{cases} \qquad (3.41)$$

For skewed to right and odd layers, if the rth filament does not have contact with right lateral support:

$$\begin{cases} a_{r6} = 1 \\ a_{(-r+2\times n_{prev\_lay})(11)} = 1 \end{cases} \qquad (3.42)$$

and, for all the filaments of the layer:

$$\begin{cases} a_{r3} = 1 \\ a_{(-r+2\times n_{prev\_lay}+1)(9)} = 1 \end{cases} \qquad (3.43)$$

For skewed to left and even layers, for all the filaments of the layer:

$$\begin{cases} a_{r6} = 1 \\ a_{(-r+2\times n_{prev\_lay}+1)(11)} = 1 \end{cases} \qquad (3.44)$$

and, if the rth filament does not have contact with left lateral support:

$$\begin{cases} a_{r3} = 1 \\ a_{(-r+2\times n_{prev\_lay})(9)} = 1 \end{cases} \qquad (3.45)$$

For skewed to left and even layers, if the rth filament does not have contact with right lateral support:

$$\begin{cases} a_{r6} = 1 \\ a_{(-r+2\times n_{prev\_lay}+1)(11)} = 1 \end{cases} \qquad (3.46)$$

72

and, if the rth filament is not the first of the layer:

$$\begin{cases} a_{r3} = 1 \\ a_{(-r+2 \times n_{prev\_lay} + 2)(9)} = 1 \end{cases}$$

(3.47)

> ➤ *Perpendicular filaments*

As explained before, due to the orientation changes in perpendicular sequences, the filaments are subdivided into square elements of width w, which are characterized by the layer number, the vertical position and the horizontal position (Figure 3.42). Since temperatures of each element are computed, contacts and initial conditions must be also computed for each one. Contacts are activated depending on the orientation of the filaments of the actual layer and the number of filaments of the previous layers. However, while that for unidirectional sequences, the definition of contacts only depend on the position of the layer (odd or even position number), for perpendicular sequences, four distinct situations must be considered, for each orientation. Figure 3.48 shows the four possible senses of deposition for vertical filaments, characterized by the start point *canto_0*. These start points are numbered from 1 to 4, and must be established for each layer in order to define the orientation of the deposition.
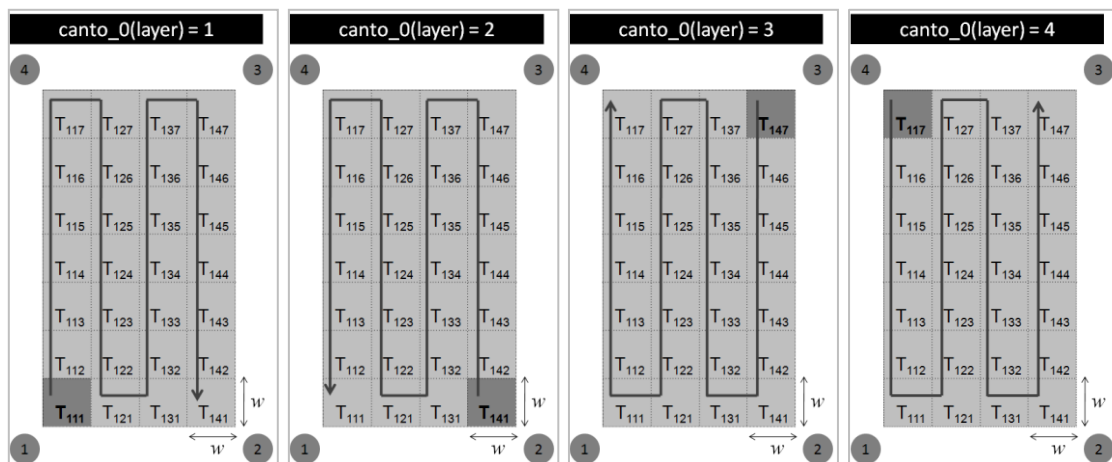
Figure 3.48 – Possible deposition orientations for a layer of vertical filaments of a perpendicular sequence.

For horizontal filaments, four situations must be also considered being each of them defined by the start corner number (Figure 3.49).
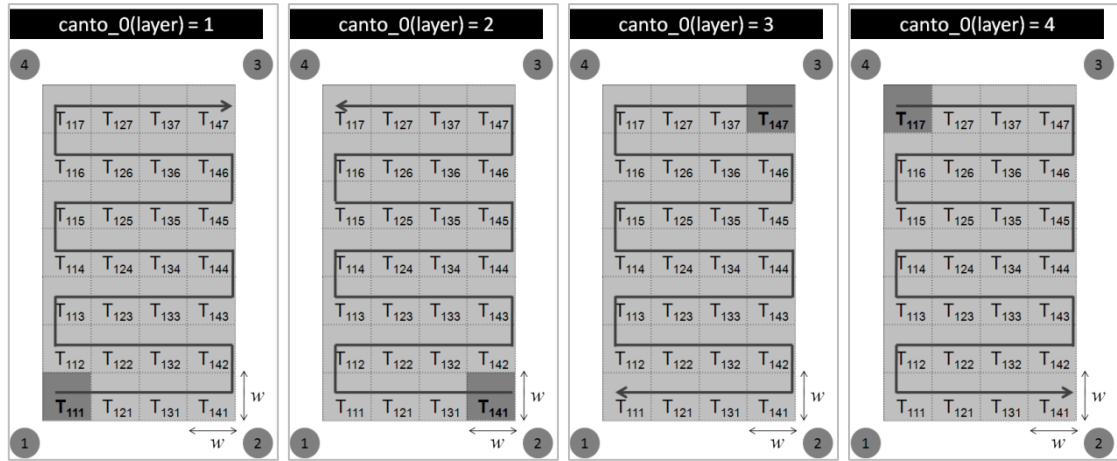
Figure 3.49 – Possible deposition orientations for a layer of horizontal filaments of a perpendicular sequence.

In the code, the start corners are saved in the vector *canto_0* of dimension $m \times 1$:

$$canto\_0 = \begin{bmatrix} canto\_0(1) = 1 \\ canto\_0(2) \\ canto\_0(3) \\ \vdots \\ canto\_0(m) \end{bmatrix} \begin{matrix} \rightarrow \text{ start corner of } 1^{st} \text{ layer} \\ \rightarrow \text{ start corner of } 2^{nd} \text{ layer} \\ \rightarrow \text{ start corner of } 3^{rd} \text{ layer} \\ \vdots \\ \rightarrow \text{ start corner of } m^{th} \text{ layer} \end{matrix} \qquad (3.48)$$

The start corner of the actual layer is computed based on three parameters:

- Filaments orientation of previous layer (horizontal or vertical);

- Filaments number of previous layer (odd or even number);

- Start corner *canto_0* of previous layer (1, 2, 3 or 4).

The relationships between these and the start corner of the actual layer are shown in Table **3.11** and implemented in the code. By using this, the definition of the horizontal contacts can thus be defined.

74

Table 3.11 – Procedure to determine the start corner of the actual layer *lay* (*lay* > 1).

The filaments of the previous layer are VERTICAL			The filaments of the previous layer are HORIZONTAL		
Start corner of the previous layer ↓	ODD number of filaments in the previous layer	EVEN number of filaments in the previous layer	Start corner of the previous layer ↓	ODD number of filaments in the previous layer	EVEN number of filaments in the previous layer
canto_0(lay-1)=1	canto_0(lay)=3	canto_0(lay)=2	canto_0(lay-1)=1	canto_0(lay)=3	canto_0(lay)=4
canto_0(lay-1)=2	canto_0(lay)=4	canto_0(lay)=1	canto_0(lay-1)=2	canto_0(lay)=4	canto_0(lay)=3
canto_0(lay-1)=3	canto_0(lay)=1	canto_0(lay)=4	canto_0(lay-1)=3	canto_0(lay)=1	canto_0(lay)=2
canto_0(lay-1)=4	canto_0(lay)=2	canto_0(lay)=3	canto_0(lay-1)=4	canto_0(lay)=2	canto_0(lay)=1

Horizontal contacts (contacts n.º 2 and 8) between elements depend on start corners. If the actual deposited element allows to a layer of vertical filaments, then:

$$
\begin{aligned}
&canto\_0(lay) = 1 \vee canto\_0(lay) = 4 \Rightarrow a_{(lay),2,i,j} = 1 \wedge a_{(lay),8,(i-1),j} = 1 \\
&canto\_0(lay) = 2 \vee canto\_0(lay) = 3 \Rightarrow a_{(lay),8,i,j} = 1 \wedge a_{(lay),2,(i+1),j} = 1
\end{aligned}
\tag{3.49}
$$

and, if the actual deposited element allows to a layer of horizontal filaments:

$$
\begin{aligned}
&canto\_0(lay) = 1 \vee canto\_0(lay) = 2 \Rightarrow a_{(lay),2,i,j} = 1 \wedge a_{(lay),8,i,(j-1)} = 1 \\
&canto\_0(lay) = 3 \vee canto\_0(lay) = 4 \Rightarrow a_{(lay),8,i,j} = 1 \wedge a_{(lay),2,i,(j+1)} = 1
\end{aligned}
\tag{3.50}
$$

On the other hand, vertical contacts don't depend on the start corners. If the actual deposited element allows to the layer *lay*, and has vertical position *i* and horizontal position *j*, the bottom contact (contact n.º 5) for it is activated:

$$
a_{lay,5,i,j} = 1
\tag{3.51}
$$

Consequently, the top contact (contact n.º 10) of the element that is under it is also activated. This element has the same vertical/horizontal position, but allows to the layer (*lay* – 1), that is, to the previous layer:

$$
a_{(lay-1),10,i,j} = 1
\tag{3.52}
$$

Procedures described above to activate the contacts are implemented in the code, depending on the deposition sequence type. After actualization of the contacts, variable b and values of TCV_1 and TCV_2 are up-dated (due to the new contacts), and temperatures are computed using the iterative process, as done for the first layer. The Biot number value is always verified along the computation process.

4 EXPANDING THE SCOPE OF THE MODEL

The objective is now to expand the model, by including the mechanical deformation and the adhesion. In fact, the knowledge of the final deformation allows determining the contact fraction and the computation of adhesion allows controlling the thermal contact conductance between adjacent filaments (Figure 4.1). Without this study, the contact lengths and thermal contact conductance are variables defined by the user in the initial section of code.
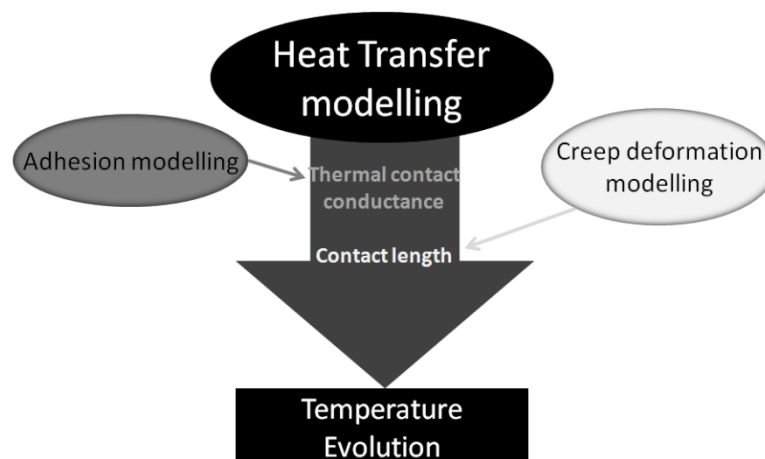
Figure 4.1 – Role of adhesion and mechanical deformation modeling in the computer code.

4.1 MECHANICAL DEFORMATION

The mechanical deformation must be now studied and possibly included in the developed MatLab® code in order to expand the modelling of FFE heat transfer. Since the used material is a polymer, an analysis of the viscoelastic behaviour of the filaments needs to be made, depending on the temperature evolution along deposition time. This analysis was concretized with ABAQUS® software in order to evaluate the importance of the viscoelastic component in the deformation of the filaments.

4.1.1 Conditions of the mechanical deformation study

For the mechanical deformation analysis, an extreme situation was considered: 200 vertically filaments, where each is deposited every 0.5 second. The objective is to compute the deformation of the first, which supports the biggest weight.

Figure 4.2 illustrates the case study, where *h* and *w* are respectively the initial height and width of the first filament: ABAQUS® 3D simulation will devolve the values of *h'* and *w'*, the respective final height and width of the first filament.
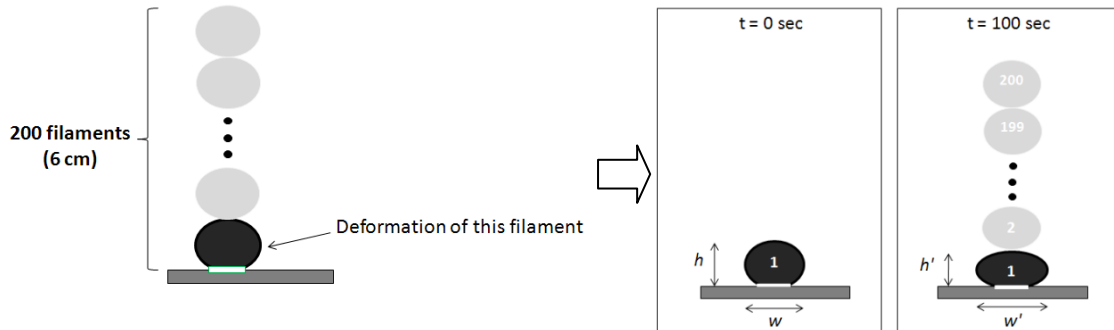
Figure 4.2 – Case study for the mechanical deformation study (Cross section view).

For this case study, two 3D simulations were made: with elastic and viscoelastic properties. The objective is to compare the values of |*h'* − *h*| and |*w'* − *w*| between the two analysis and conclude about the importance of considering a viscoelastic response. In the two simulations, the following conditions were applied to the 1st filament: the gravity force and a pressure of 2067.8 N/m^2, which corresponds to the weight of 199 top filaments. Since these top filaments are deposited successively, the applied pressure cannot be activated instantaneously (Default Load Variation with Time, Table 4.1).

Table 4.1 – ABAQUS® parameters for the mechanical deformation study.

Property	Value
Elements Number	4832
Mesh Type	Wedge
Element Type	C3D8R: 8-node linear brick, reduced integration, hourglass control.
Step Type	Simulation 1: Static General
	Simulation 2: Visco
Increment Size	Initial = 10^{-25} s
	Minimum = 10^{-50} s / Maximum = 0.5 s
Solution Technique	Full Newton
Default Load Variation with Time	Ramp linearly over step
Output Request	U, Displacement

4.1.2   Definition of the viscoelastic properties of the material

In ABAQUS® software, the linear viscoelastic behaviour is described by the generalized Maxell model, also known as Prony series, which offers a straightforward fitting approach to experimental data (Drabousky 2009). Prony series representation is a finite series of exponential decay elements, which allows representing mathematically the time-dependent shear modulus $G(t)$ (Brinson and Brinson 2008) as:

$$G(t)/G_0 = 1 - \sum_{i=1}^{n_p} g_i \left(1 - e^{\frac{-t}{\tau_i}} \right)$$

(4.1)

Where $G_0 = G(0)$ is the initial shear modulus of the material (Pa), g_i is the ith Prony constant, τ_i is the ith Prony retardation time constant and n_p is the number of Prony terms. Note that:

$$\sum_{i=1}^{n_p} g_i \leq 1$$

(4.2)

Then, in order to define the viscoelastic properties of the material in ABAQUS®, three steps are required: i) to find in literature experimental data of the time-dependent shear modulus $G(t)$ for a polymer, ii) to determine the Prony terms that allow representing mathematically the selected curve in i), and, iii) to introduce the Prony terms in the ABAQUS® simulations.

Consequently, in a first step, the following graphic was considered, where the Young modulus E of Polymethyl methacrylate (PMMA) is represented in function of time. Three distinct temperatures were selected: 95ºC, 110ºC and 135ºC (Figure 4.3).
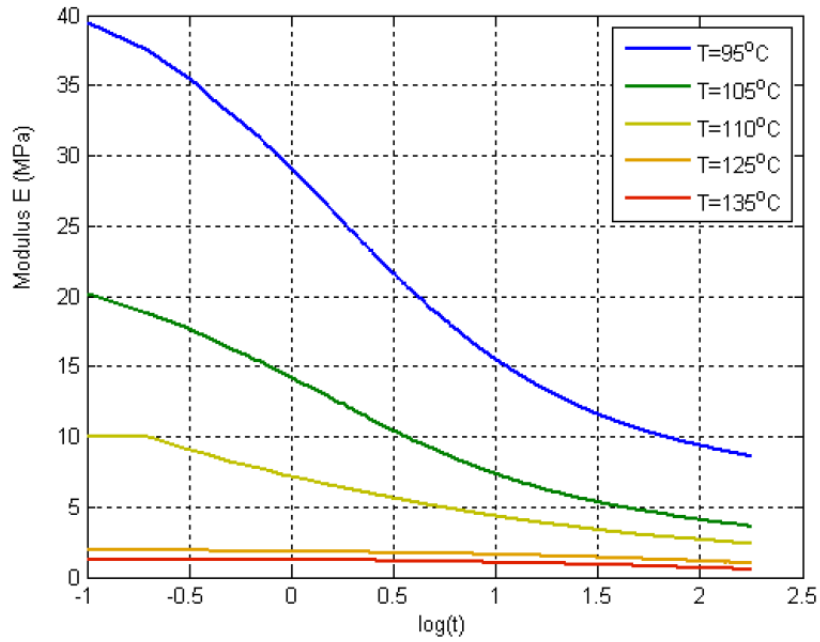
Figure 4.3 – Young Modulus E vs log(t) for PMMA at five distinct temperatures (Vogtmann 2009).

The values of $E(t)$ are then extracted from the previous graphics, and introduced in a table, for each chosen temperature (Table 4.2):

Table 4.2 – Values of $E(t)$ for PMMA deduced from Figure 4.3.

log(t)	Time (sec)	E in GPa (95 ºC)	E in Gpa (110 ºC)	E in GPa (135 ºC)
-1	0,10	39,53	10,00	1,32
-0,5	0,32	35,31	9,06	1,32
0	1,00	29,06	7,19	1,32
0,5	3,16	21,56	5,63	1,18
1	10,00	15,47	4,38	1,05
1,5	31,62	11,56	3,44	0,92
2	100,00	9,39	2,66	0,66

Assuming small deformations, the following relationship can be used to compute the shear modulus $G(t)$:

$$G(t) = \frac{E(t)}{2(1+v_p)} \tag{4.3}$$

Where v_p is the Poisson coefficient.

With $v_p = 0.4$, the following values of $G(t)$ are obtained (Table 4.3):

80

Table 4.3 – Values of $G(t)$ for PMMA.

log(t)	Time (s)	G in GPa (95ºC)	G in Gpa (110ºC)	G in GPa (135ºC)
-1	0,10	14,12	3,57	0,47
-0,5	0,32	12,61	3,24	0,47
0	1,00	10,38	2,57	0,47
0,5	3,16	7,70	2,01	0,42
1	10,00	5,53	1,56	0,38
1,5	31,62	4,13	1,23	0,33
2	100,00	3,35	0,95	0,24

Then, the Prony terms need to be determined. For this, the following MatLab® code was created:

```
function iterative_prony(n,tabela,G_0)
tau(1,1) = 0.1; tau(1,2) = 1; tau(1,4) = 100; k = 0;
for i = 1:1
   for j = 2:9
       k = k + 1; tau(1,3) = i;
       [prony_coef,erro] = prony(n,tabela,tau,G_0); matrix(k,:) = [tau,prony_coef,erro];
   end
end
[lin,col] = size(matrix);
fid = fopen('results_prony.txt','wt');
for i = 1:lin
   for j = 1:(col-1)
      fprintf(fid,'%8.2f',matrix(i,j));
   end
   fprintf(fid,'%8.4f \n',matrix(i,col));
end
fclose(fid);
```

This code allows obtaining the best Prony terms from introduced data. For $n_p = 4$ Prony terms, the following results were obtained, for each temperature (Table 4.4):

Table 4.4 – Prony series representation of $G(t)$ for PMMA.

E in GPa (95 ºC)		E in Gpa (110 ºC)		E in GPa (135 ºC)	
τ_i	g_i	τ_i	g_i	τ_i	g_i
0,1	0,01	0,1	0,01	0,1	0,01
1	0,34	1	0,35	1	0,01
7	0,33	7	0,24	5	0,15
100	0,13	100	0,21	100	0,52

These results can be compared with the experimental data of $G(t)$ for the three temperatures in Figure 4.4, Figure 4.5 and Figure 4.6, where the rigour of Prony series representation shows to be evident.
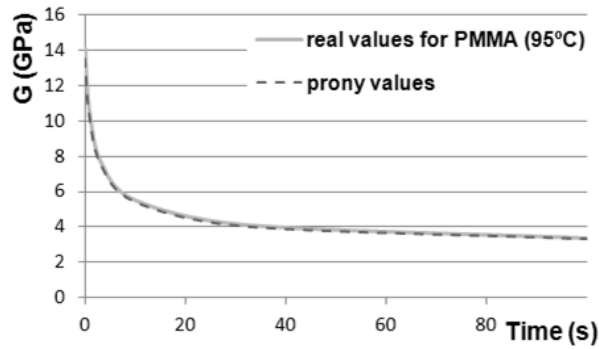
Figure 4.4 – Experimental data and Prony series representation of $G(t)$ for T = 95ºC.
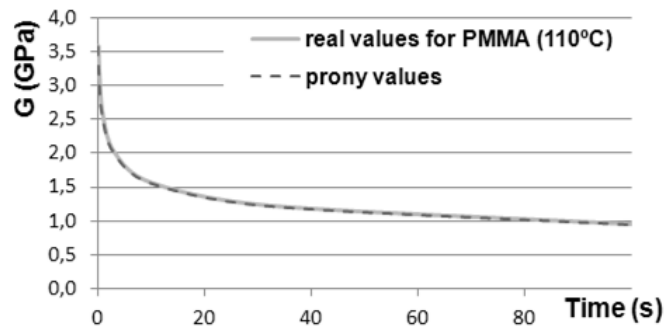
Figure 4.5 – Experimental data and Prony series representation of $G(t)$ for T = 110ºC.
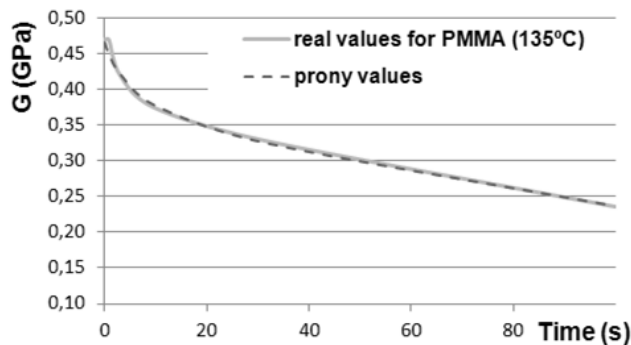
Figure 4.6 – Experimental data and Prony series representation of $G(t)$ for T = 135ºC.

4.1.3   Results and conclusions from the deformation study

The vertical deformation of the first filament (in %) with viscoelastic and elastic properties can be observed respectively in Figure 4.7 and Figure 4.8. As expected, the raise of the material temperature increased the vertical deformation. In addition, with elastic properties, the decrease of filament height is lower. However, since the deformation is very small in all the cases (< 0.5%), the observed differences are not significant.
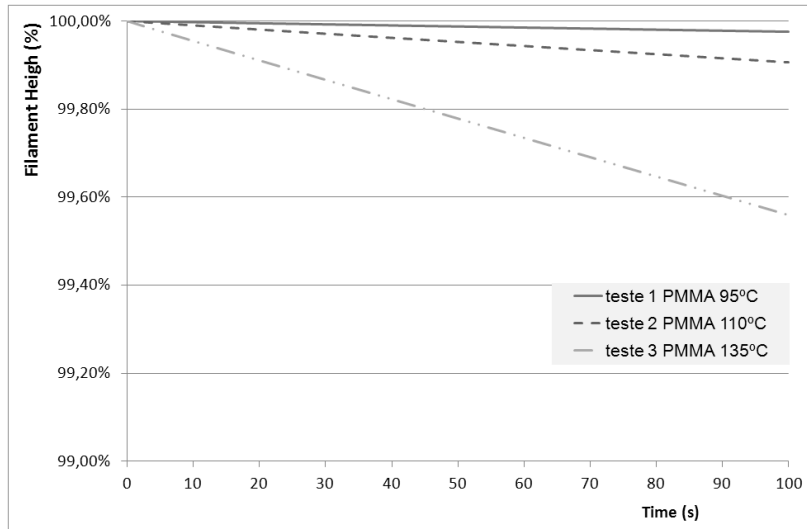
Figure 4.7 – Vertical deformation of the first filament (in %) with viscoelastic properties.
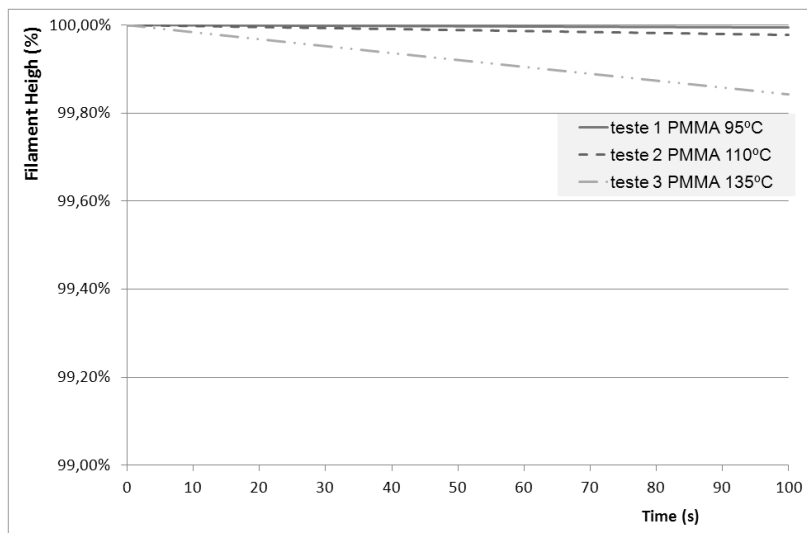
Figure 4.8 – Vertical deformation of the first filament (in %) with elastic properties.

Horizontal deformation of the first filament (in %) with viscoelastic and elastic properties are respectively shown in Figure 4.9 and Figure 4.10. The same conclusions can be made: higher material temperature and viscoelastic properties increase the horizontal deformation, which is lower than the vertical deformation ($< 0.3\%$).
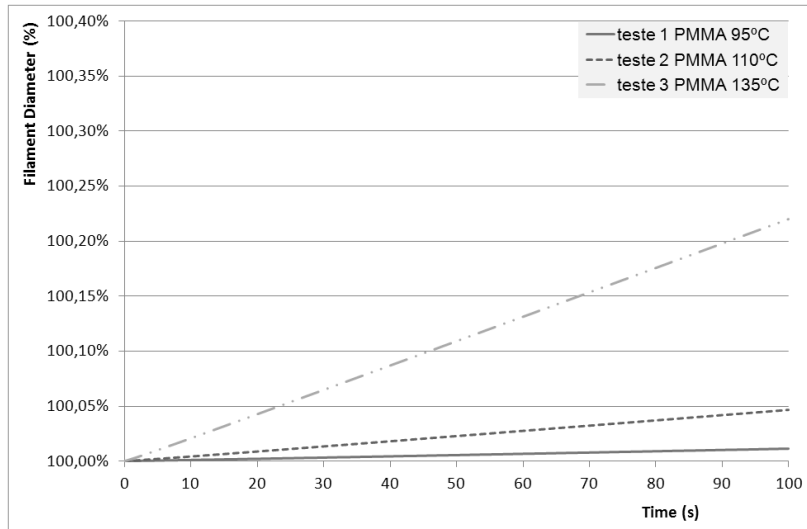
Figure 4.9 – Horizontal deformation of the first filament (in %) with viscoelastic properties.
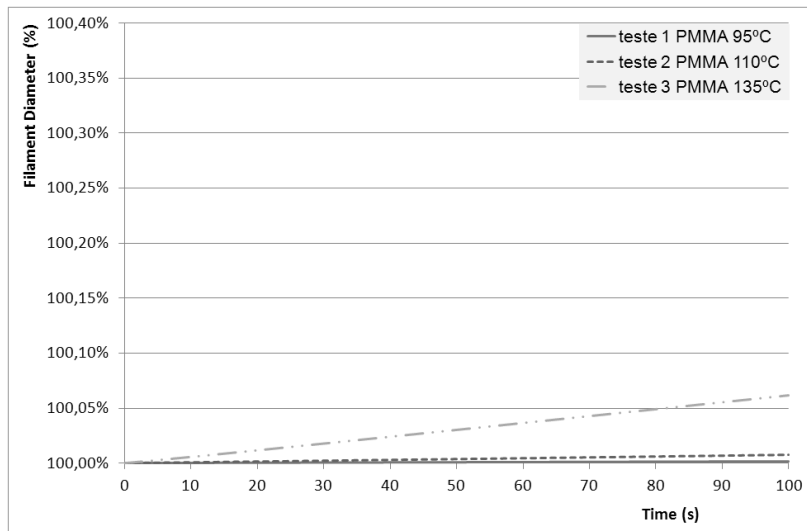
Figure 4.10 – Horizontal deformation of the first filament (in %) with elastic properties.

Since the deformation of the first filament is obtained in function of time, the total vertical deformation of the part (200 vertical filaments) can be deduced. As an example, if 4 filaments are considered (Figure 4.11), the deformation of the 4th filament, only due to the gravity force, is the same as the deformation of the 1st filament at $t = 0.5$ s, where only the gravity force is considered. As another example, the 3rd filament has only one filament on top, so, it will have the same deformation as the 1st filament after 1 second, because in the interval [0,5 s; 1 s], the 2nd filament stays on top of the 1st since $t = 0.5$ s. The same logic is used for the others filaments.

84

Consider that we have 4 filaments:
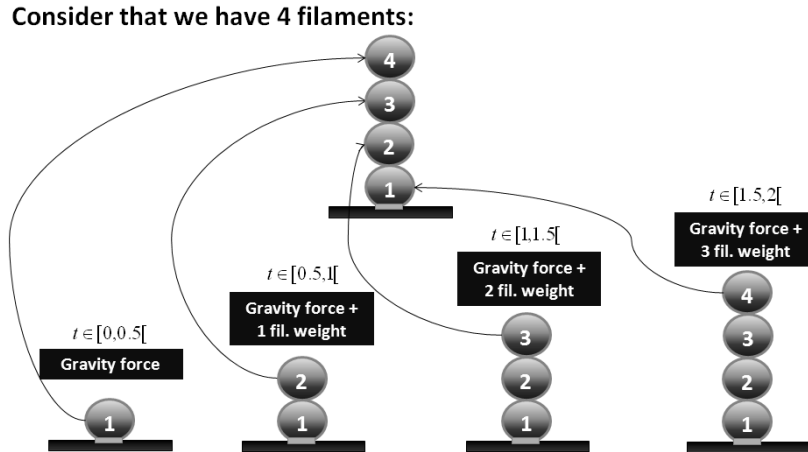
Figure 4.11 – Successive mechanical conditions along deposition time for 4 filaments.

Resuming, the total deformation can be obtained by adding the deformations of the first filament at $t = 0.5$ s, at $t = 1$ s, …, at $t = 100$ s. The results of total vertical deformation can be observed in Table 4.5.

Table 4.5 – Total vertical deformation for the part of 60 mm (200 filaments).

	Temperature PMMA		
	95ºC	**110ºC**	**135ºC**
Height Part - Viscoelastic (mm)	59.993	59.972	59.867
Deformation Height Part - Viscoelastic (%)	0.01%	0.05%	0.22%
Height Part Elastic - (mm)	59.998	59,993	59.952
Deformation Height Part - Elastic (%)	0%	0.01%	0.08%
Percentage Difference between the two models for the Height	0.01%	0.04%	0.14%

From these results, we can conclude that the vertical deformation is not significant for the two regimes (< 0.3 %), and that the differences between these are very small (< 0.2 %). Consequently, two important conclusions can be made from these results:

- Since the differences between the viscoelastic regime and the elastic regime are not significant, the viscoelastic component can be neglected;
- The total deformation is not significant, so, the deformation of the filaments during the FFE process can be ignored.

Then, the MatLab® code remains the same, that is, with an expression for temperature obtained from a heat transfer analytical study: no mechanical deformation procedure will be included in the code, since its importance is insignificant in the dimensional stability (length of contacts will so continue to be controlled by the user).

4.2 ADHESION

As described in chapter 3, heat transfer in FFE was modelled by solving a differential equation aiming develop a MatLab® code that computes the temperature evolution for any filament for a set of depositions sequences. At this point, the objective is to include a procedure that allows computing the adhesion degree between all the pairs of adjacent filaments in order to estimate the mechanical quality of the part as well as to assist the deciders about the processing variables for a specific part. For this, the bonding degree proposed by Yang and Pitchumani (2002), which showed good agreement with experimental results, was used (equation (2.9)). The computation of $D_h(t)$ requires the knowledge of two variables: the temperature in the interface between the adjacent filaments and the welding time of the material. As described in section 2.2.4, Sun (2004) also applied this model to calculate the bonding degree, but used the temperature values obtained from experiences and the welding time proposed by Rodriguez for ABS P400 (equation (2.10)). In this work, this welding time will be also used, but in conjunction with temperatures computed from MatLab® code, giving the possibility of testing the importance degree of many FFE parameters on the adhesion.

The expression (2.9) is then included in the algorithm and the following assumptions were made:

- The trapezoidal method is used to calculate the integral in the expression of $D_h(t)$;
- The adhesion is assumed to be perfect when the bonding degree $D_h(t)$ reaches the unity value 1. Therefore, $D_h(t)$ is only computed while its value is lower than 1;
- The healing degree $D_h(t)$ is computed only when the material temperature is above its glass transition point T_g (condition valid for amorphous polymers);
- The temperature at the interface between two adjacent filaments is the average temperature between them;
- Since contacts occur at different instants, for a specific pair of adjacent filaments, $D_h(t)$ is computed from $t = t_c$, where t_c is the instant at which the contact between them starts (s). Considered the two last assumptions, equation(2.9) is rewritten as:

$$D_h(t) = \left[\int_{t_c}^{t} \frac{1}{t_w(T_M(t))} dt \right]^{1/4} \qquad (4.4)$$

Where $T_M(t)$ is the average temperature between the two adjacent filaments (ºC).

- A relationship between thermal contact conductance and adhesion degree is considered (Figure 4.12): since polymers have a low thermal conductivity, the thermal contact conductance is assumed to be low (high thermal resistance) while the adhesion degree is lower than 1. When it reaches the unity value, i. e., when the interface disappears, the thermal contact conductance must be newly defined with a higher value.

The bonding degree is computed for each pair of adjacent filaments: $D_h(t) = \left[\int_{t_c}^{t} \frac{1}{t_w(T_M(t))} dt \right]^{1/4}$

If $D_h(t) < 1$:
- bad adhesion
- low thermal contact condutance.

If $D_h(t) \geq 1$:
- good adhesion
- high thermal contact condutance.
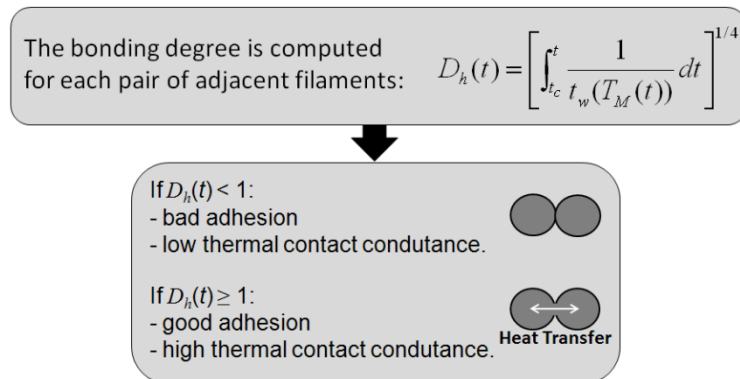
Heat Transfer

Figure 4.12 – Relation between thermal contact conductance and adhesion degree.

The heat transfer MatLab® code described in the last chapter was modified and the flowchart illustrated in Figure 3.40 up-dated in order to include the adhesion component. The resulting flowchart was shown in Figure 4.13.

MATLAB CODE	INPUT COMMAND WINDOW

MATLAB CODE

Definition of the variables

- Deposition sequence parameters
- Computation variables
- Dimensions of vectors and matrices
- **Thermal contact conductance values for all the contacts – STEP 1**
- FFE variables
- Up-dating times
- Contact matrix and contacts with support (TCV$_3$)
- Matrix of temperature values

INPUT COMMAND WINDOW

- Deposition sequence;
- Deposition mode (unidirectional and aligned, skewed, or perpendicular);

- Cross section x.

Computation of the temperature of the 1st filament (1st layer)

- Computation of b and Q
- Definition of the values TCV$_1$ and TCV$_2$ for the 1st filament
- Computation of the temperatures
- Verification of the Biot Number value (Bi)

Computation of the temperature of the rth filament, r > 1 (j^{th} layer, $j \geq 1$)

- Up-date of the contact matrix (horizontal contacts);
- **Definition of the specific position of new pairs of adjacent filaments – STEP 2**
- **Definition of the instant at which the new contacts start – STEP 3**
- Up-date of b
- Definition of an additional time period for the last filament deposited
- Definition of the values of TCV-1 and TCV-2 for the rth filament
- Up-date of the values of TCV-1 and TCV-2 for the filaments with new contacts
- Iterative process to compute the temperatures of the filaments
- **Computation of the bonding degree D_h – STEP 4**
- **Verification of the bonding degree D_h for each pair of adjacent filaments – STEP 5**
- Verification of the value of Bi.

OUTPUT

Text Document with:
- Evolution of temperature during deposition for all the filaments.
- **Evolution of adhesion degree for all the contacts.**

Figure 4.13 – General procedure to compute all the temperatures and bonding degree.

Thermal contact conductance values for all the contacts – STEP 1

Previously, when only the heat transfer was considered, the thermal contact conductance was constant along the process and had the same value for all the contacts. However, in practice, the thermal contact conductance depends on the adhesion: when the perfect adhesion between two adjacent filaments is reached, the thermal resistance tends to zero since the interface disappears (increasing consequentially the thermal contact conductance). The thermal contact conductance is now a non-constant variable that must be defined/up-dated for each contact, depending on the adhesion degree.

A 2D matrix (valid for unidirectional sequences) H of dimension $N \times N$ was then generated to save the values of thermal contact conductance for all the contacts:

$$
\begin{aligned}
&For\, i \in \{1,2,...,N\}, j \in \{1,2,...,N\}: \\
&H_{i,j} = \text{thermal contact conductanc e for the contact} \\
&\text{between th e filaments } i \text{ and } j
\end{aligned}
\qquad (4.5)
$$

For perpendicular sequences, a 4D matrix of dimension $m \times 11 \times ver \times hor$ is defined as:

$$
\begin{aligned}
&For\, lay \in \{1,2,...,m\}, s \in \{2,5,8,10\}, i \in \{1,2,...,ver\}, j \in \{1,2,...,hor\}, \\
&H_{lay,s,i,j} = \text{thermal contact conductanc e for the } s^{th} \text{ contact} \\
&\text{of the element th at allows to the } lay^{th} \text{ layer, at the vertical} \\
&\text{position } i \text{ and the horizontal position } j
\end{aligned}
\qquad (4.6)
$$

As referred before, a low thermal contact conductance, h_{min} , is considered before the adhesion (usually 0.0001 W/m².°C), and a higher value, h_{max}, is expected after this (usually 250 W/m².°C). Therefore, the matrix H, which contains the values of thermal contact conductance for all the existing contacts (equations (4.5) and (4.6)), defined before the computation of temperatures, as:

$$
\begin{aligned}
&Unidirectional\ sequences: H_{i,j} = h_{\min}, \forall i \in \{1,2,...,N\}, j \in \{1,2,...,N\} \\
&Perpendicular\ sequences: \begin{cases} H_{lay,s,i,j} = h_{\min} \\ \forall lay \in \{1,2,...,m\}, s \in \{2,5,8,10\}, \\ i \in \{1,2,...,ver\}, j \in \{1,2,...,hor\} \end{cases}
\end{aligned}
\qquad (4.7)
$$

During the computation of the temperatures and adhesion degree, the matrix H is updated and every time a pair of adjacent filament reaches the perfect bond, the maximum value of thermal contact conductance is assumed for this contact. Then, for unidirectional sequences, when the adhesion occurs between filaments i and j:

$$
H_{i,j} = h_{\max}, for\, i \in \{1,2,...,N\}, j \in \{1,2,...,N\}
\qquad (4.8)
$$

And, for perpendicular sequences, when the adhesion occurs for the element (lay, i, j) at the sth contact:

$$\begin{cases} H_{lay,s,i,j} = h_{max} \\ for\ lay \in \{1,2,...,m\}, s \in \{1,2,...,11\}, i \in \{1,2,...,ver\}, j \in \{1,2,...,hor\} \end{cases} \qquad (4.9)$$

Definition of the specific position of new pairs of adjacent filaments – STEP 2

Since the adhesion degree must be computed for all the existing pairs of adjacent filaments, the specific position of the adjacent filaments are saved, based on the actualizations of the contact matrix a. Then, the matrix *contact_fil* was created to save these positions. For unidirectional sequences, it is a 2D matrix of dimension $N \times 11$ where:

$$\forall i \in \{1,2,...,N\}, j \in \{1,2,...,11\}:$$

$$If\ contact\_fil_{i,j} \neq 0 : contact\_fil_{i,j} = \begin{cases} \text{specific position of} \\ \text{filament adjacent} \\ \text{to the i}^{th} \text{ filament} \\ \text{for the j}^{th} \text{ contact} \end{cases},$$

$$Else: \qquad \begin{cases} \text{the j}^{th} \text{ contact} \\ \text{of the i}^{th} \text{ filament} \\ \text{is not activated} \end{cases} \qquad (4.10)$$

As an example, *contact_fil*$_{1,8}$ = 2 means that the 1st filament has the contact n.° 8 activated with the 2nd filament, and *contact_fil*$_{1,8}$ = 0 means that the 1st filament has the contact n.° 8 inactivated.

For perpendicular sequences, three 4D matrices of dimension $m \times 11 \times ver \times hor$ are used to save the specific positions of the adjacent elements: the matrices *contact_lay_o*, *contact_filh_o* and *contact_filv_o* contain, respectively, the layer, the horizontal and vertical positions of the adjacent element.

Definition of the instant at which the new contacts start – STEP 3

Since the adhesion degree between two adjacent filaments is only computed from the instant where the contact starts between them (at t_c), the actual time increment is saved

at this point, i. e. , when the actual contact is activated. These times are successively saved in the matrix *p_0_welding* and will be after used for the computation of D_h.

Computation of the bonding degree Dh – STEP 4

Since the temperatures are known, the bonding degree D_h can be computed for the pairs of filaments that did not adhere previously and while these temperatures are higher than the glass transition temperature. In these conditions, the average temperature for each pair is computed and used to calculate the bonding degree.

The values of D_h are saved in the matrix *adhesion_degree*, in order to obtain the adhesion evolution along time for all the pairs of adjacent filaments (output of code), and to deduce the FFE variables that have the highest impact on the bond quality.

Verification of the bonding degree Dh for each pair of adjacent filaments – STEP 5

At each time increment and after computation the bonding degree (STEP 4), a verification of its value is done for all the pairs of adjacent filaments, in order to up-date the matrix *bond_deg*, which indicates if a specific pair of adjacent filaments reached the perfect adhesion or not.

For unidirectional sequences, *bond_deg* is a 2D matrix of dimension $N \times N$ defined by:

$$For \ i \in \{1,2,...,N\}, j \in \{1,2,...,N\}:$$

$$\begin{cases} bond\_deg(i,j) = 1, \text{if adhesion occured} \\ \text{between filaments } i \text{ and } j \ (D_h \geq 1) \end{cases} \quad (4.11)$$

$$\begin{cases} bond\_deg(i,j) = 0, \text{if adhesion did not occur} \\ \text{between filaments } i \text{ and } j \ (D_h < 1) \end{cases}$$

For perpendicular sequences, *bond_deg* is a 6D matrix of dimension $m \times ver \times hor \times m \times ver \times hor$ defined by:

$$\forall lay_1, lay_2 \in \{1,2,...,m\}, i_1, i_2 \in \{1,2,...,ver\}, j_1, j_2 \in \{1,2,...,hor\}$$

$$\begin{cases} bond\_deg(lay_1,i_1,j_1,lay_2,i_2,j_2) = 1, \text{if adhesion occured} \\ \text{between elements at positions } (lay_1,i_1,j_1) \text{ and } (lay_2,i_2,j_2) \ (D_h \geq 1) \end{cases} \quad (4.12)$$

$$\begin{cases} bond\_deg(lay_1,i_1,j_1,lay_2,i_2,j_2) = 0, \text{if adhesion did not occur} \\ \text{between elements at positions } (lay_1,i_1,j_1) \text{ and } (lay_2,i_2,j_2) \ (D_h < 1) \end{cases}$$

The matrix *bond_deg* is then used to identify the pairs of filaments that reached the perfect quality bond: for these, the maximum thermal contact conductance is defined (up-dating of matrix *H*) and the variable *b* is up-dated. As an example, for unidirectional sequences, the following procedure is used at each time increment, for all the pairs of adjacent filaments that have not yet reached the maximum bond quality:

$$if \ bond\_deg(i,j) = 1, i \in \{1,2,...,N\}, j \in \{1,2,...,N\}:$$
$$\begin{cases} H(i,j) = h_{max} \\ Up-date \ of \ b(i) \ and \ b(j) \end{cases} \tag{4.13}$$

4.3 COMPUTATION CODE FOR HEAT TRANSFER IN FFE FOR BI-MATERIAL PARTS

The geometrical complexity of some specific parts can require the deposition of a second material, identified as a support material, which is removed at the end of the process. Therefore, and with the possibility of use two distinct materials, the material type for each filament needs to be identified during the input variables. Two arguments need to be introduced:

- A matrix representing the deposition sequence, containing *m* rows and *n* columns, for the number of layers and maximum number of filaments in a layer, respectively. Each cell is attributed a value of 0, 1, or 2 for the absence of a filament, the presence of a filament of material A or of a filament of material B, respectively. An example is given in Figure 4.14.
- The vertical cross section *x* of the part (along the filament length) where the user wishes to know the temperature evolution with time.

Since only unidirectional and aligned filaments are available, the deposition sequence type is not indicated.
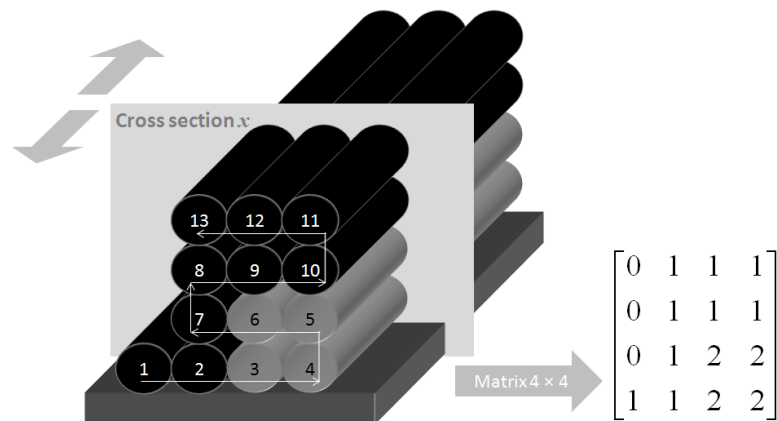
Figure 4.14 – Example of deposition sequence and corresponding input matrix.

Typical parts made by FFE/FDM have not raised dimensions (< 20 cm), but imply a deposition of a very large number of filaments due to the very small width of their cross-section: as an example, for a cube of 10 cm of length, approximately 111 000 filaments are needed. Consequently, the total computation time for testing of adhesion quality can be considerable for parts with real dimensions. To solve this problem, some simplifications were made:

- The convergence error was set to the maximum value: $\mu = 0.1$ ºC.

- A study was made in order to evaluate the maximum time increment Δt that can be used to assure the rigour of temperature results. Figure 4.15 shows the temperature evolution of a filament for 6 distinct values of Δt, with a typical extrusion velocity of $v = 0.025$ m/s, allowing conclude that for $\Delta t > 0.1$ s, differences on the form of temperature peaks occur. Consequently, the time increment is adapted along the process: close to new contacts, $\Delta t = 0.01$s while far way out of these, the maximum time increment $\Delta t = 0.1$ s is used.

- When a large number of filaments is deposited, a lot of them remains at the environment temperature during time enough until new contact occurs. The computation of temperatures of these is then useless and overloads the virtual memory of computer. In order to overcome this problem, a procedure is introduced in the code: every time a new filament is deposited, all the temperatures are computed until they stabilize close to the environment temperature. After this, the computations stop until a new filament is deposited being the procedure repeated (Figure 4.16).
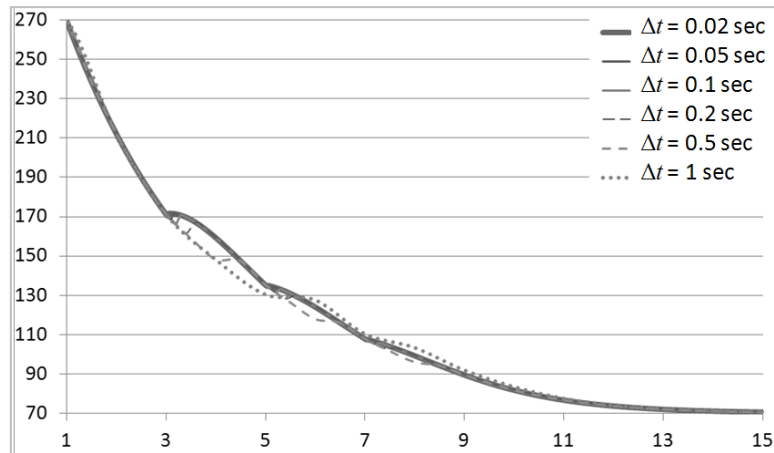
Figure 4.15 – Temperature evolution along deposition time of one filament, for 6 values of Δt, with v = 0.025 m/s.
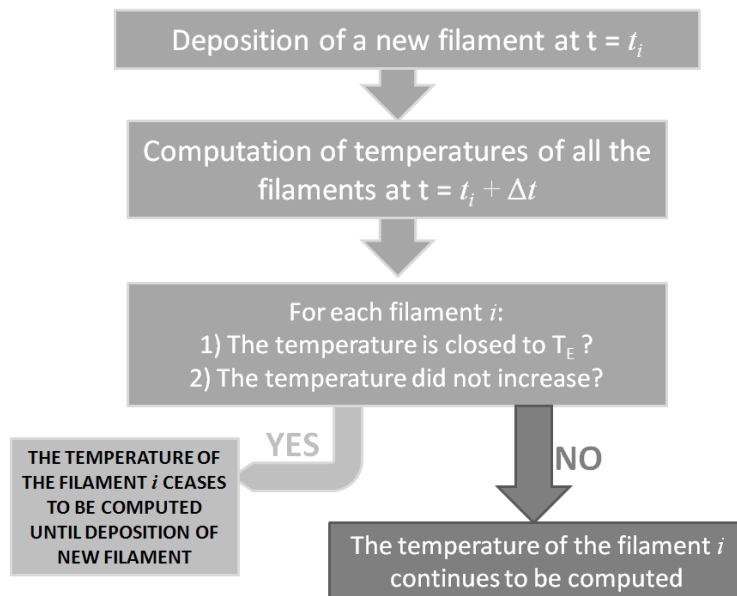
Figure 4.16 – Procedure to simplify the temperatures computation.

With these simplifications, the computation time can be reduced of 90%, problems with virtual memory of computer were solved and the code can quickly localize the regions of the part where the adhesion was not reached, for any real part made by two distinct materials. Process variables can be then modified in order to improve the adhesion and consequently mechanical resistance. In addition, an influence study can be made in order to identify the variables that have the highest impact on the part quality.

5 EXPERIMENTAL VALIDATION

5.1 MATERIALS

Two amorphous polymeric materials were selected for this experimental study: an ABS polymer (ABS FA 4475 Bordeaux – Poliversal) that provides excellent mechanical and chemical properties and a high impact polystyrene HIPS (Polystyrol 495F – BASF) due to its lower cost and most common use. Since the dimensions of the screw of the mini-extruder are low, these materials were ground by using a mill Retsch and liquid nitrogen.

5.1.1 Thermal Properties and Density:

Density ρ (kg/m^3), thermal conductivity k (W/m· ºC) and the specific heat C (J/kg· ºC) are properties needed to compute the temperatures evolution and adhesion. The values of these variables for the used materials are provided by the respective manufacturers and listed in Table 5.1.

Table 5.1 – Material properties of ABS FA 4475 and Polystyrol 495F.

Property	Material	Value
Density (kg/m^3)	ABS FA 4475	1050
	Polystyrol 495F	1030
Thermal conductivity (W/m· ºC)	ABS FA 4475	0.18
	Polystyrol 495F	0.18
Specific Heat (J/kg· ºC)	ABS FA 4475	2200
	Polystyrol 495F	1800

5.1.2 Emissivity:

The emissivity of each material was obtained experimentally using the set up described in Figure 5.1. An aluminum container with a small amount of material to be tested is heated using a laboratory temperature controlled heat plate (Selecta Combinax) until to obtained a homogeneous polymer mass. After this, the heat plate temperature was changed in a range allowing measuring the emissivity at different temperatures. For each measuring point, the heat plate was kept at constant temperature at least for 15 min to obtain an equilibrium temperature. The surface temperature of the polymer sample was measured by a fast reading type K thermocouple (Digital Handheld Thermometer, Anritsu, HFT-80) and the infrared camera SC640.

The emissivity of the material was then computed, adjusting the two measured values using the ThermaCAM Researcher Pro 2.8 SR-2® software, as illustrated in Figure 5.2. For each plate temperature at least 5 measuring temperatures of the sample were recorded. The deduced values for emissivity of ABS FA 4475 and Polystyrol 495F are respectively 0.85 and 0.80, with a standard deviation of 0.01.
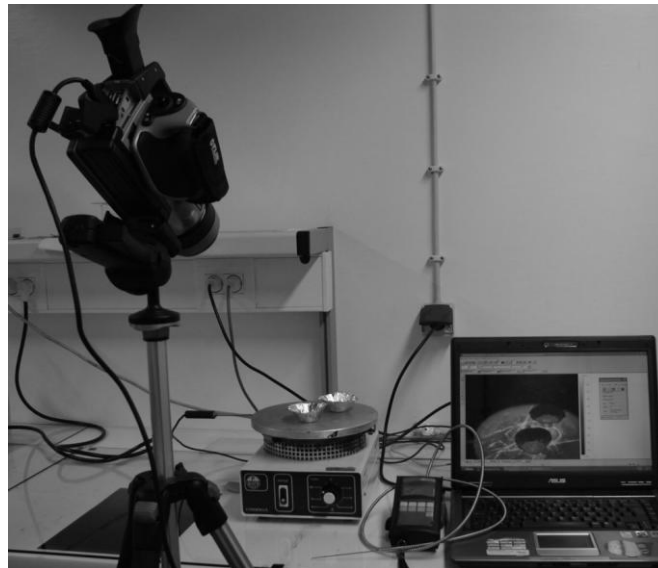
Figure 5.1 – Experimentally set up to compute the emissivity coefficient.
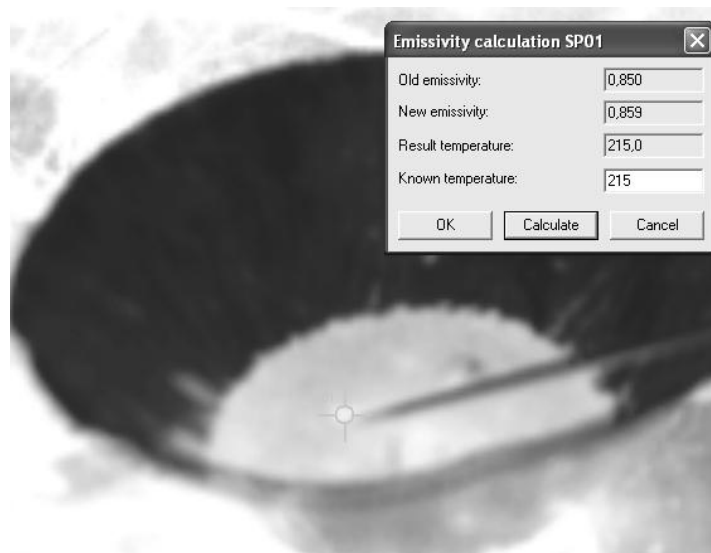
Figure 5.2 – Determination of the emissivity coefficient.

5.2 EQUIPMENT LAYOUT

The experimental setup used to perform the experimental work is presented in Figure 5.3. It comprises a home built mini extruder (Covas and Costa 2004) coupled with a gear pump (32699 Extertal Lenze) in order to ensure a constant output. At the end of these two elements is attached an extrusion extension in order to transform the horizontal flow in a vertical flow required to extrude the filament over the 3D table. The geometry of the filament is achieved by attaching a die as described in Figure 5.3, which in this work has a circular geometry with 1 mm of diameter. The mini extruder and the gear pump have independent control units being possible to control the temperature profiles and the screw or pump velocity, respectively.

The required 3D table to produce the 3D geometries is a home built equipment comprising an aluminium plate actuated by 3 independent step motors with 0.05 mm of accuracy and controlled by a personal computer with a commercial CAD/CAM software. The maximum displacement in the X and Y directions is 150 mm and 100 mm in the Z direction.
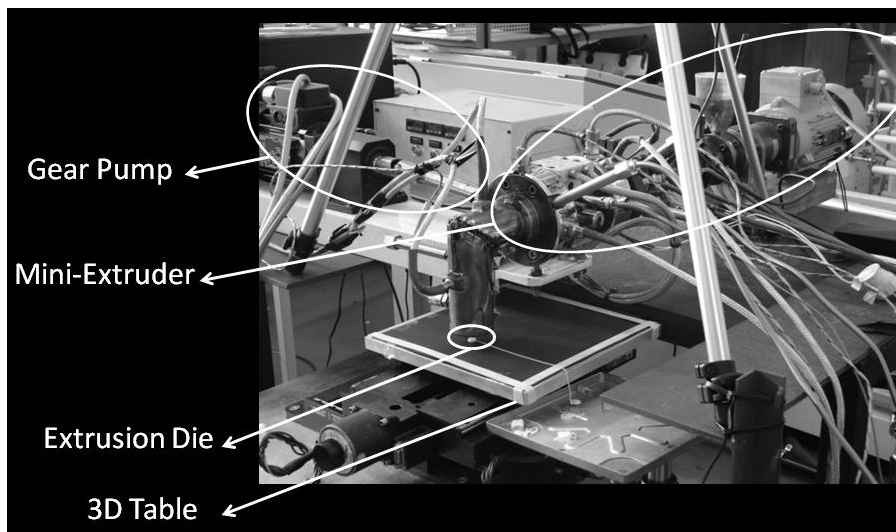
Figure 5.3 – Free Form Extrusion equipment.

The temperature evolution of the deposited filament is recorded by an infrared SC640 FLIR camera positioned above the extrusion head (Figure 5.4) connected to a computer using the ThermaCAM Researcher Pro 2.8 SR-2® software. The recorded movie was then used to measure the temperature evolution along the time at a specific point of the filament.

Figure 5.4 – Position of the thermo graphic camera to measure the temperature evolution of the deposited material.

5.3 DETERMINATION OF THE HEAT TRANSFER COEFFICIENT BY CONVECTION

In order to compare the theoretical results with the experimental measured temperature data, the heat transfer coefficient by convection, h_{conv}, must be known. Since (as abovementioned in chapter 3) the computed temperature values are quite dependent of this variable, a special attention must be done in the procedure to define this variable. Considering the experimental equipment layout described in Figure 5.3, it was observed that the cooling system of the "gear pump" generate an air flow in the surroundings of the 3D table where the filament is deposited as described in Figure 5.5.

Figure 5.5 – Air movement occurring in the surrounding of the 3D table.

Therefore, the correlation of Hilpert (Holman 1983) for the cooling down of a cylinder by forced convection will be used to estimate h_{conv}:

$$h_{conv} = \frac{Nu_d \cdot k}{d}$$ (5.1)

This correlation depends on the cylinder diameter d (m), the thermal conductivity k of the material (W/m· °C), and the Nusselt number Nu_d, defined by:

$$Nu_d = C \cdot \text{Re}^n \cdot \text{Pr}^{\frac{1}{3}}$$ (5.2)

where Re is the Reynolds's number (K), C_H and n_H are constants deduced from Hilpert data (Table 5.2) and Pr is the air pressure (Pa) at the medium temperature T_{medium} (K):

$$T_{medium} = \frac{T_{filament} + T_{ambient}}{2}$$ (5.3)

Table 5.2 – Constants for the Hilpert's correlation (Holman 1983).

Reynolds's number Re	C_H	n_H
0.4 – 4	0.989	0.330
4 – 40	0.911	0.385
40 – 4 000	0.683	0.466
4 000 – 40 000	0.193	0.618
40 000 – 400 000	0.0266	0.805

The determination of the constants C_H and n_H also depend on the value of the Reynolds's number, expressed as:

$$\text{Re} = \frac{\rho_{air} \cdot v_{air} \cdot d}{\mu_{air}} \tag{5.4}$$

Where μ_{air} is the air viscosity (kg/m.s) at the temperature T_{medium} and v_{air} is the air velocity (m/s). The air density ρ_{air} (kg/m^3) is computed by using the following expression:

$$\rho_{air} = \frac{\text{Pr}}{R \times T_{medium}} \tag{5.5}$$

Where R is the universal gas constant (R = 287 J/kg.K).

The air velocity v_{air} is experimentally measured with an anemometer. The measuring head was positioned in the 3D table near the extrusion die in order to measure the air velocity in extrusion area. The air velocity was measured at least 10 times, ranged between 0.3 and 0.5 m/s.

Alternatively, it is possible to deposit the filaments in a local far from the gear pump in order to avoid the air circulation near the 3D extrusion table as described in Figure 5.5. In this case, the heat transfer coefficient by convection can be computed by the correlation developed by Churchill and Chu (1975) for the cooling down of a long horizontal cylinder by natural convection (Kraus, Aziz e Welty, Extended Surface Heat Transfer 2001):

$$h_{conv} = \frac{k \, Nu_d}{d} \tag{5.6}$$

Nu_d is the Nusselt number given by:

$$Nu_d = \left\{ 0.60 + \frac{0.387 \, Ra_d^{1/6}}{\left[1 + (0.559/\text{Pr})^{9/16} \right]^{8/27}} \right\}^2 \tag{5.7}$$

This last expression is a function of the Rayleigh Ra_d, expressed as:

$$\begin{cases} Ra_d = Gr_d \, \text{Pr} \\ \text{Pr} = \dfrac{v_k}{\alpha} \end{cases} \qquad (5.8)$$

where v_k is the kinematic viscosity (m²/s), α is the thermal diffusivity (m²/s) and Gr_d is the Grashof number:

$$Gr_d = \frac{g \, \beta \, (T_S - T_E) \, d^3}{v_k^{\,2}} \qquad (5.9)$$

Where g is the gravity acceleration ($g = 9.8$ m/s²), β is the volumetric thermal expansion coefficient, T_s is the cylinder temperature (°C).

Figure 5.6 shows the heat transfer coefficient by convection as function of the air velocity in the range where the Hilpert's correlation is valid. An initial temperature of 200°C and an environment temperature of 20 °C are used, and the cylinder diameter is assumed to be equal to 1 mm. As can be seen, the heat transfer coefficient by convection is quite dependent on the air velocity.
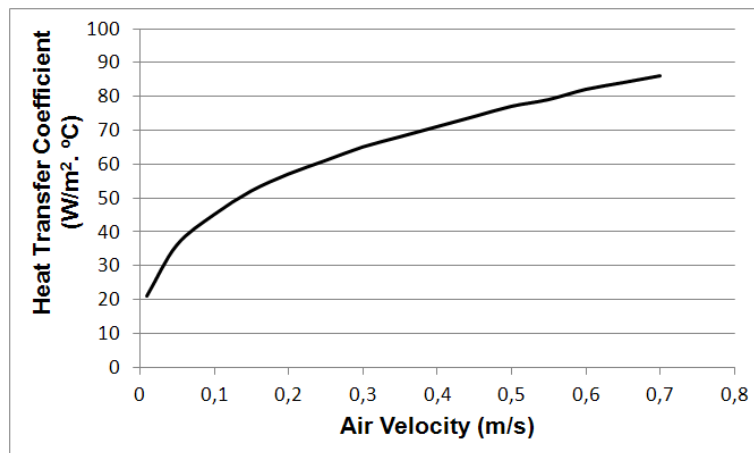
Figure 5.6 – Heat Transfer Coefficient vs air velocity using the Correlation of Hilpert, with $T_L = 200$°C, $T_E = 20$°C and $d = 0.001$ m.

In addition with the air velocity, the extrusion and environment temperatures and the cross-section diameter of the filament also influence the value of the heat transfer coefficient.

In order to access the influence of these experimental variables – filament diameter, extrusion and environment temperatures – in the heat transfer coefficient its values were now increased one by one ($d = 0.0012$ m, $T_L = 220$°C, $T_E = 40$°C). The results are shown in Figure 5.7 allowing conclude that the filament diameter has the greatest influence on the heat transfer coefficient, comparing with the extrusion and the environment temperatures. Temperature evolution at the middle of an ABS filament computed by the computer code can be observed in Figure 5.8, where the two different diameters and the two respective heat transfer coefficients are considered: temperature differences are relatively raised (until 20°C). The above results show that the determination of the heat transfer coefficient is very important, and depends strongly on the air velocity and the filament diameter, variables that must be determined with the maximal rigor.
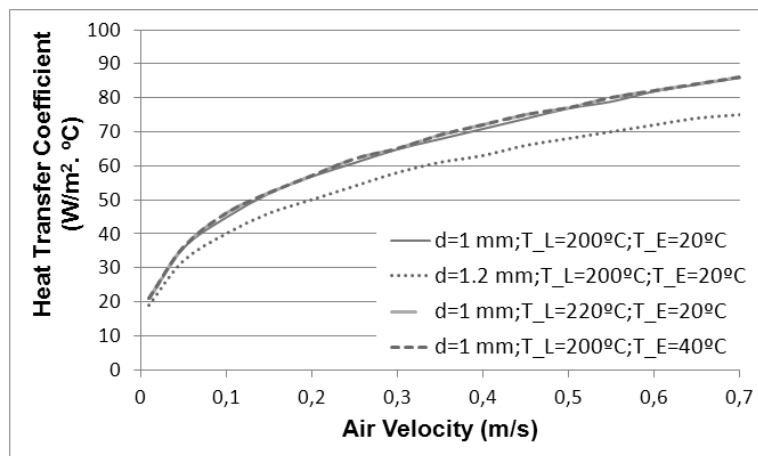

Figure 5.7 – Heat Transfer Coefficient vs air velocity using the Correlation of Hilpert, for two different diameters and temperatures.
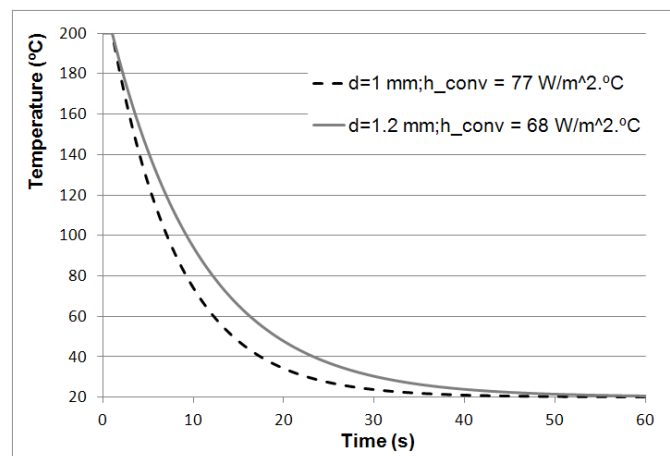

Figure 5.8 – Temperature vs time of one filament for two different heat transfer coefficient values, with $T_L = 200$°C and $T_E = 20$°C (ABS material).

102

5.4 PROCEDURES

5.4.1 Measuring temperature profiles

A protocol that allows performing experiments under controlled conditions while ensuring reproducibility of the process was followed. The procedure is as follows:

Adjust the temperature profile of the extruder, gear pump and the die to the desired values according to the material to be studied. For each material were studied two temperature profiles which corresponds in practice to two extrusion temperatures, $T_L =$ 200ºC and $T_L =$ 220ºC. After stabilizing the temperature, the rotation speed of the gear pump and screw of the mini-extruder are adjusted in order to obtain a constant flow rate. It was observed some slight variations in the instantaneous flow rate, mainly due to fluctuations in particle size of materials to be extruded. The speed of movement of the table 3D was also adjusted according to the output of the extruder in order to be deposited a uniform filament. After extrusion during a few minutes in order to stabilize the process the ThermaCAM Researcher Pro 2.8 SR-2® software starts the record of images with a frequency of 7.5 Hz and the 3D table moves according to the pre-defined trajectory. At the end of deposition, the filament extrusion is stopped while the thermal image recording is kept during a period of time sufficiently long (about two minutes), in order to ensure the complete cooling down of the filament close to environment temperature. In the software, three parameters must be introduced: the distance between the camera and the support table, the ambient temperature and the emissivity coefficient of the material (Table 5.3).

Table 5.3 – Introduced parameters in the software ThermaCAM Researcher Pro 2.8 SR-2®.

Variable	Value
Ambient controlled temperature	23 ºC
Temperature of the surrounding of the extruder	Between 40ºC and 65ºC
Distance between the camera and the support table	1 m
Emissivity of the material	0.85/0.80

Although all the experiences were performed in a closed laboratory with controlled temperature (23ºC), during the experimental work was identified by the thermographic camera that the temperature of air in the surrounding of the table 3D is higher due to the heating provided by the equipment. The air temperature ranged between 40ºC and 65ºC (closed to extrusion head).

The material temperature at the exit of the extrusion die was measured with a fast reading thermocouple in order to know the real extrusion temperature and to compare the set value. Values of all these variables are shown in Table 5.4.

Table 5.4 – Conditions of the experimental study.

Variable	Value
Initial temperature of the extruded material	190 ºC (for $T_L = 200$ºC)
	210 ºC (for $T_L = 220$ºC)
Ambient temperature	23 ºC
Temperature of the surrounding of table 3D	Between 40ºC and 65ºC (depending on the proximity of the extruder)
Extruder velocity	13.4
Pump velocity	4.5
Pressure	Between 5 and 20
Deposition Velocity	Between 0.012 and 0.017 m/s

5.4.2 Comparing with theoretical results

Confirmation of the heat transfer coefficient value:

In order to obtain points of the filaments without contact with support, a cut is made on the support table (Figure 5.9). The objective is to certify that the temperature evolution on this filament section is only controlled by heat exchanges by convection with ambient. Then, after deposition of the filament and recording of temperature profiles, the filament is cut at this point, and the diameter of the filament cross-section is experimentally measured by microscopy using a Stereoscopic Olympus Magnifier and the Leica Qwin V3 Software, in order to compute a correct value for the heat transfer coefficient. Theoretical curves are then obtained and compared with the experimental data. This procedure is described in Figure 5.10.
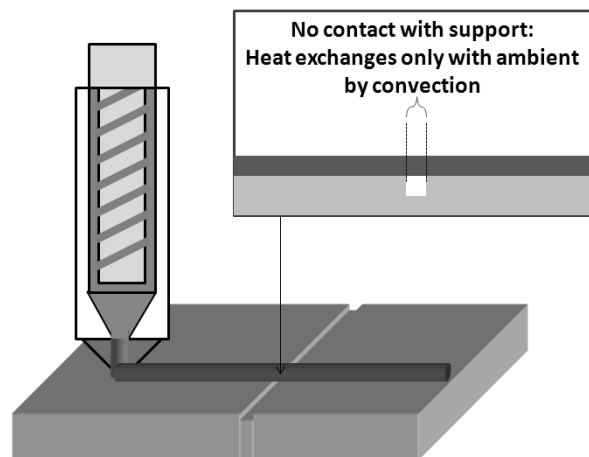
Figure 5.9 – Experimental procedure that allows obtaining points without contact with support.
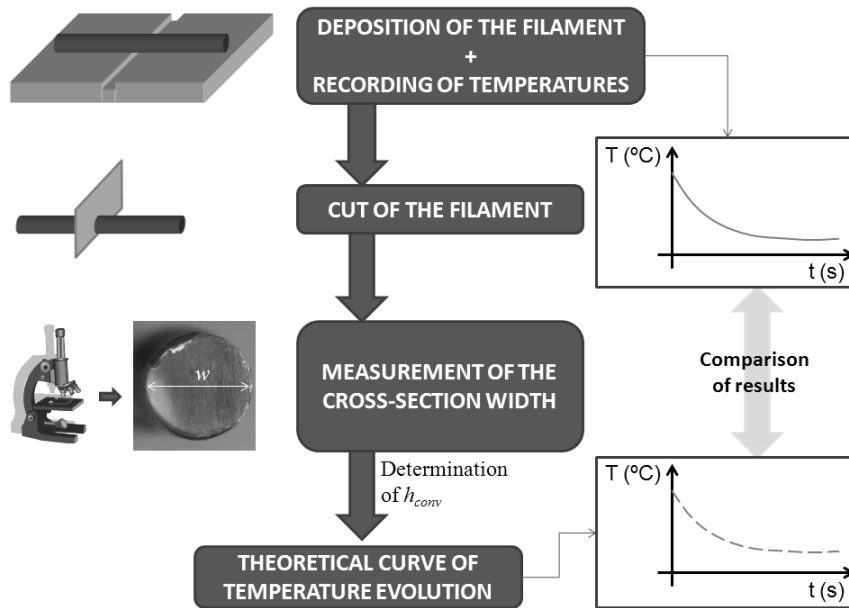
Figure 5.10 – Procedure that allows confirming the value of heat transfer coefficient.

Deduction of the thermal contact conductance between the filament and the support:

Due to the difficult determination of the value of thermal contact conductance between the filament and the support, an approximation of the theoretical to the experimental results is made (Figure 5.11). After deposition of the filament and recording of temperature profiles, points with contact with support are chosen and the filament is cut on these in order to measure the diameter of the cross-section and the length of contact. The value of thermal contact conductance is then deduced by approximating the curve devolved by the MatLab® code to the experimental data.
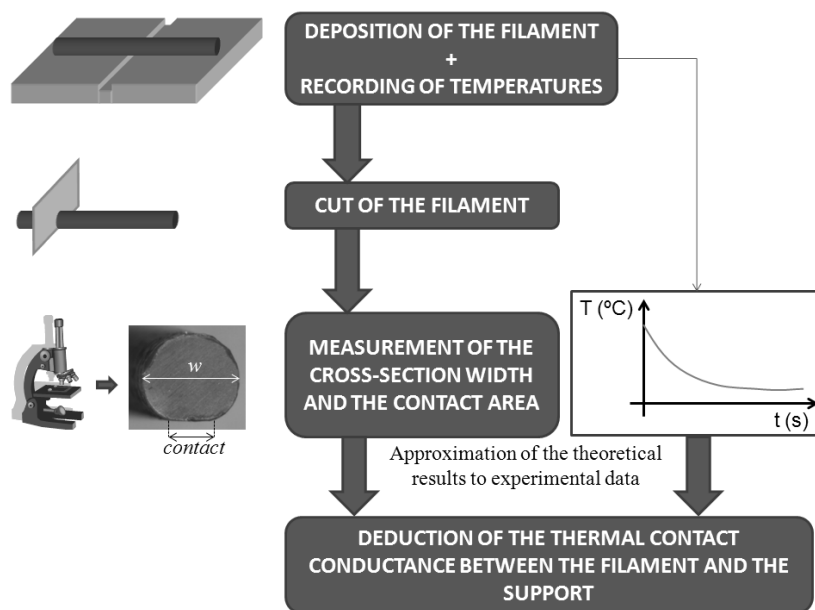
Figure 5.11 – Procedure for the determination of the thermal contact conductance with support.

After deduction of the value of thermal contact conductance, the material and the extrusion temperature are modified in order to verify if the deduced value keep constant and then validate the computer code.

Deduction of the thermal contact conductance between adjacent filaments:

If two adjacent filaments are considered, one must be deposited above the other, due to the limitations of the thermographic camera in detecting the different temperatures of two horizontal adjacent filaments. After deposition of the two filaments and recording of temperatures, the filaments are cut on the studied points in order to determine with precision the diameters of cross-sections and the length of contact with support and between the two filaments. By comparison between the theoretical and experimental results, the thermal contact conductance between adjacent filaments is deduced (Figure 5.12).
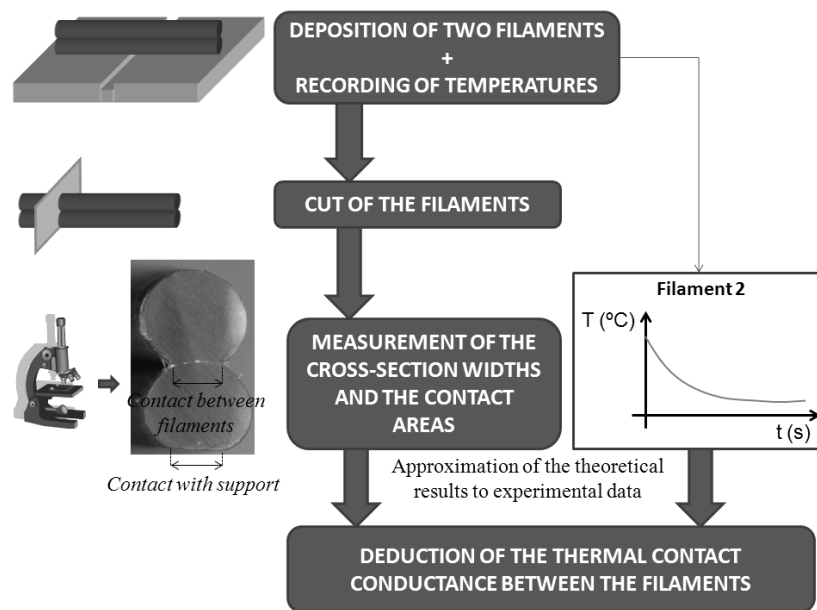
Figure 5.12 – Procedure for the determination of the thermal contact conductance between adjacent filaments.

After deduction of the thermal contact conductance between filaments, the contacts are delayed, the material and the extrusion temperature are modified and results are compared. After this, the deposition of three adjacent filaments is also made with the two materials and two different extrusion temperatures. The objective is to validate the value of thermal contact conductance between adjacent filaments.

5.4.3 Adhesion quality

In order to establish a relationship between extrusion temperature, thermal contacts and adhesion, adjacent filaments of ABS were extruded considering different conditions as described in Figure 5.13. In A, the contact between the filaments occurs immediately while for the conditions B, C and D, the contact between the two filaments is delayed, ensuring that the contact occur when the first filament it's at a lower temperature. All the filaments have a length of 14 cm and the deposition velocity was kept constant for all the experiences (0.012 m/s). Two different extrusion temperatures were considered: $T_L = 200\ °C$ and $T_L = 220\ °C$. At least 10 samples were prepared for each condition.
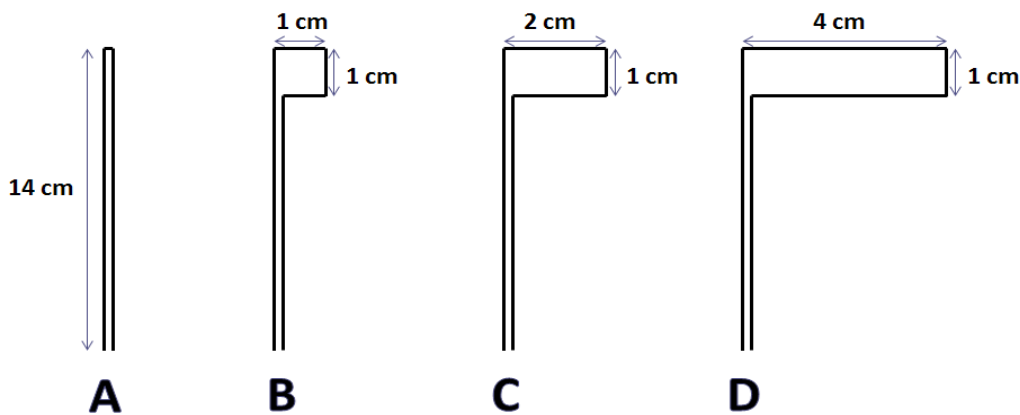
Figure 5.13 – Dimensions of the ABS specimens A, B, C and D.

In order to compare the adhesion quality, each pair is slowly detached until the break occurs. The distance between the break point and the end of filaments (as B_p in cm) is then measured as described in Figure 5.14. These results are then compared with the previsions of the MatLab® code, by using the deduced values of thermal contact conductance from the last experiences on temperature profiles.
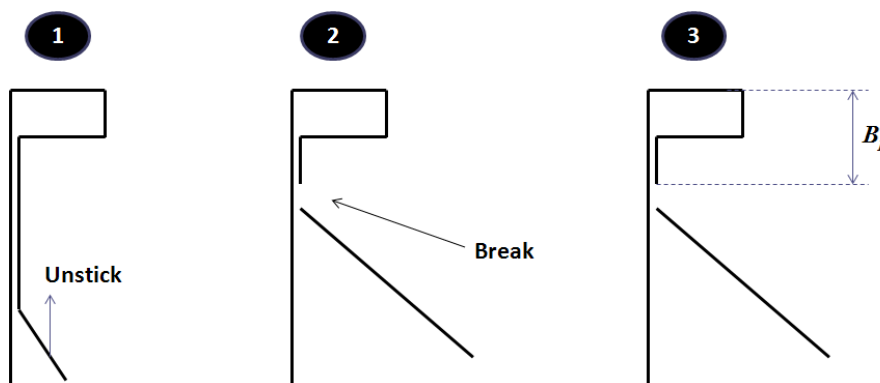
Figure 5.14 – Experimental procedure to compare the adhesion quality of specimens.

5.5 RESULTS

5.5.1 Temperatures

As explained before, a unique filament is first deposited with a deposition velocity of 0.017 m/s and a length of 120 mm. Temperatures are extracted on two points where the contact with support is not valid; on $x = 30$ mm, located far the extruder, and on $x = 80$ mm, located near the extruder. Temperatures on the surrounding of these points are different due to the heating provided by the extruder. The defined referential and the selected points are illustrated in Figure 5.15 and the reproducibility of the experiences is shown in Figure 5.19 for many conditions and materials.
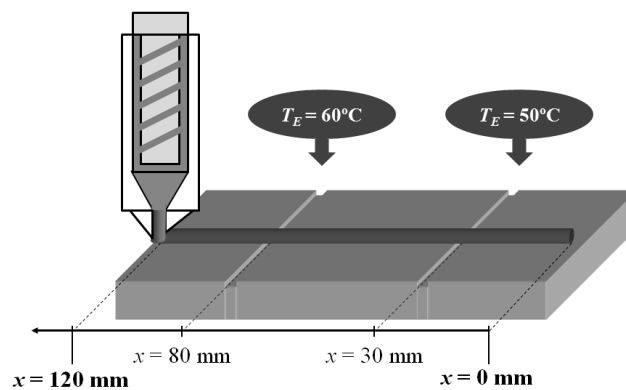
Figure 5.15 – Selected studied points.

a) $x = 30$ mm, ABS, $T_L = 200$°C

b) $x = 30$ mm, HIPS, $T_L = 200$°C

c) $x = 30$ mm, HIPS, $T_L = 220$°C

d) $x = 50$ mm, ABS, $T_L = 200$°C
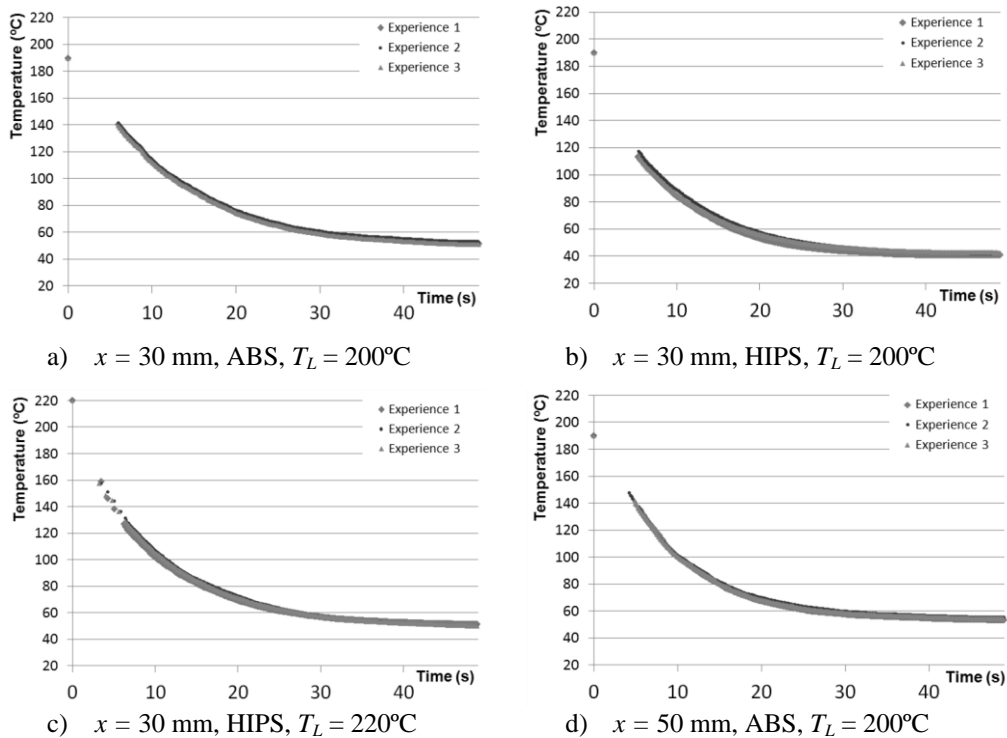
Figure 5.16 – Temperature evolution recorded by the camera for many conditions.

After deposition and recording of temperature profiles, the filament is cut on these points in order to measure with precision the diameter of the filament cross-section. For the ABS material, the deduced diameter was 1.4 mm, as illustrated in Figure 5.17. The heat transfer coefficient h_{conv} was then calculated for this diameter by using the Hilpert's correlation. Since the air velocity varies between 0.3 and 0.5 m/s, two values were found for the coefficient: $h_{conv} = 52$ W/m^2 · ºC and $h_{conv} = 62$ W/m^2 · ºC. Then, two theoretical curves were obtained for these values. With respect to the experimental data, the curve that approximates better the average of temperatures is selected and compared with the theoretical results. Figure 5.18 and Figure 5.19 show respectively the temperature evolution on the two points of the ABS filament ($x = 30$ mm and $x = 80$ mm). The extrusion temperature was set at $T_L = 200$ºC, but the thermocouple indicated that the material has a lower temperature (190 ºC) at the moment of the deposition, as referred before. These graphics show that theoretical results are in good agreement with the measured temperatures.
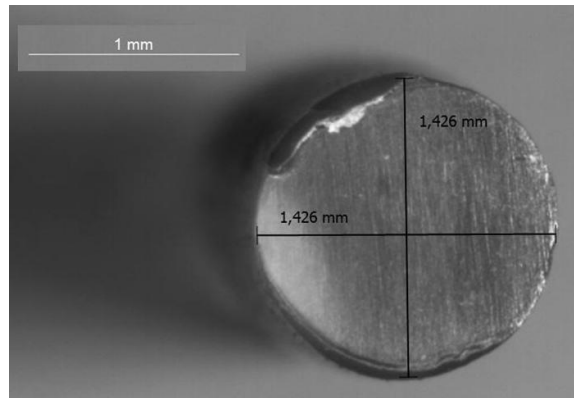
Figure 5.17 – Measurement of the diameter of the filament cross-section (ABS).
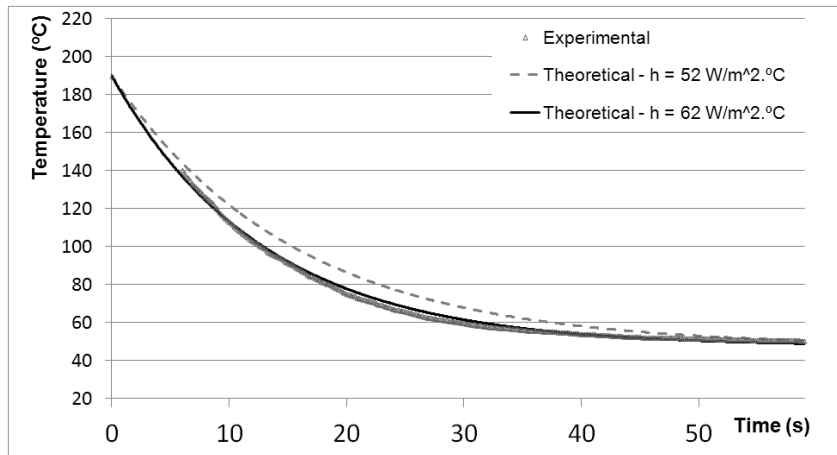
Figure 5.18 – Temperature evolution on $x = 30$ mm located far the extruder (ABS).
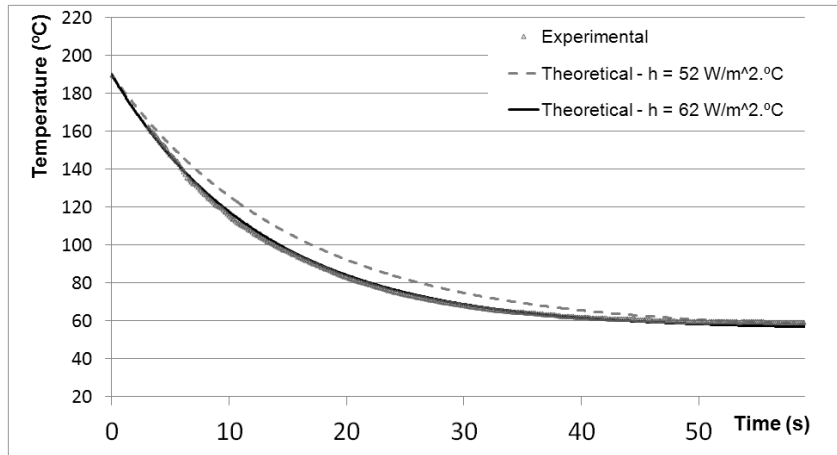
Figure 5.19 – Temperature evolution on $x = 80$ mm located near the extruder (ABS).

Figure 5.20 and Figure 5.21 show the results for the same conditions, but with a HIPS filament. The diameter was also measured (1.3 mm) then the values for the heat transfer coefficient were newly calculated: $h_{conv} = 56$ W/m$^2 \cdot$ °C and $h_{conv} = 66$ W/m$^2 \cdot$ °C. Theoretical results keep closed to experimental data.
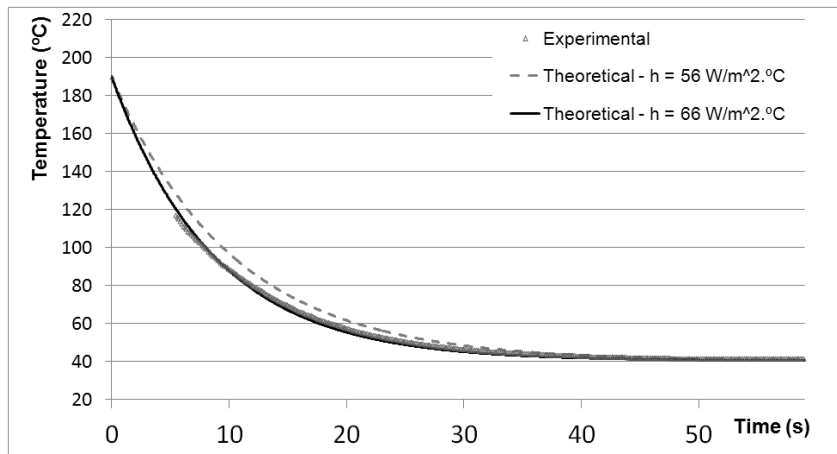
Figure 5.20 – Temperature evolution on $x = 30$ mm located far the extruder (HIPS).
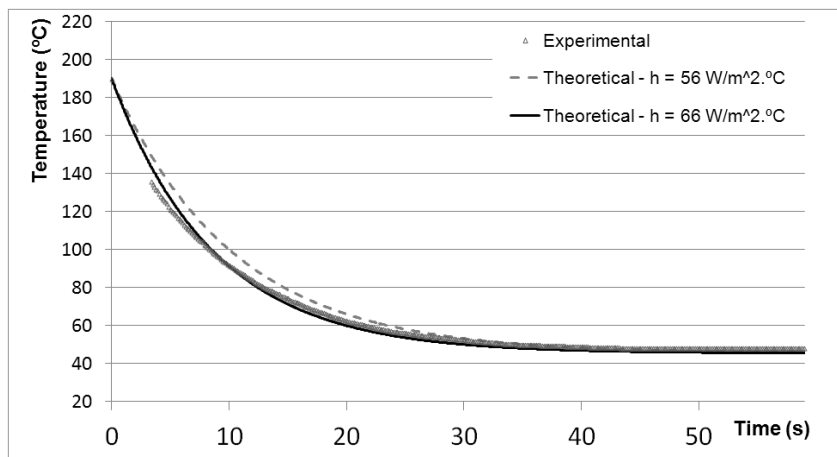
Figure 5.21 – Temperature evolution on $x = 80$ mm located near the extruder (HIPS).

These experiences were repeated with the HIPS material, but for another extrusion temperature $T_L = 220°C$. Similarly, the real initial temperature of the material is lower (210°C) and the diameter of the cross-section is lightly higher (1.35 mm). This gave rise to new values for the heat transfer coefficient: $h_{conv} = 54$ W/m^2 · °C and $h_{conv} = 64$ W/m^2 · °C. Figure 5.22 and Figure 5.23 show that the theoretical results are in good agreement with the experimental data.
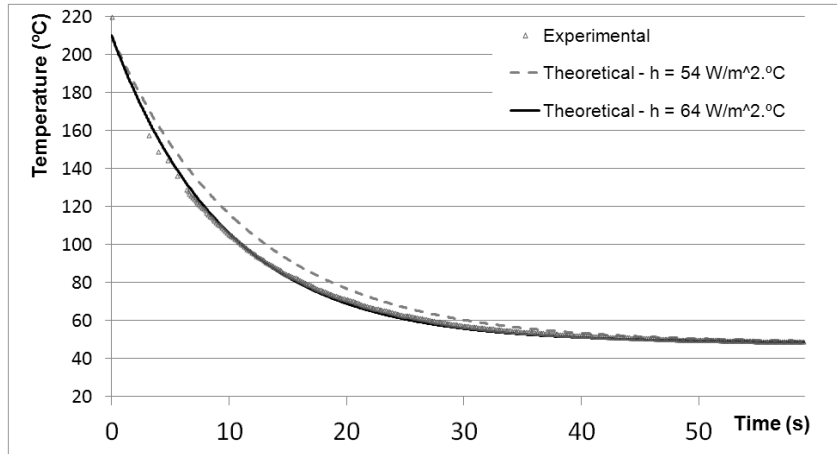
Figure 5.22 – Temperature evolution on $x = 30$ mm, for $T_L = 220°C$ (HIPS).
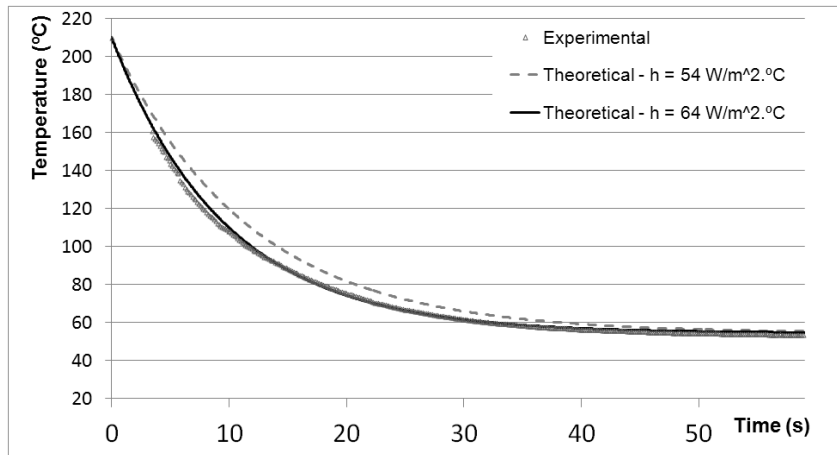
Figure 5.23 – Temperature results on $x = 80$ mm, for $T_L = 220°C$ (HIPS).

In order to investigate the importance of the air velocity, a HIPS filament is deposited in a location where the air flow is almost inexistent, that is, where the natural convection is valid. The heat transfer coefficient was then computed by using the Churchill's correlation ($h_{conv} = 30$ W/m^2 · °C) and the theoretical and experimental results were compared in Figure 5.24. Since the extruder is also distant from the support table, the ambient temperature is lower (38°C). These results show the great importance of the air flow in the cooling down of the filaments.
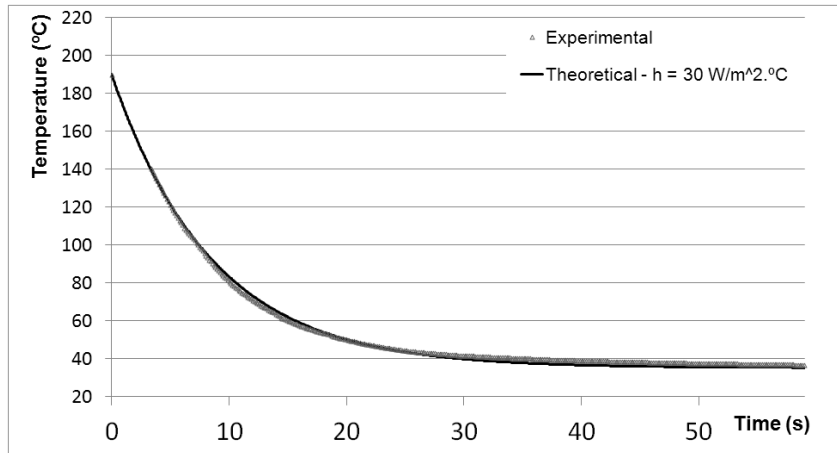
Figure 5.24 – Temperature evolution on $x = 10$ mm, for a filament deposited far the gear pump, without air flow (HIPS).

Points where the contact with support is present are now studied. The contact length is then measured on $x = 40$ mm (Figure 5.25) and the thermal contact conductance between the filament and the support was varied until coincide with experimental data: $h_4 = 250$ W/m$^2 \cdot$ °C $> h_{conv}$ was deduced, that is, points in contact with support cool down faster than the other points. Results are shown in Figure 5.26.
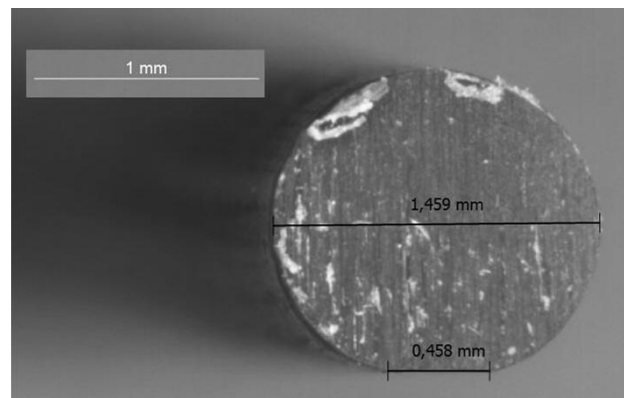
Figure 5.25 – Measurement of the contact length of the ABS filament cross-section for $T_L = 200$°C (10%).
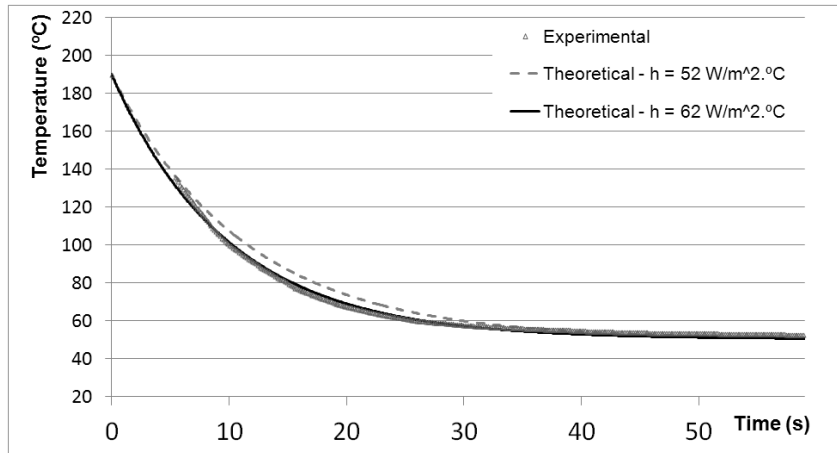
Figure 5.26 – Temperature evolution of the point $x = 40$ mm with 10% of contact with support, $T_L = 200$ºC and $h_4 = 250$ W/m$^2 \cdot$ ºC (ABS).

The point $x = 60$ mm was selected but with a higher value for extrusion temperature (T_L = 220ºC). Consequently, as shown in Figure 5.27, the contact length is also higher (14%). Results illustrated in Figure 5.28 confirmed the correct value for thermal contact conductance.
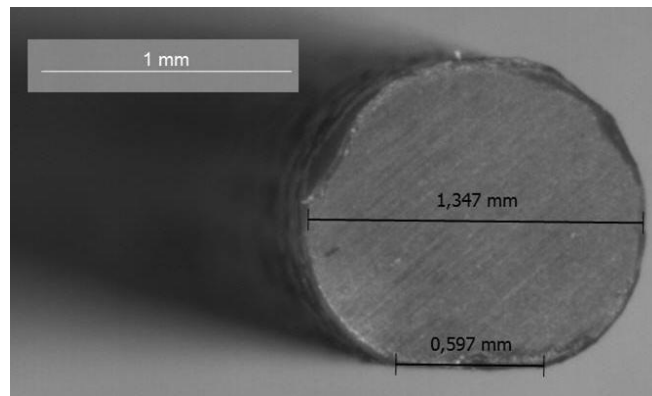
Figure 5.27 – Measurement of the contact length of the ABS filament cross-section for $T_L =$ 220ºC (14%).
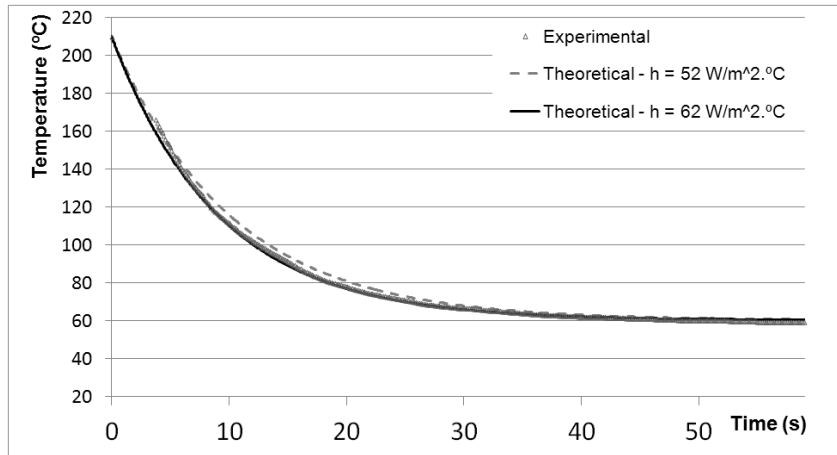
Figure 5.28 – Temperature evolution of the point $x = 60$ mm with 14% of contact with support, $T_L = 220°C$ and $h_4 = 250$ W/m$^2 \cdot$ °C (ABS).

Figure 5.29 and Figure 5.30 show the results for the same conditions, but with the HIPS material, where the contact lengths are different. Thermal contact conductance remains the same for this material.
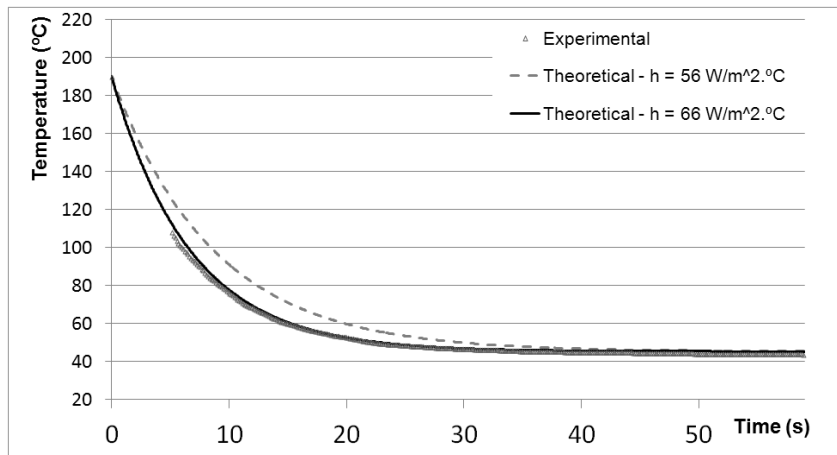
Figure 5.29 – Temperature evolution of the point $x = 40$ mm with 11% of contact with support, $T_L = 200°C$ and $h_4 = 250$ W/m$^2 \cdot$ °C (HIPS).

114
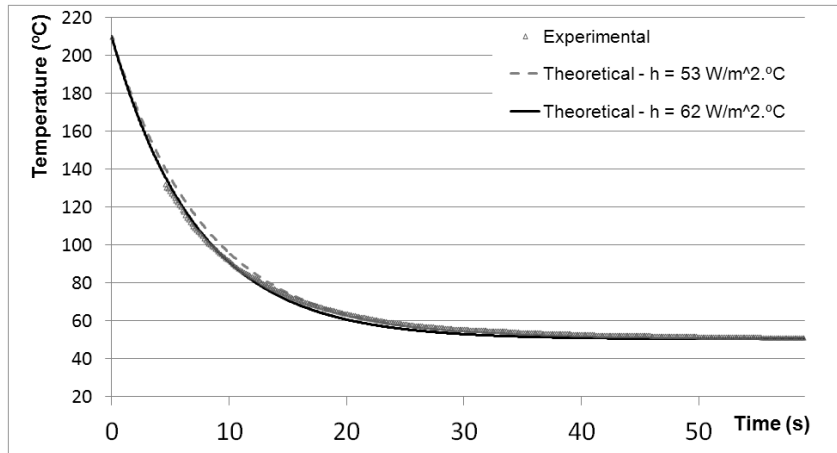
Figure 5.30 – Temperature evolution of the point $x = 60$ mm with 16% of contact with support, $T_L = 220$ºC and $h_4 = 250$ W/m$^2 \cdot$ ºC (HIPS).

Since the experimental results are always more closed to the higher heat transfer coefficient, the highest air velocity (0.5 m/s) will be considered in the future analysis.

Now, two adjacent ABS filaments are considered, one above the other. Temperature results are extracted on a point of the 2nd filament, $x = 50$ mm, which starts cooling down 8 seconds after the point of the 1st filament has begun to cool. Two others experiences were made, where the extruder is stopped between the deposition of the two filaments, in order to delay the contact between them. Then, three situations were obtained: point x starts cooling down $(8 + \Delta t)$ seconds after the 1st, for three distinct values of Δt ($\Delta t = 0$ s, $\Delta t = 2.7$ s and $\Delta t = 4.8$ s), as illustrated in Figure 5.31.
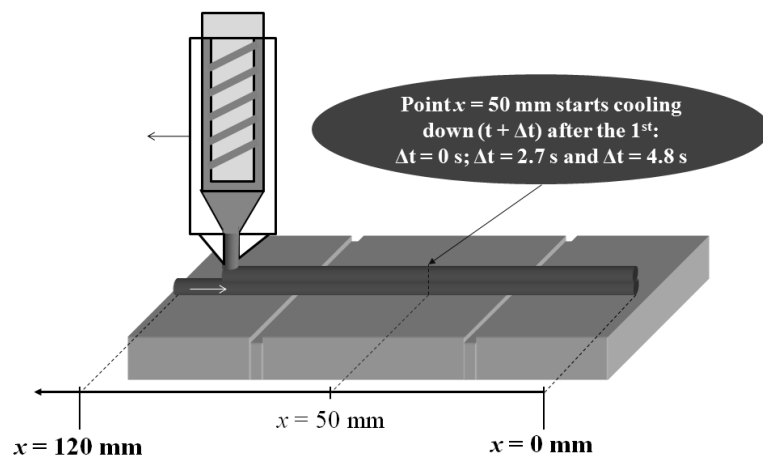
Figure 5.31 – Selected point and conditions for the deposition of two filaments.

Contact lengths are then measured (Figure 5.32) and the thermal contact conductance between the adjacent filaments was varied until coincide with experimental data: $h_5 = h_{10} = 50$ W/m$^2 \cdot$ °C was deduced. Results for the three conditions are shown in Figure 5.33.

Figure 5.32 – Measurement of the contact lengths of the ABS filament cross-section for $T_L = 200$°C (14% with support and 10% between filaments).

a) $\Delta t = 0$ s

b) $\Delta t = 2.7$ s

c) $\Delta t = 4.8$ s
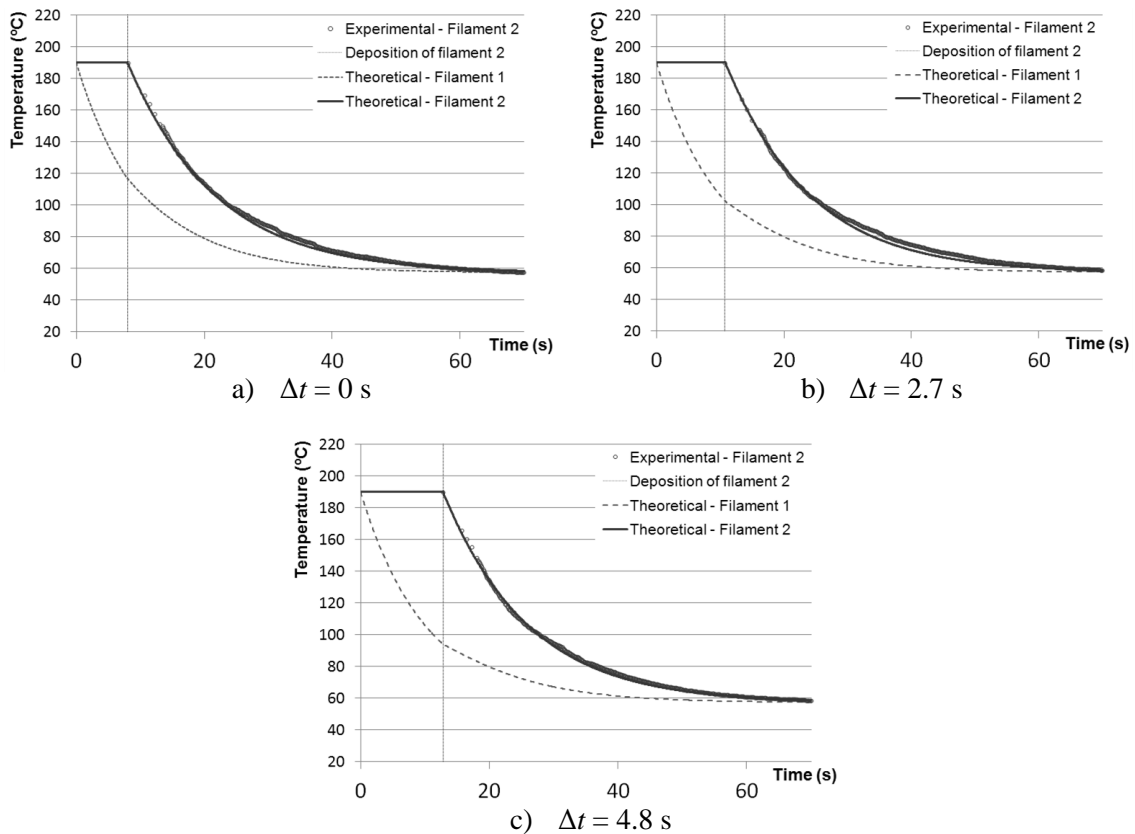
Figure 5.33 – Temperature evolution on the point $x = 50$ mm of the 2nd ABS filament with 14% of contact with support, 10% of contact with the 1st filament, $T_L = 200$°C and $h_5 = h_{10} = 50$ W/m$^2 \cdot$ °C.

The same experiences were made with the HIPS material and allow concluding that the thermal contact conductance between filaments remains the same. Figure 5.34 shows the results of these experiences.

a) $\Delta t = 0$ s (11% of contact with support and 10% of contact with the 1st filament)

b) $\Delta t = 2.7$ s (13% of contact with support and 9% of contact with the 1st filament)

c) $\Delta t = 4.8$ s (13% of contact with support and 9% of contact with the 1st filament)
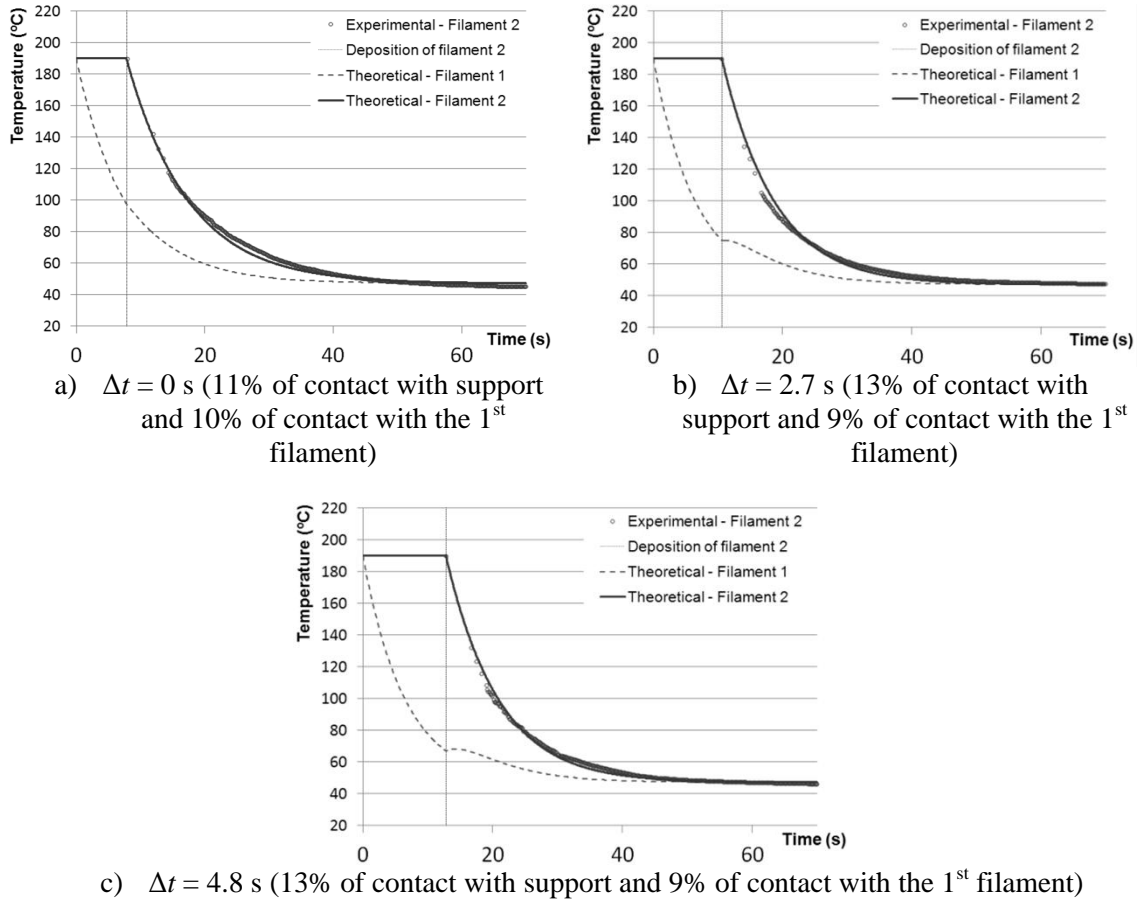
Figure 5.34 – Temperature evolution on the point $x = 50$ mm of the 2nd HIPS filament, for $T_L = 200$ºC and $h_5 = h_{10} = 50$ W/m^2 · ºC.

The extrusion temperature was then increased, and contact lengths are newly measured on the same point ($x = 50$ mm). As shown in Figure 5.35 for the ABS filaments, the contact lengths increased with the higher temperature. Results for ABS and HIPS in confirmed the value for thermal contact conductance between adjacent filaments (Figure 5.36 and Figure 5.37).
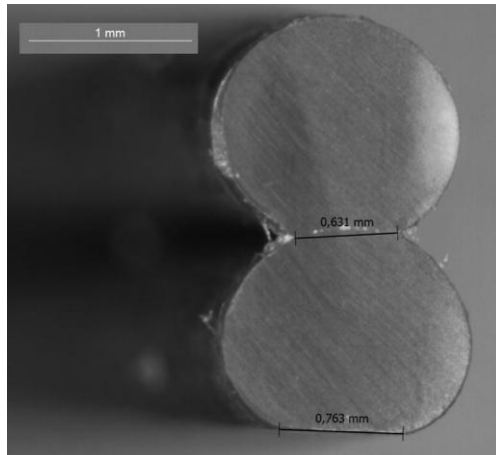
Figure 5.35 – Measurement of the contact lengths of the ABS filament cross-section for $T_L =$ 220°C (17% with support and 14% between filaments).
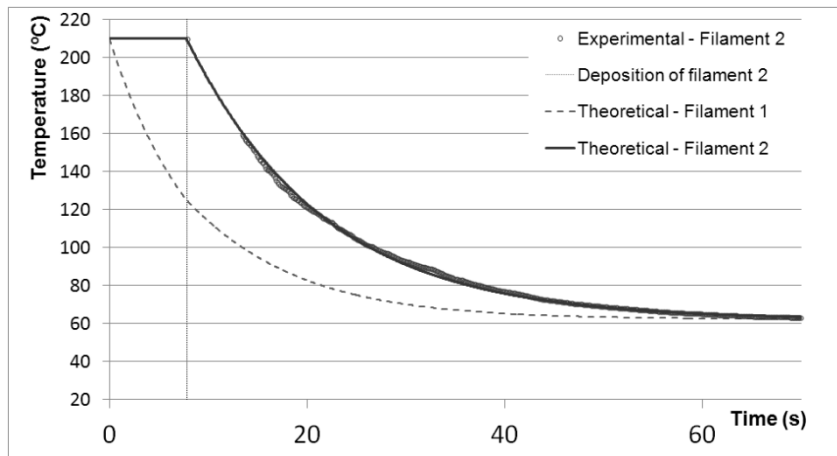
Figure 5.36 – Temperature evolution on the point $x = 50$ mm of the 2nd ABS filament with 17% of contact with support, 14% of contact with the 1st filament, $T_L = 220$°C and $h_5 = h_{10} = 50$ W/m^2·°C.
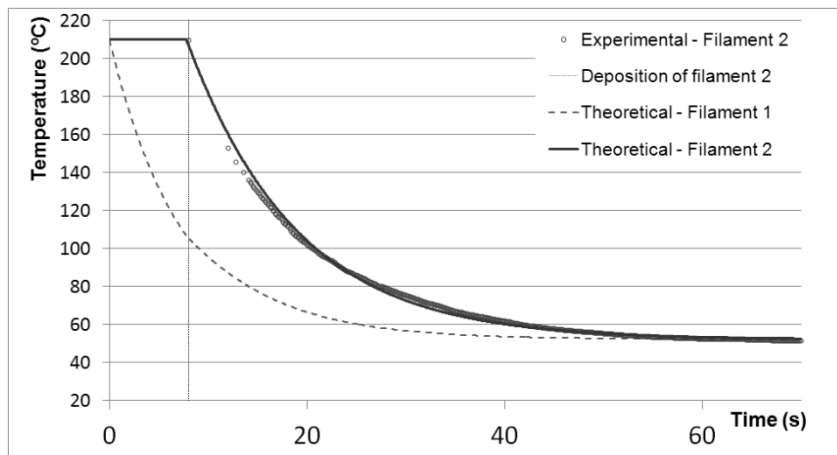
Figure 5.37 – Temperature evolution on the point $x = 50$ mm of the 2nd HIPS filament with 17% of contact with support, 14% of contact with the 1st filament, $T_L = 220$°C and $h_5 = h_{10} = 50$ W/m^2·°C.

118

Now, three adjacent ABS filaments are considered, one above the other. Temperature results are extracted on the point $x = 45$ mm of the 3rd filament, which starts cooling down 17.6 seconds after the point of the 1st filament has begun to cool. Contact lengths are then measured for the higher extrusion temperature (Figure 5.38). Results for ABS material with an extrusion temperature of $T_L = 220$ºC are shown in Figure 5.39.
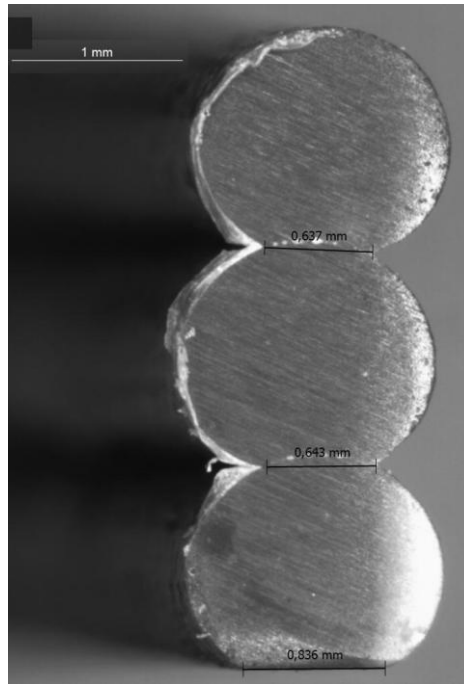
Figure 5.38 – Measurement of the contact lengths of the ABS filament cross-section for $T_L =$ 220ºC (18% with support and 13% between filaments).
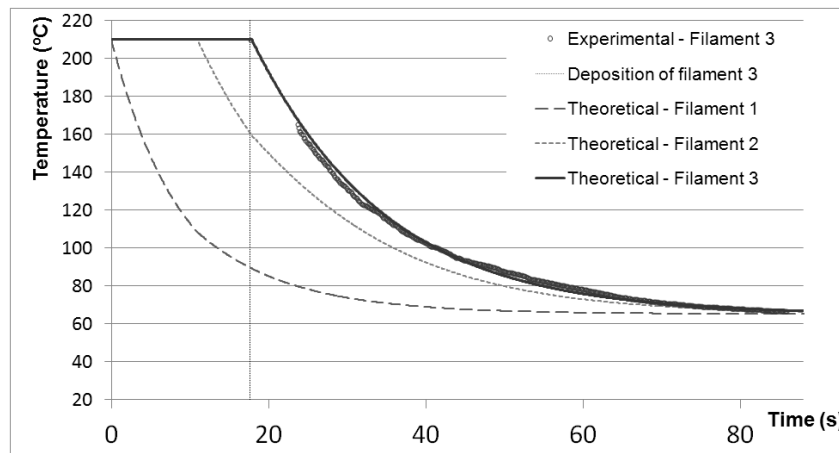
Figure 5.39 – Temperature evolution on the point $x = 45$ mm of the 3rd ABS filament with 18% of contact with support, 13% of contact with the 2nd filament, $T_L = 220$ºC and $h_5 = h_{10} = 50$ W/m^2·ºC.

Three HIPS filaments are deposited at an extrusion temperature $T_L = 200$ºC and another point was selected ($x = 65$ mm). Contact lengths are lower (11% with support and 10% with adjacent filaments). Figure 5.40 shows the temperature results.

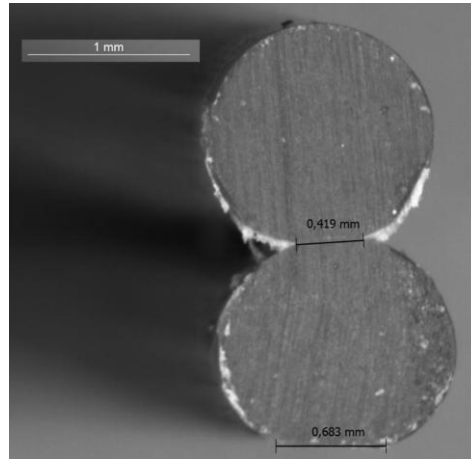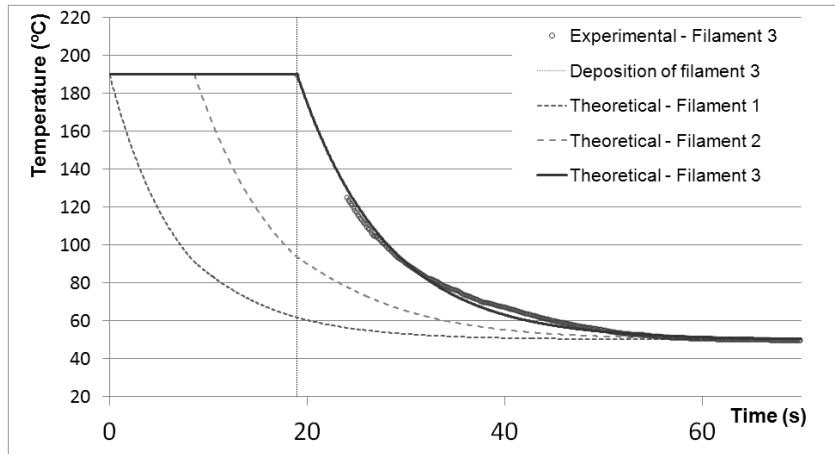**Figure 5.40** – Temperature evolution on the point $x = 65$ mm of the 3rd HIPS filament with 11% of contact with support, 10% of contact with the 2nd filament, $T_L = 200$ºC and $h_5 = h_{10} = 50$ W/m$^2 \cdot$ ºC.

5.5.2 Adhesion results

Figure 5.41 shows an example of a specimen for each set. The values of B_p for each specimen are measured and the respective average and standard deviation are calculated for the sets A, B, C and D. Table 5.5 and Table 5.6 show respectively these results for the two extrusion temperatures $T_L = 200$ ºC and $T_L = 220$ ºC. As a first general observation, the average value for B_p is lower for the lower extrusion temperature, that is, a higher value for the extrusion temperature improves the adhesion quality between adjacent filaments.
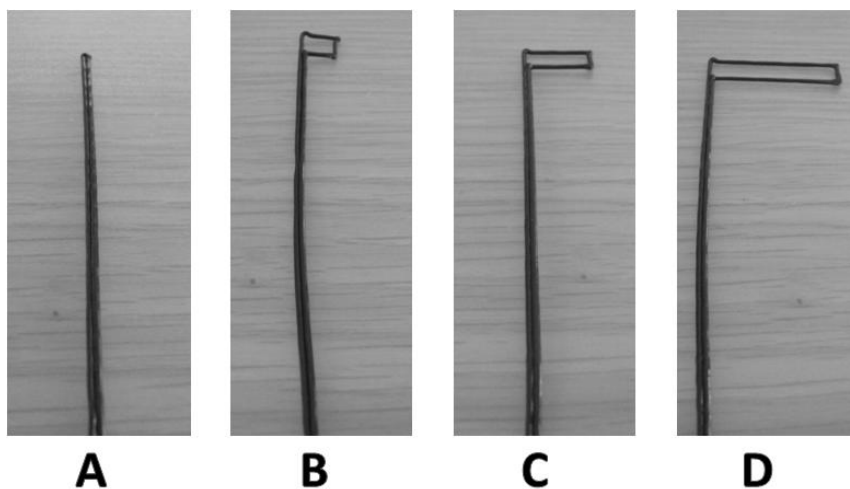
Figure 5.41 – Photo of each specimen type.

Table 5.5 – Experimental measured break point values for $T_L = 200$ ºC.

Specimen Type	Average break point (cm)	Average break point (%)	Standard Deviation (cm)	Standard Deviation (%)	Photo
A	0.00	0%	0.00	0%	
B	0.99	7%	0.66	5%	
C	0.00	0%	0.00	0%	
D	0.00	0%	0.00	0%	

Table 5.6 – Experimental measured break point values for $T_L = 220$ ºC.

Specimen Type	Average break point (cm)	Average break point (%)	Standard Deviation (cm)	Standard Deviation (%)	Photo
A	4.15	30%	1.87	13%	
B	0.64	5%	0.50	4%	
C	2.22	16%	1.16	8%	
D	1.42	10%	1.21	9%	

If the results are analyzed with more details, for the lower extrusion temperature ($T_L =$ 200 ºC), the filaments of sets C and D exhibit insufficient adhesion since no break occurs. On the other hand, due to the contact that occurs earlier, adhesion between filaments of set B is better (higher average value for B_p). So, logically, filaments of set A should show the best adhesion, with the highest value for B_p. However, this did not occur and can be explained by the deposition velocity that showed to be non-constant, as illustrated by Figure 5.42, where a photo of a pair of filaments of set A is zoomed: the irregularities in the deposition velocity led to a reduction of contact points, which contributes to a worst adhesion. These irregularities did not occur for the others specimen, but the control of deposition velocity is very difficult, despite the use of the gear pump.
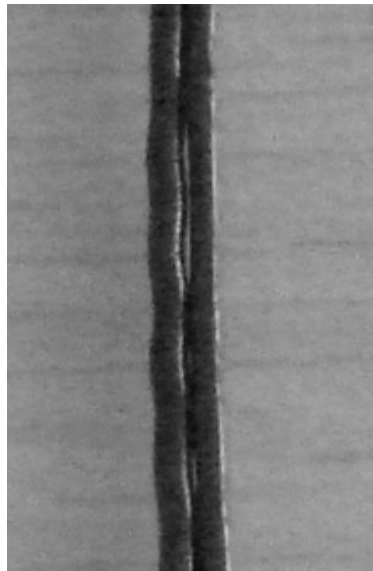
Figure 5.42 – Zoomed image of a specimen of set A, for $T_L = 200$ ºC.

For the higher extrusion temperature ($T_L = 220$ ºC), the non-constant deposition velocity also avoided a great adhesion for specimens of set B. However, the results respective to the specimen of sets A, C and D show a decreasing adhesion when contacts occur later: this shows the great importance of thermal contacts between adjacent filaments in the bonding quality.

The experimental measurements were now compared with the MatLab® results. The code allows obtaining the adhesion degree evolution of any cross section of the pair of filaments, so the cross-section point from which the adhesion degree does not reach the unity value is registered. The results can be compared in Table 5.7 and Table 5.8 for the two respective extrusion temperatures. For the lower extrusion temperature, theoretical results showed to be in good agreement with experimental results (maximum difference

of 3%), except for the set A, due to the problems of non-constant deposition velocity referred before, fact that can be also observed for the set B, with the higher extrusion temperature. With T_L = 220 ºC, the results for the specimen of sets B and C are also much closed to the MatLab® break point values (maximum difference of 4%), except for the specimen of set D, which broke at B_p = 1 cm, that is, at the local where the two filaments have the first contact. However, the computation code predicts that the break doesn't occur: this is due to the higher value of extrusion temperature and the direction change of support table, which leads to a stronger contact point at this local. This phenomenon can be observed in Figure 5.43, where a specimen of set D is zoomed.

Table 5.7 – Break point values for T_L = 200 ºC: comparison between experiences and MatLab® results.

Specimen Type	Experimental break point (%)	MatLab® break point (%)
A (non-constant deposition velocity)	0%	17%
B (constant deposition velocity)	7%	10%
C (constant deposition velocity)	0%	0%
D (constant deposition velocity)	0%	0%

Table 5.8 – Break point values for T_L = 220 ºC: comparison between experiences and MatLab® results.

Specimen Type	Experimental break point (%)	MatLab® break point (%)
A (constant deposition velocity)	30%	34%
B (non-constant deposition velocity)	5%	26%
C (constant deposition velocity)	16%	19%
D (constant deposition velocity)	10%	0%
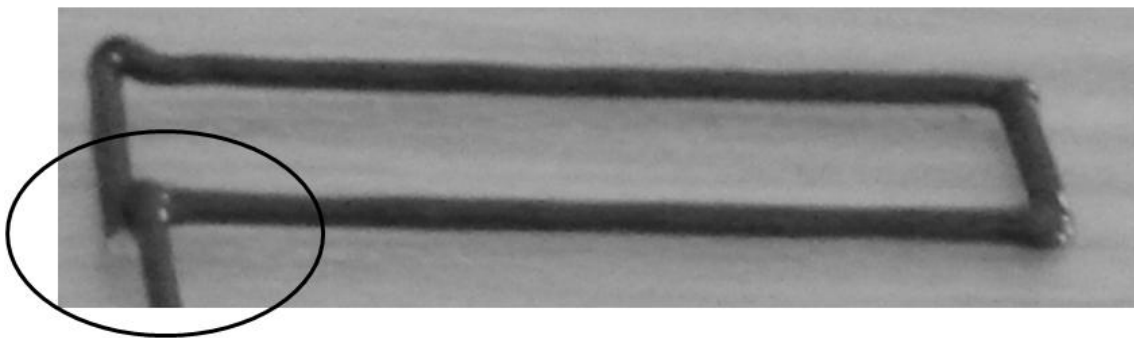
Figure 5.43 – Zoomed image of a specimen of set D, for T_L = 220 ºC.

6 DEDUCTION OF THE MOST IMPORTANT PROCESS VARIABLES ON THE FINAL QUALITY OF FFE PARTS

The objective of this chapter is evaluating the importance degree of some variables on the quality of parts made by FFE and identifies strategies that can improve the performance of these.

In a first phase, two deposition sequences are chosen in order to observe the heat transfer and the adhesion evolution for different conditions:

- The first will be used for the observation of temperature evolution, where the 3rd filament was selected due to the large number of contacts (Figure 6.1). Note that the length of the filaments is $L = 0.1$ m.

- The second will be used for the evolution of adhesion degree ($L = 0.02$ m), where 16 contacts are available. The aim is to verify if the conclusion made from the results obtained with the last deposition still valid for this deposition sequence (Figure 6.2).

$$\longrightarrow \quad M = \begin{bmatrix} 4 & 0 \\ 2 & -1 \\ 2 & 0 \end{bmatrix}$$
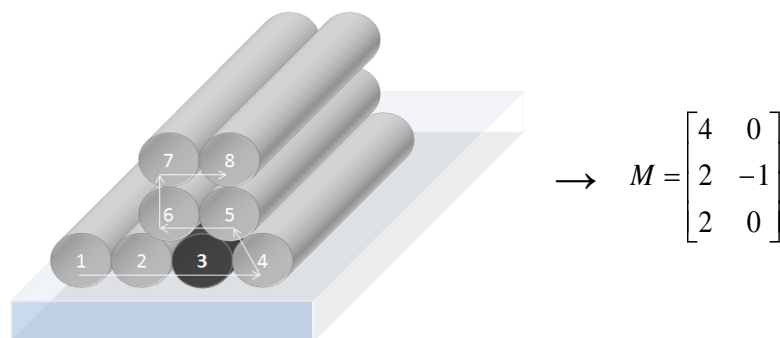
Figure 6.1 – Sequence of filaments deposition for $L = 0.1$ m and corresponding matrix for the temperature results.

$$\longrightarrow \quad M = \begin{bmatrix} 6 & 0 \\ 6 & 0 \end{bmatrix}$$
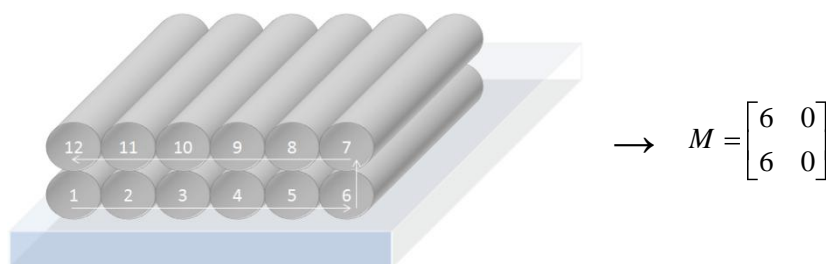
Figure 6.2 – Sequence of filaments deposition for $L = 0.02$ m and corresponding matrix for the adhesion degree results.

The influence of the following parameters on temperature evolution was studied (Table 6.1):

Table 6.1 – FFE variable parameters.

Property	Value
Heat Transfer Coefficient for the natural convection with air (W/m^2.K)	65
Extrusion Temperature (ºC)	270
Environment Temperature (ºC)	70
Deposition velocity (m/s)	0.02
Orientation Strategy	---

The constant parameters and the computational variables are respectively shown in Table 6.2 and Table 6.3. The material properties values (density, thermal conductivity and specific heat) are also relative to a P400 ABS plastic, usually used in FDM technology (Rodriguez, Thomas and Renaud 1999).

Table 6.2 – FFE constant parameters.

Property	Value
Density of ABS P400 (kg/m^3)	1050
Thermal Conductivity of ABS P400 (W/m.K)	0.1768
Specific Heat of ABS P400 (J/kg.K)	2019.7
Thermal Contact Conductance for the contacts between adjacent filaments (W/m^2.K)	From 10^{-4} (for no adhesion) to 250 (adhesion)
Thermal Contact Conductance for the contact between filaments and support (W/m^2.K)	10
Fraction of Contact length	0.2
Cross-section Geometry	Circle
Cross-section Width (m)	0.0003
Cross section x	*Filament middle* (*L*/2)

Table 6.3 – Computational variables.

Property	Value
Computation time (s)	0.01
Additional computation time after the part construction (s)	15
Temperature convergence error (ºC)	10^{-3}

In a second phase, two bi-material parts with real dimensions were considered and a detailed study about their adhesion quality is made with the computer code.

6.1 Heat Transfer Coefficient

In order to test the influence of convection coefficient, three values were tested: $h = 10$ W/m$^2 \cdot$ °C, $h = 65$ W/m$^2 \cdot$ °C and $h = 100$ W/m$^2 \cdot$ °C. Temperature results show that the heat transfer coefficient has a large influence on the evolution of temperature (Figure 6.3). Smaller values for heat transfer coefficient imply a smaller rate of cooling down and vice versa, making its determination as very relevant. The obtained results for adhesion degree vs time (Figure 6.4) also verify this last observation: for $h = 100$ W/m$^2 \cdot$ °C, the adhesion degree reaches the unit value after a longer time period than for $h = 10$ W/m$^2 \cdot$ °C. Then, with higher values of convection coefficient, temperatures decrease faster, and the adhesion is prejudiced, as concluded by Yardimci (1996). On the other hand, if the adhesion results of $h = 100$ W/m$^2 \cdot$ °C are compared between the two sequences, for the 2nd one, the maximum adhesion is reached for all the pairs of adjacent filaments, but not for the 1st one: filaments 2 and 6, and filaments 5 and 8 don't reach the maximum adhesion. This is due to the higher length of filaments for the 1st sequence, which implies a more raised time period between two consecutive filaments. The part geometry is then very important in the adhesion control, that is, longer parts have lower mechanical resistance.
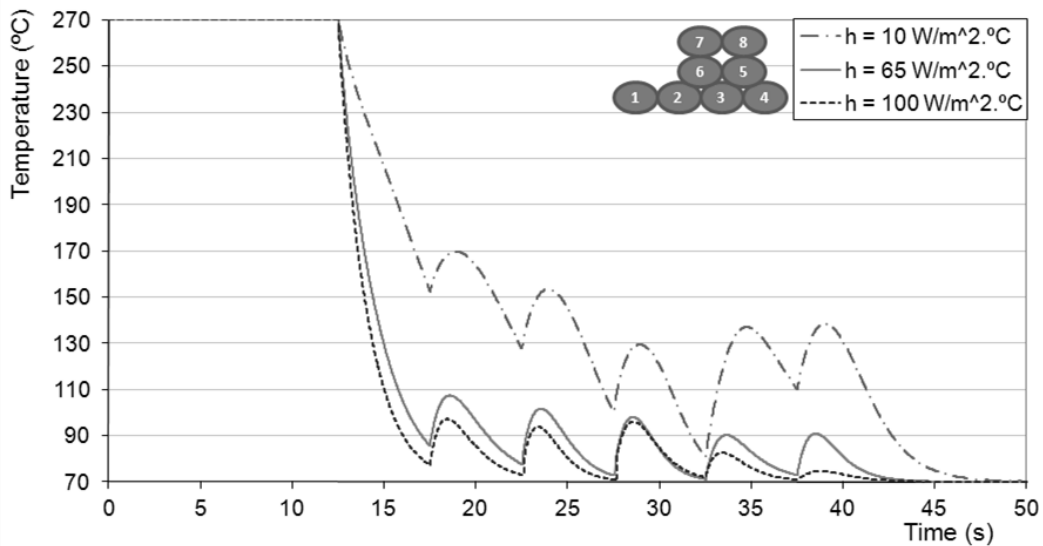
Figure 6.3 – Temperature vs. time for some values of heat transfer coefficient.
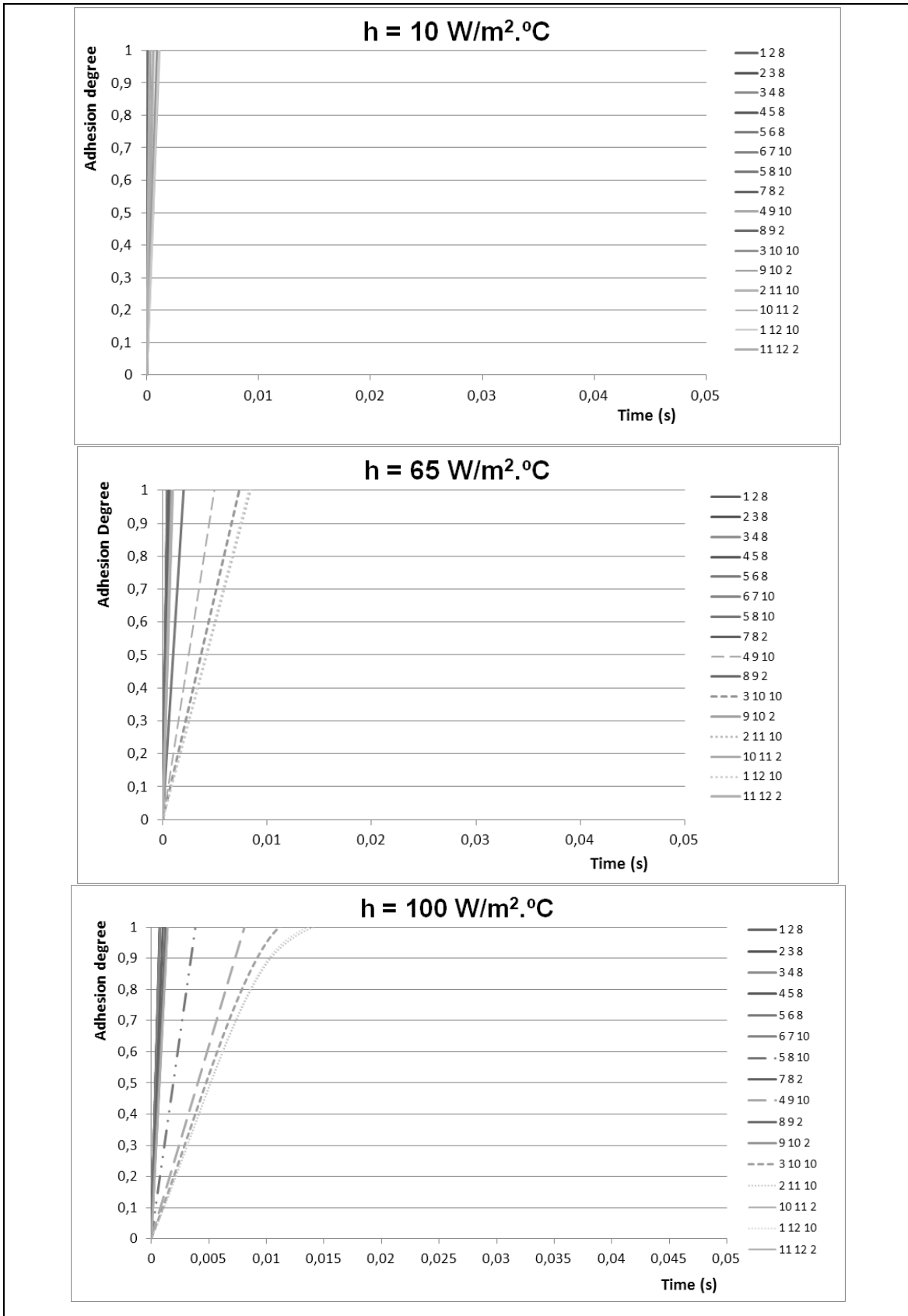
Figure 6.4 – Adhesion degree evolution along deposition time for $h = 10$ W/m$^2 \cdot$ ºC, $h = 65$ W/m$^2 \cdot$ ºC and $h = 100$ W/m$^2 \cdot$ ºC.

6.2 EXTRUSION TEMPERATURE

To test the influence of extrusion temperature, three values were tested: $T_L = 270°C$, $T_L = 250°C$ and $T_L = 230°C$. For each of these values, the temperature and the adhesion degree along time were computed for the two sequences, and respectively shown in Figure 6.5 and Figure 6.6. As expected, the diminution of extrusion temperature implies a faster cooling down and a worst adhesion. For the lowest temperature ($T_L = 230.°C$), Figure 6.6 shows that the adhesion degree for filaments 1 and 12, 2 and 11, 3 and 10, and 9 and 4, were not reach the value 1 (perfect adhesion), so, these pairs of filaments don't adhere. For the medium value ($T_L = 250°C$), adhesion occurs for all the pairs of filaments, but the necessary time to reach this adhesion is longer than for the highest temperature ($T_L = 270°C$).
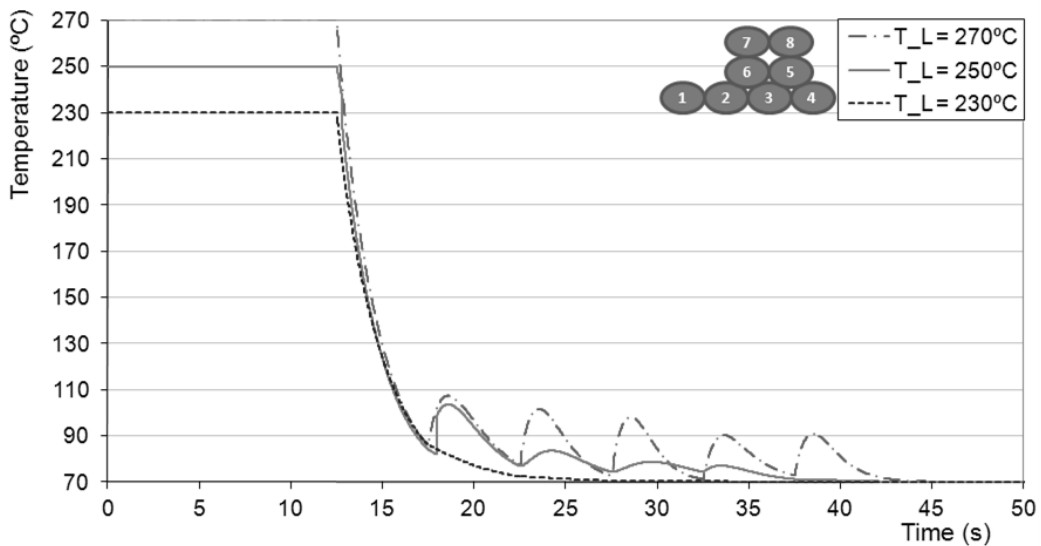
Figure 6.5 – Temperature vs. time for some values of extrusion temperature.
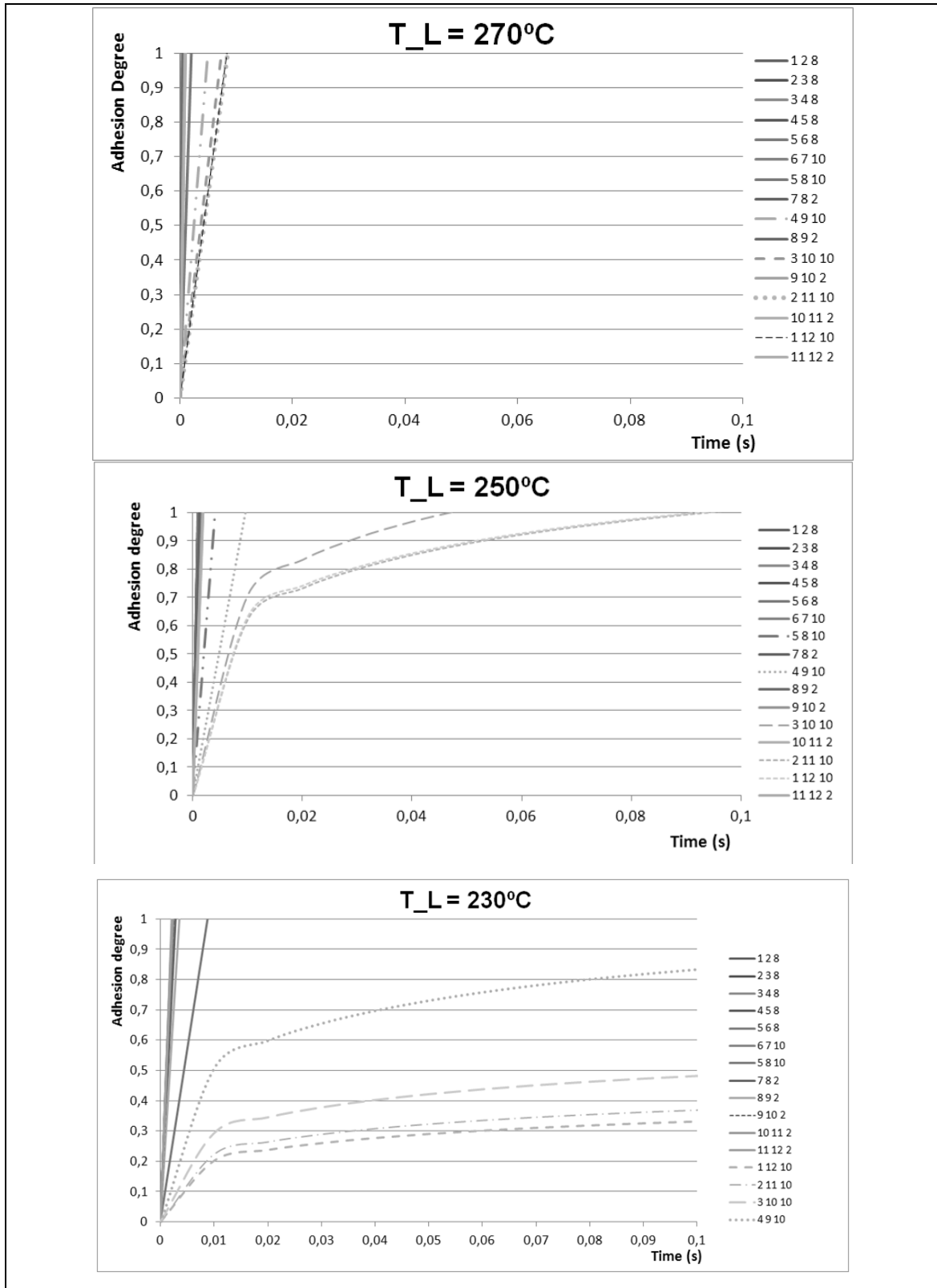
Figure 6.6 – Adhesion degree evolution along deposition time for $T_L = 270$ºC, $T_L = 250$ºC and $T_L = 230$ºC.

6.3 ENVIRONMENT TEMPERATURE

The influence of environment temperature was too studied for three values: $T_E = 70ºC$; $T_E = 60ºC$ and $T_E = 50ºC$. Temperature and adhesion results are respectively shown in Figure 6.7 and Figure 6.8. As deduced by Rodriguez (1999), the environment temperature has a higher influence than the extrusion temperature: with a reduction of 20 ºC in the environment temperature, differences can reach 40ºC; with the same reduction in the extrusion temperature, maximum differences only round the 20ºC.

Respecting to the adhesion, this is reached in the three cases, but for the lowest temperature ($T_E = 50ºC$), the necessary time to accomplish the bonding is higher. Since this variable is controllable, it can be used to improve the adhesion.
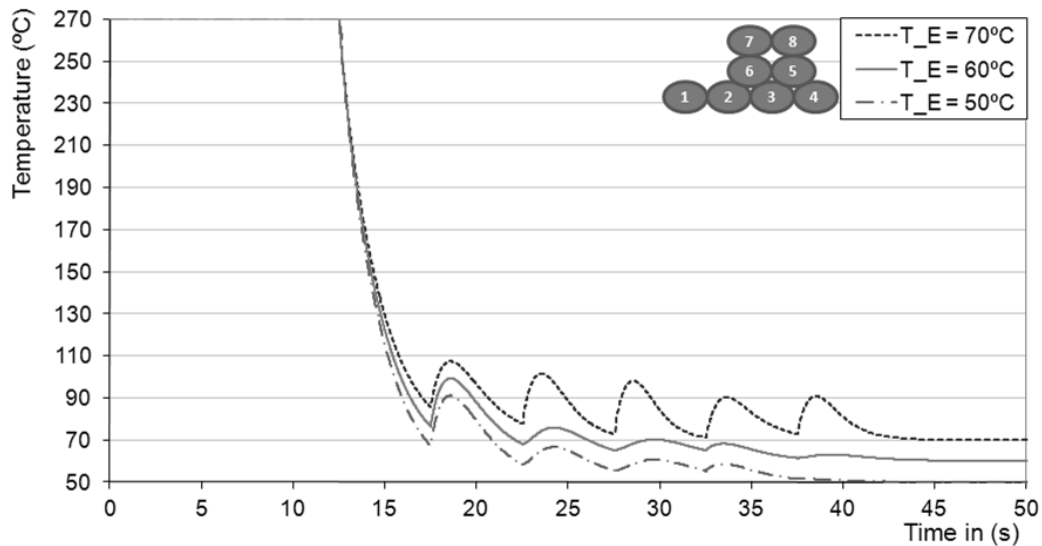
Figure 6.7 – Temperature vs. time for some values of environment temperature.
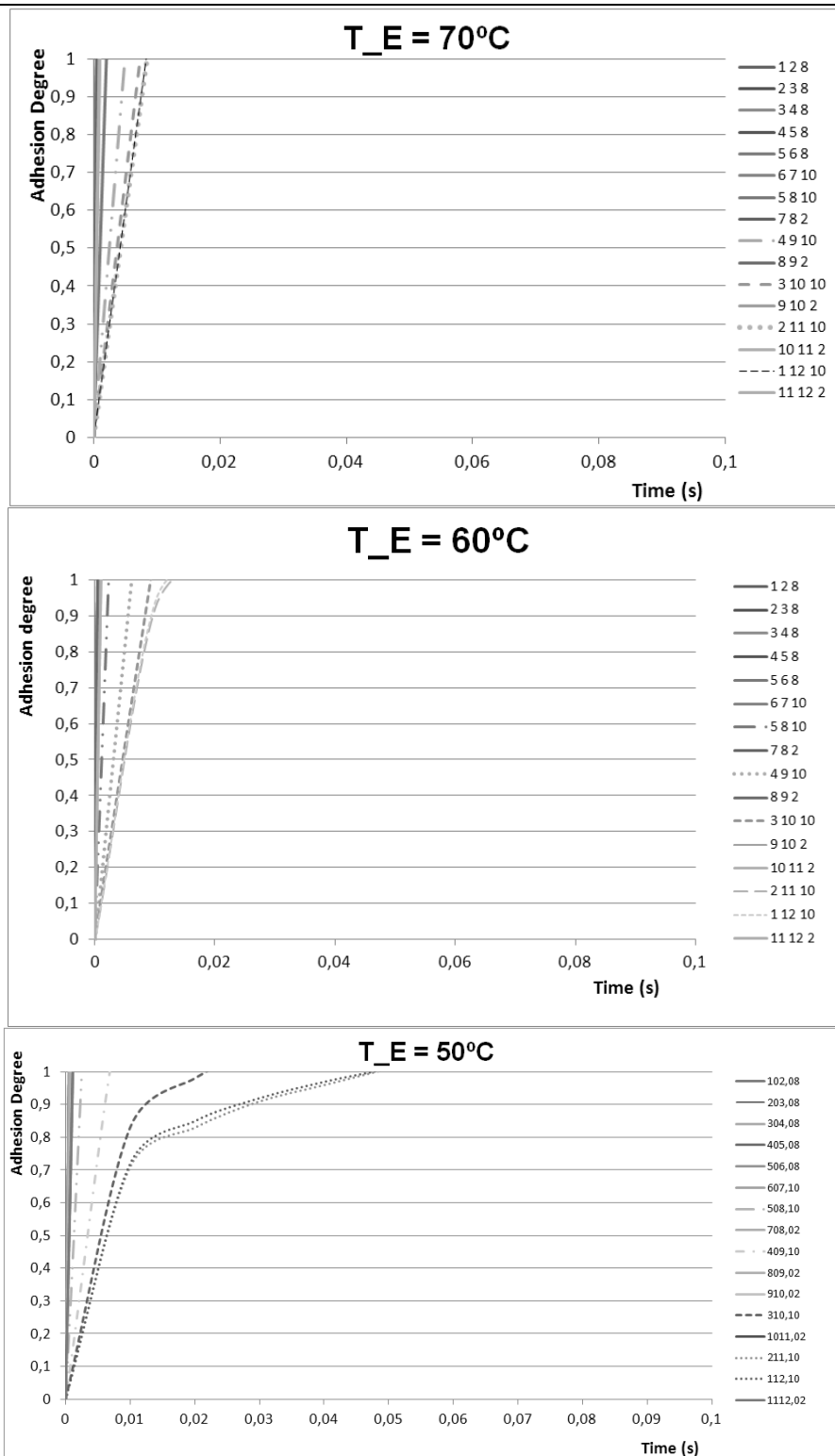
Figure 6.8 – Adhesion degree evolution along deposition time for $T_E = 70°C$, $T_E = 60°C$ and $T_E = 50°C$.

6.4 DEPOSITION VELOCITY

Three values were used to test the weight of extrusion velocity: $v = 0.02$ m/s; $v = 0.01$ m/s and $v = 0.005$ m/s. Figure 6.9 shows the temperature evolution for the three cases: the velocity of extrusion head influences very much the evolution of temperature, due to the thermal contacts that occur at different times. Then, the extrusion velocity has a very important paper in the FFE process, and can be adapted to improve the quality of the final part.
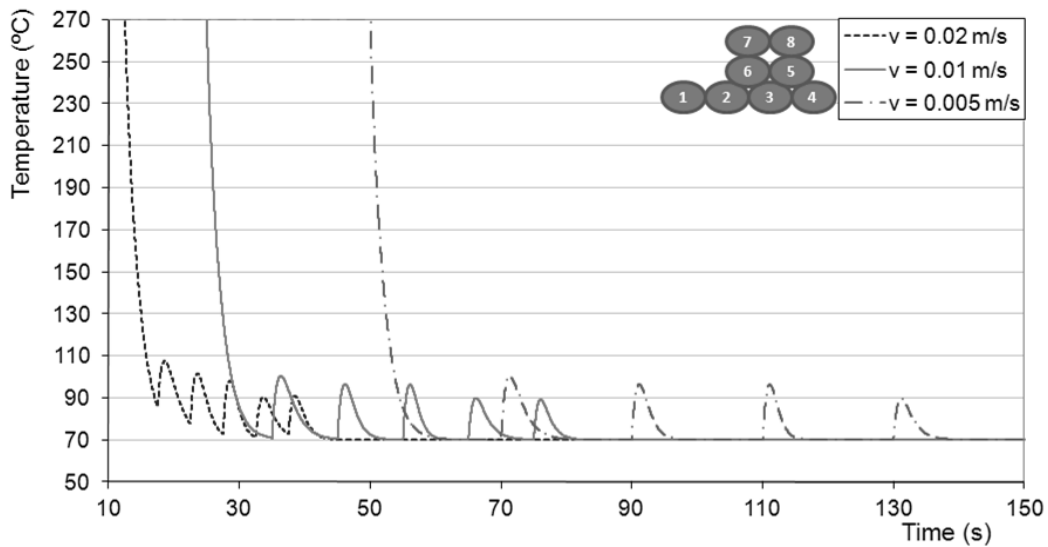
Figure 6.9 – Temperature vs. time for some values of extrusion velocity.

Figure 6.10 also prove this conclusion; as expected, lower values of deposition velocity imply lower values of adhesion degree. So, although the influence of this variable on heat transfer has never been studied in previous studies, this is very important and can be used to improve the mechanical resistance of the part.
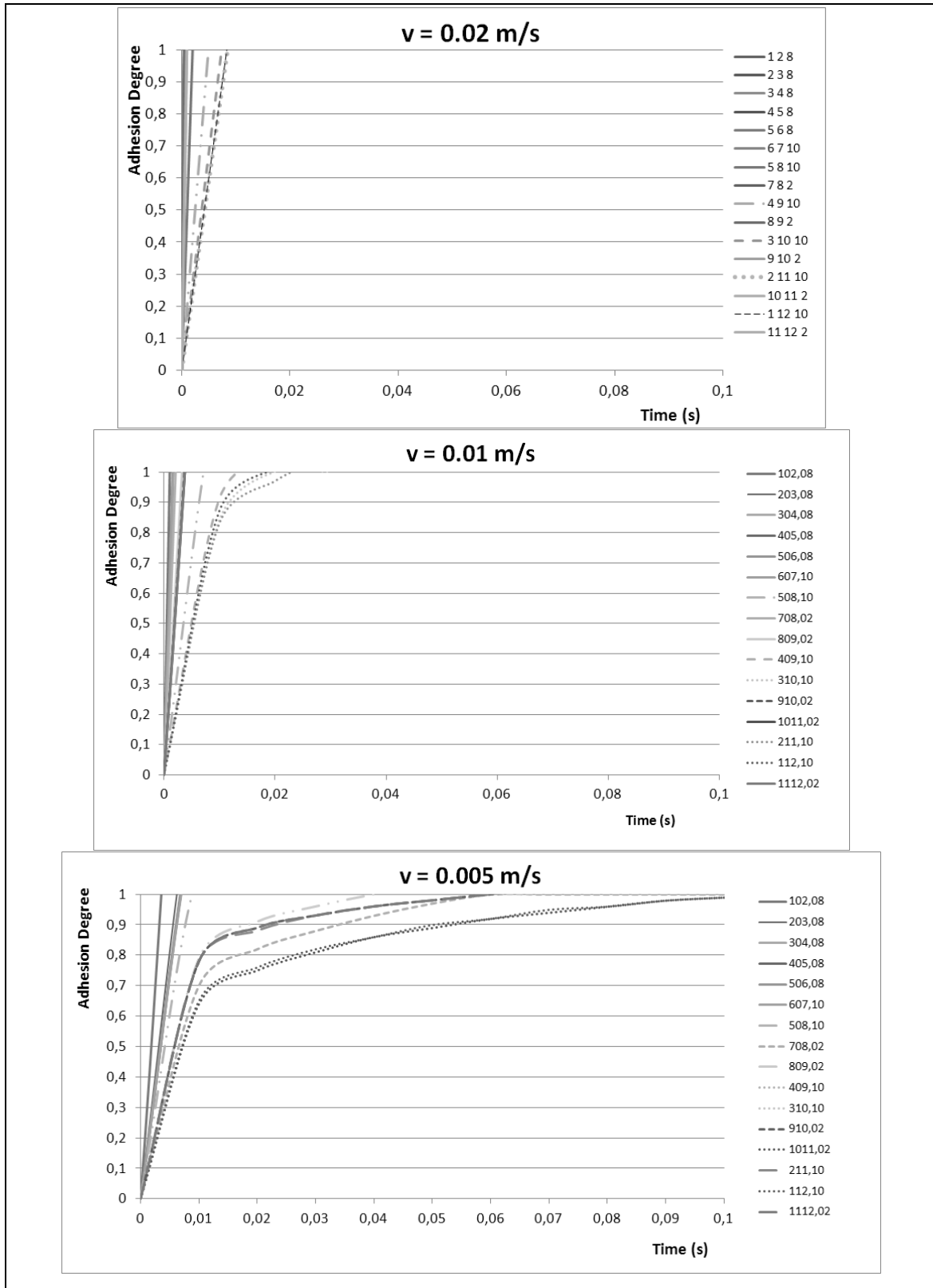
Figure 6.10 – Adhesion degree evolution along deposition time for $v = 0.02$ m/s, $v = 0.01$ m/s and $v = 0.005$ m/s.

6.5 ORIENTATION STRATEGY

The 2nd previous sequence can be made on some different orientations. Two orientations were tested to study its importance degree in the adhesion phenomena (Figure 6.11).

Orientation 1   Orientation 2
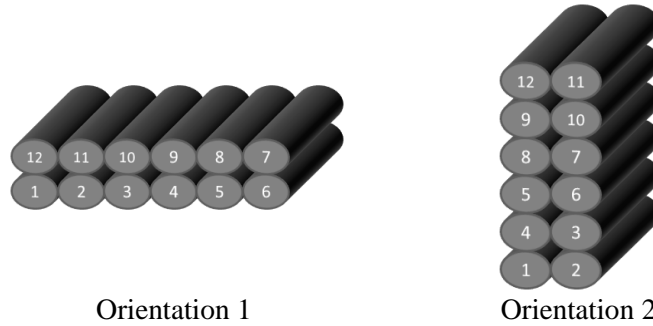
Figure 6.11 – Considered possible orientations for the construction of the part.

The evolution of adhesion degree is shown for the two orientations in Figure 6.12.
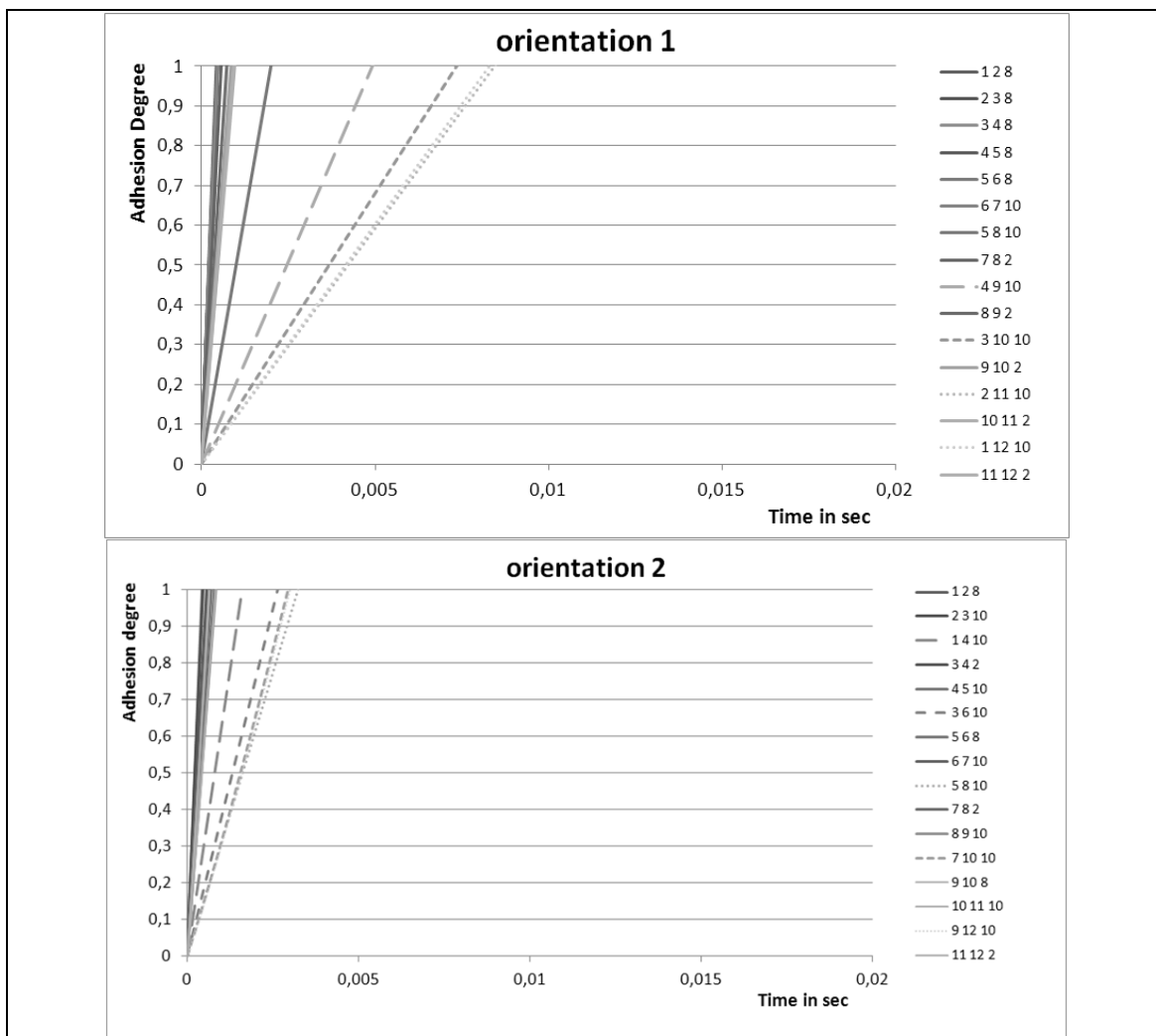
Figure 6.12 – Adhesion degree evolution along deposition time for the two different orientations.

These results show that the orientation construction has influence on the adhesion process. Adhesion is reached in the two cases, but for the orientation 2, the bonding is faster reached than for the orientation 1. This is due to the higher width of the part for the 1st orientation: the maximum time period between two adjacent filaments is longer than for the 2nd orientation. So, to maximize the mechanical resistance of this part, orientation 2 must be chosen and, as a general conclusion, orientations where the width is raised must be avoided.

6.6 BI MATERIAL PARTS

Consider the engineering parts that fit together, with the geometry presented in Figure 6.13, to be manufactured under the processing conditions summarized in Table 6.4.

Part A   Part B
Figure 6.13 – Geometry of the parts.

Table 6.4 – Processing conditions.

Property	Value
Extrusion Temperature (ºC)	270
Environment Temperature (ºC)	70
Extrusion velocity (m/s)	0.025
Heat Transfer Coefficient (W/m$^2 \cdot$ ºC)	20
Cross-section geometry	Square
Cross-section width (m)	0.0003
Deposition sequence type	Unidirectional and aligned
Density of ABS P400 (kg/m^3)	1050
Thermal conductivity of ABS P400 (W/m· ºC)	0.1768
Specific Heat of ABS P400 (J/kg· ºC)	2019.7

The manufacture of these parts requires the use of a support material. The deposition sequence for each part is shown in Figure 6.14 and Figure 6.15, where gray filaments are made of part material (ABS) and white filaments are made of support material.

136
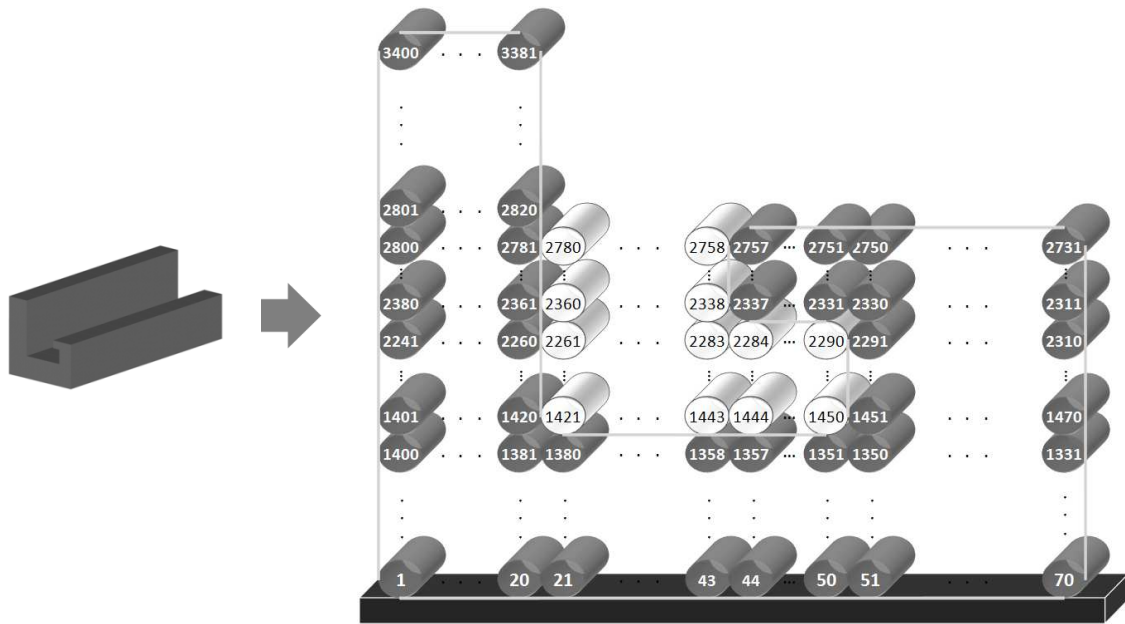
Figure 6.14 – Filaments deposition sequence for part A.
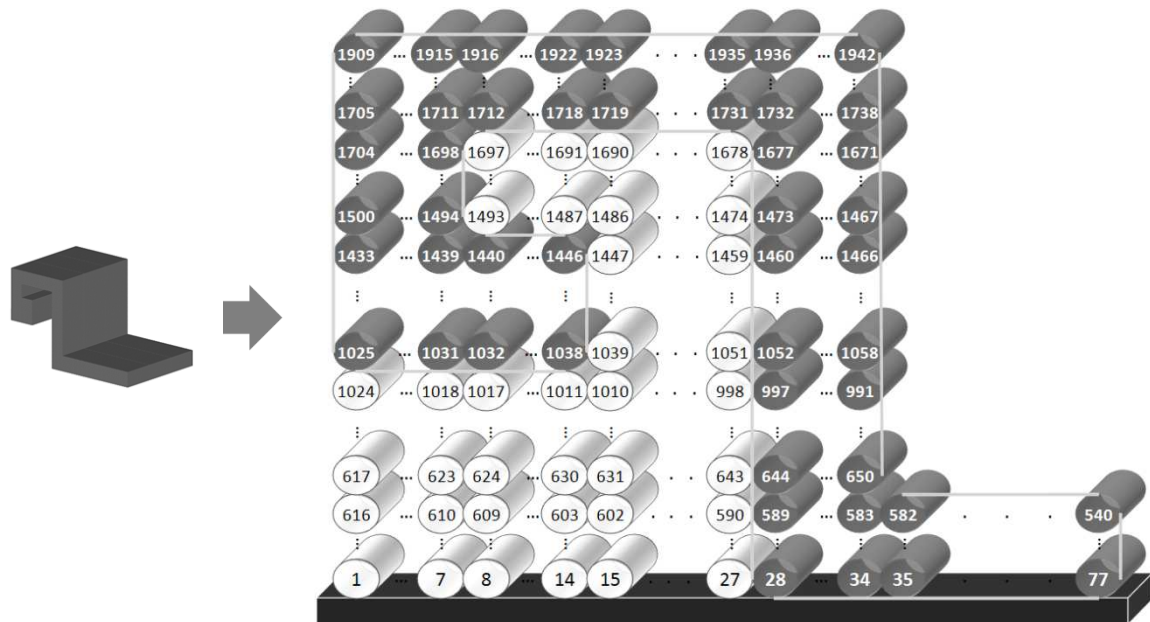
Figure 6.15 – Filaments deposition sequence for part B.

PLA was considered as support material: the properties of this material are described in Table 6.5.

Table 6.5 – Material properties of support material PLA.

Property	Value
Density (kg/m^3)	1300
Thermal conductivity (W/m· ºC)	0.2
Specific Heat (J/kg· ºC)	2100

Figure 6.16 shows the problematic adhesion areas of the parts constructed by FFE technique, for the conditions described before. According to the computation results, the parts have a satisfactory mechanical resistance.
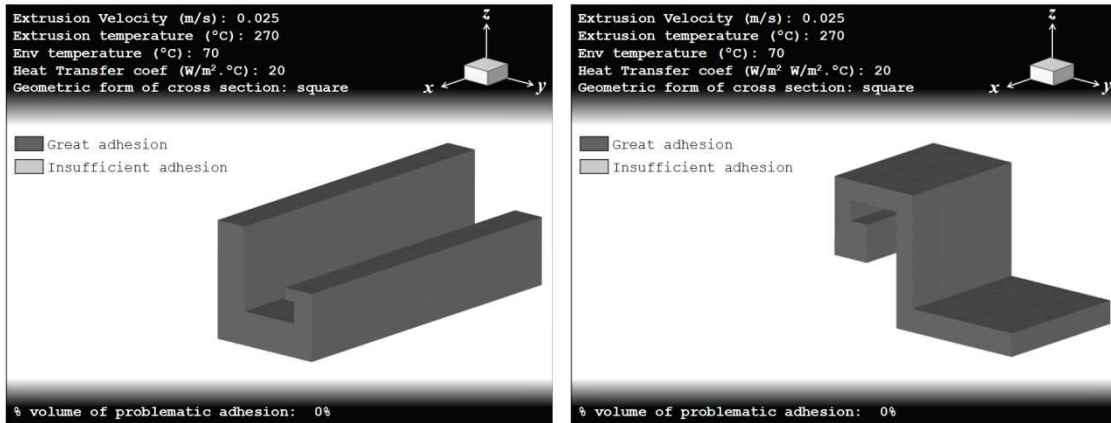
Figure 6.16 – Problematic adhesion areas of part A and part B.

The two parts were newly tested, but with a lower extrusion temperature (T_L = 260ºC): Figure 6.17 shows that the parts remain with a good performance.
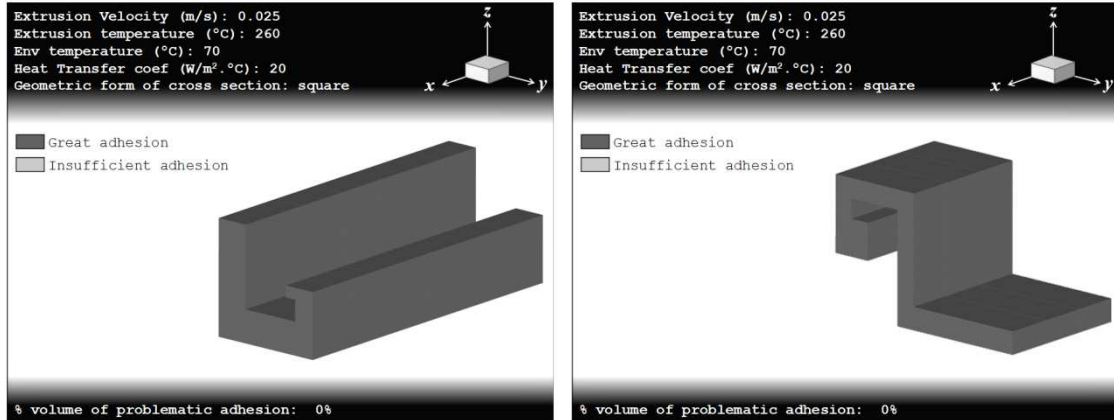
Figure 6.17 – Problematic adhesion areas of part A and part B for T_L = 260ºC.

However, if the extrusion temperature is again reduced (T_L = 250ºC), the part A losses quality unlike the part B: a problematic adhesion volume of 9.6% was obtained for part A (Figure 6.18). These results show the great importance of the geometry: parts with higher dimensions are more sensitive to bonding problems, as concluded before.
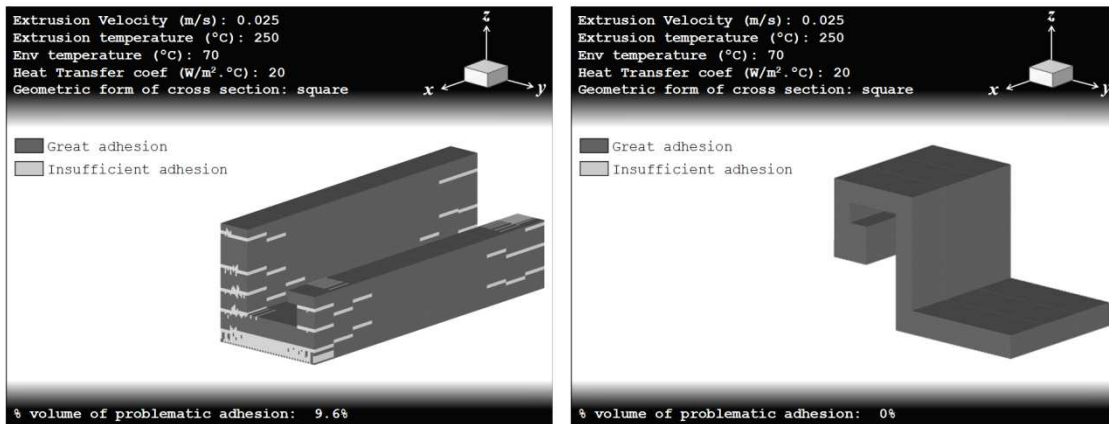
Figure 6.18 – Problematic adhesion areas of part A and part B for $T_L = 250$ºC.

Some additional tests were made to conclude that the smaller part B starts having problems only from $T_L = 230$ºC (Figure 6.19).
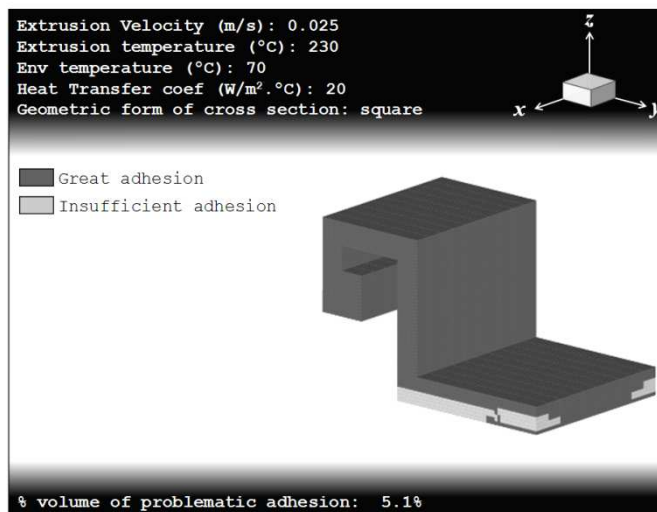
Figure 6.19 – Problematic adhesion areas of part B for $T_L = 230$ºC.

In order to understand where the adhesion was not reached, three cuts were made along the part B for this last test ($T_L = 230$ ºC): on $x = 0.001$ m (Figure 6.20), $x = 0.0075$ m (Figure 6.21) and $x = 0.014$ m (Figure 6.22). These results allowed concluding that: i) adhesion problems are more present on the extremities of the part, ii) bonding is always reached on horizontal contacts and, iii) the most of filaments that didn't reach the adhesion allows to the first layers, due to the low number of filaments that prejudices the global heating of part and the contact with support table.
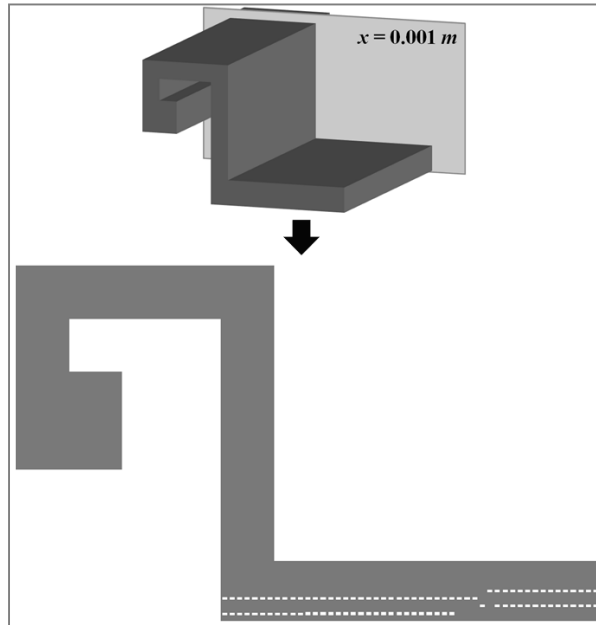
Figure 6.20 – Problematic adhesion areas of part B for $T_L = 230$ºC, on $x = 0.001$ m.
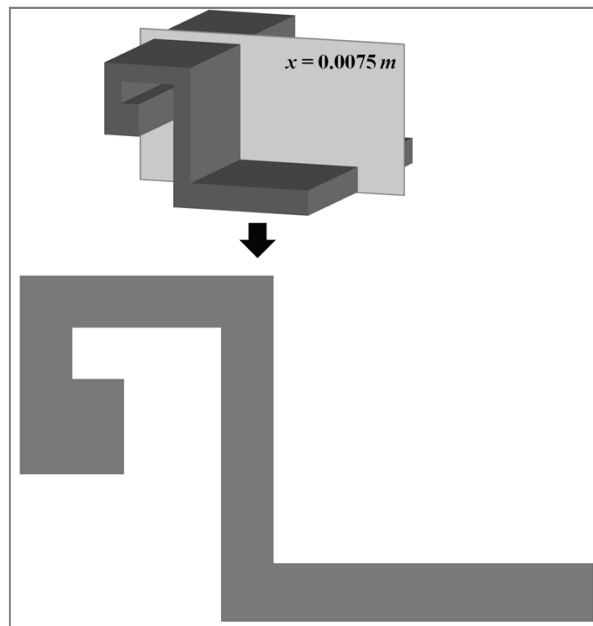
Figure 6.21 – Problematic adhesion areas of part B for $T_L = 230$ºC, on $x = 0.0075$ m.
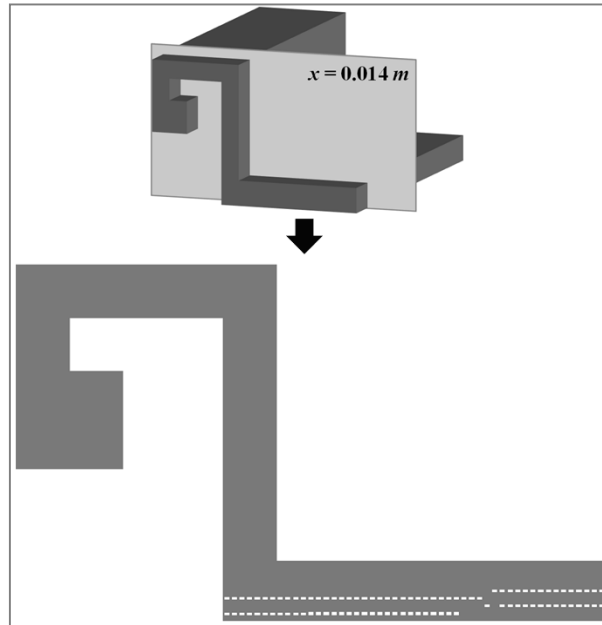
Figure 6.22 – Problematic adhesion areas of part B for $T_L = 230$ºC, on $x = 0.014$ m.

In order to solve this insufficient bonding, five layers of support filaments were added below the part and the adhesion test was newly made with $T_L = 230$ºC: the problematic adhesion volume decreased from 5.1% to 0% (Figure 6.23). This shows the potential of the code in modifying the process conditions to optimize the performance of the part.
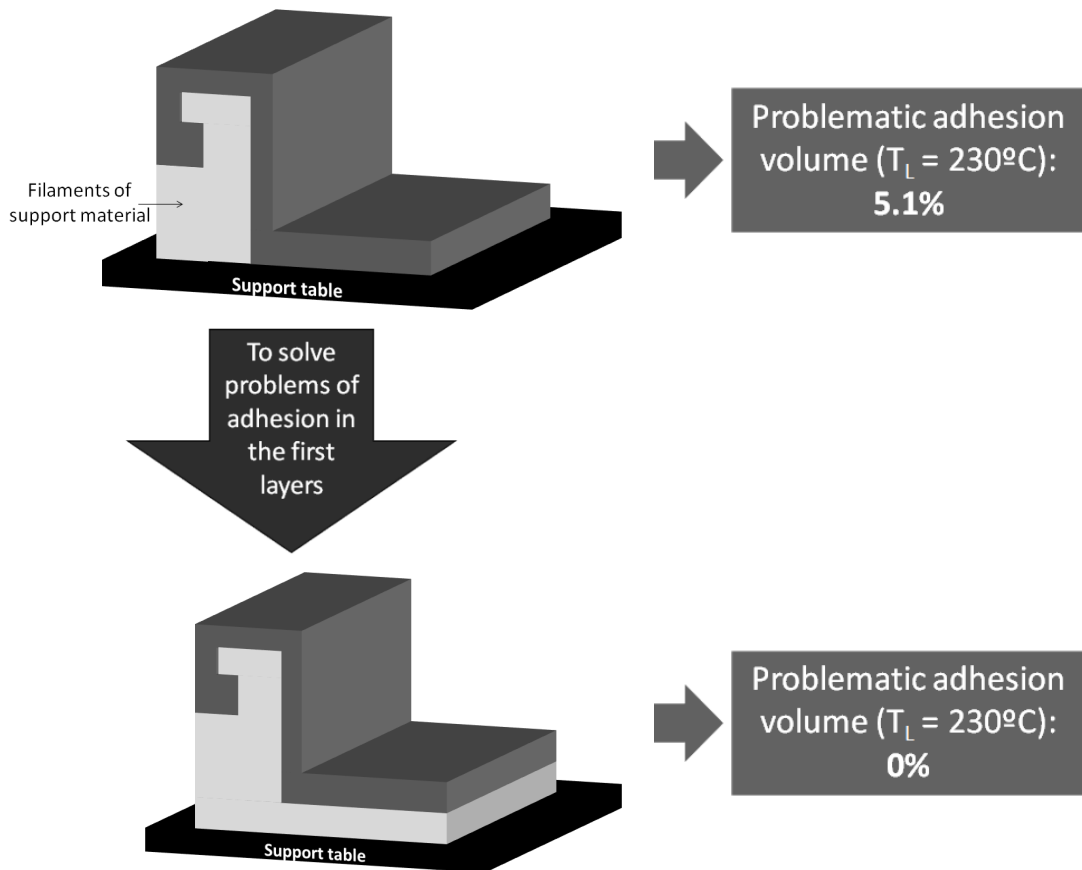
Figure 6.23 – Solution for improving the bonding degree in the first layers.

Part A was newly submitted to the adhesion test with a lower environment temperature $T_E = 50°C$ (Figure 6.24). A problematic adhesion volume of 7.2% was obtained, which is closed to the deduced volume for $T_L = 250°C$. Once more, the problematic adhesion points are located on the extremities of the part, and concentrated on the first layers.
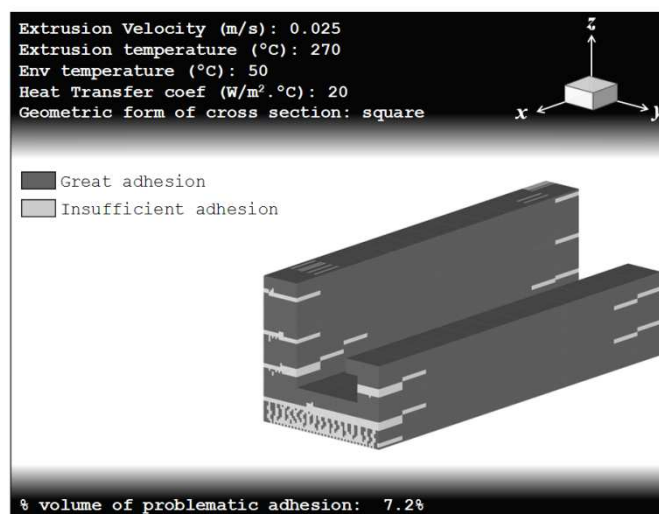
Figure 6.24 – Problematic adhesion areas of part A for $T_E = 50°C$.

The environment temperature was again decreased ($T_E = 40$ºC) and bonding results for part A are shown in Figure 6.25. The problematic adhesion volume increased significantly (52.03%): this shows the importance of constructing the part within an oven with a high temperature in order to maximize the mechanical resistance.
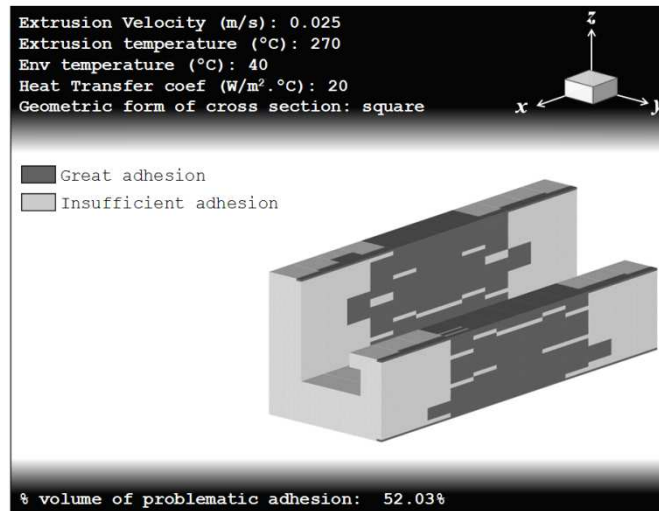
Figure 6.25 – Problematic adhesion areas of part A for $T_E = 40$ºC.

The weight of heat transfer coefficient on bonding was studied by increasing its value ($h_{conv} = 150$ W/m$^2 \cdot$ ºC): the adhesion remains perfect between all the adjacent filaments of the part (Figure 6.26).
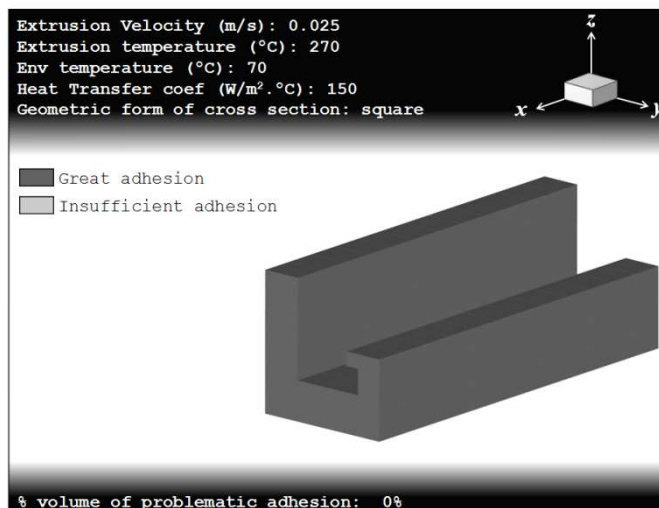
Figure 6.26 – Problematic adhesion areas of part A for $h_{conv} = 150$ W/m$^2 \cdot$ ºC.

The geometry of filament cross-section was also modified: a circular cross-section was considered (smaller contacts between adjacent filaments) but the part still exhibits a good mechanical resistance (Figure 6.27).
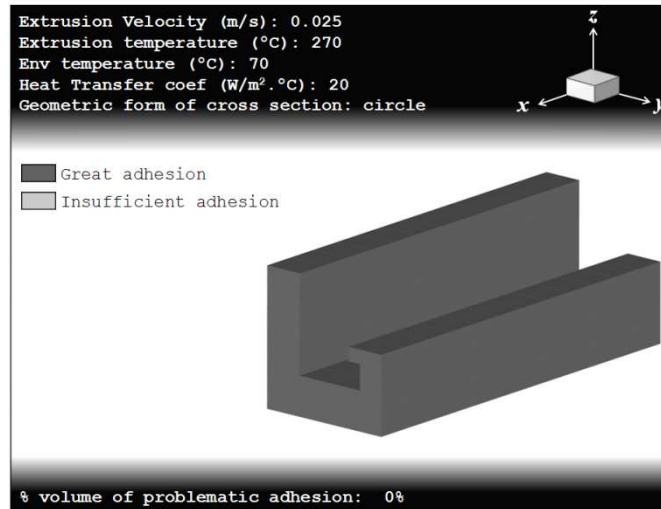
Figure 6.27 – Problematic adhesion areas of part A for circular cross-section filament.

6.7 DEPOSITION SEQUENCE TYPE

The influence of the deposition strategy on adhesion can be studied for parts made by a unique material. As a case study, consider the part with the geometry presented in Figure 6.28 to be manufactured under the processing conditions summarized in Table 6.6.
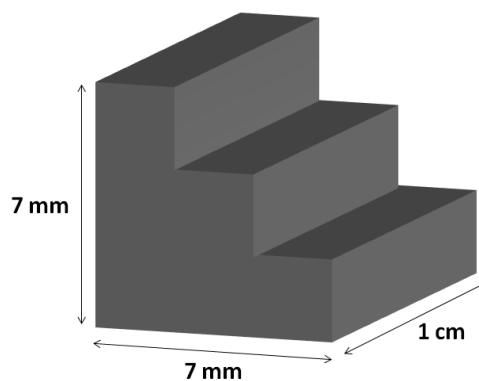
Figure 6.28 – Geometry of the part.
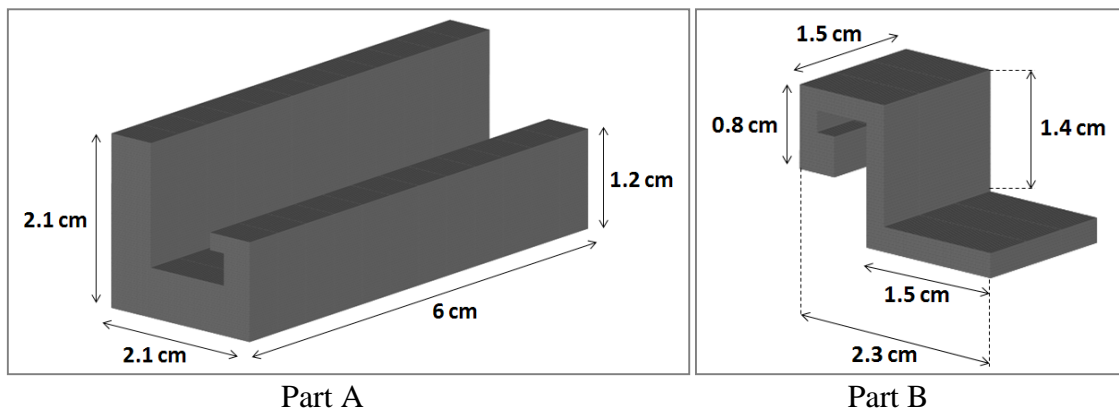
Table 6.6 – Processing conditions.

Property	Value
Extrusion Temperature (ºC)	240
Environment Temperature (ºC)	70
Extrusion velocity (m/s)	0.02
Heat Transfer Coefficient (W/m$^2 \cdot$ ºC)	60
Cross-section geometry	Circular
Cross-section width (m)	0.0004
Deposition sequence type	<u>Case 1</u>: Unidirectional and aligned
	<u>Case 2</u>: Perpendicular
Density of ABS P400 (kg/m^3)	1050
Thermal conductivity of ABS P400 (W/m $\cdot$ ºC)	0.1768
Specific Heat of ABS P400 (J/kg $\cdot$ ºC)	2019.7

The part was submitted to the adhesion test with two distinct deposition sequences: unidirectional and aligned filaments (Figure 6.29) and perpendicular filaments (Figure 6.30).
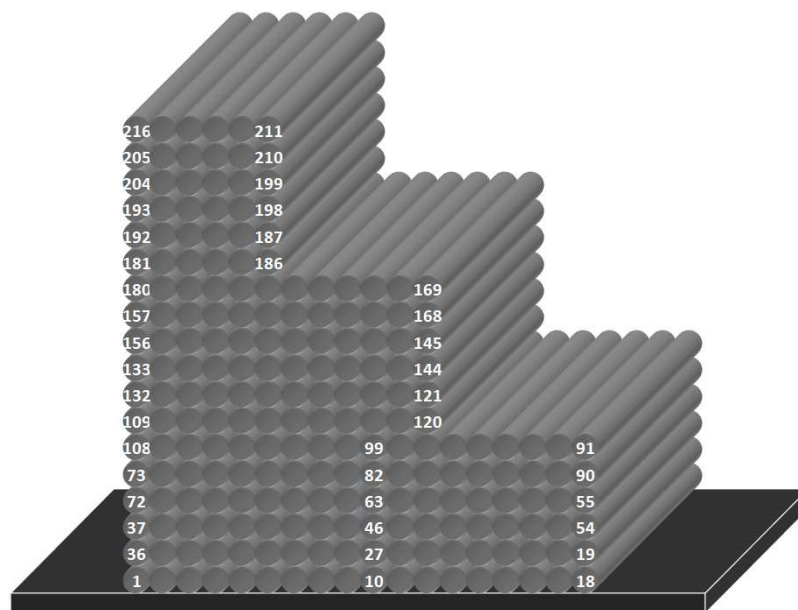
Figure 6.29 – Filaments deposition sequence (unidirectional and aligned).
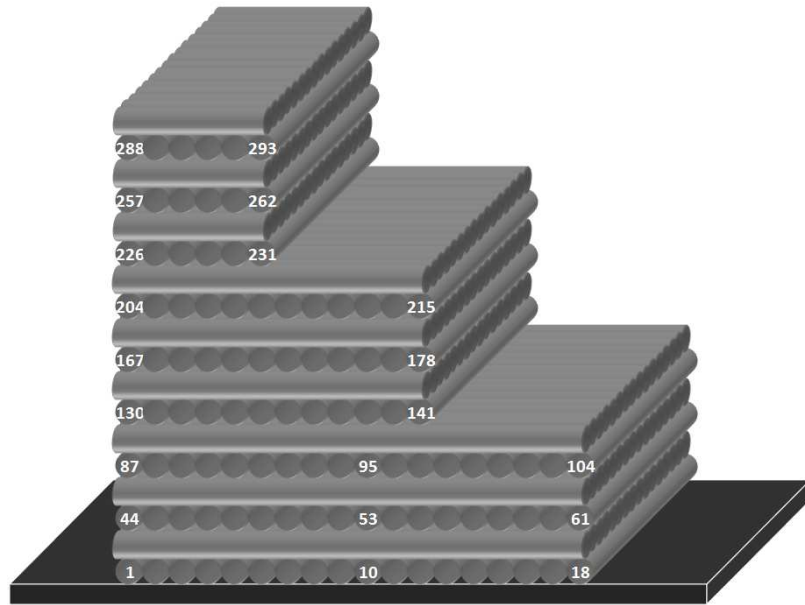
Figure 6.30 – Filaments deposition sequence (perpendicular).

Figure 6.31 and Figure 6.32 show the problematic and adequate adhesion areas for the two different deposition sequences. When adopting unidirectional deposition, 70% of the volume will evidence poor adhesion, whereas this value increases to 86.2% for perpendicular filaments. Beyond the percentage difference, the localization of the problematic adhesion areas also differs. This shows that the deposition type sequence has an important role on the bond quality, depending on the part geometry.
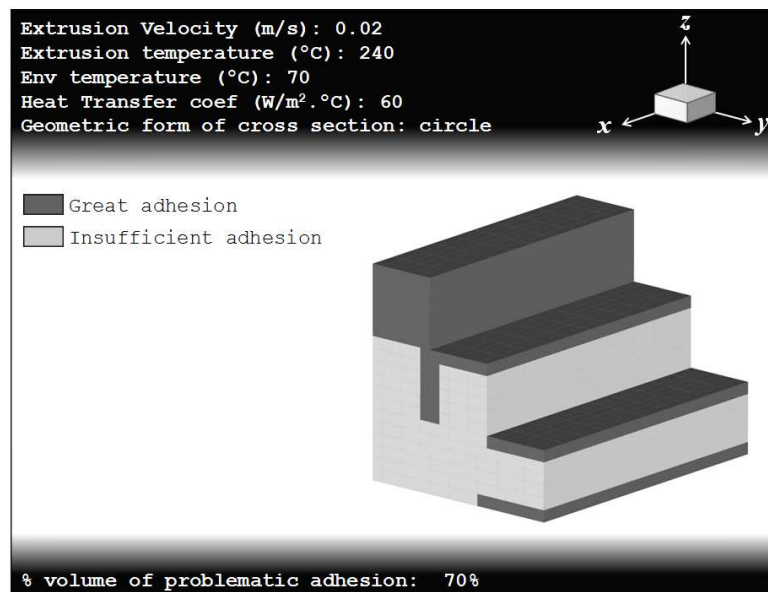
Figure 6.31 – Problematic adhesion areas of part for unidirectional filaments.
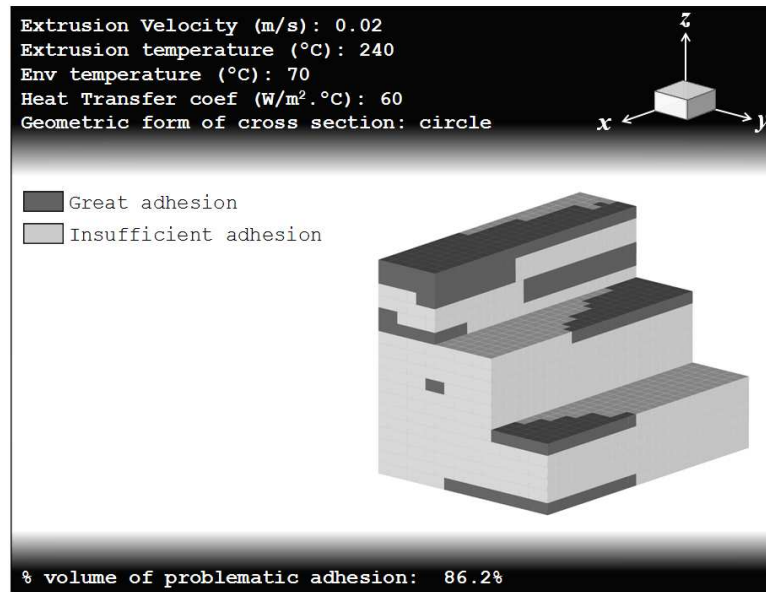
Figure 6.32 – Problematic adhesion areas of part for perpendicular filaments.

6.8 CONCLUSIONS

This study allowed us to make many conclusions:

- Heat transfer coefficient has a great influence on temperature and adhesion;

- Environment temperature has a higher influence on adhesion than extrusion temperature;

- All the variables that modify the instants at which the contacts occur have a much raised weight in temperature evolution and adhesion quality. These variables include deposition velocity, filament length, build orientation, part dimensions, cut x of the part and deposition sequence type. None of these variables were studied in previous heat transfer models, but these results show their unquestionable importance.

- The geometric form of the filament cross-section has a little influence on the adhesion degree.

7 CONCLUSIONS AND RECOMMENDATIONS FOR FUTURE WORK

The modelling of FFE was concretized through a rigorous study of the three phenomena and their inter-relations, which gave rise to a MatLab® computer code that devolves the temperature and the adhesion degree along deposition time of all the filaments, for any the three possible deposition sequences (unidirectional and aligned, unidirectional and skewed and perpendicular). This code was the consequence of the following studies:

- An influence study was first made with ABAQUS® software in order to deduce the thermal conditions that have the highest impact on heat transfer: heat exchanges with ambient by convection and between adjacent filaments by conduction showed to be the most important phenomena;

- An analytical study was carried out, by considering only these two thermal conditions: the differential equation was solved to yield an expression for temperature in function of time;

- Some procedures were created to generate a MatLab® code that devolves the temperature history for all the filaments of any deposition sequence, by using the previously deduced analytical expression;

- The computation of creep deformation was not included in the code, since the study with ABAQUS® software revealed that the deformation of filaments can be neglected;

- The expression for the adhesion degree proposed by Yang and Pitchumani (2002) was used to add a section in the code that allows computing the bonding degree between all the pairs of adjacent filaments, depending on the previously computed temperatures: this value is used to determine the thermal contact conductance values and to qualify the mechanical resistance of the final part.

This code was the base of others applications that can assist the FDM/FFE user in selecting the ideal process variables, for real complex parts. One of these applications is a code that devolves a *.txt* document as output; this document can be read by the Tecplot® software, which allows visualizing the 3D part with the locals where the adhesion did not reached. This gives us a fast feedback of the mechanical resistance of the final part, depending on the introduced process variables. In this code, only parts made by a unique material can be evaluated, which reduces the complexity degree of the geometry, but the three distinct deposition sequence types can be used, in order to conclude about the influence of the deposition strategy.

The other application is another code that also allows visualizing the 3D part with the problematic locals, but can be applied for parts made by two distinct materials. Since some simplifications were made in order to reduce the computation time, this code is a powerful tool that allows testing parts with a complex geometry and real dimensions. The description of these two applications is shown in Figure 7.1.

Code "FFE_complete 2011.m" allows:
- Obtaining the temperature/adhesion evolution along deposition time of all the filaments of any sequence. Three possible deposition sequences are available: unidirectional and aligned, unidirectional and skewed and perpendicular.

Code "FFE_two_mat_func.m" allows:
- Obtaining the pairs of adjacent filaments that not reach the perfect adhesion, for parts made by two distinct materials, for one deposition sequence type (unidirectional and aligned);
- Obtaining a .txt document that can be read by Tecplot® software, where the part can be visualized and the locals with poor adhesion are sinalized.

Code "FFE_complete_2011_func.m" allows:
- Obtaining the pairs of adjacent filaments that not reach the perfect adhesion, for parts made by a unique material, for any of these deposition sequence types: unidirectional and aligned, unidirectional and skewed and perpendicular.
- Obtaining a .txt document that can be read by Tecplot® software, where the part can be visualized and the locals with poor adhesion are sinalized.

Figure 7.1 – Applications deduced from the MatLab® computer code.

The proposed MatLab® code for bi-material parts can assist the FFE user in selecting the process variables values that will contribute to the good performance of final parts (Figure 7.2). For a selected object, the user determines the filaments number and identifies the filaments made of support material, depending of the specific geometry. This deposition sequence is introduced in the computer on matrix form, and the simulation code starts, in order to devolve the fractional volume of part (%) with problematic adhesion. If this volume is equal to 0%, it seems that the object has a good mechanical resistance, due to the absence of locations with insufficient bonding. In this case, FFE process can start to create the required part, with the assurance that the mechanical properties are satisfactory. Otherwise, the process variables are modified by the user (by increasing environment temperature, deposition velocity....), and simulation is newly made. The modification of these variables must be based on inter-relationships deduced from previous influence studies and depend on others objectives namely reduction of costs and manufacturing time. With this "test quality cycle", the performance of the initial part is guaranteed.

149

However, this code requires some improvements in order to apply this procedure. Contour fill is not available, the length of all the filaments must be the same, and perpendicular filaments cannot be used for bi-material parts. Consequently, some objects with circular faces, or with specific complex geometries, are not available by the software. These limitations can be eliminated through additional investigation, where the code would be extended in order to increase the diversity of available geometries and the possible filaments orientations. With these improvements, it would be possible to evaluate the quality of any FFE part before its construction, and, if necessary, to modify the process variables that allow maximizing their performance.
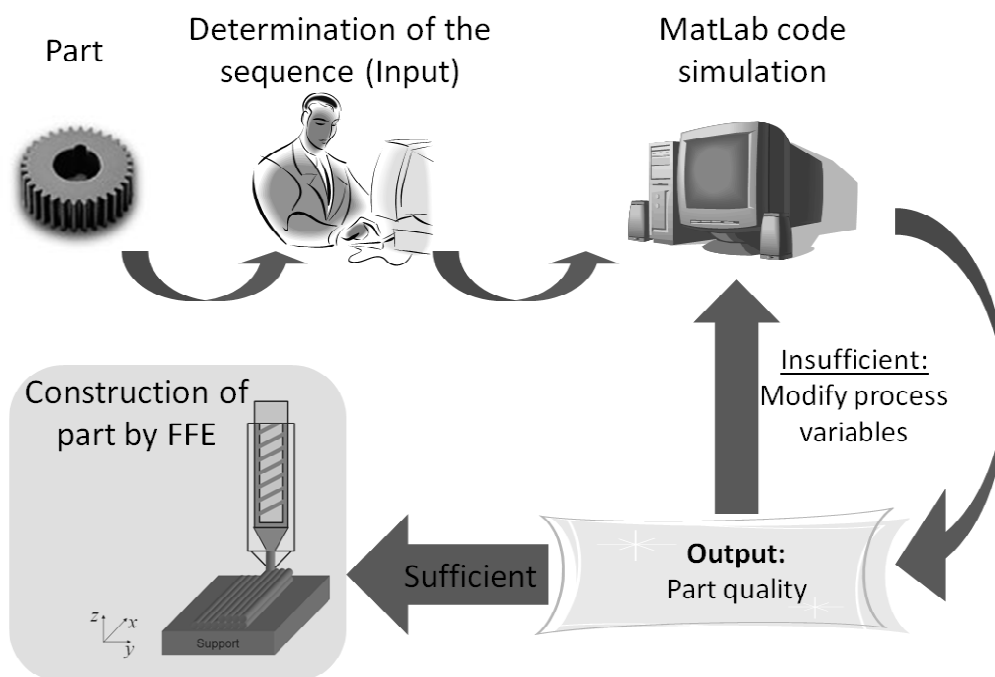
Figure 7.2 – Possible future application of the computer code for FFE modeling.

REFERENCES

- Agarwala, M. K., V. R. Jamalabad, N. A. Langrana, A. Safari, P. J. Whalen, and S. C. Danforth. "Structural quality of parts processed by fused deposition." *Rapid Prototyping Journal, Vol. 2*, 1996: 4-19.

- Ahn, S-H, M. Montero, D. Odell, S. Roundy, and P. K. Wright. "Anisotropic material properties of Fused Deposition Modelling ABS." *Rapid Prototyping, Vol.8*, 2002: 248-257.

- Bártolo, P. *Stereolithography: Materials, Processes and Applications.* Leiria, Portugal: Springer, 2011.

- Bastien, L.J., and J.W. Gillespsie. "A non-isothermal healing model for strength and toughness of fusion bonded joints of amorphous thermoplastics." *Polymer Engineering and Science, Vol.31*, 1991: 1721–1730.

- Bejan, A. *Heat Transfer.* USA, New York: John Wiley & Sons, Inc., 1993.

- Bellini, A. *Fused Deposition of Ceramics: a comprehensive experimental, analytical and computational study of material behavior, fabrication process and equipament design.* PhD thesis: Department of Mechanical Engineering and Mechanics, Drexel University, Philadelphia, PA, 2002.

- Bellini, A., and Bertoldi, S. M. Güçeri. "Liquefier Dynamics in Fused Deposition." *Journal of Manufacturing Science and Engineering, Vol. 126*, 2004: 237-246.

- Bellini, A., and S. Güçeri. "Mechanical characterization of parts fabricated using fused deposition modeling." *Rapid Prototyping Journal, Vol. 9*, 2003: 252-264.

- Bellini, A., L. Shor, and S. I. Güçeri. "New developments in Fused Deposition Modelling of Ceramics." *Rapid Prototyping Journal, Vol.11*, 2005: 214-220.

- Brinson, H. F., and L. C. Brinson. *Polymer engineering science and viscoelasticity: an introduction.* USA, Houston: Springer, 2008.

- Chua, C. K., K. F. Leong, and C. S. Lim. *Rapid Prototyping – Principles and Applications (2nd Chinese Edition).* Singapore: World Scientific Publishing, 2005.

- Cooper, K.G. *Rapid Prototyping Technology – Selection and Application.* USA, New York: Ed. Marcel Dekker Inc., 2001.

- Covas, J.A., and P. Costa. "A miniature extrusion line for small scale." *Polym Test*, 2004: 763-773.

- DeGarmo, E. P., J. T. Black, and R. A. Kohser. *Degarmo's Materials and Processes in Manufacturing.* USA: John Wiley & Sons, 2011.

- DeGennes, P.G. De. "Reptation of a polymer chain in the presence of fixed obstacles." *J. Chem. Phys. Vol.55*, 1971: 572 - 579.

- deGennes, P.G. "Reptation of a Polymer Chain in the Presence of Fixed Obstacles." *J. Chem. Phys. Vol.55*, 1971: 572-579.

- Drabousky, D. P. "Prony Series representation and interconversion of viscoelastic material functions of equine cortical bone." *Dissertation for the degree of Master of Science.* Department of Mechanical and Aerospace Engineering - Case Western Reserve University, August 2009.

- Elias, H. G. *Macromolecules:Volume 3: Physical Structures and Properties.* USA, Tulsa: Wiley-VCH, 2008.

- Ewen, B., and D. Richter. "Neutron spin echo spectroscopy, viscoelasticity, rheology." *Advances in polymer science, Vol. 134*, 1997: 1-129.

- Fellow, R. C. L., and J. H. Tzou. "The Development of an Intelligent Web_Based Rapid Prototyping Manufacturing System." *IEEE Transactions on Automation Science and Engineering, Vol.1*, 2004: 4-13.

- Gaal, D. S., and P. S. Gaal. *Thermal Conductivity 30/Thermal Expansion 18:Proceedings of the 30th International Thermal Conductivity Conference and the 18th International Thermal Expansion Symposium.* USA, Pittsburgh: DEStech Publications, Inc., 2010.

- Gebhardt, A. *Rapid Prototyping.* USA, Cincinnati: Hanser Gardner Publications, 2003.

- Gibson, I., D. W. Rosen, and B. Stucker. *Additive Manufacturing Technologies: Rapid Prototyping to Direct Digital Manufacturing.* USA, New York: Springer, 2009.

- —. *Manufacturing Techonologies: Rapid Prototyping to Direct Digital Manufacturing.* USA, New York: Springer, 2010.

- Gray, R.W., D.G. Baird, and D.G. Bohn. "Effects of processing conditions on short TLCP fiber reinforced FDM parts." *Rapid Prototyping Journal, Vol. 4*, 1998: 14-25.

- Gregorian, A., et al. "Accuracy improvement in rapid prototyping machine (FDM-1650)." *Solid Freeform Fabrication Proceedings*, 2001: 77-84.

152

- Grimm, T. *User's Guide to Rapid Prototyping.* USA, Dearborn: Society of Manufacturing Engineers, 2004.

- Helwany, S. *Applied soil mechanics with ABAQUS applications.* USA, Hoboken: John Wiley and Sons, 2007.

- Hibbitt, Karlsson and Sorensen, Inc. *ABAQUS User's Manual Version 5.7.* Pawtucket, USA: RI, 1997.

- Hoekstra, N. L., B. P. Kraft, and J. L. Newcomer. "Effect of Layer Orientation on the Mechanical Properties of ABS Test Specimens Produced By FDM." *Journal of Injection Moulding Technology, Vol.5*, 2001: 193-199.

- Hoekstra, N. L., B. P. Kraft, and J. L. Newcomer. "Effect of Layer Orientation on the Mechanical Properties of ABS Test Specimens Produced By FDM." *Journal of Injection Moulding Technology, Vol.5, No.3*, 2001: 193-199.

- Holman, J. P. *Transferência de Calor.* São Paulo, Brasil: McGraw-Hill, 1983.

- Hopkinson, N. *Rapid Manufacturing: an industrial revolution for the digital age.* Loughborough University, UK: John Wiley & Sons, Ltd., 2006.

- Jacobs P. F. *Rapid Prototyping and Manufacturing: Fundamentals of Stereolithography.* USA, Rochester Hills: Society of Manufacturing Engineers, 1992.

- Jacobs. *Stereolithography and other RP&M technologies:from rapid prototyping to rapid tooling.* Los Angeles, USA: Society of Manufacturing Engineers in cooperation with the Rapid Prototyping Association of SME, 1996.

- Kamrani, A. K., and E. A. Nasr. *Rapid Prototyping – Theory and Practice.* USA, New York: Springer Science, 2006.

- Kaviany, M. *Principles of heat transfer.* USA, New York: John Wiley & Sons, Inc., 2002.

- Kochan, D. *Solid Freeform Manufacturing, Advanced Rapid Prototyping. Manufacturing Research and Technology.* USA, New York: Elsevier, 1993.

- Kothandaraman, C.P., and S. Subramanyan. *Fundamentals of heat and mass transfer.* India, New Dehli: New Age International, 2006.

- Kraus, A. D., A. Aziz, and J. R. Welty. *Extended Surface Heat Transfer.* USA, New York: John Wiley & Sons, Inc., 2001.

- —. *Extended Surface Heat Transfer.* USA: John Wiley & Sons, Inc. , 2001.

- Kulkarni, P., A. Marsan, and D. Dutta. "A review of process planning techniques in layered manufacturing." *Rapid Prototyping Journal, Vol.6*, 2000: 18-35.

- Lee, L.H. *Fundamentals of adhesion.* USA, New York: Springer-Verlag, 1991.

- Li, L. *Analysis and Fabrication of FDM Prototypes with locally controlled Properties.* Ph.D. Thesis: Department of Mechanical and Manufacturing Engineering, University of Calgary, Canada, 2002.

- Liu, G. R., and S. S. Quek. *The finite element method:a practical course.* USA, Oxford: Butterworth-Heinemann, 2003.

- Liu, X., C. Wu, and X. Wang. "Synthesis, characterization, and infrared-emissivity study of Ni–P–CB nanocomposite coatings by electroless process." *Journal of Coatings Technology an Research, Vol.7*, 2010: 659-664.

- Luo, R. C., and J. H. Tzu. "The Development of an Intelligent Web-Based Rapid Prototyping Manufacturing System." *IEEE Transactions on Automation Science and Engineering, Vol.1*, 2004: 4-13.

- Madhusudana, C. V. *Thermal Contact Conductance.* Sidney: Springer, 1996.

- Meirovitch, L. *Methods of Analytical Dynamics.* USA, New York: Courier Dover Publications, 1970.

- Menges, G., W. Michaeli, and P. Mohren. *How to make injection molds.* USA, Cincinnati: Hanser Verlag, 2001.

- Ogot, M., and G. Okudan-Kremer. *Engineering Design: a pratical guide.* Canada, Victoria: Trafford Publishing, 2004.

- Palais, R. S., and R. A. Palais. *Differential equations, mechanics, and computation, Volume 51.* USA, Providence: American Mathematical Soc., 2009.

- Pandey, P. M., N. V. Reddy, and S. G. Dhande. "Improvement of surface finish by staircase machining in fused deposition modeling." *Journal of Materials Processing Technology, Vol.132*, 2003: 323-331.

- Pandey, P. M., N. V. Reddy, and S.G. Dhande. "Surface roughness simulation for FDM processed parts." *Proceedings of 18th International Conference on Computer Aided Production Engineering, Vol. 44*, 2003: 413-421.

- Pennington, R. C., N. L. Hoekstra, and J. L. Newcomer. "Significant factors in the dimensional accuracy of fused deposition modelling." *Journal of Process Mechanical Engineering, Vol. 219*, 2005: 89-92.

- Pérez, C. J. L. "Analysis of the surface roughness and dimensional accuracy capability of fused deposition modelling process." *International Journal of Production Research, Vol.40*, 2002: 2865-2881.

- Prager, S., and M. Tirrell. "The healing process at polymer-polymer interfaces." *J. Chem. Phys., Vol.75*, 1981: 5194-5198.

- Rathore, M.M., and Raul R. A., Jr. Kapuno. *Engineering Heat Transfer, 2nd Edition.* USA, Sudbury: Jones & Bartlett Learning, 2010.

- Rauwendaal, C. *Polymer Extrusion.* USA: Hanser, 2001.

- Rodriguez, J. F. *Modelling the mechanical behaviour of fused deposition acrylonitrile-butadiene-styrene polymer components, Ph.D. Dissertation.* USA: Department of Aeorospace and Mechanical Engineering, University of Notre Dame, 1999.

- Rodriguez, J. F., J. P. Thomas, and J. E. Renaud. "Characterization of the mesostructure of fused-deposition acrylonitrile-butadiene-styrene materials." *Rapid Prototyping Journal, Vol.6*, 2000: 175-185.

- Rodriguez, J. F., J. P. Thomas, and J. E. Renaud. "Tailoring the mechanical properties of fused-deposition manufactured components." *Proc. Rapid Prototyping and Manufacturing '99, Vol.3*, 1999: 629-643.

- Rodriguez, J.F., J.P. Thomas, and E.R. Renaud. "Mechanical Behavior of acrylonitrile butadiene styrene fused deposition materials modeling." *Rapid Prototyping Journal, Vol. 4*, 2003: 219-230.

- Rodríguez, J.P. Thomas and J.F. "Modeling the fracture strength between fused deposition extruded roads." *Proc. 11th Solid Freeform Fabrication Symposium Proceeding.* Austin, 2000. 16-23.

- Shome, S. N., J. Basu, and G. P. Sinha. *Proceedings of the National Conference on Advanced Manufacturing & Robotics.* India, New Dehli: Allied Publishers, 2004.

- Siegel, R., and J. R. Howell. *Thermal Radiation; Heat Transfer.* USA, New York: Hemisphere Publishing Corporation, 1992.

- Silva, A., and R. Simões. *Handbook of Research on Trends in Product Design and Development:Technological and Organizational Perspectives.* USA, Hershey: Idea Group Inc (IGI), 2010.

- Sonmez, F.O., and H.T. Hahn. "Thermoviscoelastic analysis of the tape placement process." *Journal of Thermoplastic Composite Materials, Vol.10*, 1997: 381–414.

- Sperling, L.H. *Introduction of Physical Polymer Science - Fourth Edition.* USA, New York: John Wiley & Sons, Ltd., 2006.

- Sun, Q. *Bond Formation between Polymer Filaments in Fused Deposition Modeling Process.* Ph.D. Thesis: Department of Chemical and Petroleum Engineering, University of Calgary, Canada, 2004.

- Tan, C. M., Z. Gan, W. Li, and Y. Hou. *Applications of Finite Element Methods for Reliability Studies on ULSI Interconnections.* UK, London: Springer, 2011.

- Thrimurthulu, K., P. M. Pandey, and N. V. Reddy. "Optimum part deposition orientation in fused deposition modeling." *International Journal of Machine Tools & Manufacture, Vol.44*, 2004: 585-594.

- Timings, R. L., and S. P. Wilkinson. *E-manufacture: application of advanced technology to manufacturing processes.* England, Harlow: Pearson Education, 2003.

- Tseng, A.A., and M. Tanaka. "Advanced deposition techniques for freeform fabrication of metal and ceramics parts." *Rapid Prototyping Journal, Nol.7*, 2001: 6-17.

- Venkata, R. *Advanced Modelling and Optimization Of Manufacturing Processes: International Research and Development.* UK, London: Springer, 2010.

- Venuvinod, P. K., and W. Ma. *Rapid prototyping: laser-based and other technologies.* USA, Boston: Kluwer, 2004.

- Vogtmann, D. "Stress relaxation in PMMA During Large-Strain Compression Testing Near the Glass Transition Temperature." *Thesis.* Ohio State University, May 2009.

- Wang, F., et al. "Precision extruding deposition and characterizationof cellular poly-caprolactone tissue scaffolds." *Rapid Prototyping Journal, Vol.10*, 2004: 42-49.

- Wool, R.P. *Polymer Interfaces: Structure and Strength.* USA, New York: Hanser, 1995.

- Wool, R.P., and K.M. O'Connor. "A Theory of crack healing in polymers." *Jornal of Applied Physics, Vol.52*, 1981: 5953-5963.

- Wool, R.P., B.L. McGarel, and O.J.Yuan. "Welding of Polymer Interfaces." *Polymer Engineering and Science, Vol.29*, 1989: 1340-1367.

- Wu, Z., S. Azhi, F.W. Paul, E. Hunt, and A.A. Ogale. "Modeling of mechanical behavior of SLA parts." *Proceedings of the Solid Freeform Fabrication Symposium*, 1997: 725-732.

- Yang, F., and R. Pitchumani. "Healing of Thermoplastic Polymers at an interface under Nonisothermal Conditions." *Macromolecules, Vol.35*, 2002: 3213-3224.

- Yardimci, M. A. *Process Analysis and Planning for Fused Deposition.* Ph.D. Thesis: Department of Mechanical Engineering, University of Illinois at Chicago, 1999.

- Yardimci, M. A., and S. Güçeri. "Conceptual framework for the thermal process modelling of fused deposition." *Rapid Prototyping Journal, Vol. 2*, 1996: 26-31.

- Ziemian, C.W., and P.M. Crawn. "Computer Aided Decision Support for Fused Deposition Modelling." *Rapid Protyping Journal, Vol. 7*, 2001: 138-147.

APPENDIX 1

An energy balance was proposed for the FFE heat transfer. A differential equation was then deduced (equation (3.12)) and some simplifications were made in order to obtain equation (3.15). These simplifications are below:

$$-kA\frac{\partial T_r}{\partial x} - h_{conv}(A_r)_{conv}(T_r - T_E) - \sum_{i=1}^{n} h_i(A_r)_i(T_r - T_{r_i}) =$$

$$= \rho\,CA\frac{\partial T_r}{\partial t}dx - A\left[k\frac{\partial T_r}{\partial x} + \frac{\partial\left(k\frac{\partial T_r}{\partial x}\right)}{\partial x}dx\right]$$

$$\Leftrightarrow -kA\frac{\partial T_r}{\partial x} - h_{conv}(A_r)_{conv}(T_r - T_E) - \sum_{i=1}^{n} h_i(A_r)_i(T_r - T_{r_i}) = \rho\,CA\frac{\partial T_r}{\partial t}dx -$$

$$- kA\frac{\partial T_r}{\partial x} - A\frac{\partial\left(k\frac{\partial T_r}{\partial x}\right)}{\partial x}dx$$

$$\Leftrightarrow -h_{conv}(A_r)_{conv}(T_r - T_E) - \sum_{i=1}^{n} h_i(A_r)_i(T_r - T_{r_i}) = \rho\,CA\frac{\partial T_r}{\partial t}dx - A\frac{\partial\left(k\frac{\partial T_r}{\partial x}\right)}{\partial x}dx$$

Using the expressions of $(A_r)_{conv}$ and $(A_r)_i$, and considering that k is a constant, we obtain:

$$\rho\,CA\frac{\partial T_r}{\partial t}dx - Ak\frac{\partial^2 T_r}{\partial x^2}dx + h_{conv}\left(1 - \sum_{i=1}^{n} a_{r_i}\lambda_i\right)P(T_r - T_E)dx + \sum_{i=1}^{n} h_i a_{r_i}\lambda_i\,P(T_r - T_{r_i})dx = 0$$

$$\Leftrightarrow \rho\,CA\frac{\partial T_r}{\partial t} - Ak\frac{\partial^2 T_r}{\partial x^2} + h_{conv}\left(1 - \sum_{i=1}^{n} a_{r_i}\lambda_i\right)P(T_r - T_E) + \sum_{i=1}^{n} h_i a_{r_i}\lambda_i\,P(T_r - T_{r_i}) = 0$$

$$\Leftrightarrow \frac{\partial T_r}{\partial t} - \frac{Ak}{\rho\,CA}\frac{\partial^2 T_r}{\partial x^2} + \frac{h_{conv}P}{\rho\,CA}\left(1 - \sum_{i=1}^{n} a_{r_i}\lambda_i\right)(T_r - T_E) + \sum_{i=1}^{n} \frac{h_i a_{r_i}\lambda_i\,P}{\rho\,CA}(T_r - T_{r_i}) = 0$$

$$\Leftrightarrow \frac{\partial T_r}{\partial t} = \frac{k}{\rho\,C}\frac{\partial^2 T_r}{\partial x^2} - \frac{h_{conv}P}{\rho\,CA}\left(1 - \sum_{i=1}^{n} a_{r_i}\lambda_i\right)(T_r - T_E) - \sum_{i=1}^{n} \frac{h_i a_{r_i}\lambda_i\,P}{\rho\,CA}(T_r - T_{r_i})$$

$$\Leftrightarrow \frac{\partial T_r}{\partial t} = \frac{k}{\rho\,C}\frac{\partial^2 T_r}{\partial x^2} - \frac{P}{\rho\,CA}\left(h_{conv}\left(1 - \sum_{i=1}^{n} a_{r_i}\lambda_i\right)(T_r - T_E) + \sum_{i=1}^{n} h_i a_{r_i}\lambda_i(T_r - T_{r_i})\right)$$

APPENDIX 2

The objective is to solve the differential equation (3.16). Then, the characteristic polynomial method was used. Details of the resolution can be observed below:

$$\frac{\partial T_r}{\partial t} = -\frac{P}{\rho\,CA}\left(h_{conv}\left(1-\sum_{i=1}^{n}a_{r_i}\lambda_i\right)(T_r-T_E)+\sum_{i=1}^{n}h_i a_{r_i}\lambda_i\left(T_r-T_{r_i}\right)\right)$$

$$\Leftrightarrow \frac{\partial T_r}{\partial t} = -\frac{PL}{\rho\,CAL}\left(h_{conv}\left(1-\sum_{i=1}^{n}a_{r_i}\lambda_i\right)(T_r-T_E)+\sum_{i=1}^{n}h_i a_{r_i}\lambda_i\left(T_r-T_{r_i}\right)\right)$$

$$\Leftrightarrow \frac{\partial T_r}{\partial t} = -\frac{PL}{\rho\,CV}\left(h_{conv}\left(1-\sum_{i=1}^{n}a_{r_i}\lambda_i\right)(T_r-T_E)+\sum_{i=1}^{n}h_i a_{r_i}\lambda_i\left(T_r-T_{r_i}\right)\right)$$

$$\Leftrightarrow \frac{\rho\,VC}{PL}\frac{\partial T_r}{\partial t} = -\left(h_{conv}\left(1-\sum_{i=1}^{n}a_{r_i}\lambda_i\right)(T_r-T_E)+\sum_{i=1}^{n}h_i a_{r_i}\lambda_i\left(T_r-T_{r_i}\right)\right)$$

$$\Leftrightarrow \frac{\rho\,VC}{PL}\frac{\partial T_r}{\partial t} = h_{conv}\left(1-\sum_{i=1}^{n}a_{r_i}\lambda_i\right)T_E +\sum_{i=1}^{n}h_i a_{r_i}\lambda_i T_{r_i} -\left(h_{conv}\left(1-\sum_{i=1}^{n}a_{r_i}\lambda_i\right)+\sum_{i=1}^{n}a_{r_i}h_i\lambda_i\right)T_r$$

$$\Leftrightarrow \frac{\rho\,VC}{PL}\frac{\partial T_r}{\partial t} = \frac{h_{conv}\left(1-\sum_{i=1}^{n}a_{r_i}\lambda_i\right)T_E +\sum_{i=1}^{n}h_i a_{r_i}\lambda_i T_{r_i}}{h_{conv}\left(1-\sum_{i=1}^{n}a_{r_i}\lambda_i\right)+\sum_{i=1}^{n}a_{r_i}h_i\lambda_i}\left(h_{conv}\left(1-\sum_{i=1}^{n}a_{r_i}\lambda_i\right)+\sum_{i=1}^{n}a_{r_i}h_i\lambda_i\right)+$$

$$-\left(h_{conv}\left(1-\sum_{i=1}^{n}a_{r_i}\lambda_i\right)+\sum_{i=1}^{n}a_{r_i}h_i\lambda_i\right)T_r$$

If we consider that:

$$b\!\left(a_{r_1},...,a_{r_n}\right)= h_{conv}\left(1-\sum_{i=1}^{n}a_{r_i}\lambda_i\right)+\sum_{i=1}^{n}a_{r_i}h_i\lambda_i$$

And:

$$Q\left(a_{r_1},...,a_{r_n}\right) = \frac{h_{conv}\left(1 - \sum_{i=1}^{n} a_{r_i}\lambda_i\right)T_E + \sum_{i=1}^{n} a_{r_i}h_i\lambda_i T_{r_i}}{h_{conv}\left(1 - \sum_{i=1}^{n} a_{r_i}\lambda_i\right) + \sum_{i=1}^{n} a_{r_i}h_i\lambda_i}$$

We can rewrite the differential equation:

$$\frac{\rho VC}{PL}\frac{\partial T_r}{\partial t} = Q\left(a_{r_1},...,a_{r_n}\right)b\left(a_{r_1},...,a_{r_n}\right) - b\left(a_{r_1},...,a_{r_n}\right)T_r$$

$$\Leftrightarrow \frac{\rho VC}{PL\, b\left(a_{r_1},...,a_{r_n}\right)}\frac{\partial T_r}{\partial t} = Q\left(a_{r_1},...,a_{r_n}\right) - T_r$$

$$\Leftrightarrow \frac{\rho VC}{PL\, b\left(a_{r_1},...,a_{r_n}\right)}\frac{\partial T_r}{\partial t} + T_r = Q\left(a_{r_1},...,a_{r_n}\right)$$

Since the coefficients are constants, we can use the characteristic polynomial method in order to solve this last differential equation. The homogeneous equation associated to the last is:

$$\frac{\rho VC}{PL\, b\left(a_{r_1},...,a_{r_n}\right)}\frac{\partial T_r}{\partial t} + T_r = 0$$

The characteristic equation corresponded to the last is:

$$\frac{\rho VC}{PL\, b\left(a_{r_1},...,a_{r_n}\right)}y + 1 = 0$$

The solution of can be obtained from:

$$\frac{\rho VC}{PL\, b\left(a_{r_1},...,a_{r_n}\right)}y + 1 = 0 \Leftrightarrow$$

$$\Leftrightarrow \frac{\rho VC}{PL\, b\left(a_{r_1},...,a_{r_n}\right)}y = -1 \Leftrightarrow$$

$$\Leftrightarrow y = \frac{-PL\, b\left(a_{r_1},...,a_{r_n}\right)}{\rho VC}$$

So:

$$T_r(t) = C_1 e^{\frac{-PL\, b\left(a_{r_1},...,a_{r_n}\right)}{\rho VC}(t-t_r)}$$

Where C_1 is a constant and $t_r(x)$ is the instant where the filament starts cooling down or enters in contact with another ($j \in \{1,...,n\}$, n is the physical number of contacts). We can conclude that the general solution is:

$$T_r(t) = C_1 e^{\frac{-PL\, b\left(a_{r_1},...,a_{r_n}\right)}{\rho VC}(t-t_r)} + Q\left(a_{r_1},...,a_{r_n}\right)$$

Let T_{r0} the temperature of the filament at the instant t_r :

$$T_r(t_r) = T_{r0}$$

The constant C_1 can be obtained from the two last expressions:

$$T_r(t_r) = T_{r0}$$
$$\Leftrightarrow C_1 e^{\frac{-PL\, b\left(a_{r_1},...,a_{r_n}\right)}{\rho VC}(t_r-t_r)} + Q\left(a_{r_1},...,a_{r_n}\right) = T_{r0}$$
$$\Leftrightarrow C_1 e^0 + Q\left(a_{r_1},...,a_{r_n}\right) = T_{r0}$$
$$\Leftrightarrow C_1 = T_{r0} - Q\left(a_{r_1},...,a_{r_n}\right)$$

The expression of $T_r(t)$ is so rewritten:

$$T_r(t) = \left(T_{r0} - Q\left(a_{r_1},...,a_{r_n}\right)\right)e^{\frac{-P\, b\left(a_{r_1},...,a_{r_n}\right)}{\rho AC}(t-t_r)} + Q\left(a_{r_1},...,a_{r_n}\right)$$

APPENDIX 3

This code below allows obtaining the temperature along deposition time for the first layer of filaments, using one or two distinct materials. The real complete code has the same logic and structure for the remaining layers.

```matlab
function FFE(matrix,x)

%Definition of the vector that contains the number of total filaments in each layer
matrix_lin = size(matrix,1);
matrix_col = size(matrix,2);
vector = zeros(matrix_lin,2);
contar = 0;
for i = matrix_lin:-1:1
    contar = contar + 1;
    for j = 1:matrix_col
        if matrix(i,j) ~= 0
            vector(contar,1) = vector(contar,1) + 1;
        end
    end
end

%Number of layers
m = length(vector(:,1));

%Number of filaments
n = 0;
for j = 1:m
    if m == 1
        n = vector(1,1);
    else
        if vector(j,2) <= 1
            n = n + vector(j,1);
        end
    end
end

%Computation variables
passo = 0.05;        %Step time
temp_mais = 15;      %Additional time computation after construction of the part
erro = 0.001;        %Convergence error

%Definition of the size of the variables
h = zeros(1,5); lambda = zeros(1,5); a = zeros(n,5); T = zeros (n,5);
vec_b = zeros(n,5); vec_Q = zeros(n,5); b = zeros(1,n); Q = zeros(1,n);
T_begin = zeros(1,n); dif = zeros(1,n); Biot = zeros(1,n); save_T = zeros(1,n);
old_T = zeros(1,n); save_lim = zeros(1,n); viz = zeros(11,n);

%Process Variables
T_L = 270;       %Extrusion temperature (ºC)
T_E = 70;        %Temperature of the envelope (ºC)
v = 0.02;        %Velocity of the extrusion head (m/sec)
for lin = 1:n    %Temperature of support (ºC)
    T(lin,1) = T_E;
end
```

162

```
%Filament dimensions
w = 0.0003;           %Layer Thickness (meters)
L = 0.02;             %Length of the filament (meters)
area = pi * (w/2)^2;  %Area of the cross section of filament (meters^2)
per = pi * w;         %Perimeter of the cross section of filament (meters)
vol = area*L;         %Volume of the filament
A_p = per*L;          %Superficial area of the filament


% Material Properties
%Thermal conductivity (W/m.K)
conductivity(1) = 0.1768; % material A
conductivity(2) = 0.5;    % material B
%Density (kg/m^3)
ro(1) = 1050;             % material A
ro(2) = 1500;             % material B
%Specific heat (J/kg.K)
C(1) = 2019.7;            % material A
C(2) = 2500.7;            % material B


% Heat transfer coefficient (lost of heat by natural convection)
h_conv = 45;


%Thermal contact conductances between
h(1,1) = 200;         % filament and left adjacent filament
h(1,2) = 200;         % filament and down adjacent filament
h(1,3) = 200;         % filament and right adjacent filament
h(1,4) = 200;         % filament and top adjacent filament
h(1,5) = 10;          % filament and support


%Fraction of perimeter contact between
lambda(1,1) = 0.2;    % filament and left adjacent filament
lambda(1,2) = 0.25;   % filament and down adjacent filament
lambda(1,3) = 0.2;    % filament and right adjacent filament
lambda(1,4) = 0.25;   % filament and top adjacent filament
lambda(1,5) = 0.25;   % filament and support


%Definition of the parameters influenced by the contacts
for col = 1:5
   for lin = 1:n
      vec_b(lin,col) = h(1,col)*lambda(1,col);
      vec_Q(lin,col) = vec_b(lin,col)*T(lin,col);
   end
end


%Definition of the parameters influenced by the material properties
contar = 0;
number_filament = 0;
for i = matrix_lin:-1:1
   contar = contar + 1;
   if isodd(contar) == 1
      for j = 1:matrix_col
         if matrix(i,j) ~= 0
            number_filament = number_filament + 1;
            escalar(number_filament) = -per/(ro(matrix(i,j))*area*C(matrix(i,j)));
            esc(number_filament) = h_conv/(ro(matrix(i,j))*L*C(matrix(i,j)));
            kt(number_filament) =  conductivity(matrix(i,j));
         end
      end
   else
```

163

```matlab
        for j = matrix_col:-1:1
            if matrix(i,j) ~= 0
                number_filament = number_filament + 1;
                escalar(number_filament) = -per/(ro(matrix(i,j))*area*C(matrix(i,j)));
                esc(number_filament) = h_conv/(ro(matrix(i,j))*L*C(matrix(i,j)));
                kt(number_filament) =  conductivity(matrix(i,j));
            end
        end
    end
end


%Definition of the periods of time between two successive contacts
for i = 1:(n+2)
    if isodd(i) == 1
        limite(i,1) = (i*L-x)/v;
        limite(i,2) = (i*L+x)/v;
    else
        limite(i,1) = limite(i-1,2);
        limite(i,2) = ((i+1)*L-x)/v;
    end
end
for road = 1:n
    linha = 0;
    for i = 0:passo:limite(n,2)
        linha = linha + 1;
        temp(linha,road) = T_L;
    end
end
for layer = 1:m
    if layer == 1
        for num = 1:vector(layer,1)
            if num == 1

                %Activation of the contact with support
                a(num,5) = 1;

                %Definition of the variables b and Q defined in equation Eq. 7
                b(num) = h_conv*(1-lambda*a(num,:)') + vec_b(num,:)*a(num,:)';
                Q(num) = (h_conv*(1-lambda*a(num,:)')*T_E + vec_Q(num,:)*a(num,:)')/b(num);

                p = 0;
                for t = 0:passo:limite(num,1)
                    p = p+1; abcissa(p) = t;
                end

                %Computation of the temperatures of the first filament
                for t = (limite(num,1)+passo):passo:limite_final
                    p = p+1; abcissa(p) = t;
                    temp(p,num)=(T_L-Q(num))*exp(escalar(num)*b(num)*(t-limite(num,1)))
                    +Q(num);
                End

                %Saving the last temperature of the period time of cooling down
                T_begin(num) = temp(p,num);

                %Verification of the value of Biot Number
                Biot(num) = (vol/A_p)*(b(num)/kt(num));
                if Biot(num)>=0.1
                    'WARNING! We cannot use a Lumped System'
```

164

```
            end
        else
            %Activation of the contacts
            a(num-1,3) = 1; a(num,1) = 1; a(num,5) = 1;

            %Up-dating of the variable b
            for j = 1:num
                b(j) = h_conv*(1-lambda*a(j,:)') + vec_b(j,:)*a(j,:)';
            end

            if m == 1
                if num == vector(layer,1)
                    limite_final = limite(num,2) + temp_mais;
                else
                    limite_final = limite(num,2);
                end
            else
                limite_final = limite(num,2);
            end
            for t = (limite(num,1)+passo):passo:limite_final
                p = p+1; abcissa(p) = t;
                last = p-1;
                for j = 1:num
                    save_T(j) = temp(last,j);
                end

                %Iterative process
                for q = 1:100000
                  %Saving contacts and temperatures of adjacent filaments
                    for j = 1:num
                        if j == 1
                            T(j,3) = save_T(j+1);
                            viz(3,j) = j+1;
                        end
                        if j > 1 & j < num
                            T(j,1) = save_T(j-1);
                            viz(1,j) = j-1;
                            T(j,3) = save_T(j+1);
                            viz(3,j) = j+1;
                        end
                        if j == num
                            T(j,1) = save_T(j-1);
                            viz(1,j) = j-1;
                        end
                        for k = 1:5
                            if T(j,k) ~= 0 & k ~= 5
                                vec_Q(j,k) = vec_b(j,k)*T(j,k);
                            end
                        end

                        %Up-dating of the variable Q
                        Q(j) = (h_conv*(1-lambda*a(j,:)')*T_E + vec_Q(j,:)*a(j,:)')/b(j);
                        old_T(j) = save_T(j);
                      end

                    %Computation of the temperatures
                     if num == 2
                        save_T(1) = (T_begin(1)-Q(1))*exp(escalar(1)*b(1)*
                                    (t-limite(1,1)))+Q(1);
```

165

```matlab
                    save_T(2) = (T_L-Q(2))*exp(escalar(2)*b(2)*(t-limite(1,1)))+Q(2);
                    save_lim(1,1) = limite(num,1);
                    save_lim(1,2) = limite(num,1);
                else
                    for j=1:num-2
                        save_T(j) = (T_begin(j)-Q(1))*exp(escalar(j)*b(j)*
                                    (t-save_limite(1,j)))+Q(j);
                    end
                    save_T(num-1) = (T_begin(num-1)-Q(num-1))*
                                exp(escalar(num-1)*b(num-1)*(t-limite(num,1)))+Q(num-1);
                    save_T(num) = (T_L-Q(num))*
                                exp(escalar(num)*b(num)*(t-limite(num,1)))+ Q(num);
                    save_lim(1,num-1) = limite(num,1);
                    save_lim(1,num) = limite(num,1);
                end
                for j = 1:num
                    dif(j) = abs(save_T(j)-old_T(j));
                end
                try = 1;
                stop = 0;
                for j = 1:num
                    if dif(try) < erro
                        try = try+1;
                    end
                    if try == num+1;
                        stop = 1;
                    end
                end
                if stop == 1
                    for j = 1:num
                        temp(p,j) = save_T(j);
                    end
                    break;
                end
            end
        end
        T_begin(num) = temp(p,num);
        %End of iterative process

        %Verification of the Biot Number
        for j=1:num
            Biot(j) = (vol/A_p)*(b(j)/kt(j));
            if Biot(j)>=0.1
                'WARNING! We can not use a Lumped System'
                j
                Biot(j)
            end
        end
    end
  end
 end
end
```